

https://dspace.org/

Resolving the atmospheric sulphur budget over the Elandsfontein area of the Mpumalanga Highveld

Igbafe, Anselm Iuebego

2008-09-02T09:46:49Z
http://hdl.handle.net/10539/5587

Downloaded from a DSpace repository. https://dspace.org/

RESOLVING THE ATMOSPHERIC SULPHUR BUDGET OVER THE ELANDSFONTEIN AREA OF THE MPUMALANGA HIGHVELD

Anselm Iuebego Igbafe

A Thesis submitted to the Faculty of Engineering and the Built Environment, University of the Witwatersrand, in fulfilment of the requirements for the degree of Doctor of Philosophy in Engineering

Johannesburg 2007

Preface

This work was supervised by:

Dr S J Piketh, Director, Climatology Research Group, University of the Witwatersrand, Johannesburg

and

Dr L L Jewell, Senior Lecturer, School of Chemical and Metallurgical Engineering, University of the Witwatersrand, Johannesburg.

Copyright © 2007 by Anselm Iuebego Igbafe, University of the Witwatersrand, Johannesburg, Republic of South Africa.

Subject Key Headings

- Temporal scale assessment of *in situ* sulphur observations
- Sulphate characterisation and forecast using meteorology
- Computational chemistry model analyses
- Gas-phase, aqueous-phase and radical atmospheric sulphur reactions
- Thermochemical properties and reaction path analyses
- Kinetic Modelling with dispersion during advection

This work is part of the research project on air pollution studies jointly conducted by the Climatology Research Group in collaboration with Consulting, Research and Development, Eskom Resources and Strategy, Johannesburg. Funding was provided by the Climatology Research Group, Eskom Research and Innovation and the National Research Fund.

The work described in this thesis is novel as regards the *in situ* assessment of particulate sulphate in the Mpumalanga Highveld subregion of South Africa. It also shows the relative importance of the several known reactions involving SO_2 in the atmosphere against one another, through the determination of the most favourable reaction pathways, using first principle model chemistry techniques. Finally it shows the reaction kinetics of atmospheric sulphur (IV) during advection in the planetary boundary layer as it affects the downwind concentration distribution.

Articles, Conferences and Reports from the Study

Igbafe, A. I., Jewell, L. L., Piketh, S. J. and Dlamini, T. S. (2006): **A Wintertime Impact of Dilution on Transformation Rate in the Planetary Boundary Layer**, *Journal of Environmental Informatics*, Vol. 8, No. 1, pp. 34 – 48.

Igbafe, A. I., Jewell, L. L. and Piketh, S. J. (2006): **Assessment of Total Sulphur in the Planetary Boundary Layer on the Mpumalanga Highveld**, South Africa Society of Atmospheric Scientist (SASAS) Conference Proceedings, 4 – 6 October, Bloemfontein, p97.

Igbafe, A. I., Jewell, L. L. and Piketh, S. J. (2006): **Theoretical Determination of Thermodynamic Properties for Gas-Phase and Aqueous-Phase Reactions of Atmospheric Sulphur, Atmospheric Chemistry at the Interface,** CACGP/IGAC/WMO Conference Proceedings, S1P4, 17 – 22 September, Cape Town, p19.

Igbafe, A. I., Piketh, S. J., Jewell, L. L. and Snow, N. H. (2006): **Preliminary Sulphate Budget Findings at Elandsfontein AQM Station**, Eskom Report RES/RR/05/26693, pp. 1 – 21.

Igbafe, A. I., Piketh, S. J., Jewell, L. L. and Snow, N. H.: **An In situ Evaluation of Atmospheric Sulphur Species on the South African Highveld**, Submitted to *Journal of Geophysical Research*.

Igbafe, A. I., Piketh, S. J. and Jewell, L. L.: **Variations in the Order of Reaction: An Implication on Oxidation Rate during Atmospheric Diffusion of SO_2 in the Planetary Boundary Layer**, Submitted to *Journal of Environmental Informatics*.

Igbafe, A. I., Jewell, L. L. and Piketh, S. J.: **Thermochemical Analyses of Sulfur Compounds: Implications for Atmospheric Sulfur Oxidation**, Submitted to *South African Journal of Science*.

Declaration

I declare that this thesis is my own, unaided work. It is being submitted for the Degree of Doctor of Philosophy in the University of the Witwatersrand, Johannesburg. It has not been submitted before for any degree or examination in any other University.

_____

This **1st** day of **April 2007**

Abstract

A novel study on the investigation of three very common atmospheric sulphur species relevant to the Mpumalanga Highveld subregion was conducted. Long-term *in situ* measurements were applied in the diurnal and seasonal evaluation of the observed sulphur species. Ambient pollutant concentrations and surface meteorological data were collected at an air quality monitoring station at Elandsfontein. Elandsfontein air quality monitoring station was ideal for the observations due to its high elevation within the Mpumalanga Province surrounded by few rolling hills and negligible windbreaks which easily allows for extensive plume-contact with the surface during convective daytime mixing. The temporal characteristics of the sulphur species have been assessed relative to one another with varying meteorological conditions. The diurnal and seasonal concentration variations were used to describe the physical characteristics exhibited by the compounds over Elandsfontein. Pollution roses were used to target the source of the major release points and areas of these sulphur species relative to the Elandsfontein monitoring station. Gas and particle concentrations were analysed in relation to varying meteorological parameters with a view to ascertaining the sulphur transformation and concentration distribution in the planetary boundary layer. Particulate sulphate distribution has been modelled through multivariate regression analyses in relation to three meteorological parameters, namely, wind speed, relative humidity and ambient temperature for the various seasons observed over southern Africa.

This study has shown that hydrogen sulphide, sulphur dioxide and sulphate species are present throughout the year in the Mpumalanga Highveld at notably significant levels. The presence of ambient particulate sulphate has been shown to result from the combination of chemical interactions during long-range aerosol transport; atmospheric recirculation processes shown from back trajectories over the southern Africa sub-region, as well as the variation in the removal mechanisms and rates for the different seasons throughout the year. These transport and removal processes all contribute to the overall sulphur mass balance in the planetary boundary layer. Dosage of the three sulphur species was evaluated to provide data for sulphur pollution loading that could form a basis for health and

environmental impact assessments over the area. In view of the characteristic patterns displayed by particulate sulphate, multivariate mathematical models have been developed on a seasonal basis with variations in meteorological parameters. This was seen to predict an accuracy of up to 70 % of the particulate sulphate loading for different seasons over the South African Highveld.

In order to understand the chemical interactions of atmospheric sulphur species, it is important to be able to predict the route taken and expected products of transformation on any given condition. Theoretical analyses of the chemical thermodynamic properties of the known reacting species and a well-established approach were used in predicting reaction paths and establishing the possible and feasible products of chemical transformation in relation to the ambient temperature. The determination of reaction paths and possible products of chemical transformation provides a measure of the relative importance of the reacting species and the mechanism of reaction. Gas-, aqueous-phase and radical reactions involving sulphur (IV) were investigated with a view to establishing their relative importances. Thermochemical properties of several sulphur-containing compounds not available in the literature have been generated for evaluation of Gibbs free energy (ΔG) and enthalpy (ΔH). An electronic energy structural approach has been applied to model for ΔG and ΔH of 88 sulphur species in 90 chemical reactions comprising gas-phase, aqueous-phase and radical reactions. Modelling was evaluated for their relative importances over a temperature range of –100 °C to +100 °C. The temperature range is well above the known tropospheric temperature range to account for variations in the atmospheric environment.

To further comprehend the chemistry of sulphur with regards to distribution of the species in the atmosphere, a kinetic model is developed and incorporated into a dispersion model. The kinetic evaluation of the oxidation rate of SO_2 to sulphate has been determined with advection and dispersion over the Elandsfontein area. Gas-phase transformation with advection and dispersion has been used to evaluate the extent of the distribution of SO_2 relative to the major contributing sources. The dry deposition was considered to be the dominant removal mechanism. It was assumed that the reaction rate was second order in concentration and that the rate of deposition was first order. The oxidation rates obtained for the seasons were 10.9 % h^{-1} for summer; 8.83 % h^{-1} for autumn; 6.56 % h^{-1} for winter;

10.8 % h^{-1} for spring, while an overall rate of 9.6 % h^{-1} was obtained for the one year study period. The transformation rate model produced a reaction constant and an activation energy of 4.92 x 10^{-6} µg m^{-3} s^{-1} and 36.54 kJ kg^{-1} for summer; 3.939 x 10^{-6} µg m^{-3} s^{-1} and 43.89 kJ kg^{-1} for autumn; 2.90 x 10^{-6} µg m^{-3} s^{-1} and 115.69 kJ kg^{-1} for winter; 4.82 x 10^{-6} µg m^{-3} s^{-1} and 43.29 kJ kg^{-1} for spring, while for the year 4.29 x 10^{-6} µg m^{-3} s^{-1} and 34.31 kJ kg^{-1}. A Gaussian puff unsteady state Lagrangian dispersion model with reflection at the surface and inversion layer was applied for concentration diffusion. The Lagrangian dispersion model with dry deposition was a better prediction of the observed data than the models from previous studies using a first order rate constant with or without deposition rate.

Key Words

Sulphur budget
Particulate sulphate Elandsfontein Mpumalanga Highveld
Atmospheric SO_2 oxidation rate variation in Lagrangian advection puff model
Thermochemical properties of atmospheric sulphur transformation

Dedication

To my wife,

Kate,

and

my three beautiful children,

Sylvia, Tracy and Bunmi

Acknowledgements

My deepest appreciation goes to my supervisor on air pollution climatology, Dr S J Piketh, without whom this study would not have seen the light of day and to my supervisor on chemical engineering reaction analyses, Dr L L Jewell, who was the driving force behind my involvement with atmospheric environmental studies.

Funding for this work was provided by Consulting, Research and Development, Eskom Resources and Strategy, Johannesburg. I would like to thank Neil Snow, Dr Kristy Ross, Eric Lynch, Ron Rorich, Eric Barr, Abe Segopa and Derrick Murray of Consulting, Research and Development, Eskom Resources and Strategy, Johannesburg, South Africa for assistance provided to me during the field experiments.

I also wish to thank all members of staff and especially Roelof Burger and Dragana M Jovic, and Lisanne Frewin of the Climatology Research Group, University of the Witwatersrand for their assistance and support during the field study for data acquisition and analyses. I also wish to express my appreciation to my colleagues at the School of Chemical and Metallurgical Engineering and the Climatology Research Group, University of the Witwatersrand – especially Thomas Bigala, Late Samuel Mugabe, Phillip and Joe for all the friendly support they accorded me during my programme. My sincere gratitude goes to Professor A. E. Taigbenu of the Civil and Environmental Engineering for his moral support throughout my study, and to Jeannette Menasce for the grammatical and structural review given to this document. This work was also aided with financial grants from the National Research Fund South Africa.

Finally, all glory and honour to goes to Almighty God for providing me the opportunity to study in South Africa as well as His guidance and protection of me and my family throughout my study in the country**.**

Igbafe, A I

01 April, 2007

Contents

Preface……ii

Subject Key Headings……...ii

Articles, Conferences and Reports from the Study……...iii

Declaration……v

Abstract……vi

Key Words……...viii

Dedication……..ix

Acknowledgements……x

Contents……xi

List of Figures……xvi

List of Tables……xxiii

Abbreviations, Acronyms and Symbols……..xxv

Nomenclature……xxvi

CHAPTER 1: GENERAL INTRODUCTION……1

1.1 Introduction……1

1.2 Background of Study……1

1.3 Research Goals……...2

1.4 Research Questions……2

1.5 Overall Research Objectives……3

1.6 Scope of the Research……5

1.7 Contributions to Knowledge……5

CHAPTER 2: LITERATURE SURVEY……..6

2.1 Introduction……6

2.2 Air Pollution……6

2.3 Air Pollution from Coal Combustion……7

2.4 Targeting of Air Pollutants Source Areas……...10

2.4.1 Receptor Modelling……..10

2.4.2 Back Trajectories……..11

2.5 The Mpumalanga Highveld……..12

2.6 Climatology and Meteorology of the Mpumalanga Highveld……...14

2.6.1 Surface and Elevated Inversions over the Mpumalanga Highveld……...17

2.6.2 Transport Mechanisms over the Mpumalanga Region…….20

2.7 Atmospheric Sulphur: An Overview……...22

2.7.1 Atmospheric Sulphur from Natural and Man-Made Sources……..23

2.7.2 Gaseous Atmospheric Sulphur……..26

2.7.3 Atmospheric Sulphate Aerosols……....28

2.7.4 Health Implications of Atmospheric Sulphur……...33

2.7.5 Formation and Distribution of Sulphur in the Atmosphere……...35

2.7.6 Deposition: A Removal Mechanism of Atmospheric Sulphur……..36

2.8 Atmospheric Ammonia-Related Sulphur Compounds……..36

2.9 The Microphysics and Chemistry of Aerosol Particles…….38

2.9.1 The Impact of Sulphate Aerosol on Climate……39

2.9.2 Mechanism of Climate Forcing by Atmospheric Sulphate……39

2.9.3 Sulphate Aerosol Contribution to Direct Forcing……40

2.9.4 Particulate Sulphate Contribution to Indirect Forcing……..42

2.9.5 Atmospheric Water Vapour Impact on Aerosols……..43

2.9.6 Effects of Temperature Lapse Rate on Aerosols…….....51

2.9.7 Phoretic Dynamics of Sulphate Aerosols……...……..51

2.10 Atmospheric Sulphur Budget…….…… 52

2.10.1 Atmospheric Time Scales…….53
2.10.2 Box Model for Atmospheric Sulphur Budget……..58
2.10.3 Transboundary Model for Atmospheric Sulphur Budget….58

2.11 Chemical Transformations of Atmospheric Sulphur……58
2.11.1 Kinetics of Chemical Transformations…….61
2.11.2 Thermodynamic Equilibrium of Chemical Reactions……..69

2.12 Transport Models……..….84
2.12.1 Air Pollution Dispersion……...86
2.12.2 Air Quality Dispersion Models…….93
2.12.3 Atmospheric Diffusion Principles and Mechanisms…….94

2.13 Conclusion……108

CHAPTER 3: EXPERIMENTAL……..110

3.1 Introduction……110

3.2 Site Description……...110

3.3 Sampling Approach for Temporal Analysis……111
3.3.1 Materials and Methods……...112
3.3.2 Sampling Procedure……113

3.4 Computational Chemistry Approach to Modelling Atmospheric Transformations…….……123
3.4.1 Computational Method for Thermochemical Analyses….123

3.5 Data Evaluation for Kinetic and Dispersion Modelling……..124
3.5.1 Materials and Method…….……124
3.5.2 Sampling Description…….……125

CHAPTER 4: ANALYSIS OF TEMPORAL VARIATIONS OF ATMOSPHERIC SULPHUR OVER ELANDSFONTEIN……126

4.1 Introduction to Total Sulphur Evaluation……126

4.2 Evaluations of Measured Concentrations……128

4.3 Analyses of Measured Concentrations……..129
4.3.1 The Effect of Wind on Concentration Distribution……129

4.3.2 Temporal Variations of Atmospheric Sulphur at Elandsfontein……..134
4.3.3 Relationships between SO_2 and Particulate Sulphate in the Atmosphere……...145
4.3.4 Meteorological Contributions to Particulate Sulphate Distribution…….149
4.3.5 Statistical Analyses for Total Atmospheric Sulphur Distribution…….156

4.4 Conclusion……169

CHAPTER 5: THEORETICAL ANALYSES OF THERMOCHEMICAL PROPERTIES OF ATMOSPHERIC SULPHUR……172

5.1 Introduction to Theoretical Analyses for Atmospheric Sulphur Reactions……...172

5.2 Analyses of Computational Energies……..…176

5.3 Analyses of Computational Methods……..178

5.4 Effect of Temperature on Equilibrium Constant……179

5.5 Equilibrium Conversion over Tropospheric Temperature Range……188

5.6 The Most Significant Atmosphere Sulphur Transformations……189

5.7 Conclusion……190

CHAPTER 6: ANALYSES OF SO_2 OXIDATION DURING DISPERSION OVER ELANDSFONTEIN……192

6.1 Introduction……192

6.2 Model Development……193

6.2.1 Estimation of SO_2 Concentration at the Source…….195
6.2.2 Chemical Sub-models……195
6.2.3 Comparison of the Three Predicted Rate Constants……..208
6.2.4 Application of Transformation Rates to Atmospheric Diffusion……208

6.3 Outcomes of the Dispersion Modelled with Transformations……217

6.4 Conclusion……218

CHAPTER 7: OVERALL CONCLUSION……...220

RECOMMENDATION FOR FUTURE WORK……225

REFERENCES……...227

APPENDIX A: MODEL DEVELOPMENT AND CALCULATIONS FOR ATMOSPHERIC SO_2 OXIDATION DURING DIFFUSION……..274

A-1: Rate Model Development for Atmospheric SO_2 Oxidation……274

A-2: Temperature Dependency on Reaction Rates……..283

A-3: Model Development for Concentration Dispersion with Transformation……...284

APPENDIX B: COMPUTATIONAL METHODS FOR EVALUATION OF THERMOCHEMICAL PROPERTIES……297

B-1: Model Input Requirements……297

B-2: Quick Tour of Gaussian Output……298

B-3: Enthalpies and Gibbs Free Energy Computed Using G03 Model Package……309

List of Figures

Figure 2-1: Map of South Africa showing the study area....13

Figure 2-2: Mean monthly winds and contours (gpm) of the 850 and 500 hPa pressure surfaces in January and July....16

Figure 2-3a: Annual surface inversion frequency (percentage) at 01:30 and 13:3018

Figure 2-3b: Generalised winter early morning inversion depth (m) and strength (°C) over southern Africa....18

Figure 2-4: Mean minimum and mean maximum mixing heights in summer and winter over South Africa....19

Figure 2-5: Seasonal variation of the mean 800 hPa winds and contours....22

Figure 2-6: The atmospheric sulphur cycle....24

Figure 2-7: Diameter change of $(NH_4)_2SO_4$, NH_4HSO_4 and H_2SO_4 particles as a function of relative humidity....45

Figure 2-8: Gibbs free energy of a solid salt and its aqueous solution as a function of relative humidity....47

Figure 2-9a: Deliquescence relative humidity as a function of temperature for $(NH_4)_2SO_4$....48

Figure 2-9b: Deliquescence relative humidity as a function of temperature for Na_2SO_4, $NaNO_3$ and mixed salt....49

Figure 2-10: Two air pollution sources at the Elandsfontein area on the Mpumalanga Highveld....87

Figure 2-11: Typical plume shapes with wind and temperature profiles....89

Figure 2-12: Plume boundary and time-averaged envelope....96

Figure 2-13: An aerial view of a plume flow pattern....97

Figure 2-14: Vertical dispersion coefficient as a function of downwind distance101

Figure 2-15: Horizontal dispersion coefficient as a function of downwind distance 101

Figure 2-16: Plume dispersion by Gaussian distribution and coordinate system 104

Figure 3-1: Front view of the model 43C trace SO_2 pulse fluorescence analyser 114

Figure 3-2: Front view of model 450 H_2S-SO_2 pulse fluorescence analyser 115

Figure 3-3: Series 8400S ambient particulate sulphate monitor 117

Figure 3-4: Schematic of the Rupprecht and Patashnick Series 8400S monitor consisting of a pulse generator and pulse analyser 118

Figure 3-5: Correlations between the semi-continuous sulphate concentrations and the 24-h filter data, collected at the Queens College site 120

Figure 3-6: Model 05305-L R. M. Young Wind Monitor-AQ 121

Figure 3-7: The model 41003-5 10-Plate Gill Radiation Shield 122

Figure 4-1: Wind rose for Elandsfontein between September 2004 and August 2005 130

Figure 4-2: Mean H_2S concentration distribution at Elandsfontein between September 2004 and August 2005 131

Figure 4-3: Mean SO_2 concentration distribution at Elandsfontein between September 2004 and August 2005 132

Figure 4-4: Mean particulate sulphate concentration distribution at Elandsfontein between September 2004 and August 2005 133

Figure 4-5: Monthly mass fraction distributions of particulate sulphate relative to total sulphur at Elandsfontein between September 2004 and August 2005 136

Figure 4-6: Diurnal variations of mean H_2S concentrations at Elandsfontein for the various seasons observed over southern Africa 137

Figure 4-7: Diurnal variations of mean SO_2 concentrations at Elandsfontein for the various seasons observed over southern Africa 138

Figure 4-8: Diurnal variations of mean particulate sulphate concentrations at Elandsfontein for the various seasons observed over southern Africa 140

Figure 4-9: Seasonal variations of mean concentrations of the observed sulphur species at Elandsfontein between September 2004 and August 2005 142

Figure 4-10: Seasonal variations of maximum concentrations of the observed sulphur species at Elandsfontein between September 2004 and August 2005 142

Figure 4-11: Seasonal variations of minimum concentrations of the observed sulphur species at Elandsfontein between September 2004 and August 2005 143

Figure 4-12a: Regression correlation between SO_2 and particulate sulphate in spring from measurements at Elandsfontein 146

Figure 4-12b: Regression correlation between SO_2 and particulate sulphate in summer from measurements at Elandsfontein 147

Figure 4-12c: Regression correlation between SO_2 and particulate sulphate in autumn from measurements at Elandsfontein 147

Figure 4-12d: Regression correlation between SO_2 and particulate sulphate in winter from measurements at Elandsfontein 148

Figure 4-13: Relationship between SO_2 and particulate sulphate obtained as an average of all measured data at Elandsfontein, from wind directional sectors A and B. 148

Figure 4-14: A diurnal episode on 02 July 2005 indicating the first observed maximum particulate sulphate concentration at Elandsfontein 150

Figure 4-15: A diurnal episode on 15 July 2005 indicating the second observed maximum particulate sulphate concentration at Elandsfontein 151

Figure 4-16: NOAA HYSPLIT backward trajectories ending at 23:00 UTC for 02 July 2005 from Elandsfontein 152

Figure 4-17: NOAA HYSPLIT backward trajectories ending at 23:00 UTC for 15 July 2005 from Elandsfontein 153

Figure 4-18: Frequency distribution of deliquescence and crystallisation relative humidities for particulate NH_4HSO_4 and $(NH_4)_2SO_4$ at Elandsfontein 155

Figure 4-19: Frequency distribution of H_2S concentrations from September 2004 to August 2005 at Elandsfontein 156

Figure 4-20: Frequency distribution of SO_2 concentrations from September 2004 to August 2005 at Elandsfontein 157

Figure 4-21: Frequency distribution of particulate sulphate concentrations from September 2004 to August 2005 at Elandsfontein 157

Figure 4-22: Frequency and cumulative distribution of raw measured H_2S, SO_2 and particulate sulphate concentrations from September 2004 to August 2005 at Elandsfontein 159

Figure 4-23: Frequency and cumulative distribution of the natural logarithmic transformed H_2S, SO_2 and particulate sulphate concentrations from September 2004 to August 2005 at Elandsfontein 159

Figure 4-24: Frequency and cumulative distribution of the inverse transformed H_2S, SO_2 and particulate sulphate concentrations from September 2004 to August 2005 at Elandsfontein 160

Figure 4-25: Frequency and cumulative distribution of the square root transformed H_2S, SO_2 and particulate sulphate concentrations from September 2004 to August 2005 at Elandsfontein 161

Figure 4-26: Diurnal characteristics of observed and predicted particulate sulphate in spring at Elandsfontein 164

Figure 4-27: Diurnal characteristics of observed and predicted particulate sulphate in summer at Elandsfontein....164

Figure 4-28: Diurnal characteristics of observed and predicted particulate sulphate in autumn at Elandsfontein....165

Figure 4-29: Diurnal characteristics of observed and predicted particulate sulphate in winter at Elandsfontein....165

Figure 4-30: Comparison of the predicted against the mean observed particulate sulphate in spring at Elandsfontein....167

Figure 4-31: Comparison of the predicted against the mean observed particulate sulphate in summer at Elandsfontein....168

Figure 4-32: Comparison of the predicted against the mean observed particulate sulphate in autumn at Elandsfontein....168

Figure 4-33: Comparison of the predicted against the mean observed particulate sulphate in winter at Elandsfontein....169

Figure 5-1: Comparison of the level of accuracy for the various compounded and density functional methods from calculated enthalpies of reactions178

Figure 5-2a: The effects of ambient temperature on equilibrium constants at atmospheric pressure for the gas-phase sulphur reactions shown in the legend....180

Figure 5-2b: The effects of ambient temperature on equilibrium constants at atmospheric pressure for the gas-phase sulphur reactions shown in the legend....180

Figure 5-2c: The effects of ambient temperature on equilibrium constants at atmospheric pressure for the gas-phase sulphur reactions shown in the legend....181

Figure 5-2d: The effects of ambient temperature on equilibrium constants at atmospheric pressure for the gas-phase sulphur reactions shown in the legend....181

Figure 5-3a: The effects of ambient temperature on equilibrium constants at atmospheric pressure for the aqueous-phase sulphur reactions shown in the legend 182

Figure 5-3b: The effects of ambient temperature on equilibrium constants at atmospheric pressure for the aqueous-phase sulphur reactions shown in the legend 182

Figure 5-3c: The effects of ambient temperature on equilibrium constants at atmospheric pressure for the aqueous-phase sulphur reactions shown in the legend 183

Figure 5-3d: The effects of ambient temperature on equilibrium constants at atmospheric pressure for the aqueous-phase sulphur reactions shown in the legend 183

Figure 5-4a: The degree of importance of the gas-phase atmospheric sulphur reactions shown in the legend from thermochemical analyses arranged from the most relevant (top plot) to the least (bottom plot)..... 184

Figure 5-4b: The degree of importance of the gas-phase atmospheric sulphur reactions shown in the legend from thermochemical analyses arranged from the most relevant (top plot) to the least (bottom plot)..... 184

Figure 5-4c: The degree of importance of the gas-phase atmospheric sulphur reactions shown in the legend from thermochemical analyses arranged from the most relevant (top plot) to the least (bottom plot)..... 185

Figure 5-4d: The degree of importance of the gas-phase atmospheric sulphur reactions shown in the legend from thermochemical analyses arranged from the most relevant (top plot) to the least (bottom plot)..... 185

Figure 5-5a: The degree of importance of the aqueous -phase atmospheric sulphur reactions shown in the legend from thermochemical analyses arranged from the most relevant (top plot) to the least (bottom plot)..... 186

Figure 5-5b: The degree of importance of the aqueous -phase atmospheric sulphur reactions shown in the legend from thermochemical analyses arranged from the most relevant (top plot) to the least (bottom plot).....186

Figure 5-5c: The degree of importance of the aqueous -phase atmospheric sulphur reactions shown in the legend from thermochemical analyses arranged from the most relevant (top plot) to the least (bottom plot).....187

Figure 5-5d: The degree of importance of the aqueous-phase atmospheric sulphur reactions shown in the legend from thermochemical analyses arranged from the most relevant (top plot) to the least (bottom plot).....187

Figure 6-1: A diffusion model pattern for the disappearance of SO_2 to sulphate197

Figure 6-2: Comparison of the mean monthly SO_2 observations to the corresponding monthly predicted model outcomes 217

List of Tables

Table 2-1: Deliquescence relative humidities of electrolyte solutions at 298K . 46

Table 2-2: Humidity constants for saturated water 50

Table 2-3: Components of the complete basis set methods..... 82

Table 2-4: Structural configuration for sulphur oxide..... 83

Table 2-5: Pasquill atmospheric stability classes 99

Table 4-1: Estimation of sulphur dosage in the planetary boundary layer at Elandsfontein 134

Table 4-2: Monthly mean ambient total sulphur, gaseous sulphur and particulate sulphate concentrations at Elandsfontein..... 135

Table 4-3: Rainfall data over Mpumalanga between September 2004 and August 2005..... 145

Table 4-4: Summary data of the central tendency of the sulphur species 158

Table 4-5: Summary output of regression analysis 166

Table 5-1: Gas-phase and aqueous-phase atmospheric sulphur reactions considered in this study..... 174

Table 6-1: Meteorological conditions during sampling period 202

Table 6-2: Monthly rate constant for SO_2 disappearances between the source power station and Elandsfontein..... 203

Table 6-3: Rate constants of SO_2 disappearances with seasonal variations obtained from *model type-1* 205

Table 6-4: Rate constants of SO_2 disappearances with seasonal variations obtained from *model type-1* from observations against least squares fitted values..... 205

Table A-1: Calculated kinetics variables using the least squares method..... 283

Table B-3a: Computed enthalpies of the individual chemical species in Hartrees at 298K.....309

Table B-3b: Computed Gibbs free energies of the individual chemical species in Hartrees at 298K 314

Table B-3c: Calculated and experimental enthalpies of the gas-phase reactions (kJ mol^{-1}) at 298K 319

Table B-3d: Calculated and experimental enthalpies of the aqueous-phase reactions (kJ mol^{-1}) at 298K 322

Table B-3e: Calculated and experimental Gibbs free energies of the gas-phase reactions (kJ mol^{-1}) at 298K.....325

Table B-3f: Calculated and experimental Gibb's free energies of the aqueous-phase reactions (kJ mol^{-1}) at 298K.....328

Abbreviations, Acronyms and Symbols

AGL	Above ground level
AMSL	Above mean sea level
ASL	Above sea level
AQMA	Air quality modelling area
θ	Ambient temperature
ψ	Atmospheric water partial pressure
D	Brownian diffusivity of the gas in ambient air
CCN	Cloud condensation nuclei
CRH	Crystallisation relative humidity
DRH	Deliquescence relative humidity
DFT	Density functional theory
F_d	Deposition rate
k_d^i	Deposition rate constant of component i
v_d	Deposition velocity
$\dot{y}$	Mass fraction
PM_{10}	Particulate matter <10 μm in diameter
PBL	Planetary boundary layer
υ	Velocity

Nomenclature

y_{SO_4} = mass concentration of particulate sulphate (μg m^{-3})

υ = wind speed (m s^{-1})

ψ = water vapour partial pressure (hPa)

θ = ambient air temperature (°C)

RH = relative humidity (%)

q = mass of specie in puff (μg)

$\overline{u}$ = mean wind speed at emission height (m s^{-1})

$\overline{K}_{xx}$ = mean eddy diffusivity in the along-wind direction (m^2 s^{-1})

$\overline{K}_{yy}$ = mean eddy diffusivity in the crosswind direction (m^2 s^{-1})

$\overline{K}_{zz}$ = mean eddy diffusivity in the vertical direction (m^2 s^{-1})

σ_x = the along-wind dispersion coefficient (m)

σ_y = the crosswind dispersion coefficient (m)

σ_z = the vertical dispersion coefficient (m)

x = downwind receptor point from puff centre (m)

y = crosswind receptor point from puff centre (m)

z = vertical receptor height from ground (m)

H = inversion layer height above ground (m)

g = acceleration due to gravity (m s^{-2})

v_d = deposition velocity that measures the degree of absorption of the Earth's surface (cm s^{-1})

Chapter 1: General Introduction

1.1 Introduction

Air is an indispensable requirement for human existence. It is housed in the atmosphere with more than 60 % of its total mass present in the lower atmosphere (troposphere). The distortion of the chemical composition of the natural atmosphere, affects the air we breathe as well as the ecosystem of the environment –hence the need for continuous monitoring and assessment of air quality with time cannot be overemphasised. Air quality assessments for air pollution over any area, region or country would be incomplete without an evaluation of the levels of the common varieties of atmospheric sulphur species.

1.2 Background of Study

Over the years anthropogenic emissions released from industrial complexes such as power plants, open-cast coal mines, fuel refining processes and domestic coal-fired heaters have significantly altered the budget –the inflow and outflow– of atmospheric sulphur over the Mpumalanga Highveld subregion of South Africa. Over an extended period, released air pollutant gases are transformed into particle aerosols during air mass transport from their various sources. Several studies of the oxidation of sulphur species from surface and stack emissions in open-cast coal mines and coal-fired power plants during plume transport have been made at varying atmospheric conditions (Dittenhoefer and de Pena, 1978; Rodhe, 1978; Fugas and Gentilizza, 1978) which result in the formation of aitken particles and particulate sulphate.

Since the 1980s, the South African government has become conscious of the state of the country's atmospheric environment, culminating in the promulgation of an Air Quality Act (RSA, 2005) for local, provincial and national sectors. This act provides for the establishment of emissions standards for industries and factories of different types as is the common practice in other developed countries such as the United States of America and

the United Kingdom. As a part of the contribution to the solution of the air quality assessment, additional programmes are required by the present legislation for studies involving air pollution investigations with a view to providing end-of-pipe solutions for abatement, especially for industries which are major contributors to the problem. This study tries to answer a number of questions relating to a pollutant-type (sulphur) with special reference to assessment of the overall levels in the planetary boundary layer over Elandsfontein on the Mpumalanga Highveld subregion. The assessment entails an evaluation of the major forms of sulphur observed [namely: hydrogen sulphide (H_2S), sulphur dioxide (SO_2) and sulphate (SO_4^{2-})]; the major sources at Elandsfontein; the removal mechanisms and rates, as well as the development of a predictive mechanism for ascertaining the possible products of transformation of the emitted primary pollutants (sulphur gases) over a wide range of tropospheric temperatures. The last part of this study involves the modelling of chemical transformation rate with variation in meteorological parameters during plume advection.

1.3 Research Goals

The study aims to determine parametric relationships between the primary and secondary atmospheric sulphur species principally observed over the Mpumalanga Highveld subregion in South Africa.

The study also aims to investigate the effect of atmospheric chemistry and meteorology on the concentration variations on a temporal scale and during the advection process over the region.

1.4 Research Questions

An important question that relates to atmospheric pollution from the industrialised Mpumalanga Highveld subregion of South Africa is how to determine the net total sulphur over the region. It is well-known that sulphur is released into the atmosphere over the Mpumalanga Highveld from anthropogenic sources as sulphur dioxide and biogenic emissions as hydrogen sulphide. Also, during air mass transportation, windborne gaseous

sulphur undergoes chemical transformation and deposition from the source area downwind. Furthermore, hydrogen sulphide and sulphur dioxide in the atmosphere are known to oxidise to sulphuric acid (H_2SO_4) aerosols and subsequently to particulate sulphate. Therefore, in order to achieve the aforementioned goals, a number of questions need to be answered. These questions are:

(a) Quantify the sulphur compounds relevant to the Mpumalanga Highveld for a year and determine the major source contributors.

(b) Evaluate the temporal (diurnal and seasonal) variation in the concentrations of these sulphur species, taking into consideration the contribution of meteorological effects.

(c) Evaluate the important atmospheric sulphur reactions expected over the Mpumalanga Highveld and predict the most likely secondary sulphur pollutants as a function of ambient temperature.

(d) Develop a kinetic model for the oxidation of atmospheric sulphur dioxide (the most common and long-lived sulphur compound) during advection with diffusion occurring. Produce rate dependant parameters for the observed ambient temperatures.

1.5 Overall Research Objectives

The overall research objectives are to:

(a) Measure –on a continuous basis for twelve months– the ambient concentrations of hydrogen sulphide, sulphur dioxide and particulate sulphate with time at Elandsfontein, while simultaneously observing the prevailing meteorological parameters, so as to determine the major source area. This is because the Elandsfontein area is on a high ground with few surrounding rolling hills and no windbreaks that allow for well-mixed plumes to make contact with the surface during convective daytime.

(b) Determine the *in situ* temporal behaviours of H_2S, SO_2 and, for the first time, particulate sulphate concentrations over Elandsfontein. Characterise the behaviour of these atmospheric sulphur species with meteorological variations for day- and night-times. Determine relationships between the various sulphur species on a diurnal and seasonal scale with variations in meteorological parameters.

(c) Establish the effects of different seasons in the year on the *removal mode* through analyses of the meteorology. Examine any contributions of air recirculation over southern Africa to sulphate loading at Elandsfontein. Provide temporal concentration dosage for atmospheric sulphur (comprised of H_2S, SO_2 and particulate sulphate) traversing the Mpumalanga Highveld for one year. Develop mathematical relationships using a multivariate approach to predict the presence of particulate sulphate in the planetary boundary layer as a function of the prevailing meteorological parameters.

(d) Apply computational molecular modelling to the gaseous sulphur species to establish the most likely reaction pathways followed during atmospheric sulphur transformations. And categorise the predicted reactions in order of increasing significance of favourability at temperatures of between –100 °C and +100 °C.

(e) Develop a kinetic model that establishes the oxidation of SO_2 with deposition as the removal mechanism during advection.

(f) Compare the developed rate model with those from previous studies –in the Literature– by estimating the ground-level sulphur concentrations at the sampling station using a Lagrangian puff diffusion model. Thereafter, deduce the model with the best correlation coefficient of reaction rate.

1.6 Scope of the Research

The research is restricted to the planetary boundary layer (PBL) since sulphate aerosols reside predominantly within this layer of the lower troposphere. As a result, the contributions of surface meteorological conditions to turbulent diffusion during advection are described by the variations in the planetary boundary layer parameters. Also included is the determination of the relative importance of several known atmospheric sulphur reactions for the most favourably occurring tropospheric transformations of hydrogen sulphide and sulphur dioxide over the Mpumalanga Highveld which will be developed using thermochemical analysis. Additionally included is the development of a chemical reaction rate model with regard to the disappearance of sulphur dioxide during advection with dispersion.

1.7 Contributions to Knowledge

This study will provide good information on the total sulphur species relevant to the South African Highveld and, in particular, on the particulate sulphate levels on a short averaging time-scale over the region. In addition, it will provide an estimate of the particulate matter loading at Elandsfontein and over the Mpumalanga Highveld which could be applicable to studies of the impact of air pollution on health over the area.

This study will provide –for the first time– an *in situ* relationship between hydrogen sulphide, sulphur dioxide and particulate sulphate in the atmosphere using high response time sampling of the sulphur species in the planetary boundary layer of the Mpumalanga Highveld.

Thermochemical property data for 92 species, of which fewer than 10 % are available in literature (handbooks) are generated.

Chapter 2: Literature Survey

2.1 Introduction

Sulphur is commonly observed in the atmosphere over Elandsfontein primarily as hydrogen sulphide (H_2S), sulphur dioxide (SO_2) and sulphate (SO_4^{2-}) (Held *et al*, 1993; 1994; Scheifinger and Held, 1997). It is the intention of the South African government's programme on air pollution, to gain an understanding of the nature, composition and removal pattern of these sulphur compounds. Gaseous sulphur compounds undergo chemical transformation with advective diffusion in the atmosphere, yielding an end-product known as particulate sulphate. In the Mpumalanga Highveld subregion of South Africa, the emission of gaseous sulphur compounds from anthropogenic sources, comprised overwhelmingly of emissions from industrial sources with special reference to coal-fired power plants, open-cast coal mines, fuel oil refining and petrochemical plants as major contributors occurs significantly. Another significant contributor of atmospheric sulphur is indoor domestic coal-fired heaters.

2.2 Air Pollution

Usually, the most important sources of anthropogenic air pollution, particularly on a national or continental scale, are combustion processes, at least with regard to SO_2 and other trace gas emissions (Fernandez-Martinez *et al*, 2001). The combustion of coal, in addition to SO_2 formation, leads to the emission of small but significant amounts of volatile organic compounds (VOCs) and toxic organic micropollutants, such as aromatic hydrocarbons, into the environment. These compounds are the products of incomplete combustion of coal and when released into the atmosphere, pose a potential risk to both human and animal health and the environment (Chagger *et al*, 1999). VOCs have been observed in particulate matter from power stations during coal-burning activities (Santos *et al*, 2004). They are inherent air pollutants because of their contributions to the initiation of the formation of atmospheric oxidants which are required in the propagation of the

transformations of the several sulphur compounds (Pienaar and Helas, 1996). Evaporation losses from the use of fossil fuels for combustion in engines, as well as solvents, constitute the major sources of VOCs and hence emissions, while coal-fired electric power plants contribute a significant amount of the approximate 37 % of all anthropogenic VOCs (Bocola and Cirillo, 1989). Emissions of H_2S and SO_2 from fossil fuel processing and burning in power plants and refining processes can have serious environmental effects via chemical transformations to sulphate which is deposited either as acids or as salty particles (McGonigle *et al*, 2004). Also, particulate matter and VOCs are well-known to be associated with emissions from electric power plants (Santos *et al*, 2004).

Anthropogenic gaseous sulphur emissions are chemically converted to sulphurous and sulphuric acids in the atmosphere in the gaseous (primarily via reaction with OH^-) and aqueous phases. When these acids are precipitated, damage is caused to the ecosystems, particularly where soils are lacking sufficient alkalinity to buffer these acids (Hewitt, 2000; Wright and Schindler, 1995). Aerosol particles resulting from the acids can cause human respiratory morbidity and mortality. In the industrialised countries of the world, especially in the United Kingdom, emissions of SO_2 from fossil fuel-burning power plants account for approximately 70 % of the total anthropogenic sulphur species released into the atmosphere and about 55 % of the SO_2 emissions result from the automobiles. This has since been reduced gradually as a result of the burning of low-sulphur coal coupled with the desulphurisation of flue gas (McGonigle *et al*, 2004).

2.3 Air Pollution from Coal Combustion

Coal is the world's most abundant and widely distributed solid-state fossil fuel. It is presently the primary energy source for several countries in the world. It is used primarily as the fuel for boiler heaters in electric power generation plants and steel smelting process plants. Coal is classified according to its rank which is a measure of the amount of alteration that the coal has undergone (that is, the amount of heat and pressure that the coal underwent during formation). The increase in rank describes an increase in temperature and pressure which results in the coal having a lower volatile content and, therefore, an increased carbon content. Coal is also classified according to its sulphur, phosphorous,

volatiles and ash content, whose proportions generally vary according to its rank. Consecutive stages in the evolution of rank, from an initial peat stage, are brown coal (or lignite), sub-bituminous coal, bituminous coal and anthracite.

Coking coal is used in the steel production industry because it is required to have specific qualities such as low sulphur and phosphorous content. Approximately 630 kg of coal are used for every ton of steel produced. Electricity generation uses thermal coal, which is ground to a fine powder prior to combustion. In addition to southern Africa, some of the world's major coal producing countries include China, Australia and India (Edna, 1957).

In South Africa the major source of energy is coal. The Highveld region houses almost all the coal deposits of the country, thereby providing a suitable location for the establishment of coal-based industries (Figure 2-1). Over 90 % of the coal-fired power plants and a variety of other large process industries, such as metal smelting and petrochemical plants, make use of coal for heat generation. Coal is also consumed by activities such as spontaneous combustion processes in open-cast coal mines (Timko and Derrick, 1989). These processes, in addition to gas vents, fugitive emissions and leaks of waste gases in process plants, contribute to the air pollution load in the atmosphere. These forms of emissions of air pollutants make the troposphere over the Mpumalanga Highveld a fairly consistent composition in terms of the different species of gaseous and aerosol sulphur-containing compounds. The Highveld region is located towards the northern part of South Africa and is a region of grassland, similar to an arid region with several irregular terrains. It provides a suitable environment for effective convective mixing and advection of pollution species from source areas close to the Earth's surface.

A very large part of Witbank, KaNgwane and the former Eastern Transvaal coalfields are included in the Mpumalanga Province which is the most important coal-producing area in South Africa. This area has a number of significant coal seams possessing diverse characteristics to suit a variety of potential markets. These markets include the power generation, export, domestic, metallurgical, liquefaction and chemical processing sectors. The Witbank coalfield contains a large and important resource of high-yield export quality

steam coal. The other coalfields on the Mpumalanga Highveld contain low-grade bituminous coal which is better suited to syn-gas fuel and electric power production. About eight farms in the Ermelo district are underlain by substantial resources of peat coal, which could have potential value for the horticultural industry (Edna, 1957; Barker and Associates, 1985; Gayer and Harris, 1996).

Coal combustion emits SO_2, NO_x, CO, VOCs and particulate matter and, during air mass transport, SO_2 transforms to sulphate (SO_4^{2-}) (Latimer and Samuelsen, 1978; Gillani and Wilson, 1983). Coal-fired power plants generate most of the electrical power in South Africa and a significant fraction of this electrical power is supplied to its neighbouring countries. These power stations face the continuous challenge to provide an essential service for South Africa's rapidly increasing population. The ability to meet the demand of the ever-increasing population poses a challenge to energy providers to produce cleaner power that is still affordable. In performing this function, environmental impact assessments as well as routine observations are essential on the air quality and the aesthetic qualities of the existing environment (Santos *et al*, 2004; Mc Gonigle *et al*, 2004). The environmental impact of emissions from power plants is the contributions of SO_2, NO, NO_2, CO, CO_2, O_3 and particulate matter relative to their adverse ecological and health effects over the life time of the process. The increase in energy demand, especially in winter, results in a significant rise in SO_4^{2-} and PM_{10} emissions (Snyman *et al*, 1990).

Although coal is relatively plentiful in South Africa, concern about the emissions from coal-fired power generation plants is overwhelming. This is due to the environmental health-related problems emanating from the release of gaseous emissions into the atmosphere (Priest *et al*, 1981). This has resulted in the establishment of some stringent environmental standards regulating the emission levels for PM_{10}, SO_2, NO_2, CO, O_3, dust fall and benzene in South Africa (CTMR, 1988: RSA, 2005). In this regard, the chemical constituents of smoke plumes from coal-fired power stations and polluted air from coal mines (Terblanche *et al*, 1993) are of interest to this study, with particular reference to the Mpumalanga Highveld subregion –the region where coal is the common fossil fuel used both for small- and large-scale industrial processes.

2.4 Targeting of Air Pollutants Source Areas

Air pollutants are known to travel from more- or less-distant industrial or urban zones towards rural zones in industrialised countries (Priest *et al*, 1981). On a local scale, the wind direction may influence the air quality at a particular monitoring site. The air transport regimes are useful in determining the pathways travelled by pollutants from their sources thereby providing a measure for source-sink targeting (Timko and Derrick, 1989; Davison and Hewitt, 1997).

In the past, studies have utilised elemental residue analysis of ambient air as means of attributing sources associated with SO_2 emissions. This is because the interventions of natural SO_2 sources (such as plants and anaerobic biotic processes in soils contaminated by decades of fumes and smoke deposits) affect the source apportioning (Emberlin, 1980a; 1980b; Prahm *et al*, 1980). The elemental analysis approach is inappropriate for the Mpumalanga Highveld due the variety of process industries within the region.

In order to establish the various SO_2 sources over Elandsfontein, a simple representation of air pollutant distribution resulting from wind action known as a 'pollution rose' is used. This approach has been used in previous studies to apportion emissions of trace gases from open-cast coal mines over the Witbank area of the Mpumalanga Highveld (Igbafe *et al*, 2006). Two other source identification techniques (receptor modelling and back trajectory) are described below.

2.4.1 Receptor Modelling

Receptor modelling is used to determine the origin of air-borne particles, the basic idea being the resolution of observed concentration patterns of particles at sampling sites, "receptors", into contributions from several sources (Gordon, 1980). Receptor modelling has been performed in a number of instances. These include: the allocation of light scattering associated with regional haze (composed of secondary particles from photochemical smog and a smaller fraction from forest fires) from gas and particle compositions using air-mass trajectories (Macias *et al*, 1981). Shaw and Paur (1983) assessed the impact of coal-fired power plants upon their immediate air quality through

particle collection and analyses. Similarly to Shaw and Paur's (1983) methodology, fine particles of less than 2.5 μm diameter have been analysed for identification of particulate species, such as sulphate and elemental composition for trace metals and non-metals (Shaw *et al*, 1982). Steven *et al* (1984) performed similar measurements in addition to anionic and cationic chemical analyses of emissions attributed to coal-fired power plants. Rahn and Lowenthal (1984) devised a tracer technique to identify and characterise particles from large regions of up to 1000 km^2.

Despite the advances, receptor modelling simulations do not account for the modification of particle composition when the transporting air mass encounters areas with industries such as power generation complexes within the region. It is known that particles with a diameter greater than 5 μm travel short distances before settling, and if only particles less than 2.5 μm are considered, the composition would be retained over several hundreds of kilometres. This was resolved through receptor modelling, a tool that accounts for distant source particles linked to acid and/or sulphate, which cause visibility degradation in addition to acid deposition (Tuncel *et al*, 1985). Trace elemental analyses of fine fractions of atmospheric particulate samples collected, coupled with back-trajectories of air masses, were applied in receptor models to assess regional sulphate within a valley (Tuncel *et al*, 1985). The same researchers ascertained that if the component originates from coal combustion, there is modification of the elemental composition pattern during transport from distant power plants to the receptors, even in the less than 2.5 μm fraction.

2.4.2 Back Trajectories

To quantify the source/receptor relationship, back trajectories (Stohl, 1998) are popular for identifying possible sources of pollutants measured qualitatively at a receptor location because their computational demands are smaller than for the Eulerian models (Jacobson, 1997a, 1997b; Lurmann *et al*, 1997; ENVIRON, 1998; Nenes *et al*, 1999; Villasenor *et al*, 2001). Conventionally, to quantitatively determine the source-receptor relationship for trajectory models, a trajectory model is coupled with physical-chemical models –known as Lagrangian models– which include aerosol chemistry, gas-to-particle conversion and a diffusion mechanism (Pandis *et al*, 1992; Seigneur *et al*, 1997; Gabruk *et al*, 1999;

Karamchandani *et al*, 2000; Scire *et al*, 2000a; 2000b). Thereafter, sensitivity analysis is performed to determine the source-receptor relationship in the model by varying emission rates of one source at a time. This model is run repeatedly to quantify the change in the simulated concentration at the receptor with new emission profiles. In comparison with the statistical analysis methods that can further increase the probability of identifying possible sources (Cheng *et al*, 1993a; 1993b) with good angular resolution and poor radial solution of the convergence of all trajectories (Vasconcelos *et al*, 1996), Tsuang (2003) quantifies the formation of secondary sulphate aerosols from the oxidation of gaseous SO_2 emissions using a Gaussian trajectory transfer-coefficient model as well as by performing a sensitivity analysis to simulate a source-receptor relationship and to obtain the relative importance of the source quantification.

2.5 The Mpumalanga Highveld

The industrial heart of South Africa is the rich coal fields and mineral resource area of the Highveld. The resource materials present on the Highveld are concentrated in the Mpumalanga subregion. Air pollution over the Mpumalanga Highveld is the result of continuous emissions from coal-fired power plants, and chromium, manganese and vanadium smelting plants. In addition, flue gases and fugitive hydrocarbon compounds from fuel-processing plants also contribute to the air pollution.

The Mpumalanga Highveld subregion lies on a plateau some 1600 m above mean sea level (AMSL) on the GPS location shown in Figure (2-1). The regional scale topography slopes gradually downward towards the west and south. To the east lies the escarpment of the Drakensberg and to the south is the Vaal basin about 1400 m AMSL, which tends to drain cold air from the surrounding high-lying plateau of the Gauteng Province (Held *et al*, 1996).

The major pollution sources found within this area include nine coal-fired power stations of which seven are government-owned, while two are privately owned by syn-gas hydrocarbon fuel-processing plants. The total installation capacity of the government-owned power plants is 45.5 GW. The hydrocarbon fuel process plants together with the

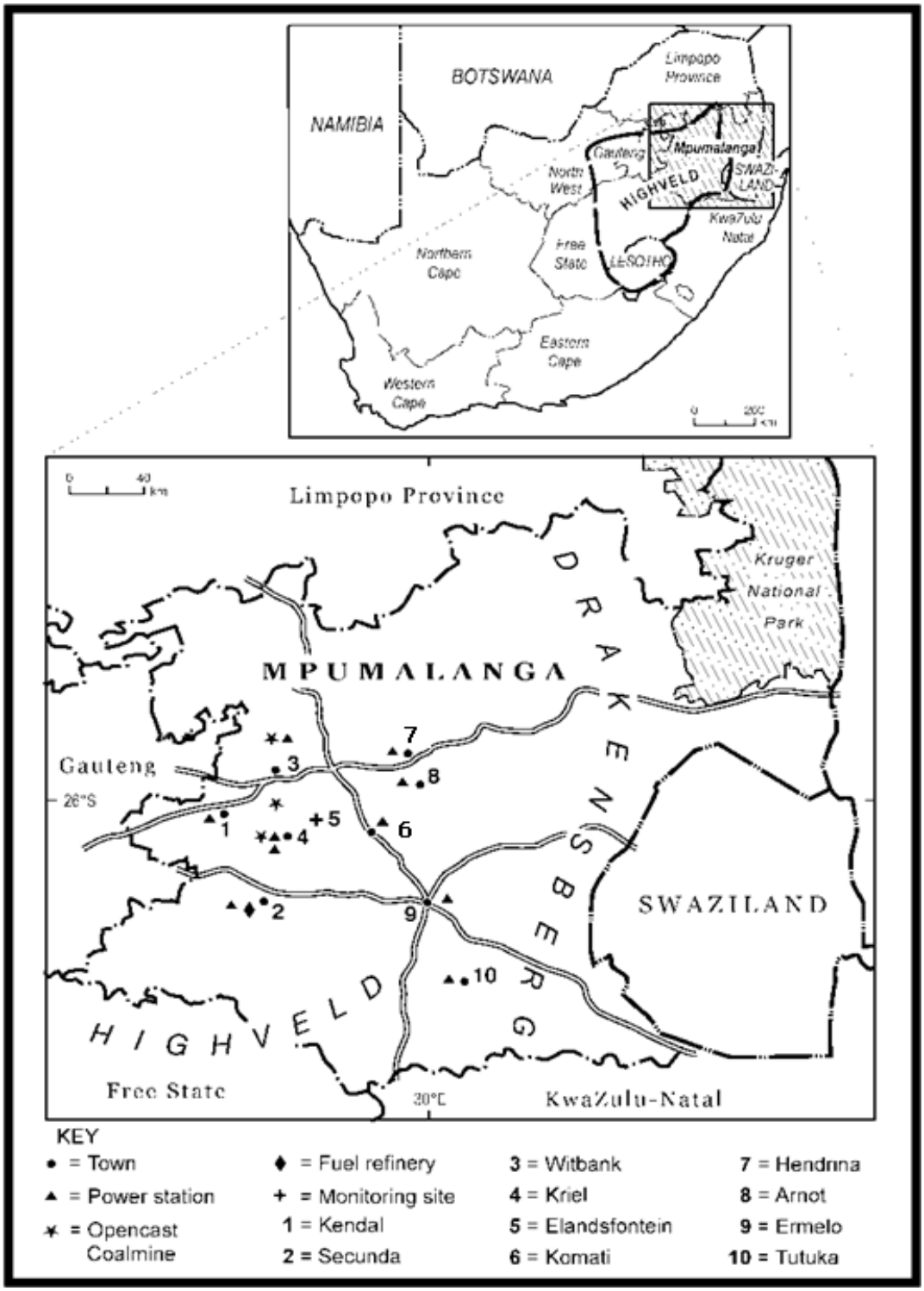

(Legend: (a) The Highveld region (thick broken lines); (b) The Mpumalanga Highveld subregion (enlarged section)

Figure 2-1: Map of South Africa showing the study area

open-cast coal mines adjacent to the power plants are added sources of several sulphur-based pollutant compounds within the area. These various source types liberate huge amounts of hydrogen sulphide and sulphur dioxide gases per year (Snyman *et al*, 1990), especially during winter as the demand for electric power increases leading to an increased demand for coal burnt.

In order to combat the poor dispersion potential and the adverse climatological conditions of windborne pollutants, tall-stack policies (Lucas, 1975) were implemented on the types of stacks used in government-owned power plants to reduce ground-level emission concentrations near the source points.

However, this policy only produced elevated layers containing more secondary pollutants forming an accumulation zone of pollutants in the vicinity of the inversion layer (Lucas, 1975). The sulphur content of the coal burnt is relatively low but there are no end-of-pipe abatement technological practices in place for the recovery of sulphur in the flue gas. This could partly contribute to increase in the atmospheric sulphur near the ground over the area subject to surface absorption (Scriven and Fisher, 1975), deposition and transformation with advection (Forrest and Newman, 1977; Newman, 1981; Lee and Kingdon, 2001).

2.6 Climatology and Meteorology of the Mpumalanga Highveld

The prediction of what will happen to pollution when it is released into the atmosphere relies on the knowledge of the complex and individual nature of local climates and weather. From day to day, and at different times of the day, pollution concentration levels fluctuate in response to the changing state of atmospheric stability, to concomitant variations in mixing depth and to the effect of mesoscale and microscale wind systems upon transport and dispersion of air pollution (Preston-Whyte and Tyson, 1993). The introduction of sulphur compounds into the atmosphere has been observed to contribute in a number of ways to the magnitude of the greenhouse gas concentrations and aerosols loading (Twomey, 1991; Ross, 2003).

The Mpumalanga Highveld subregion is dominated by dry conditions with scanty annual rainfall, north-westerly winds in summer and westerly winds in winter. Air mass transport is predominantly by anticyclonic circulations over southern Africa (Tyson *et al*, 1976). The macroscale climatology and meteorology of the Highveld provide the means by which atmospheric transport prevails over southern Africa. South Africa is situated in the sub-tropical high pressure belt which causes the general circulation over the subcontinent to be anticyclonic above 700 hPa for most of the time. During the summer months at the 850 hPa level cyclonic circulations occur when troughs develop over the central Highveld plateau of the country. This region is influenced to a great extent by the sub-tropical anticyclonic belt of the general circulation (Tyson and Preston-Whyte, 2000). This effect is more pronounced during winter than in summer, resulting in low-level atmospheric stability and rainfall between the two seasonal extremes.

However, circulation over the eastern parts of the Highveld remains under an anticyclonic influence for most of the time (Figure 2-2). The frequency of anticyclonic circulations and associated atmospheric subsidence reaches a maximum in winter from July to September (Held *et al*, 1996). This subsidence is conducive for the formation of elevated temperature inversions with base heights varying from 2000 to 3000 m AGL during summer and 1700 m AGL during winter (Held *et al*, 1996).

During winter, temperature inversions occur almost nightly at the surface and, with high frequency, elevated inversions occur. However, even during summer, nocturnal surface inversions are as frequent as 70 %, although they are not as strong as in winter (Pretorius *et al*, 1986). The moist, unstable conditions and rainfall are almost exclusively confined to the summer period when the anticyclonic belt is located further south. These conditions –in addition to increased ambient temperature and solar radiation– are favourable for the formation of secondary pollutants. Hence, there are several occasional episodes with notably high aerosol concentrations of sulphates in summer. The dry, highly stable winter period is obviously of great importance in connection with the accumulation of atmospheric pollutants.

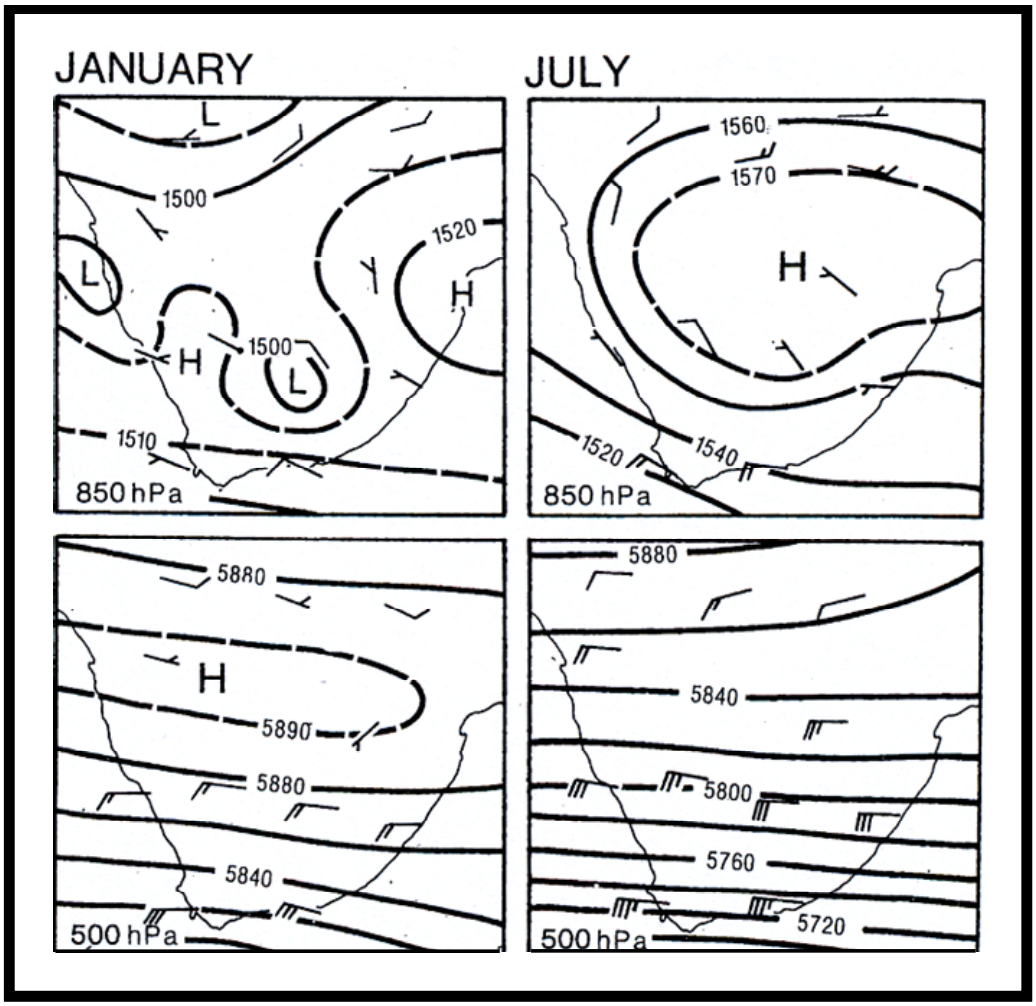

(Source: Held *et al*, 1996)

Figure 2-2: Mean monthly winds and contours (gpm) of the 850 and 500 hPa pressure surfaces in January and July

Winds over the Highveld are dependant almost exclusively on the strength and position of the anticyclone over the southern Indian Ocean all year round. But occasionally, during the winter, the passage of frontal disturbances results in unstable flows from the southwesterly sector as opposed to the commonly occurring easterly and northerly sector winds (Snyman *et al*, 1990).

The diffusion of atmospheric pollutants into a greater volume of the atmosphere reduces the concentration of the materials. This occurs most effectively under conditions of free convection when the mixing layer is deep. Unstable conditions of this type occur most frequently in summer during the day. Conversely, diffusion is inhibited by stable conditions in the boundary layer. Most surface pollution is trapped in surface inversions. On occasions and at certain times of the day, however, the surface inversion may not be present and pollution will disperse, only to be prevented from diffusing freely upward by the presence of an elevated inversion (Preston-Whyte and Tyson, 1993).

2.6.1 Surface and Elevated Inversions over the Mpumalanga Highveld

When the Earth's surface cools at night and heat is lost through radiation, surface inversions will occur. The more stable the atmosphere, the more likely stronger inversions will develop. Surface inversions have been observed on a frequency of between 80 and 90 % during winter over the Highveld (Held *et al*, 1996). Mean early morning winter surface inversions over the Highveld region vary from 3 to 11 °C, with extreme cases reaching up to 15 °C in strength and in depth from 100 to 400 m AGL. Over the Mpumalanga Highveld subregion, inversions of greater than 10 °C commonly occur during 25 to 30 % of all winter nights for approximately 16 hours (Held *et al*, 1996).

Radiative surface inversions are particularly important in air pollution meteorology because of their nightly occurrence under clear, calm and dry conditions. They start developing shortly before sunset and terminate by 21:00 and may be several hundreds of metres deep (Preston-Whyte and Tyson, 1993). Stable anticyclonic conditions over the Highveld are ideal for the formation of surface-based inversions. Large scale averages of winter surface inversions vary in strength from 5 °C to 7 °C and in depth from less than 300 to 500 m AGL over the Highveld plateau {Figures (2-3a) and (2-3b)}. In summer, surface inversion depths are similar to those in winter, but with strength less than or equal to 2 °C (Held *et al*, 1996).

Elevated inversions are caused by subsidence or by frontal movement of air masses. They have been found to occur throughout the year with frequencies of about 60 % at heights of

between 1300 m in winter and 2600 m in summer (Held *et al*, 1996). On a mesoscale, the first elevated inversion above the surface inversion over the Mpumalanga Highveld was observed for about 36 % of all days with soundings producing heights between 250 and 400 m AGL and strengths of up to 5.4 °C (Held *et al*, 1996).

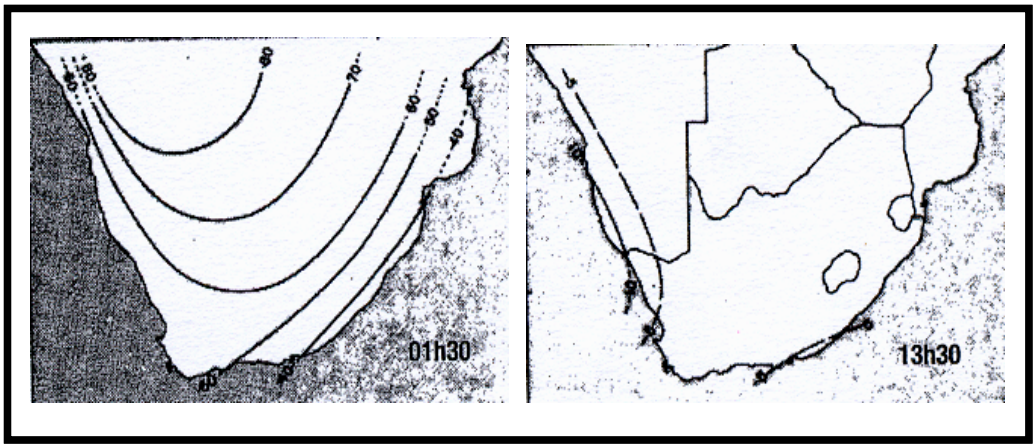

(Source: Held *et al*, 1996)
Figure 2-3a: Annual surface inversion frequency (percentage) at 01:30 and 13:30

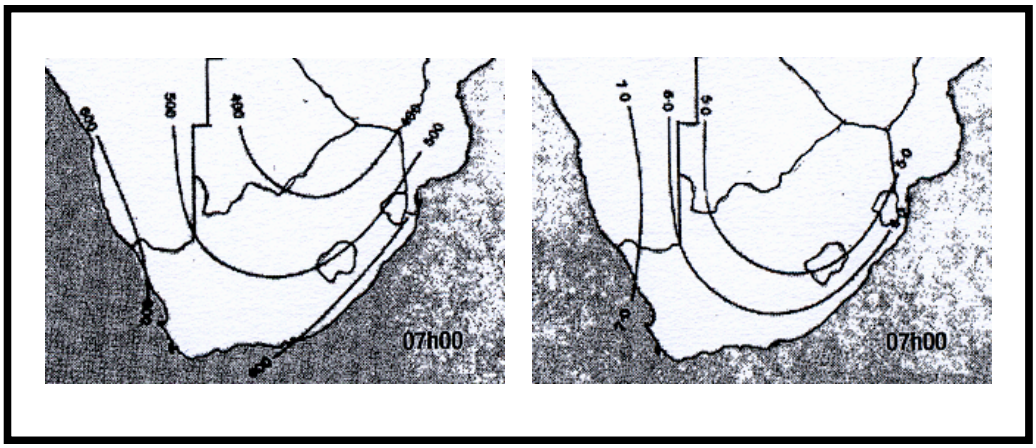

(Source: Held *et al*, 1996)
Figure 2-3b: Generalised winter early morning inversion depth (m) and strength (°C) over southern Africa

Elevated inversions suppress the diffusion and vertical dispersion of pollutants by reducing the height to which such pollutants are able to mix, and consequently result in a

concentration of pollutants below their bases (Scorgie, 1999). Such inversions contribute to long-range transport and re-circulation of pollution (Diab, 1975; Harrison, 1993; Garstang *et al*, 1996). Elevated inversions occur commonly in high pressure areas (Preston-Whyte and Tyson, 1993). The basal height of the lowest absolutely stable layer is 733 hPa which is approximately 2700 m ASL (D'Abreton *et al*, 1998). In summer the mean mixing heights are higher over the interior plateau than in winter. Average summer values for the Mpumalanga Highveld range from 200 to 300 m whereas average winter values are in the region of 150 to 200 m due to the position of the continental high over the interior in winter and the high frequency of calm air, which does not allow for the mechanical generation of turbulence. The average daily maximum mixing heights over the Highveld are in the region of 1000 to 1500 m AGL in summer and winter (Figure 2-4).

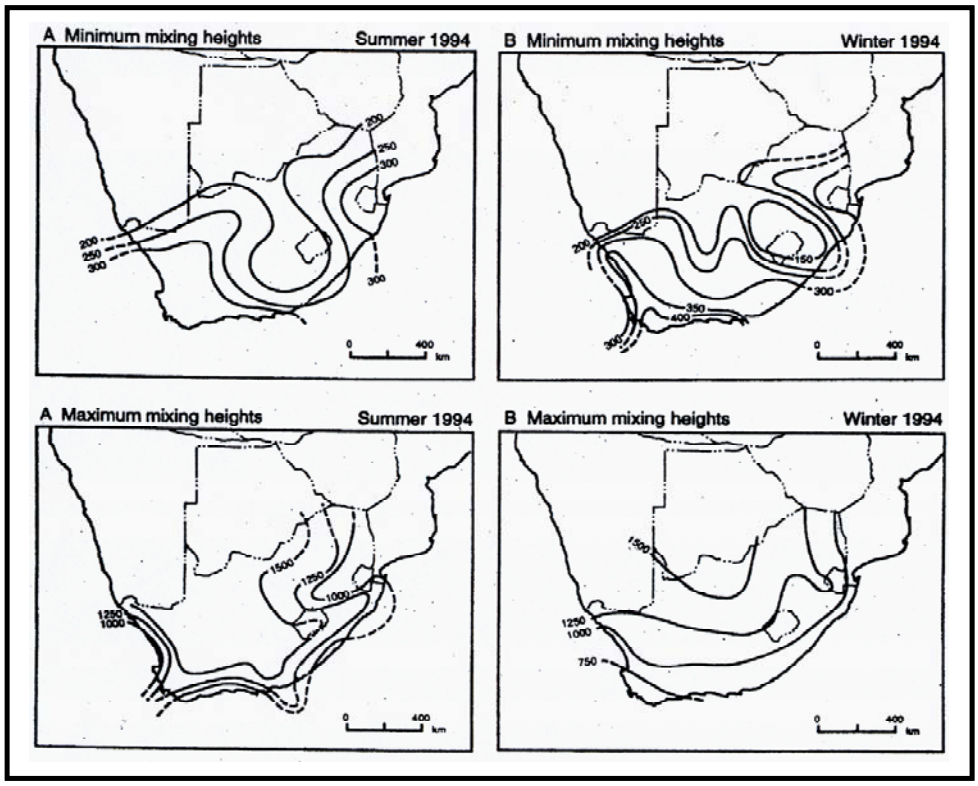

(Source: D'Abreton *et al*, 1998)

Figure 2-4: Mean minimum and mean maximum mixing heights in summer and winter over South Africa

Seasonal variation in mixing layer depth is not as marked on the coast as over the interior. In winter, the mixing layer height reduces significantly with reduction in the surface inversion (Annegarn *et al*, 1996), resulting in higher concentrations of surface pollutants.

2.6.2 Transport Mechanisms over the Mpumalanga Region

The driving force of atmospheric constituents is the wind. In the planetary boundary layer, winds may be grouped in two broad classes, namely, surface winds and boundary layer winds.

Surface Winds

Over the Mpumalanga Highveld, mean daytime surface winds over much of the region show a predominance of north to north-westerly winds, with easterly winds being the next most frequent. However, during winter the frequency of south-westerly winds increases as a result of increased cyclonic occurrences associated with westerly weather disturbances. During the night a greater incidence of north-easterly winds occurs than north-westerly winds. However, substantial increases of light, topographically induced winds occurring from the east and southerly sectors during the night. Annual surface wind speeds vary between 2 and 4 m s^{-1} with a maximum occurring during late winter and spring between August and October (Held *et al*, 1996).

When temperature inversion occurs after sunset, it causes a reduction in frictional drag and the formation of nocturnal low level jet. The low-level jet is a fast moving ribbon of air in the low levels of the atmosphere. It can rapidly transport air at high speeds. Nocturnal jet is strongest in early morning hours and decreases during the day due to a reverse in the temperature gradient (Jury and Tosen, 1989). Low-level jets over various regions of southern Africa have also been observed as a result of a thermal gradient established over gently sloping terrain that extend beyond the nocturnal temperature inversions. Winds

reaching 10 ms^{-1} in the jet core at altitude of about 200 m AGL (Zunckel *et al*, 1996) have been observed hence the contributions from low-level jets in regional-scale wind systems may be partly responsible to the transport of pollutants during night time.

Boundary Layer Winds

Winter on the Highveld is dominated by the presence of anticyclonic circulation, mostly sustained by the expansion of the south Indian Ocean anticyclone over the relatively colder interior of Mpumalanga.

The "winter mode" 800 hPa wind circulation (about 350 m AGL) indicates that boundary layer winds are dominated by the Indian Ocean anticyclone which extends inland to the Northern Province (Tosen and Jury, 1986). As a result of northerly movement of the anticyclonic pressure belts in winter, the Mpumalanga Highveld is dominated by westerly and west-north-westerly winds. However, in summer due to the southward migration of these pressure belts, the circulation is distinguished by the presence of northerly-component winds (Figure 2-5). These winds change direction progressively towards the north-north-west in late summer and thereafter reverse at the onset of autumn to westerly (Held *et al*, 1996).

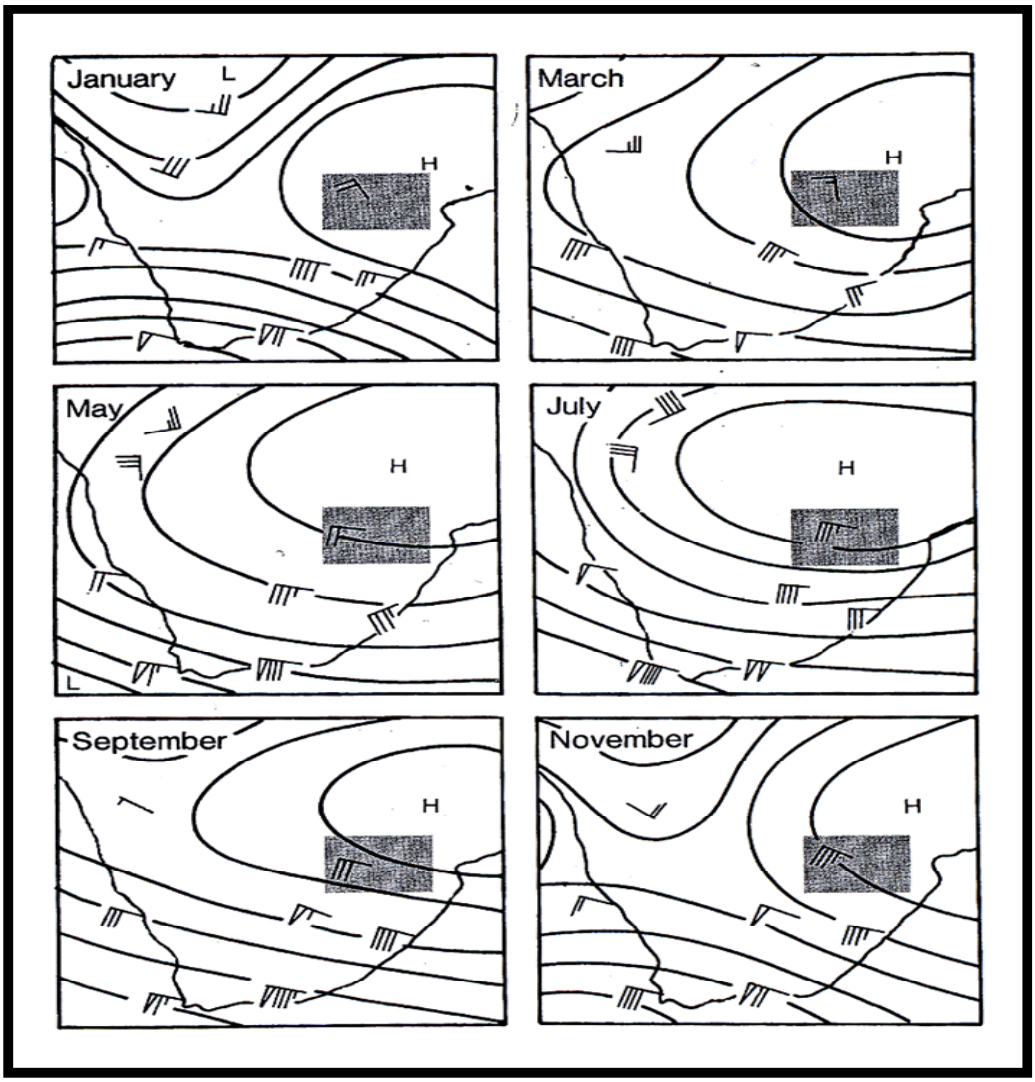

(Source: Held *et al*, 1996)
(Legend: The 800 hPa surface occurs at around 1950 m, that is, the shaded region)
Figure 2-5: Seasonal variation of the mean 800 hPa winds and contours

2.7 Atmospheric Sulphur: An Overview

Numerous sulphur compounds are associated with urban areas and oceans. It is known that sea bubble spray is associated with about 2.65 mg of sulphate per gram of water (Kellogg *et al*, 1972) generated from the oxidation of hydrogen sulphide (Cox and Sandalls, 1974), dimethyl sulphide (Lovelock *et al*, 1972) and sulphur dioxide (Cuong *et al*, 1974). In the

Antarctic and sub-Antarctic regions, where the effects of anthropogenic sulphur are negligible, the budget of sulphur dioxide and sulphate –which could be approximated as the background– range from 0.04 to 0.09 μg m^{-3} for sulphur dioxide and 0.5 to 1.0 μg m^{-3} for sulphate aerosol (Cuong *et al*, 1974; 1975; Duce and Hoffman, 1976). It has been observed that there is a rapid disappearance of sulphur dioxide in the oceans by oxidation and direct absorption by sea water, thus making the ocean –which was regarded as a source of sulphate– also a sink for sulphur dioxide. Gaseous and particulate pollutants released into the atmosphere build up in the micro-environment as microparticles called aerosols (Gillani *et al*, 1983; Terblanche *et al*, 1993). At Elandsfontein the sulphur species of importance are hydrogen sulphide, sulphur dioxide and sulphate (Held *et al*, 1993; 1994; Scheifinger and Held, 1997; Becker, 2004).

2.7.1 Atmospheric Sulphur from Natural and Man-Made Sources

Sulphur is a relatively abundant element that plays an essential role in the environmental cycle. It is found mainly as sulphide and sulphate ores, whilst in the oceans it is present as dissolved sulphate. In the atmosphere, the principal sulphur compounds are hydrogen sulphide (probably together with other reduced sulphur species), sulphur dioxide and sulphate aerosols and mists (Figure 2-6). These compounds follow a cycle whereby sulphur is continuously transported between different phases (Cullis and Hirschler, 1980).

The main natural source of atmospheric sulphur is biogenic activity. About 90 % of the total sulphur emitted by man's activities is the result of coal and petroleum combustion processes as well as the smelting of copper ore (Cullis and Hirschler, 1980).

Atmospheric Sulphur from Natural Sources: Non-Biogenic

These sources of sulphur compounds include geothermal emissions resulting from underground activities such as in sulphur springs. However, the greatest amount of sulphur

generated in this way is derived from volcanoes which release mainly sulphur dioxide, while, at relatively low temperatures, hydrogen sulphide dominates the emissions, along with small amounts of sulphur trioxide and more-reduced sulphur (Cullis and Hirschler, 1980).

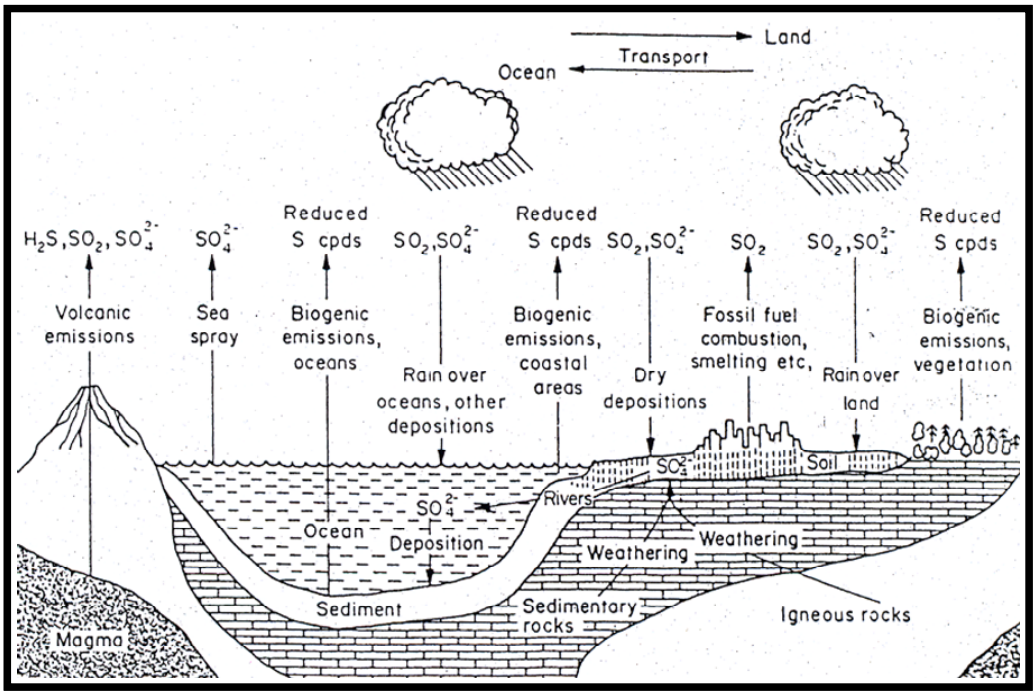

(Source: Cullis and Hirschler, 1980)
Figure 2-6: The atmospheric sulphur cycle

Another important source of atmospheric sulphur is the fine spray formed above the oceans from individual liquid droplets which evaporate, leaving smaller solid particles that consist mainly of sodium sulphate (Cullis and Hirschler, 1980).

Atmospheric Sulphur from Natural Sources: Biogenic

The biological reduction of sulphur compounds is the most important biogenic natural source of atmospheric sulphur. This occurs readily in the presence of organic matter and

under oxygen-deficient conditions. Sulphur (hydrogen sulphide, carbon disulphide and dimethyl sulphide) derived in this way is produced by marine algae in soils with decaying vegetation and sulphate-reducing bacteria such as *Sporovibrio desulphuricans* present in fine-grained muds (Cullis and Hirschler, 1980).

Due to the expected wet scavenging by rain, coupled with the strong oxidising environment of open sea-water, there is very little or no net contribution of atmospheric sulphur in the form of sulphide from long distances from the natural sources. However, in the deep parts of the ocean, where oxygen cannot penetrate, much of the sulphur may be present as sulphide rather than sulphate (Cullis and Hirschler, 1980).

Atmospheric Sulphur from Anthropogenic Sources

The main anthropogenic sources of atmospheric sulphur are industries. These industrial sources include combustion of coal and petroleum products in furnaces and boilers especially in power generating plants; in refining processes (as waste flue gases), and in the smelting of non-ferrous ores. The most abundant source of atmospheric sulphur is the burning of coal and its by-products. Sulphur emissions from coal vary with the type of coal. Hard and lignite coal, especially that used in power plants, metallurgical and cement industries, contains a significant amount of sulphur in the ash. The rate of sulphur emissions from petroleum products is still lower than that from coal despite the high and escalating rate of petroleum consumption around the world. This is due to several treatments associated with petroleum production, refining processes and product specifications requiring desulphurisation and sulphur recovery processes. The last major industrial source of anthropogenic sulphur is the non-ferrous, ore-smelting factories. Here sulphur-based compounds are associated with the ores of these metals (such as copper, lead or zinc) such that, during heat treatment operations, they are released as oxides of sulphur (Cullis and Hirschler, 1980).

2.7.2 Gaseous Atmospheric Sulphur

In the atmosphere, sulphur exists in the gaseous phase mostly as sulphides and oxides. The sulphide forms include: hydrogen sulphide, carbon disulphide, carbonyl sulphide and, dimethyl sulphide, whilst the common oxide forms are sulphur dioxide and trioxide (Calvert *et al*, 1978; Pienaar and Helas, 1996; Warneck, 1988; Seinfeld and Pandis, 1998; Herrmann *et al*, 2000; Hewitt, 2000). Gaseous sulphur compounds are observed over the South African Highveld in significant amounts that are alarming to the region (Annegarn *et al*, 1996). The common gaseous sulphur species over this area are hydrogen sulphide and sulphur dioxide from anthropogenic sources (Held *et al*, 1994). In winter, the tropospheric emission load is increased due to heating requirements, leading to more rapidly catalysed gas-phase oxidations of SO_2 (Terblanche *et al*, 1993).

Hydrogen Sulphide in the Atmosphere

Similar to the observation for sulphur dioxide, over the Mpumalanga Highveld hydrogen sulphide (H_2S) is released from a variety of sources which include open-cast coal mines, fuel processing and smelting plants. The Mpumalanga Highveld, together with adjacent communities, at certain periods of the year experiences high levels of malodorous air emissions from nearby sources. The hydrogen sulphide undergoes thermal gas-phase photo-oxidation to yield SO_2 in the atmosphere (Eggleton and Cox, 1978; Warneck, 1988).

Sulphur Dioxide in the Atmosphere

Sulphur dioxide (SO_2) is a colourless gas with a strong pungent odour, belonging to the family of gases called sulphur oxides (SO_x). It is 2.3 times heavier than air with a penetrating smell when the concentration exceeds 1.3 mg m^{-3}. It reacts on the surface of a variety of airborne solid particles, and is soluble in water as well as can be oxidised within airborne water droplets (Becker, 2004). Sulphur dioxide is released when substances containing sulphur –such as fossil fuels– are burned, and is a component of smog. It is released to the atmosphere in many industrial and domestic processes, mainly as a result of burning fossil fuels in quantities that are somewhat hazardous to the environment.

Sulphur dioxide is toxic to plants even at low concentrations of less than 0.3 mg m^{-3}, whilst at concentrations between 2.5 and 5.2 mg m^{-3} it constitutes a public and occupational health risk as well as causes ecological damage within and around source areas. In urban areas, space heating is, among others, a substantial source of SO_2 emissions especially in winter (Spengler *et al*, 1990; Mayer, 1999; Mage *et al*, 1996). When released into the atmosphere, SO_2 is oxidised in the presence of water vapour to form sulphurous and sulphuric acids which, when neutralised, result in the production of sulphate aerosols (Manahan, 1991).

Sulphur dioxide from coal-fired power plants can be reduced by cleaning the coal (beneficiation) prior to burning to reduce the sulphur content or by using lime solution spray in scrubbers to reduce the concentration of SO_2 from combustion leaving the smoke stack. Scrubbing processes are effective in removing more than 90 % of the sulphur in the flue gas. The acceptable levels of sulphur dioxide in ambient air, as published in the South African National ambient air quality standards (RSA, 2005), include an average 10-minute exposure of 500 µg m^{-3} (or 0.19 ppm), a 24-hour exposure of 125 µg m^{-3} (or 0.05 ppm), and an annual exposure of 50 µg m^{-3} (or 0.02 ppm).

Since the 1990s the issue has been raised that, as a result of the release of SO_2 by the principal industries over the Mpumalanga Highveld, adjacent communities were affected to the point that acidic precipitations had been observed (Held *et al*, 1996). To date the real reasons for this problem of highly acidified air have not been fully established since several processes play important roles in the area. These processes include mechanised agricultural practices, refining of petroleum products, metal smelting, open-cast coal mines and electric power generation. Thus it is still not clear to what extent SO_2 emissions are responsible for the problem of acidified air and also what fraction of this windborne material comes from nearby sources in the Mpumalanga Highveld in comparison to that from distant sources, especially neighbouring countries within the southern African sub-continent.

Sulphur dioxide can travel considerable distances in the atmosphere and it is deposited at a rate expressed as the product of the deposition velocity and the low-level concentration.

The deposition velocity is usually of the order of 1 cm s^{-1}. During long-range atmospheric transport, it is converted photochemically to sulphate aerosol which, in-turn, transforms to particulate matters (Latimer and Samuelsen, 1978; Maul *et al*, 1980) via several reaction mechanisms and in typical industrially polluted air at a transformation rate which appears to be dependent essentially on the relative humidity (Smith and Jeffrey, 1975).

Absorption and Oxidation of Sulphur dioxide

Many pollutants are removed from the surface layer by vegetation through the process of dry deposition. This may occur by the mass transfer of pollutants through the atmosphere to the surface followed by the uptake of the pollutants by vegetation and other materials at the surface. In this process, the control variables are a resistance to mass transport and a resistance to surface removal. The transport resistance is evaluated from turbulent transfer in the atmospheric boundary layer and the surface resistance is experimentally measured on the uptake of the pollutant by the various surface features (Platt, 1978; Roedel and Junkermann, 1978).

It is recognised (Scriven and Fisher, 1975) that a large fraction of the SO_2 emitted is taken up by the ground during advection, while the remaining fraction becomes sulphate and is deposited steadily in both dry- and wet-conditions. This SO_2 absorption by the ground is thought to provide a major sink of the long-term effect of sulphur emissions on soil.

In the atmosphere SO_2 becomes oxidised and is deposited as sulphate at greater distances. However, the SO_2 which deposits at short distances rapidly becomes oxidised in the soil, creating a greater acidifying effect on the surface at short distances where concentrations are high, than at great distances where they are low (Scriven and Fisher, 1975; Liberti *et al*, 1978).

2.7.3 Atmospheric Sulphate Aerosols

Atmospheric aerosols are important materials observed in several processes, such as the formation of clouds, radiative transfer and transport of chemical species. The various

processes often determine the chemical compositions and sizes of the aerosols. These aerosol properties can vary over a wide range for different meteorological conditions.

The properties of the aerosol are determined based on the complex interactions between the aerosol and the environment. These interactions include processes such as condensation and evaporation, coagulation, nucleation, gravitational settling, emission- and deposition-rates, advection and diffusion (von Salzen and Schlünzen, 1999). A dominant fraction of the tropospheric aerosols consists of fine secondary aerosols which include sulphate salts of ammonium and coarse marine aerosols such as calcium sulphate.

The secondary aerosol is produced from gas-phase or aqueous-phase chemical reactions that generate condensable compounds while the marine aerosol is generated from myriads of sea-spray bubbles blown off from sea waves. The chemical composition and size of tropospheric aerosols are modified significantly during their life cycles by condensation and evaporation of gaseous precursors such as ammonia, sulphuric acid, nitric acid, hydrogen chloride and water vapour (von Salzen and Schlünzen, 1999; Walker *et al*, 2004). The reactivity of sulphate and bisulphate aerosols of ammonium with regard to hydrolysis is lower than that of sulphuric acid aerosol under tropospheric conditions. The uptake coefficient, which indicates the reactivity rate of salty ammonium aerosols at high humidity in liquid droplets, is essentially the same for the same particles in water droplets. In comparison, at low humidities, when the particles may be crystalline, the uptake coefficient falls due to reduced liquid water volume. Also, uptake on sea-salt aerosols, such as sodium chloride, appears to be faster than on aqueous aerosols at equivalent humidity (Hallquist *et al*, 2000; 2003).

Atmospheric aerosol particles consist of sulphates, nitrates, ammonium, organic material, elemental carbon, crustal species, sea salt, hydrogen ions, certain transition metals and water. A typical urban aerosol size and composition as shown in John *et al* (1990) indicates that sulphate particles exist in condensation and droplet modes in the 0.1 to 1.0 μm diameter size range and in the coarse form for sizes greater than 1.0 μm in diameter. The condensation mode peaks at 0.2 μm and is the result of condensation of secondary aerosol

components in the gas-phase. While the droplet mode that peaks at around 0.7 μm is produced from heterogeneous and aqueous-phase reactions (Seinfeld and Pandis, 1998).

During combustion of fossil-fuel oxides of sulphur and other inorganic compounds are released into the atmosphere and are transported through the movement of air masses over long distances. Some of these oxides are converted into sulphate in the atmosphere and may be removed through wet- and dry-deposition. Apart from the formation of sulphate within the transported air masses, the total sulphate content within an area also depends on the amount of sulphate in the air masses from other sources along the same transport path (Husain *et al*, 1984).

Sulphuric acid (H_2SO_4) is known to exist as a liquid irrespective of the atmospheric relative humidity (Tang and Munkelwitz, 1994), but gaseous H_2SO_4 is formed in the exhaust of aircraft engines (Frenzel and Arnold, 1994; Prather *et al*, 1999; Sorokin *et al*, 2004). SO_3 molecules represent a major fraction of sulphur (VI) gases at the exit of an aircraft gas-turbine combustor and essentially the conversion of SO_3 to H_2SO_4 occurs in the exhaust line where the exhaust gases encounter a longer residence time as well as where the temperature is lower than in the hot exhaust (Reiner and Arnold, 1993; 1994). Like liquid H_2SO_4, it plays an important role in the formation and activation of aerosol particles which act as water vapour condensation nuclei (Zhao and Turco, 1995; Karcher, 1996) for subsequent cloud formation (Ross, 2003).

Gaseous H_2SO_4 is formed via rapid oxidation of fuel sulphur to SO_2 and immediately to SO_3, which in the cooling exhaust readily reacts with water vapour leading to H_2SO_4 (Reiner and Arnold, 1993). The gaseous H_2SO_4 at the exhaust tail-end concentrates and produces a super-saturated solution which condenses along with some water vapour on pre-existing soot particles leading to a partial H_2SO_4 / H_2O coating on soot particles (Zhao and Turco, 1995; Karcher, 1996). Coating of soot and new particle formation and growth become more efficient as the mass of gaseous H_2SO_4 produced per second increases (Hidy *et al*, 1978a). The H_2SO_4 / H_2O coating increases the hygroscopicity of the soot particle, hence allowing the coated soot particle to act as a water vapour condensation nucleus at a lower water vapour supersaturation than particles without coating. Furthermore, H_2SO_4

may also experience homogeneous and/or heterogeneous ion-induced nucleation (Katz and Mirabel, 1974; Yu and Turco, 1997) leading to a new volatile aerosol particle which grows by H_2SO_4 / H_2O condensation (Reiner and Arnold, 1994).

Particulate sulphate, like most other sulphate salts, is a chemically stable compound at tropospheric temperatures. Its formation can be attributed to the radical initiated gas-to-particle transformation processes of emitted gaseous sulphur compounds. These sulphur species include hydrogen sulphide, dimethyl sulphide, methyl mercaptans, dimethyl disulphide, carbonyl sulphide and sulphur dioxide.

Sulphate aerosols from photochemical oxidation have been observed to be more harmful to human health as PM_{10} than as deposited acid (Carmichael and Peters, 1984a; Tuncel *et al*, 1985). These sulphate aerosols are to some extent coated with dust during long-range transport. Within the atmosphere, sulphate-coated dusts are formed through heterogeneous co-nucleation of water, sulphuric acid and ammonia vapours (Korhonen *et al*, 2003; Katz and Mirabel, 1974). These sulphate-coated dusts do not inhibit the formation of new particles but prevent their growth to detectable sizes since they act as condensation and coagulation sinks for the new particles.

In South Africa there has been a significant reduction in the levels of particulate emissions over the years from industrial complexes (such as power plants) through the use of electrostatic precipitators and air bags on industrial flue gas leaving the smoke stack. While the particulate matter is removed, the SO_2 is released without any end-of-pipe abatement technology in place, especially for coal-fired power plants (Snyman *et al*, 1990). Secondary pollutants (such as sulphates) are produced from both natural and man-made emissions of primary gas-phase sulphur compounds in the presence of oxidants in photochemical reactions (Bari *et al*, 2003a; WHO, 1979). These products of chemical transformations are accompanied by other short- and long-lived pollutants which may be locally generated or arise from long-range air transport.

Atmospheric aerosols containing sulphate ions have become the focal point for the environmental and energy-related programmes of many developed countries. This is due to the increasing atmospheric sulphur resulting from the use of coal containing a small

percentage of sulphur for domestic and industrial energy generation. These sulphur emissions can undergo chemical transformation in the atmosphere to produce sulphate aerosols. Sulphate aerosols can be produced with relatively constant mass concentration (Sharpe *et al*, 2004). Like most other aerosols, particulate sulphate is known to contribute to climate forcing. Climate forcing creates warming of the troposphere which provides a thermodynamically favourable condition for several other emitted gaseous pollutants to become thermally activated and participate in chemical transformations yielding more complex compounds (Twomey, 1991; Blanchet, 1995). Sulphate aerosols contribute to acidification of precipitation, in other words acid rain (Granat, 1972; Cogbill and Likens, 1974; Likens, 1976; Galloway *et al*, 1976; Calvert and Stockwell, 1983).

An important analysis performed on sulphates is the study of their optical properties. The extinction of light in the atmosphere by ambient aerosols is well known, and the principles of molecular and particle optics are reasonably well understood. Also, mathematical models can be created to compute the optical properties of the atmosphere by considering the time- and space-variation of chemical composition, concentration, and particle-size distribution of ambient aerosols under specific meteorological conditions (Tang *et al*, 1981). In addition, thermodynamic and optical data especially for the most observed species are lacking when dealing with the chemical equilibrium and phase transformation of a given multicomponent sulphur aerosol system (Tang *et al*, 1981).

Atmospheric visibility is largely determined by the concentration, size distribution and chemical composition of ambient aerosols and the extent of light extinction by aerosol particles depends on whether the aerosol is present in multicomponent solution droplets of identical composition or as single salt aerosols (Eggleton, 1969; Tang *et al*, 1981). A deliquescence point at 80 % relative humidity is clearly reflected in the extinction coefficient for ammonium sulphate aerosols and multicomponent identical composition droplet sulphate aerosols contribute overwhelmingly to visibility reduction (Eggleton, 1969; Waggoner *et al*, 1976; White and Roberts, 1977; Cass, 1979; Tang *et al*, 1981). These sulphates have a characteristic size range of 0.1 to 1.0 μm (Roessler *et al*, 1965; Lundgren, 1970; Kadowaki, 1976; Whitby, 1978 and Chy'lek *et al*, 1983), making them efficient in scattering light in hot and humid weathers typical of summer periods, creating

very low visibility covering several thousands of kilometres. This diminished visibility is believed to be the result of the presence of sulphate aerosols over the area (Hall *et al*, 1975; Samson and Ragland, 1977 and Wolff *et al*, 1977). Likewise in winter, several studies, which include the Winter Haze Intensive Tracer Experiments (WHITEX), have demonstrated the contributions of sulphates in coal-fired power plant plumes to visibility degradation (Eatough *et al*, 1991).

2.7.4 Health Implications of Atmospheric Sulphur

While gaseous sulphur species are known to contribute to respiratory tract infections, atmospheric particulate sulphates, which are the end-products of SO_2 transformation, are a more harmful secondary pollutant than other particulate matter (such as pollens) (Newman *et al*, 1975a; 1975b; Carmichael and Peters, 1984a; Tuncel *et al*, 1985).

During several episodes of extreme air pollution in various countries, an increase in morbidity and mortality has been observed as the result of adverse effects of air pollution on human health. Exposure to elevated concentrations or long-continued exposure to low levels of ambient air pollutants has received increasing attention due to the wide range of adverse effects of air pollutants on ecological and human health (Dockery and Pope, 1994; Koenig *et al*, 1993; Norris *et al*, 1999; Pope *et al*, 2002). Kitagawa (1984) reported severe cases of lung disease near a plant emitting sulphuric acid aerosols. The number of incidents decreased with increasing distance away from the plant, and when sulphuric acid was removed completely from the emissions, the incidence of lung disease decreased sharply. Inhaled sulphurous acid (H_2SO_3) aerosols act as a stimulus to bronchoconstriction in persons with asthma (Balmes *et al*, 1989).

Air pollution has been positively associated with death from lung cancer and cardiopulmonary disease, as well as increased mortality with respect to the presence of fine particulates, including sulphate (Dockery *et al*, 1993). There is also strong evidence that long-term exposure to fine particulate air pollution, which is common to many metropolitan areas, is an important aggravating factor for cardiopulmonary mortality (Pope *et al*, 2002). Studies have shown that there is a relationship between the concentration of

SO_4^{2-} and the number of hospital admissions for respiratory diseases (Bates and Sizto, 1987). Moreover, an increase in morbidity and mortality was observed near a sulphuric acid production plant (Bari *et al*, 2003a; 2003b).

The ambient air quality over the South African sub-region improved over the last decade due to the reduction of gas and aerosol emission rates from industrial and urban origin –such as vehicular emissions. However, little has been documented on a continual temporal scale appraisal on the transformations of the released gaseous sulphur pollutants and their corresponding particle sulphate products which historically have been considered the most harmful of atmospheric pollutants. The hazardous potential of particulate sulphate, coupled to the unusual variability of the weather patterns observed over the South Africa, have warranted this investigation.

Mortality Effects of Sulphate Compared with Other Particulates

About 90 % of the energy supplies in sub-Saharan Africa are derived from fossil fuels which are affordable but are associated with numerous environmental (such as greenhouse) and health effects (WHO, 1991). In South Africa, more than 80 % of the electric power plants operate on coal-fired combustion processes, while a significant number of the informal settlement population depend partially or completely on coal or wood for cooking and space heating (Terblanche *et al*, 1993; Mdluli, 2007). Combustion of coal and wood has been associated with the release of multiple gases and particulate matter.

In indoor coal-fired heaters, the emitted pollutants build up within the micro-environment, reaching alarming levels which exceed the acceptable limit by more than 20 % (Terblanche *et al*, 1993). Acute asthma, with several associated respiratory tract infections, has been observed to arise mainly as a result of the intake of particulate sulphates rather than from other forms of gaseous and particle compounds (Thurston *et al*, 1993). Sulphates are known to have chronic deleterious effects on the ecosystem and on human health (Amdur, 1971; McJilton *et al*, 1973; EPA, 1974).

2.7.5 Formation and Distribution of Sulphur in the Atmosphere

The gas-to-particle formation of sulphate from SO_2 is easily derived from the mass distribution of continental and sub-continental aerosols. Sulphate aerosols are entrained in submicron particles similar in size to other wind-generated particles, such as sea salt and mineral dust greater than 1 μm radius (Weis *et al*, 1977). In the atmosphere, SO_2 available for oxidation to sulphate is lower in summer than in winter. This is due to rapid aqueous-phase oxidation in summer and an increase in the consumption of fossil fuels during winter (DeBary and Junge, 1963; Martin and Barber, 1981).

Ambient SO_2 has been shown to vary consistently with sulphate levels, yielding a uniform correlation (Shaw and Paur, 1983). This variation which was observed in the Ohio River Valley occurred in the reverse manner with minimum sulphate and maximum SO_2 in winter and the opposite in summer. These trends indicate the increase in the rate of SO_2 oxidation during the warmer and brighter period of the year –presumably as a result of enhanced photochemical processes specifically with the increase in OH^- concentration during the summer. Similar observations have been reported for diurnal and seasonal cycles of power-plant plume emissions both in rural and urban areas (Hidy *et al* 1978b; Husar *et al*, 1978; Chan *et al*, 1980; Wilson, 1981; Meagher *et al*, 1983; Malm *et al*, 1994).

In polluted regions, ground-level sulphate concentrations are usually smaller than those of SO_2, whereas in the upper atmosphere both concentrations are approximately the same (Warneck, 1988). Also due to the difference in the scale heights of sulphates and total aerosol mass in the boundary layer, at higher altitudes aerosols become enriched with sulphate (Warneck, 1988).

Snyman *et al* (1990) observed that near-ground concentrations of sulphate were generally moderate. They noticed that between ground and 200 m AGL, the distribution of sulphate varies greatly with other constituents of the aerosols. In the summer of 1990, a distinct gentle increase with height was observed for sulphate with a temperature inversion existing up to 100 m AGL with very low wind speed at ground level which increased slightly to the top and above the inversion.

2.7.6 Deposition: A Removal Mechanism of Atmospheric Sulphur

SO_2 and other trace gaseous sulphur are released into the planetary boundary layer (PBL) primarily as by-products of combustion. The mechanisms for the removal of air pollutants such as the sulphur compounds from the atmosphere occur predominantly through wet- and dry-deposition on the surface either directly or after oxidation to sulphate. H_2S and SO_2 are removed by surface absorption, transformation and precipitation, while sulphate-bearing particles are removed from the atmosphere through wet- and dry-depositions. The sulphate particles can easily fall to the ground during precipitation (Smith and Jeffrey, 1975). The sinks are greatest in the PBL where the relatively warm temperatures, high humidity and proximity to the Earth's surface lead to rapid removal of sulphur. Studies on sulphur deposition have shown that dry deposition rates decrease faster than wet deposition rates with decrease in emissions. The non-linear response of sulphur deposition rate to SO_2 emissions is the result of variations in the effective release height of emissions and canopy resistances of SO_2 change in response to ambient cation (such as ammonia) concentrations (Lee and Kingdon, 2001). A significant removal of the anions (SO_3^{2-} and SO_4^{2-}) increases the local acidity downwind of the emission sites (Cogbill and Likens, 1974; Likens *et al*, 1984; Ragland and Wilkening, 1982). Wet deposition of sulphate increased periodically in Europe but not as significantly as the increase in anthropogenic SO_2 over the same period (Granat, 1978). During the dry period in the year, sulphate deposition ranged between 9 and 29 % of the total air-borne sulphate with a mean of 20 %. Also, sulphate concentration in the air underneath the canopy has been observed to be up to 35 % lower than in the air above it and rain water rinses the dry deposited materials off the foliage such that rain water collected below the canopy is enriched with sulphate and other trace substances (Warneck, 1988). Hence the dry deposition at canopy layer is affected by the wet deposition, yielding variations in the ratio of dry-to-wet deposition for different varieties of vegetation.

2.8 Atmospheric Ammonia-Related Sulphur Compounds

One very common compound often found associated with sulphate is ammonia. In areas with large ammonia concentrations compared to acids, any H_2SO_4 present would be

neutralised forming NH_4HSO_4 and $(NH_4)_2SO_4$ (Bari *et al*, 2003a). Ammonia, a primary gas-phase pollutant, is the major neutralising agent in the atmosphere and plays an important role in the chemistry of the atmosphere. Major sources of ammonia emission are livestock and ammonia-based chemical fertilisers (Bari *et al*, 2003a; Chimka *et al*, 1997). Other sources of ammonia include humans' excretory products, sewage treatment plants and vehicles equipped with catalytic converters. Ammonia formation has also been observed to occur via the heterogeneous reaction of reduced nitrogen monoxide by carbon monoxide in the presence of excess water vapour (Cant *et al*, 2003; Gassan-zedeh and Seyidbayova, 2003; Ferraris *et al*, 2003).

Most of the ammonia is emitted in the planetary boundary layer and may react irreversibly with sulphuric acid-containing aerosols, and reversibly with both nitric and hydrochloric acids to form relatively neutral ammonium salt aerosols, which can again dissociate, with the dissociation being dependent upon temperature and humidity (Bari *et al*, 2003a). Ammonia is the most reduced form of nitrogen, and is released in small quantities from anaerobic degradation of organic matter containing nitrogen and from reduction of isocyanic acid produced in the troposphere by the interaction of reduced nitrogen oxides with carbon monoxide in the presence of water vapour (Cant *et al*, 2003).

Ammonium (formed by the protonation of ammonia) is known to be the principal cation associated with sulphate in continental aerosol (Warneck, 1988). This confirms the origin of the ammonium ion from the gas-to-particle neutralisation of sulphuric acid by ammonia. This reaction rate depends on the ammonia concentration relative to that of sulphuric acid in a mole ratio of between 1 and 2 corresponding to the intermediate between ammonium bisulphate (NH_4HSO_4) and ammonium sulphate ($(NH_4)_2SO_4$). The deficiency in the ammonium ion which results in the formation of bisulphates has been attributed to the presence of mainly uncompensated acids (Brosset, 1978 and Tanner *et al*, 1979; Watson *et al*, 1994).

2.9 The Microphysics and Chemistry of Aerosol Particles

An important issue in the evaluation of air pollution is the impact of pollutants on the visibility and aesthetic quality of the atmosphere. In this regard, emissions from coal-fired power plants generate conspicuous visible plumes as a result of high levels of particulate matter (Cass, 1979). Visibility impairment is produced as a result of the presence of primary particles, such as fly ash and combustion-generated particulate matter, and secondary particles, such as sulphates and nitrates, which are produced from chemical reactions of the emitted precursors in the presence of oxidising compounds (Cass, 1979). The particulate matter, which comprises mainly sulphates, also scatters and absorbs sunlight, thereby altering the albedo of the troposphere. In addition, water vapour entrained in waste flue gas emitted to the atmosphere may produce an adverse visibility effect if condensation occurs, forming small droplets of water. Another agent that impairs atmospheric visibility is gaseous nitrogen dioxide. It absorbs light selectively and hence discolours the atmosphere. It is a reddish-brown gas that produces a yellow-to-brown coloured plume if present in sufficient concentrations. It is produced in plumes due to photochemical reactions of the primary nitrogen oxide (NO) released from combustion mainly from vehicular emissions (Latimer and Samuelsen, 1978; WHO, 1979; Seinfeld and Pandis, 1998; Spengler *et al*, 1990; Mage *et al*, 1996; Mayer, 1999).

Since the physical and chemical properties exhibited by atmospheric aerosols are described from the microphysics and chemistry of particles, it is essential to understand the physics of aerosols in the atmosphere as it affects several parameters of meteorology. The transformation and removal mechanisms are based on known thermochemical parameters which are derived from the chemical properties of the reactants and products.

The state of existence of atmospheric aerosols is regularly altered by two well-established processes: condensation and evaporation. The condensation of gas molecules at the particle surface occurs in two steps. The first is molecular diffusion transport of the gas molecules to the surface of the particle. Once the molecule encounters the particle surface, it may be taken up by the particle. The net uptake of molecules occurs when the partial pressure of the gas at the particle surface is lower than the ambient partial gas pressure. At equilibrium

there is no change in both partial pressures. Studies have shown that there are kinetic constraints on attainment of chemical reaction equilibrium between gases and particles (Allen *et al*, 1989; Wexler and Seinfeld, 1990; Harrison and Mckenzie, 1990; Harrison *et al*, 1990). A longer time is required for coarse aerosol particles to reach equilibrium and they are not always in equilibrium with gases within the troposphere (Meng and Seinfeld, 1996).

2.9.1 The Impact of Sulphate Aerosol on Climate

In the troposphere, sulphate aerosol particles from natural and anthropogenic sources result in climate forcing. Climate forcing is the result of the alteration of meteorological variables on produced CCN. These processes and variables include the solar scattering and variation in relative humidity. More specifically, tropospheric sulphate aerosols of anthropogenic activities are highly non-uniform globally, because of their atmospheric residence time (about 170 hours).

The light interferences of sulphate aerosols are illustrated from their optical properties defined by the light-scattering coefficient. The light-scattering coefficient for sulphate aerosol, b_{sp}, is the product of the light-scattering mass efficiency of the sulphate aerosol and mass concentration of sulphate. The light-scattering mass efficiency of the sulphate aerosol, depends on the mass of sulphate, particle diameter, wavelength of absorption and on the ambient relative humidity (Seinfeld and Pandis, 1998).

2.9.2 Mechanism of Climate Forcing by Atmospheric Sulphate

Unlike greenhouse gases, atmospheric sulphate aerosols impact on climate through several mechanisms which include aerosol acidification, aerosol interaction with boundary layer stability, surface-aerosol interactions and changes in the atmospheric water vapour cycle (Blanchet, 1995). Sulphate coating on background aerosols is known to alter the CCN concentration, enhance precipitation and weaken the greenhouse effect of water vapour during air transformation (Twomey, 1974). This process causes climate cooling from infrared radiation. The climate -which is in a state of quasi-equilibrium- is balanced by

several huge energy fluxes of radiation, sensible heat, latent heat and to some extent chemical and kinetic energies. The chief energy flux is solar radiation. Several external processes, referred to as forcing agents, alter this energy balance independent of the climate system (Oke, 1987). These external processes include variations in sunlight intensity and the magnitude of a volcanic eruption. These processes alter the climate due to the aerosol content introduced into the atmosphere from smoke and formation by gas-to-particle conversion. Sulphate and other aerosols from anthropogenic sources contribute to external forcing significantly because of the rapid progression of global population and technology (Blanchet, 1995).

2.9.3 Sulphate Aerosol Contribution to Direct Forcing

Direct forcing mechanisms are those produced when the net energy flux (solar radiation [source] – terrestrial radiation [sink]) affects the adiabatic heating and consequently the temperature of the atmosphere (Oke, 1987; Blanchet, 1995; Seinfeld and Pandis, 1998). Similarly, other climate variables such as precipitation, winds, pressure, and humidity are automatically altered since they are related to temperature. The induced climate forcing is limited to regions of significant aerosol concentrations. The aerosol circuitously alters the microphysics by changing the population of the condensation nuclei. This alteration affects the surface albedo (heat transfer) and the energy balance in turn affects convection and precipitation (Blanchet, 1995). As a consequence, in the troposphere, the formation of sulphate from the oxidation of sulphur dioxide significantly affects the meteorology which in turn distorts the phase change of atmospheric chemical interactions and rates. In addition the composition of aerosols and the water vapour content influence the chemistry of transformation in the atmosphere (Moller, 1980; Toon *et al*, 1986; Pienaar and Helas, 1996). The contributions of sulphate aerosols to climate forcing can be described in terms of the processes resulting from the forcing mechanisms.

Solar Scattering by Sulphate Aerosols

Two main competing processes of aerosols on solar radiation are scattering and absorption of visible light. The scattering property is highly significant in direct forcing. Fine sulphate particles are considered to be the most effective aerosol cooling agent when combined with condensed water in moist air. Sulphate aerosols are often perceived as the model of purely scattering aerosols in the atmosphere because they are widespread and produced in enormous quantities by both natural and anthropogenic sources (Charlson *et al*, 1991). However, as a result of their submicron sizes, long residence time and the uneven distribution of atmospheric sulphate aerosols, climate forcing is highly regional with the source region experiencing higher concentrations. Apart from sea salts, soil particles and pollens with short atmospheric residence times, most other inorganic salts such as $(NH_4)_2SO_4$ are deliquescent (Twomey, 1977) characterised by the sub-saturation growth above a threshold referred to as the deliquescence point. But H_2SO_4, which is predominantly found in cold regions, is hygroscopic to such an extent that even at very low relative humidities it exists as solution droplets. The enlargement of these droplets enhances the aerosol scattering coefficients by adsorption of water vapour.

Terrestrial Radiation on Particulate Sulphate

The direct effect of sulphate aerosol on terrestrial long-wave infrared radiation is generally weak due to its relatively small particle size as compared to giant size particles such as soil, sea salts and pollen as well as significantly enlarged wet aerosol particles. Because these particles are confined to the lower troposphere there is not much temperature difference between them and the Earth's surface, resulting in low infrared radiative cooling (Blanchet, 1995).

The impacts of the solute material of aerosols on the internal heat exchange between atmospheric layers relative to cooling-to-space have been studied (Blanchet and List,

1987). Acidic aerosols can form thick haze layers where the surface inversion is pronounced. These affect the infrared radiation as it is sensitive to differences in temperature and optical depth. Also, in wet aerosol layers, a sharp moist haze can radiate to space more effectively than a vertically diffused haze layer even with same optical depth. Salt aerosols above the deliquescence point, like activated aerosol particles, result in a larger optical depth gradient at the top of a moist layer than sulphuric acid particles of comparable optical depth. Since sulphuric acid grows at all relative humidities, it produces vertically diffuse haze layers and favours the production of internal heat transport between atmospheric layers rather than cooling-to-space (Blanchet and List, 1987).

2.9.4 Particulate Sulphate Contribution to Indirect Forcing

Effects of Sulphate Cloud and Surface Albedo

Most of the observed active cloud condensation nuclei (CCN) are sulphate derived. They act as cooling agents by the *Twomey effect*. It is yet uncertain whether the additional sulphate produces new CCN or becomes internally mixed with existing CCN. Since SO_2 is generally oxidised in the liquid phase, the sulphate formed is often found with other particles. In remote areas, most particles are coated by sulphate while pure sulphate particles are rarely seen (Bigg, 1980). When water insoluble particles are coated with sulphate, only a few particles can be activated resulting in larger droplets and earlier precipitation. Hence, the cloud albedo can either increase or decrease with increasing sulphate concentration depending on the sulphate mixture with pre-existing CCN and on the CCN concentration (Blanchet, 1995).

The surface albedo is an important parameter that indicates both the magnitude and the sign of the forcing term. High surface albedo favours warming by aerosols with a high absorption-to-backscattering ratio and low surface albedo favours cooling by aerosols with a low absorption-to-backscattering ratio. In the latter case, sulphate aerosols have been observed to be responsible for the cooling above the ocean (Charlson *et al*, 1991; Blanchet, 1995).

The major source of CCN over the oceans appears to be dimethyl sulphide, produced by planktonic algae in sea water, which oxidises in the atmosphere to form sulphate aerosols (Charlson *et al*, 1987). The reflectance (albedo) of clouds, and thus the earth's radiation budget, is sensitive to the CCN density, while biological regulation of climate is possible through the effects of temperature and sunlight on the phytoplankton population and on dimethyl sulphide production. This process of CCN production is a form of natural counteraction to atmospheric CO_2 formation which is a major component of the global warming effect.

Sulphur-containing compounds on the Earth's surface present as sulphates are thermochemically stable in the presence of oxygen. But the sulphates can be reduced by organisms through two mechanisms: dissimilatory and assimilatory sulphate reduction. The dissimilatory pathway is restricted by sulphate-reducing bacteria in anaerobic environments due to physical and microbial restrictions. Only a small fraction of the H_2S produced by this process can escape to the atmosphere. The products of the assimilatory pathway are a variety of organosulphur compounds, the largest being the amino acids cysteine and methionine. Gaseous sulphur species in the form of H_2S and SO_2 are oxidised in air, largely by OH^- (Graedel, 1979; Niki *et al*, 1983; Yin *et al*, 1986).

Clouds of liquid water droplets form only in the presence of CCN. The size distribution of the cloud droplets changes with the size distribution or concentration of the CCN (Hobbs *et al*, 1974). This could affect the coalescence and rain production process and possibly the time-averaged cloud cover. This change in the size distribution of the droplets is known to change the reflectance (albedo) of clouds (Paltridge, 1980; Charlock, 1982; Somerville and Remer, 1984; Bohren, 1985).

2.9.5 Atmospheric Water Vapour Impact on Aerosols

The atmospheric moisture budget alters climate forcing by aerosols in several ways. One of the ways is the transformation of warm-moist maritime air to cold-dry continental polar air. Here, the cooling rate of the air mass depends to some extent on the atmospheric water vapour content because, when air cools, condensation and precipitation takes place. Also a

reduction of the water vapour in the atmosphere reduces the downward atmospheric infrared radiation largely responsible for greenhouse effects. Consequently, a reduction in greenhouse effects would increase the cooling rate of the lower troposphere-surface region and accelerate the formation of continental polar air. When continental polar air is produced more rapidly, the region is observed to be a cold region (Blanchet, 1995).

Once a gas molecule has been captured by a particle, it immediately interacts with the chemical compounds of the particle. These interactions are different for solid particles and aqueous particles (von Salzen and Schlünzen, 1999). A gas molecule captured by an aqueous aerosol is involved in several aqueous-phase processes following its uptake. This molecule may dissociate to form ions while it is transported within the particle. It may also react with other charged or neutral chemical components in the particle. These processes are strongly affected by electrostatic interactions between dissolved ions due to the high concentrations of the species favouring mostly dissolved charged species over the neutral species (Bassett and Seinfeld, 1983; Kim *et al*, 1993b).

In their study of the contributions of solute content of the aerosols to continental polar air formation Blanchet and Girard, (1994), observed that sulphuric acid coating on aerosols reduces the number of activated droplets as well as the concentration of ice formed. It also reduces the erosion of the aerosol variety and prolongs the residence time. As a result, the reduced number of activated CCN then grows at a faster rate and becomes larger. Consequently, the precipitation rate is increased and air-mass dehydration is accelerated (Blanchet and Girard, 1994).

Liquid Water Content of Aerosols

Secondary aerosols are mainly composed of inorganic electrolytes, ions and water. An important agent that affects the aerosol content in the atmosphere is the water level. Most of the water associated with atmospheric particles is chemically unbounded (Pilinis *et al*, 1989). In the atmosphere, aerosol particles of inorganic salts are solid at very low relative humidities and, as the ambient humidity increases, the particles remain solid until the

relative humidity reaches a threshold value specific for each aerosol particle specie. At this relative humidity, the solid particle spontaneously absorbs water to produce a saturated aqueous solution of the salt. This threshold relative humidity is known as the deliquescence relative humidity (DRH). With further increase in the ambient relative humidity, additional water condenses onto the salt solution to maintain thermodynamic equilibrium (Figure 2-7).

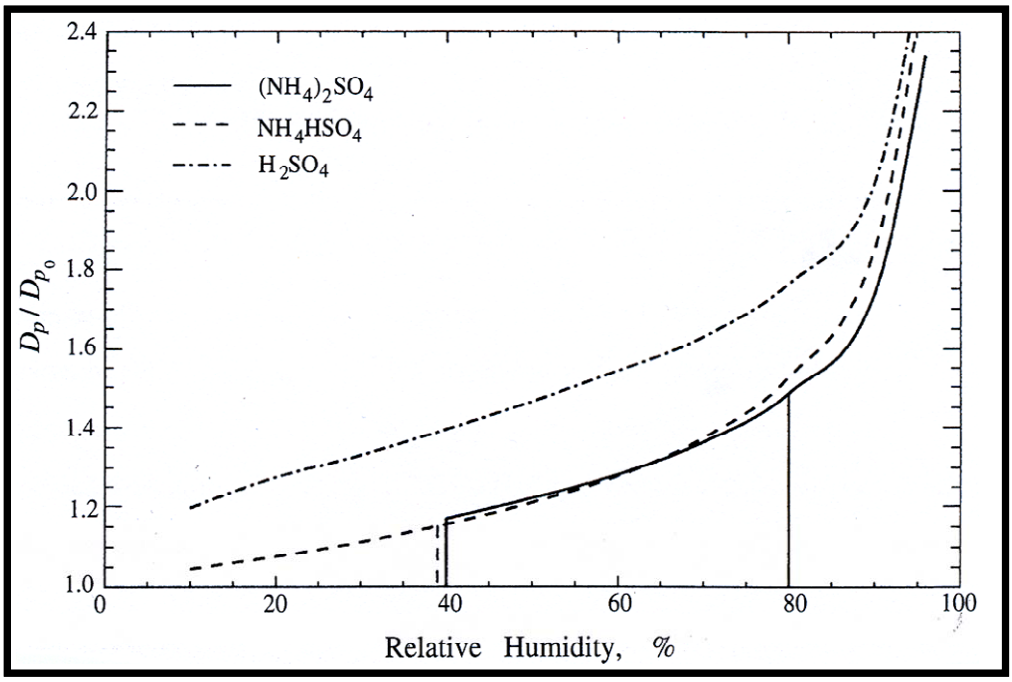

(Source: Seinfeld and Pandis, 1998)
(Legend: Dp_0 is the diameter of the particle at 0 % relative humidity)
Figure 2-7: Diameter change of $(NH_4)_2SO_4$, NH_4HSO_4 and H_2SO_4 particles as a function of relative humidity

Alternatively, when the ambient relative humidity starts to drop over a very wet particle, water is evaporated from the particle. Although the solution does not crystallise at DRH, but remains in a metastable state as saturated solution until a much lower relative humidity at which crystallisation occurs. The relative humidity at which the crystallisation occurs is known as the crystallisation relative humidity (CRH) (Shaw and Rood, 1990; Seinfeld and Pandis, 1998). The CRH of an electrolyte may be at a much lower RH than it's DRH (McMurry and Stolzenburg, 1989; Shaw and Rood, 1990; Carrico *et al*, 1995; Tang, 1997;

Seinfeld and Pandis, 1998). The metastable aqueous aerosols are more likely to exist than particles containing dehydrated salts, even at very low relative humidities (Guise-Bagley *et al*, 1994). The salts of sulphate become deliquescent in the atmosphere at 80% for $(NH_4)_2SO_4$ and 39% for NH_4HSO_4, while crystallisation relative humidity occurs at 37% for $(NH_4)_2SO_4$ and less than 5% for NH_4HSO_4 (Tang, 1980; Tang and Munkelwitz, 1993; Tang and Munkelwitz, 1994). The deliquescence relative humidities of some common atmospheric particulate sulphate aerosols are given in Table (2-1) below. At any given relative humidity, an inorganic salt can exist either as a solid or as an aqueous solution. When the relative humidity is lower than the DRH, the Gibbs free energy of the solid salt is lower than that of the corresponding solution (Seinfeld and Pandis, 1998).

Table 2-1: Deliquescence relative humidities of electrolyte solutions at 298K

Salt	**DRH (%)**
KCl	84.2 ± 0.3
Na_2SO_4	84.2 ± 0.4
NH_4Cl	80.0
$(NH_4)_2SO_4$	79.9 ± 0.5
NaCl	75.3 ± 0.1
$NaNO_3$	74.3 ± 0.4
$(NH_4)_3H(SO_4)_2$	69.0
NH_4NO_3	61.8
Na_2HSO_4	52.0
NH_4HSO_4	40.0

Source: Tang, 1980 and Tang and Munkelwitz, 1993

This keeps the salt in the solid state (Figure 2-8). As the relative humidity increases, the Gibbs free energy of the aqueous solution decreases while that of the solid salt remains constant.

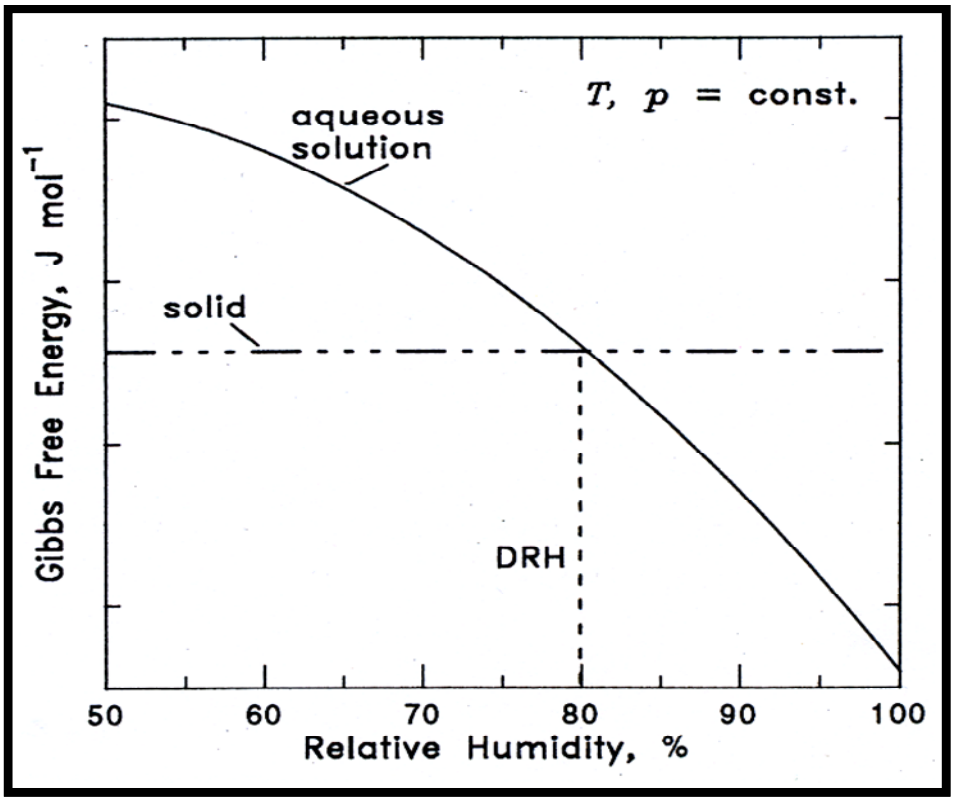

(Source: Seinfeld and Pandis, 1998)
(Note: At the DRH these energies become equal)
Figure 2-8: Gibbs free energy of a solid salt and its aqueous solution as a function of relative humidity

At the DRH, the energy of the aqueous solution equals that of the solid salt. With further increase in the RH, the solution attains a lower energy state and the aerosol spontaneously absorbs water to form a saturated solution. This change of state is accompanied by a significant growth in the mass of the particle. For a wet particle at RH higher than the DRH, the aerosol remains in the solution state. But, when the RH decreases reaching the DRH, the energies of the two states become equal once again. However, with a further decrease in RH, the particle attains a lower energy state, resulting in the formation of a supersaturated solution with the water evaporating from the particle. The solution eventually reaches a critical supersaturation and crystallisation (nucleation) results, producing a solid particle at an RH significantly lower than the DRH (Tang and Munkelwitz, 1994). Some aerosol species do not exhibit deliquescent behaviour at 298K

because they are hygroscopic with only a very small change in water content with change in relative humidity. Such species include sulphuric acid (Seinfeld and Pandis, 1998). It was shown practically that the DRH value for sulphates, such as $(NH_4)_2SO_4$ and Na_2SO_4, varies only slightly with ambient temperature, while for other compounds, such as $NaNO_3$, the variation is significant {Figures (2-9a) and (2-9b)}.

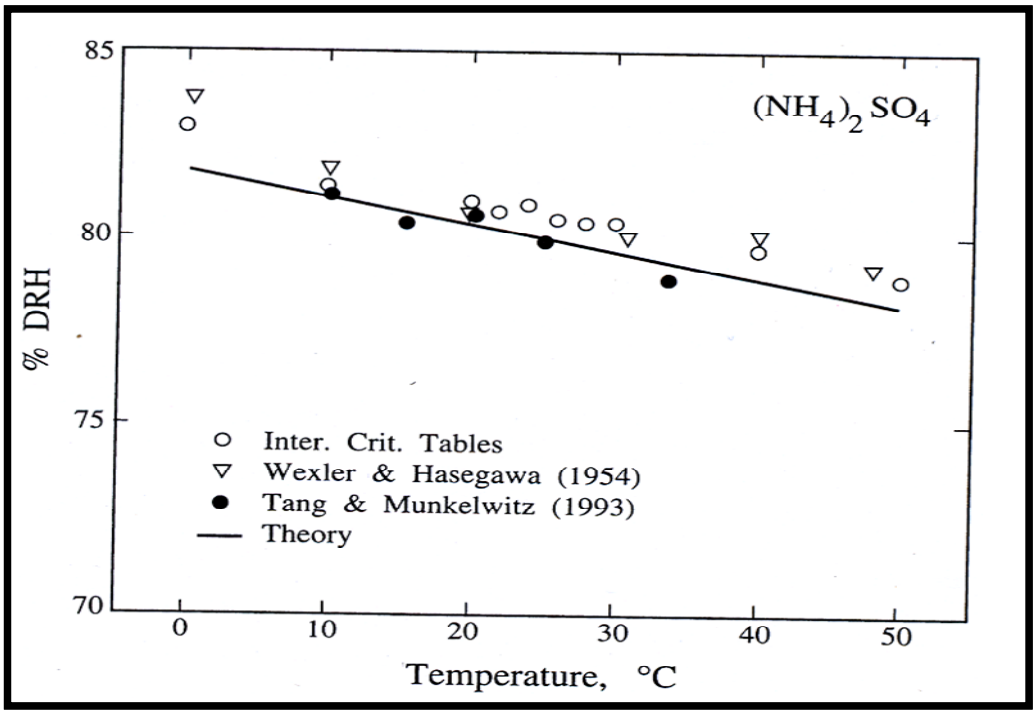

(Source: Tang and Munkelwitz, 1993)

Figure 2-9a: Deliquescence relative humidity as a function of temperature for $(NH_4)_2SO_4$

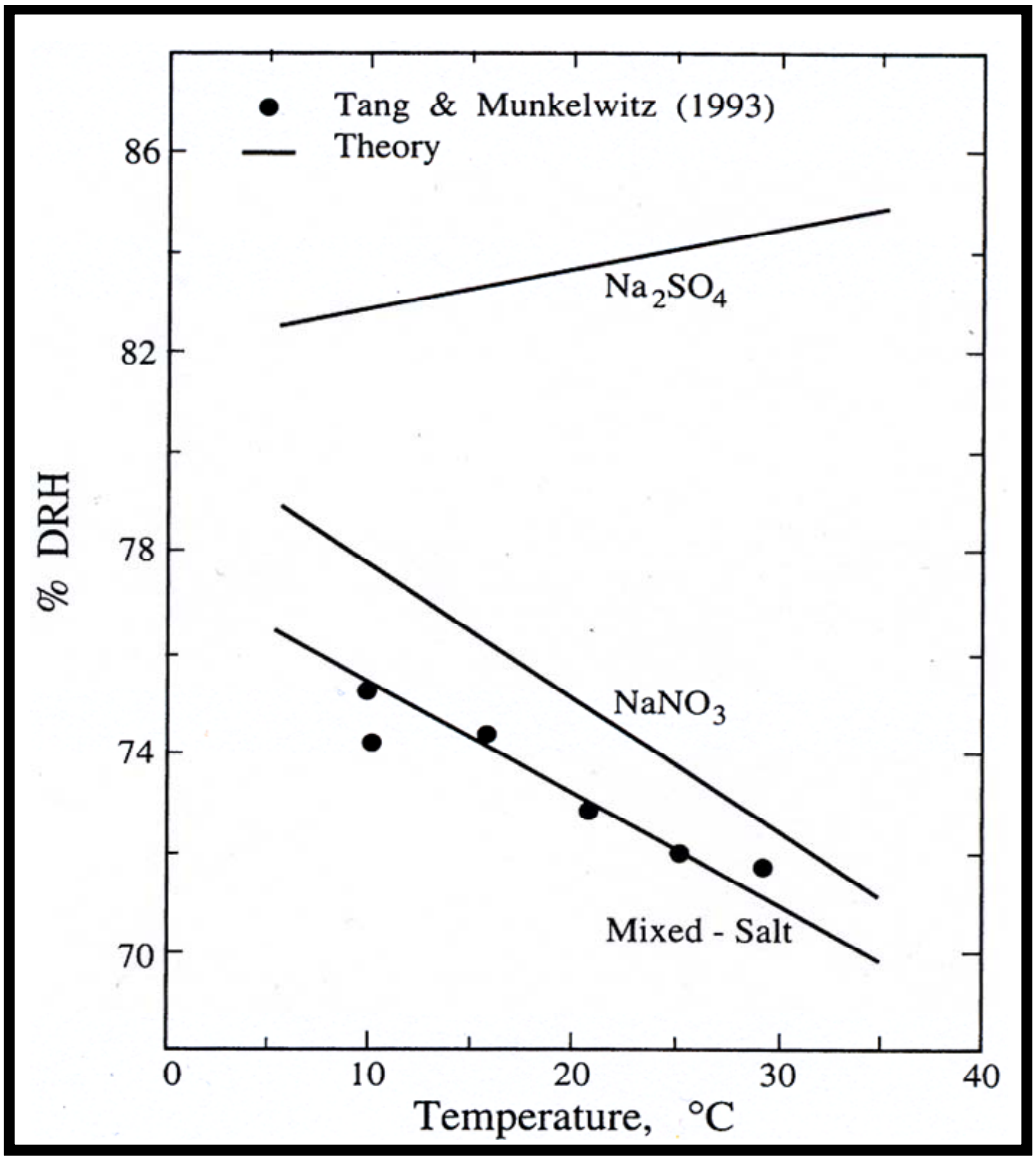

(Source: Tang and Munkelwitz, 1993)

Figure 2-9b: Deliquescence relative humidity as a function of temperature for Na_2SO_4, $NaNO_3$ and mixed salt

Temperature Dependence of Relative Humidity

It is assumed that the ambient vapour pressure of water in the atmosphere is not affected by the transport of water to and from aerosols in the atmosphere for thermodynamic calculations (Pilinis and Seinfeld, 1987; Pilinis *et al*, 1989; Seinfeld and Pandis, 1998).

The ambient RH is related to the atmospheric water vapour pressure, p_w, for atmospheric aerosols by:

$$\frac{p_w}{p_w^0} = \frac{RH}{100} \tag{2.1}$$

where p_w (hPa) and p_w^0 (hPa), are the water vapour and saturation water vapour pressures, respectively, RH (%), is the relative humidity.

Table 2-2: Humidity constants for saturated water

Constants	α values between -50 °C and +50 °C
α_1	0.0610779961 x 10^{2}
α_2	0.4436518521
α_3	1.428945805 x 10^{-2}
α_4	2.650648471 x 10^{-4}
α_5	3.031240396 x 10^{-6}
α_6	2.034080948 x 10^{-8}
α_7	6.136820929 x 10^{-11}

Source: Seinfeld and Pandis, 1998

The saturation water vapour pressures have been determined as a function of the ambient temperature range of –50 °C and +50 °C as:

$$p_w^0 = \alpha_1 + \alpha_2 T + \alpha_3 T^2 + \alpha_4 T^3 + \alpha_5 T^4 + \alpha_6 T^5 + \alpha_7 T^6 \tag{2.2}$$

where α is an empirical constant and, T (K) is ambient temperature.

When equations (2.1) and (2.2) are combined, the water vapour content over tropospheric temperature is estimated as:

$$p_w = \left(\alpha_1 + \alpha_2 T + \alpha_3 T^2 + \alpha_4 T^3 + \alpha_5 T^4 + \alpha_6 T^5 + \alpha_7 T^6\right)\frac{RH}{100} \tag{2.3}$$

In relation to the atmospheric pressure over a particular area, the water vapour concentration expressed as a mixing ratio, y_w, in the troposphere could be expressed as:

$$y_w = \frac{\left(\alpha_1 + \alpha_2 T + \alpha_3 T^2 + \alpha_4 T^3 + \alpha_5 T^4 + \alpha_6 T^5 + \alpha_7 T^6\right)\frac{RH}{100}}{P} \qquad (2.4)$$

where y_w (dimensionless), is the water vapour concentration and P (hPa) is the total (atmospheric) pressure of the system.

2.9.6 Effects of Temperature Lapse Rate on Aerosols

Aerosols are known to increase the static stability of the lower atmosphere by reducing the solar radiation reaching the surface. In turn, a lower temperature reduces convection. Static stability is enhanced by warming the upper levels of the aerosol layer. The consequences of the increasing static stability are that the aerosol lifetime is increased which extends further their effects on the climate. An effect of the increasing aerosol at the Earth's surface is the reduction of the sensible- and latent-heat convective flux, and indirectly creating warming at the surface. Carlson and Benjamin (1980) reported that radiation helps to maintain boundary layer stability, hence favouring long-range dust transport, while observations of McCracken *et al* (1986) indicated that a reduction in solar radiation at the Earth's surface is compensated for by increased downward atmospheric infrared radiation from warmer and more opaque aerosol layers in the upper atmosphere.

2.9.7 Phoretic Dynamics of Sulphate Aerosols

Like most aerosols, particulate sulphate experiences external influences induced by forces other than gravity or electrical field effects. When there is a gradient of fluid temperature, concentration and solar radiation, there are differences in the momentum conveyed by gas molecules in all directions, producing Brownian motion. The Brownian effects are thermophoresis, diffusiophoresis and photophoresis. The photophoresis does not play any role in atmospheric aerosol behaviour (Seinfeld and Pandis, 1998).

Thermophoresis

This is the effect generated when a sulphate aerosol particle is suspended in a fluid with temperature gradient. When a mass of gas molecules is subjected to high temperatures close to the Earth's surface, their kinetic energy increases as well as the rate of collision with particles, resulting in the movement of particles in the hot surface region to the cold upper troposphere. This is directly applicable to small aerosol particles, while for larger aerosol particles a temperature gradient is developed around the layer and the surface of the particle as hot gas moves from a warmer to a colder region along the surface of the large aerosol particle, resulting in a force in the cold direction (Seinfeld and Pandis, 1998).

Diffusiophoresis

This is a phenomenon occurring in the presence of a concentration gradient of gas molecule such as the evaporation of water molecules in the atmosphere. When water vapour decreases in concentration with distance away from the Earth's surface due to evaporation, there is an upward water vapour flux away from the surface. Simultaneously, all the surrounding air molecules must move downward towards the surface to replace the upward-moving water molecules. Aerosol particles suspended above the water vapour surface will partake in the molecular traffic. They collide with the water molecules and are carried upward as well as encountering air molecules that are pushed downward. Since the air molecules are more massive than the water molecules in the atmosphere, the process is dominated by the air molecules, resulting in a net downward movement of the aerosol particles (Seinfeld and Pandis, 1998).

2.10 Atmospheric Sulphur Budget

The atmospheric sulphur budget has been studied extensively (Eriksson, 1963; Robinson and Robbins, 1970; Rodhe, 1970; Georgii, 1970; Kellog *et al*, 1972; Friend, 1973; Granat

et al, 1976; Galloway and Whelpdale, 1980; Katsoulis and Whelpdale, 1990; Whelpdale, 2002). Except in the works of Nguyen *et al* (1983), which considered the oceans, all other studies have sulphur sources accounting for about one-half of the sulphur sinks.

The circulation of chemical compounds in the atmosphere is described essentially on time scales that characterise the transformation and removal processes. The knowledge of time scale, coupled with ambient concentrations of the compounds, allows for the determination of the transformation and removal properties. Also, the dispersion pattern and fallout can be obtained when the sources and dispersive characteristics are known. In addition, the time scale of deposition serves to provide information on the amount of the compound in the atmosphere as well as its rate of accumulation (Rodhe, 1978).

Most previous atmospheric sulphur budgets have dealt with global totals of sources and sinks. Since man-made sulphur sources are randomly distributed over the globe and because of the limited residence time of sulphur dioxide in the atmosphere, it is obvious that possible ecological impacts of the interferences on the sulphur cycle by anthropogenic activities are most likely local or, at most, regional rather than global. Hence, it is more logical to consider sulphur budgets over a limited region than globally (Granat *et al*, 1976; Fugas and Gentilizza, 1978; Rodhe, 1978).

A description that systematically compares emission sources and sinks and concentrations over reasonably large time- and space-scales was given in Rodhe (1978). This approach can be applied to estimate the time scales which characterise transformation and removal processes of sulphur compounds in the atmosphere. The box model was applied to develop the time scale followed by evaluation of the budgets of sulphur compounds (Rodhe, 1978). The intercontinental transboundary sulphur budget based on concentration overflow across a defined boundary has been established (Galloway and Whelpdale, 1980; Katsoulis and Whelpdale, 1990; Whelpdale, 2002).

2.10.1 Atmospheric Time Scales

A parameter which adequately characterises the fate of pollutants over long temporal- and spatial-scales is the residence time or turnover time of pollutants in the atmosphere.

Residence Time

The residence time of a pollutant is defined as the time required to decrease its weight in the atmosphere over a certain region by a specific factor, assuming that no further input into the atmosphere and no import across the boundaries of the region occurs (Henmi and Reiter, 1978). Simply, it is the time spent by a molecule from the moment of injection into or formation in the atmosphere to the moment of transformation or removal. Residence time could also be referred to as the transit time. This is applied in situations when the sources and sinks are situated, in most cases, at the ground level. The residence time for individual molecules of a particular compound differ, hence it is necessary to establish the frequency function, $\phi(\tau)$, which describes the residence time distribution.

Since SO_2 can be emitted directly as well as generated in the atmosphere, the fate of SO_2 in the atmosphere is determined by considering the residence times of the SO_2 molecule itself, τ_{SO_2}, and that of the sulphur atom, τ_S. The sulphur atom which exists in other compounds such as hydrogen sulphide and dimethyl sulphide, participates in atmospheric SO_2 formation. A transformation of SO_2 to sulphate implies a sink for SO_2 and a source for sulphate but not for the sulphur atom. Therefore a sulphur atom that is introduced as SO_2 and removed as sulphate will have a residence time described as:

$$\tau_S = \tau_{SO_2} + \tau_{SO_4^{2-}} \tag{2.5}$$

where τ_S, τ_{SO_2} and $\tau_{SO_4^{2-}}$ are the residence times of SO_2 entering the mixing layer, SO_2 leaving the mixing layer and sulphate leaving the mixing layer, respectively.

The average value of the residence times of all molecules is referred to as the average residence time, τ_{ar}. This average residence time is a function of the residence time distribution functional defined as:

$$\tau_{ar} = \int_0^\infty \tau\phi(\tau)d\tau \tag{2.6}$$

Equation (2.6) can be simplified by the approximation given as:

$$\tau_{ar} \cong \Delta\tau \sum_{i=0}^{i=m} \tau_i \phi_i(\tau) \qquad (2.7)$$

This average residence time is used to characterise circulation of a compound in the atmosphere.

The determination of the residence time of SO_2 in the mixing layer is based on the following assumptions regardless of season (Henmi and Reiter, 1978):

(a) Dry deposition, precipitation scavenging and chemical transformation are the removal mechanisms of the pollutant from the atmosphere.

(b) There is no leakage of the pollutant from the top of the mixing height.

(c) The import and export fluxes due to turbulent diffusion across the boundary layer are equal.

The atmospheric residence time of anthropogenic SO_2 has been reported by Meetham (1950); Junge (1960); Rodhe (1970) and Eliassen and Saltbones (1975) as ranging from 5 hours to 5 days over varying atmospheric environments and seasons. The above studies were based on measurements when no precipitation occurred. In contrast, in the work of Henmi and Reiter (1978), SO_2 residence time is generally longer in the warm season than in the cold season due to short dry periods in the cold season when compared with the warm season, coupled with the shallower depth of the mixing layer during the cold season than in the warm season. The residence times obtained for anthropogenic sulphur dioxide with wet deposition considered, ranged between 20 and 40 hours for the cold season and between 30 and 60 hours for the warm season over the eastern United States.

Age of a Molecule in the Atmospheric Reservoir

The age of a molecule in the reservoir (region within and outside the atmospheric mixing layer) is the time since it was introduced. A common assumption is that the age of a molecule when it leaves the reservoir is equal to its residence time. This is not always true. Chemical transformations are uncommon outside the mixing layer, hence a molecule released outside the mixing layer is expected to have a longer age than its residence time compared to those released directly into the mixing layer, provided the molecule was not deposited before entering the mixing layer. For example, if SO_2 is emitted and spends a long time in the reservoir remaining in the same state, when it enters the mixing layer it is transformed into sulphate. This transformed SO_2 would have a longer age compared to molecules emitted directly into the mixing layer. And if the molecule is removed almost as soon as it is released, it will have an age shorter than the expected residence time. A frequency distribution function for the age of a molecule in the reservoir is denoted as $\psi(\tau)$ (Henmi and Reiter, 1978). The difference in the molecule's age in the reservoir and its residence time is determined by the frequency distribution functional. The corresponding average age, τ_{aa}, of all molecules in the reservoir at a particular time is given as:

$$\tau_{aa} = \int_0^\infty \tau\psi(\tau)d\tau \tag{2.8}$$

Equation (2.8) can be approximately simplified as:

$$\tau_{aa} \cong \Delta\tau \sum_{i=0}^{i=n} \tau_i\psi_i(\tau) \tag{2.9}$$

Turnover Time

The turnover time is the time obtained when the total mass of a certain pollutant in the atmosphere over a specified region is numerically divided by the corresponding pollutant

removal flux (Henmi and Reiter, 1978). It is the ratio of the total mass of the pollutant in the reservoir to the total flux out of (or into) it. It is expressed as:

$$\tau_o = \frac{M}{\dot{m}} \tag{2.10}$$

τ_o is identical to τ_{ar} on the basis that $\tau_{aa} = \tau_{ar}$ such that the turn-over time is actually a measure of the average residence time spent by molecules of the compound in the reservoir (Bolin and Rodhe, 1973). The age concept is naturally applied to radioactive materials (Rodhe, 1978). The turnover time may also be applied in situations with more than one competing removal mechanism. Therefore, when dry- or wet-deposition, that is scavenging or precipitation, removes a pollutant, if the steady-state mass, M, or a well-defined mass fraction, y_M, of the pollutant in the atmosphere is known, the overall turn-over time, τ_o, expressed as a function of deposition fluxes is determined by:

$$\tau_o = \frac{M}{(\dot{D} + \dot{W})} = \frac{M}{Q} \tag{2.11}$$

where M and Q, are the mass and overall deposition rate of advecting materials respectively. Whereas $\dot{D}$ and $\dot{W}$ are the dry and wet deposition rates respectively.

While for the individual deposition mechanisms the turn-over times are given as follows:

For dry deposition, it is defined as:

$$\tau_{oD} = \frac{M}{\dot{D}} \tag{2.12}$$

And for wet deposition, it is given as:

$$\tau_{oW} = \frac{M}{\dot{W}} \tag{2.13}$$

It follows from equations (2.12) to (2.14) that

$$\frac{1}{\tau_o} = \left(\frac{1}{\tau_{oD}}\right) + \left(\frac{1}{\tau_{oW}}\right) \qquad (2.14)$$

2.10.2 Box Model for Atmospheric Sulphur Budget

In this model, it is also assumed that the conditions inside the box are homogeneous and the spatial distribution of the compound inside the box is not treated explicitly. This is in contrast to analytical or numerical dispersion models where spatial and possibly temporal distributions are explicitly considered. But the box model is advantageous as it enables an overall assessment to be made of the time-scale as well as provides the relative importance of the transformation and removal processes with simple mathematics (Husar *et al*, 1978 and Gillani *et al*, 1978).

2.10.3 Transboundary Model for Atmospheric Sulphur Budget

Local and urban scale transport yields more precise atmospheric sulphur budgets than regional and global scale transboundary sulphur budgets. The inflow and outflow flux of an advective transboundary transport of atmospheric sulphur on land has been described (Galloway and Whelpdale, 1980; Whelpdale, 2002).

Due to the limited resource materials and equipment, the resolution of the sulphur budget (which produces the net total sulphur at any particular time in air) was conducted through an approach different the aforementioned.

2.11 Chemical Transformations of Atmospheric Sulphur

In the atmosphere, the kinetics of homogeneous gas-phase sulphur transformation is well understood (Calvert *et al*, 1978; Moller, 1980; Calvert and Stockwell, 1983). Likewise, aqueous-phase and heterogeneous sulphur reactions at different atmospheric conditions have been studied via a number of pathways which include the nucleophilic displacement of water by H_2O_2 on HSO_3^- with an Fe^{2+} or Mn^{2+} catalyst (McArdle and Hoffman, 1983; Lagrange *et al*, 1993; Breytenbach *et al*, 1994; Martin and Damschen, 1981).

The photochemical oxidation of atmospheric SO_2 has its precursor oxidant formed from volatile organic compounds of nitrate anions which are stable atmospheric nitrate compounds such as peroxyacetyl nitrate (Miller, 1978; Pienaar and Helas, 1996; Chisaka, 1984; WHO, 1979). It is well established that the oxides of sulphur (SO_2 and SO_3) are oxidised to sulphuric acid and other compounds which include NH_4HSO_4. Also by nucleation and condensation several other sulphate aerosols are formed. The equilibrium concentration ratio of SO_2 to SO_3 is about 8×10^{11} in air at 25 °C and 1 atmosphere (Pienaar and Helas, 1996; Seinfeld and Pandis, 1998).

The extent of oxidation of sulphur dioxide to sulphate in the plume of coal-fired power plants has been established via a number of techniques and for several atmospheric environments and meteorological conditions (Newman *et al*, 1975a; 1975b). This includes the use of isotopic ratios of SO_2 and sulphur hexafluoride (tracer species) to observe a pseudo second-order heterogeneous oxidation, catalysed by vanadium compounds (Newman *et al*, 1975b). A conversion rate of 1 ppm^{-1} h^{-1} was achieved for emissions from oil-fired plant plumes, while, from coal-based plumes, the oxidation rate that occurred through heterogeneous mechanism pathways was less than 5 %. It was limited by the low levels of particulates in coal-based plumes (Newman *et al* 1975a; 1975b). It was presumed that a consequence of the oil-fired plume oxidation is that the water produced condenses on sulphate particulates, the magnitude of which might give rise to large particles.

Another study focussing exclusively on emissions from coal-fired plants and the use of a tracer for determining the extent of SO_2 conversion to sulphate and deposition associated with plume transport is described in Eatough *et al* (1994). The use of a specific tracer species was necessary because SO_2 to sulphate ratios, as well as the elements associated with particles released from coal-fired power plants, are not a good indicator because sulphur dioxide also evolves from several other sources. A number of studies have used spherical aluminosilicate (SAS) particles which are unique to coal-fired power plant emissions and are consequently suitable endemic tracers for source apportionment (Fisher *et al*, 1978; Webber *et al*, 1985; Eatough *et al*, 1991). Moreover, SAS particles, in combination with other endemic tracers, such as total atmospheric fluoride, selenium, arsenic and lead, have been used to discriminate between emissions from different coal-

fired power plants (Eatough *et al*, 1991). These tracers have been used to evaluate the contribution of both coal-fired and other sources of SO_2 to sulphate present at a distant site from the source. Also source apportionment has been determined using ratios of these endemic tracer species to the SO_2 from a particular region (Eatough *et al*, 1991; 1994).

It has been observed that from plume emissions the SO_2 concentration at ground level increases with downwind distance, while the sulphate concentration decreases with downwind distance (Newman *et al*, 1975b). This was attributed to a remarkably low (rarely exceeding 5 %) oxidation rate of SO_2 to sulphate from coal-fired power plant stack emissions.

Chemical reactions in the gas-phase may result in the formation of condensable products. These molecules are either deposited on pre-existing particles, or form new particles by collisions among themselves. Low vapour pressure products (such as sulphuric acid) are likely to form new particles. The particles formed by collisions are initially small but they grow due to coagulation and condensation. This was observed in the photo-oxidation of SO_2 to sulphate (Prager *et al*, 1960; McMurry and Friedlander, 1978). Several relationships exist between the surface areas of aerosols and their growth rates. One of these relationships has been shown to be independent of the chemical nature of the aerosol (McMurry and Friedlander, 1978).

Aerosols formed by the photochemical oxidation of SO_2 in the presence of NO_2 and volatile organic compounds, consisting mainly of chained olefins in air, probably consist primarily of sulphuric acid (Gerhard and Johnstone, 1955; Endow *et al*, 1963; Bouland *et al*, 1978; Chisaka, 1984) and other forms of sulphate (Groblicki and Nebel, 1971). In the presence of cyclic olefins, the sulphur aerosols formed are generally different forms of sulphate (Prager *et al*, 1960). Coarse-sized particulates, such as Aeolian dust, fly ash, soot and SiO_2, which constitutes classical smog, are possibly co-reactants in the photochemical oxidation of SO_2 to sulphate in the atmosphere in both summer and winter (Pienaar and Helas, 1996). In the atmosphere, the oxidation of SO_2 to sulphate transformation occurs during long-range pollutant transport (Eliassen and Saltbones, 1983; Benkovitz *et al*, 1994). Hence, local (within a country) and regional (across countries) pollution problems

associated with transboundary transport of SO_2 and sulphate is the production of dry- and wet-deposits especially when a tremendous amount of SO_2 and NO_x are released to the atmosphere during the burning of fossil fuels (Tang *et al*, 1981; Stockwell, 1986; Walcek *et al*, 1986).

2.11.1 Kinetics of Chemical Transformations

Chemical transformations in reacting vessels require varying lengths of time for completion, depending upon the rate constant of the limiting reactant, mixing pattern and the thermochemical conditions that favour the reaction. To study the reaction kinetics of atmospheric species, the rate expression parameters should depend not only on the flowrates but on the process variables. Some basic parameters that can affect the transformation rate of atmospheric reactants include the concentrations of reactants during advection, vertical pressure variations and ambient temperature, solar radiation, mixing layer height, wind speed and relative humidity. Higher concentrations have been known to enhance reaction rate; and at the minimum concentration the rate may be unaffected by the concentration of a particular reactant. For gases, increasing the pressure simply increases the concentration and increasing temperature up to a 10 °C rise doubles the reaction rate (Levenspiel, 1999). Also light or radiation of a particular wavelength alters the rate of photochemically propagated atmospheric reactions of released gases. In general, for a bimolecular reaction of the form

$$a\mathbf{A} + b\mathbf{B} \quad \rightarrow \quad c\mathbf{C} + d\mathbf{D} \tag{2.15}$$

where **A**, **B** and **C**, **D** represent the reactants and products, respectively, while a, b, c, d are the corresponding stoichiometric coefficients. The rate of disappearance of **A** is expressed in terms of the stoichiometric coefficients as:

$$-r_A = k_A[A]^m[B]^n \tag{2.16}$$

where m and n, are constants whose values are usually 0, 1, 2. m is the order of reaction with respect to **A** and n with respect to **B**.

And if [B] cannot be measured, it is assumed that [A] and [B] occur in stoichiometric proportions (Koch, 1977) such that

$$[B] = \frac{a}{b}[A] \qquad (2.17)$$

When equations (2.16) and (2.17) are combined, a simplified rate dependant only on the concentration of reactant A is given by:

$$-r_A = ka[A]^m\left[\frac{a}{b}[A]\right]^n = k\frac{a^{n+1}}{b^n}[A]^{m+n} = k\frac{a^{n+1}}{b^n}[A]^p \qquad (2.18)\ a$$

And $p = m + n$ (2.18) b

where p is the overall order of reaction.

Then, taking logarithms of equation (2.18a) gives:

$$\ln(-r_A) = \ln\left(k\frac{a^{n+1}}{b^n}\right) + p\ln[A] \qquad (2.19)$$

Where a plot of $\ln(-r_A)$ against $\ln[A]$ gives a slope, p, and intercept, q, defined as

$$q = \ln\left(k\frac{a^{n+1}}{b^n}\right) = \ln(k) + \ln\left(\frac{a^{n+1}}{b^n}\right) \qquad (2.20)$$

With known stoichiometric ratios, a and b, the rate constant can be derived (Koch, 1977).

Determination of Kinetics for Atmospheric Sulphur Transformation

There are four generally accepted standard methods for the determination of reaction kinetics for atmospheric sulphur (Gillani *et al*, 1978; Forrest and Newman, 1977). These methods include the tracer method; the particulate-to-total sulphate ratio method; the sulphur mass balance method, and the aerosol size spectrum kinetic method.

The Tracer Method

In this method, a tracer with similar physicochemical properties to the gas needed to be measured, which does not interfere with atmospheric sulphur species, is added to the gas released to the atmosphere at a very low concentration. The rates of change of the primary and secondary matter relative to those of the tracer substances, such as sulphur hexafluoride, are used to estimate the transformation and deposition rates of atmospheric sulphur (IV) oxide. While the method is seen to be appropriate for a time-dependent measurement, it is difficult to implement it in practice, particularly during long-range transport (Gillani *et al*, 1978).

The Particulate-to-Total Sulphur Ratio Method

This method requires the measurement of the excess plume concentrations, S_g (gaseous sulphur) and S_P (particle sulphur), averaged over any part of the travelling plume, and subsequent evaluation of the ratio of the particle sulphur to total sulphur (S_T). The total sulphur is the summation of the gaseous and particle sulphur concentrations. This method may effectively produce the particulate concentration of the transformed sulphur oxide, but it will only be meaningful if the ground removal of sulphur is negligible compared to the rate of formation of particulate sulphur. This clause thus renders the method unsuitable for kinetic sampling since deposition rate varies from one season to another (Gillani *et al*, 1978).

The Sulphur Mass Balance Method

This method combines the principles used in the methods outlined in subsections above, by a successive measurement of the cross-sections of the downwind plume explicitly in terms

of air-borne gaseous and particulate sulphur concentrations for the particle-to-total sulphur ratio determination as well as the total sulphur removed from the plume.

This mass balance method is the most fundamental method used and it is particularly suitable for estimation of plume ground removal rates, but it requires the accurate sampling of gaseous and particle sulphur concentrations at each of several plume sections and such detailed measurements are often impractical at far downwind distances where the plume is very wide and so the accuracy of the mass determinations diminishes (Gillani *et al*, 1978).

The Aerosol Size Spectrum Kinetic Method

In this method, the growth of the aerosol volume concentration is interpreted as evidence of sulphur transformation from gas to particle (Bouland *et al*, 1978). This assumes that a known fraction of the newly formed aerosol is particulate sulphur and that the growth in aerosol volume concentration downwind, indicates the age of the plume. A limitation of this method is that a definite amount of the newly formed aerosol volume would contain varying particulate sulphur concentrations as a result of changes in meteorology; the region across which it was transported (such as over an ocean), and adsorption and desorption rates favouring the formation of other particle aerosol types (Gillani *et al*, 1978).

With this method spatial variations of growth of the aerosol volume which range only from 0 to 10 km of the transport flow pattern can be verified, but it is well known that the growth of aerosol volume could undergo substantial spatial variations resulting from changes in wind directions and altitude. Further only temporal variations occurring between 06:10 – 18:50 (which is less than a day), can be verified.

Models of downwind sulphur mass balance in smoke plumes were established in Husar *et al* (1978) and Gillani *et al* (1978) using

$$S_g + S_p = S_T \qquad (2.21)$$

where S_g, S_p and S_T are the sulphur component as gas, particles and total sulphur respectively. And the mass fraction of particle sulphur, y_p, is expressed as:

$$y_p = \frac{S_p}{S_T} \tag{2.22}$$

while the average fraction of particle sulphur, $\bar{y}_p$, is:

$$\bar{y}_p = \frac{\bar{S}_p}{\bar{S}_T} \tag{2.23}$$

where $\bar{S}_p$, and $\bar{S}_T$ are the average values of particle-sulphur and total-sulphur respectively.

For applications in urban and industrial areas, a half-life of 4 hours may be applied to the analysis of SO_2 emissions. Calculations of reaction coefficients can be used to define a "half-life" to be used in a steady-state Gaussian plume or puff model with any travel time (Freiberg, 1978).

Determination of Reaction Kinetic Parameters

The reaction rate, r_i, for the disappearance of a limiting reactant, i, based on the differential method with the assumption of a constant-density reacting fluid mixture is expressed as:

$$r_i = \frac{1}{V}\frac{dN_i}{dt} = \frac{d(N_i/V)}{dt} = \frac{dC_i}{dt} = -kC_i^n \tag{2.24}$$

Where r_i (*mol.* L^{-1} s^{-1}) is the rate of disappearance of the reactant; C_i (*mol.* L^{-1}) is the concentration of the reactant *i*; *n* (unit less) is the order of reaction, and *k* is the reaction rate constant. *k* is expressed as s^{-1} for first order reactions and *L mol.* $^{-1}$ s^{-1} for second order reactions (Levenspiel, 1999). Taking logarithms of both sides of equation (2.25) gives:

$$-\ln r_i = n \ln C_i + \ln k \qquad (2.25)$$

A plot of ln r_i against ln C_i from equation (2.25), gives a straight line with a slope equal to the reaction order, n, and an intercept equal to the reaction rate constant, k (Levenspiel, 1999; Perry and Green, 1998). The rate constant, k, which is temperature dependent for a specific pressure, is defined by the Arrhenius equation (2.26a):

$$k = k_0 \exp -\left[\left(\frac{E_A}{R}\right)\frac{1}{T}\right] \qquad (2.26)\ \text{a}$$

Where k_0 is the pre-exponential factor having the same unit as k, E_A is the energy of activation in kJ kg^{-1} and R is the universal gas constant. T is the temperature at which the reaction occurred in Kelvin. Equation (2.26a) fits experiments well over a wide temperature range and is the best model approximation for true temperature dependency (Levenspiel, 1999; Perry and Green, 1998).

In order to determine E_A, two or more rate constants and their corresponding ambient temperatures are required. If only two rate constants and their corresponding temperatures are known for a particular reaction, E_A is determined using equation (2.26b) derived from the combination of two set of equation (2.26a).

$$\ln\left(\frac{r_2}{r_1}\right) = \ln\left(\frac{k_2}{k_1}\right) = \frac{E_A}{R}\left(\frac{1}{T_1} - \frac{1}{T_2}\right) \qquad (2.26)\text{b}$$

where, r_1 and r_2 are reaction rates at temperatures T_1 and T_2 with rate constants k_1 and k_2, respectively.

Applying equation (2.26b) generates the energy of activation for the oxidation reaction. While when more than two rate constants and ambient temperatures are available for the same reactions, it is preferable to apply the method of the least squares to determine E_A.

The rate constant of a chemical transformation could be related to the conversion. Likewise, the extent of transformation, x_R, of the oxidising specie can be expressed in terms of the reactant concentrations as:

$$C_R = C_{R0}(1 - x_R) \tag{2.27}$$

where C_R is the limiting reactant concentration remaining after any given time, while C_{R0} and x_R are the initial concentration and conversion respectively of the limiting reactant due to transformation.

And the concentration of the product in terms of the disappearing reactant at any given time is expressed as:

$$C_P = C_{R0}x_R \tag{2.28}$$

where C_P is the concentration of the product formed after any given time.

Then, at equilibrium, the conversion of the limiting reactant is related to the reaction rate constant, k, according to:

$$k = \frac{C_{R0}(x_R)}{C_{R0}(1 - x_R)} = \frac{x_R}{1 - x_R} \tag{2.29}$$

Rearranging equation (2.29) in terms of the reaction rate constants gives:

$$x_R = \frac{k}{1 + k} \tag{2.30}$$

Equation (2.30) gives the extent of an oxidation when the rate constant is known.

Reaction Rate Expressed in Percent per Hour

A useful way of expressing the reaction rate of a species is by using a reactant decay rate constant. Consider an SO_2 gas-phase oxidation reaction of the form:

$$SO_2 + OH^* \rightarrow HOSO_2 \qquad (2.31)\ a$$

If the rate of reaction is second order, and the rate expression for the disappearance of SO_2 is given as:

$$r_{SO_2} = -k[SO_2][OH^*] \qquad (2.31)\ b$$

then the SO_2 conversion rate in percent per hour is determined from the rate fractional loss. The fractional loss per second is expressed as:

$$fr_{SO_2} = \frac{r_{SO_2}\Delta t}{[SO_2]} = -k[OH^*]\Delta t \qquad (2.31)\ c$$

Where r_{SO_2} and fr_{SO_2} are the conversion rate and fractional loss of SO_2. Δt is the time difference at which the conversion was achieved, k is the rate constant of the reaction and $[SO_2]$ and $[OH^*]$ are the initial concentrations of the reacting species.

Therefore, the percent loss per hour is expressed as:

$$fr_{SO_2}(\%\ h^{-1}) = -k[OH^*](100)(3600) \qquad (2.31)\ d$$

Consequently, with a $[OH^*]$ of 10^6 molecules cm^{-3} remaining constant, the percent loss per hour is obtained as:

$$fr_{SO_2}(\%\ h^{-1}) = k(10^6)(100)(3600) = 3.6x10^{11}k \qquad (2.31)\ e$$

where k is the reaction rate constant with units of cm^3 (molecule $s)^{-1}$.

2.11.2 Thermodynamic Equilibrium of Chemical Reactions

In any chemical reaction, the equilibrium relationship between reactants and products is easily modelled using two thermodynamic properties of the species involved in the reaction. These properties are the Gibbs free energy and the enthalpy of the reaction. The Gibbs free energy of formation and the enthalpy of formation are important in the analysis of chemical reactions (Elliott and Carl, 1999; Smith *et al*, 2004; Yaws, 1999). The change in the Gibbs free energy of reaction is determined from the standard Gibbs free energy of formation of the individual reactants and products involved in the reaction given by:

$$\Delta G_{rxn} = \sum \left(n \Delta G_f^0 \right)_{Products} - \sum \left(n \Delta G_f^0 \right)_{Reactants} \qquad (2.32)$$

where n is the number of moles of the reactants and products and ΔG_{rxn}, $\left(\Delta G_f^0 \right)_{Products}$ and $\left(\Delta G_f^0 \right)_{Reactants}$ are the changes in the Gibbs free energy of the reaction and the standard free energies of the products and reactants, respectively. When $\Delta G_{rxn} < 0$ kJ mol^{-1}, the thermodynamics of the system favours the chemical reaction as written and when $0 < \Delta G_{rxn} < 50$ kJ mol^{-1}, the thermodynamics of the system partially favours chemical reaction, while, for $\Delta G_{rxn} > 50$ kJ mol^{-1}, the thermodynamics for the reactions are not favourable. This change is important because it affects the chemical equilibrium for the reaction (Elliott and Carl, 1999; Smith *et al*, 2004; Satterfield, 1991; Levenspiel, 1999).

In a closed system of chemical species, at constant temperature and pressure, the total Gibbs free energy of the system is a minimum. This minimum condition can be used to determine the equilibrium concentrations of the species (Pilinis and Seinfeld, 1987; Kim *et al*, 1993a).

If the equilibrium constant relationship for the gaseous chemical component, i, is expressed in terms of the component's surface partial pressure, $p_{s,i}$, then the molality of the component, m_i, in its dissolved ionic state and the component's activity coefficient, γ_i, (that accounts for the electrostatic interaction, which at infinite dilution is equal to unity), is given by:

$$K(T,P) = \frac{p_{s,i}}{\gamma_i m_i} \tag{2.33}$$

Simplified as:

$$K_{298K}(T_0, P_0) = \exp\left[-\frac{\Delta G_{Rxn}}{RT_0}\right] \tag{2.34 a}$$

where K_{298K}, R (kJ mol^{-1}K^{-1}) and T_0, P_0 are the equilibrium constant at 298K, gas constant and the reference ambient temperature and pressure at which the Gibbs free energy and enthalpy of formation were experimentally determined for the pure component, *i*, respectively. Further simplifying equation (2.34a), gives

$$K_{298K} = \exp[-0.4036\Delta G_{Rxn}] \tag{2.34 b}$$

Equation (2.34b) describes the relationship of the equilibrium constant to the free energy of the reaction at 298K.

In order to express equilibrium constant as a function of temperature change, the enthalpy of the reaction is required. In a manner similar to the determination of the Gibbs free energy, the change in the enthalpy of a reaction, which gives the heating and cooling requirements of the system, is determined from the standard enthalpy of formation of the individual reacting species as:

$$\Delta H_{rxn} = \sum\left(\Delta H_f^0\right)_{Products} - \sum\left(\Delta H_f^0\right)_{Reactants} \tag{2.35}$$

where *n* is the number of moles of the reactants and products and ΔH_{rxn}, $\left(\Delta H_f^0\right)_{Products}$ and $\left(\Delta H_f^0\right)_{Reactants}$ are the changes in the enthalpy of the reaction and the standard enthalpies of the products and reactants, respectively. If $\Delta H_{rxn} < 0$ kJ mol^{-1}, the chemical reaction is exothermic and cooling is required to maintain the reaction temperature, while, for $\Delta H_{rxn} > 0$ kJ mol^{-1}, the reaction is endothermic and heating is required to perform the reaction (Denbigh, 1981; Elliott and Carl, 1999; Smith *et al*, 2004; Satterfield, 1991). The

enthalpy of reaction enables the prediction of the equilibrium constant at temperatures other than 298K based on the assumption of a constant change in the enthalpy of reaction within the specified temperature range according to the Van't Hoff expression given by:

$$\frac{d\ln K}{dT} = \frac{\Delta H_{Rxn}}{RT^2} \tag{2.36}$$

where K is the reaction equilibrium constant, ΔH_{Rxn} is the enthalpy of reaction, T and R are the reaction temperature and gas constant respectively.

Integrating and simplifying equation (2.36) gives

$$\ln\left(\frac{K_2}{K_1}\right) = \frac{\Delta H_{Rxn}}{R}\left(\frac{1}{T_2} - \frac{1}{T_1}\right) \tag{2.37}$$

or

$$K_{T(K)} = K_{298K}.\exp\left[-\frac{\Delta H_{Rxn}}{8.314x10^{-3}}\left(\frac{1}{T(K)} - \frac{1}{298}\right)\right] \tag{2.38}$$

Explicitly the equilibrium constant may be expressed as a function of temperature, T, and total air pressure, P, as

$$K(T,P) = K(T_0,P_0)\left(\frac{P_0}{P}\right) \text{x } \exp\left[-\frac{\Delta H^0_{f,i}}{RT_0}\left(\frac{T_0}{T} - 1\right) - \frac{C^0_{p,i}}{R}\left(1 + \ln\left(\frac{T_0}{T}\right) - \frac{T_0}{T}\right)\right] \tag{2.39}$$

At equilibrium, the ratio of the product concentration to that of the reactant equals the equilibrium constant (Satterfield, 1991; Levenspiel, 1999), that is,

$$K_{T(K)} = \frac{C_{Product}}{C_{Reactant}} = \frac{C_{PE}}{C_{RE}} \tag{2.40}$$

and the concentration of the limiting reactant at equilibrium, C_{RE}, is related to conversion as:

$$C_{RE} = C_{R0}(1 - X_{RE}) \tag{2.41}$$

where C_{R0} is the initial limiting reactant concentration, while C_{RE} and X_{RE} are the concentration remaining after any given time and conversion respectively of the limiting reactant at equilibrium.

The concentration of the product at equilibrium, C_{PE}, is expressed as:

$$C_{PE} = C_{R0}X_{RE} \tag{2.42}$$

Then, at equilibrium, the conversion of the limiting reactant is related to the reaction temperature through the equilibrium constant relationship given as:

$$K_{T(K)} = \frac{C_{R0}(X_{RE})}{C_{R0}(1 - X_{RE})} = \frac{X_{RE}}{1 - X_{RE}} \tag{2.43 a}$$

Simplifying equation (2.43a) gives:

$$X_{RE} = \frac{K_{T(K)}}{1 + K_{T(K)}} \tag{2.43 b}$$

Thermochemical Properties of Atmospheric Sulphur

Gas-phase ion chemistry has played an important role in unveiling the intrinsic chemical reactivity of simple molecules under solvent-free conditions. At the same time, considerable insight has been gained into the structure and stability of ionic species from theoretical calculations of varying degrees of sophistication that have provided a lively interplay with experiments to an extent almost unparalleled in other branches of chemistry (Morgan *et al*, 1995). The study of anions has been a particularly fruitful and challenging area of gas-phase ion chemistry despite the fact that few negative ions can be produced directly by conventional ionisation or electron attachment processes. Yet the use of continuous tailored ionic or molecular reactions has considerably broadened the horizon of the synthesis of anions in the gas-phase (DePuy *et al*, 1982; Morgan *et al*, 1995).

The rates of elementary reactions of amine radicals are important inputs when an effort is made to model the energy released during transformations as well as to predict the formation and destruction of pollutants during the combustion of fossil fuels (Linder *et al*, 1995). Such radical reactions are difficult to monitor experimentally, especially when the bimolecular partners are transient species, such as hydrogen abstraction by a hydrogen atom which is an alternative to the thermal $DeNO_x$ (NO_X removal) process where ammonia is added to stack gas for NO reduction (Linder *et al*, 1995). For over 25 years the free-radical chemistry of sulphur-containing compounds has been explored and utilised in many synthetic transformations (Sze and Malcom, 1980; Schiesser and Smart, 1995). The involvement of intermediates in the attack of radicals at sulphur atom is of theoretical (computational modelling) interest in order to establish the most appropriate pathway taken during a chemical reaction.

Overview of Computational Chemistry Modelling

In molecular structure determination and reactivity analysis using computational chemistry, two theories are of relevance. These are molecular mechanics and electronic structure theory (Foresman and Frisch, 1996). They both perform the same basic types of calculations that involve:

(a) Computing the energy of a particular molecular structure with a spatial arrangement of atoms or nuclei and electrons, and for predicting the properties related to the computed energy.

(b) Performing geometry optimisations, in order to locate the lowest energy molecular structure in close proximity to the specified starting structure. The geometry optimisations depend primarily on the gradient of the energy which is determined from the first derivative of the energy with respect to atomic positions.

(c) Computing the vibrational frequencies of molecules resulting from interatomic motion within the molecule. Vibrational frequencies depend

on the second derivative of the energy with respect to atomic structure, and the frequency calculations may also predict other properties which depend on second derivatives. Frequency calculations are not possible or practical for all computational methods.

Molecular Mechanics

Molecular mechanics simulations use the laws of classical physics to predict the structures and properties of molecules. There are many different molecular mechanics methods. Each method is characterised by its specific force field. A force field consists of a set of equations defining how the potential energy of a molecule varies with the locations of its component atoms and a series of atom types defining the characteristics of an element within a specific chemical context. Atom types exhibit different characteristic behaviours for an element depending upon its environment. For example, a carbon atom in a carbonyl compound shows different behaviour than a carbon atom would if it were bonded to three hydrogen atoms. The atom type depends on hybridisation, charge and the type of the other atoms to which it is bonded. Thirdly a force field may be one or more parameter sets that fit the equations and atom types to experimental data. The parameter set defines the force constants (which are values used in the equations to relate atomic characteristics to energy components), and structural data such as bond length and angles.

Molecular mechanics calculations do not explicitly treat the electrons in a molecular system but perform computations based upon the interactions between the nuclei. Electronic effects are included in the force field through parameterisation. This renders computational approximations with molecular mechanics inexpensive and hence allows for the computation of very large systems containing many thousands of atoms. However, each force field achieves good results only for a limited class of molecules, related to those for which it was parametised. Also, no force fields can be generally used for all molecular systems of interest. Since electrons are neglected, it then means that molecular mechanics cannot treat chemical problems where electronic effects predominate. In addition molecular mechanics cannot describe processes with bond formation or breaking and it is

unable to reproduce molecular properties which depend on subtle electronic details (Foresman and Frisch, 1996).

Electronic Structure Methods

Electronic structure methods use the laws of quantum mechanics rather than classical physics as the basis for their computations. Quantum mechanics states that energy and other related properties of a molecule may be obtained by solving the Schrödinger equation which lies at the heart of much of modern science (Foresman and Frisch, 1996). It is simply expressed as:

$$\mathbf{H}\Psi = E\Psi \qquad (2.44)$$

Where Ψ is the known as the Schrödinger wave function, **H** is the Hamiltonian operator for a quantum harmonic oscillator and E is the energy (potential and kinetic) for the system.

For any but the smallest systems, exact solutions to the Schrödinger equation are computationally practical while, for larger molecules, mathematical approximations to the Schrödinger equation are feasible using the electronic structure methods. There are two major classes of electronic structure methods. The first class of electronic structure method is the semi-empirical methods such the AM1, MINDO/3 and PM3, implemented in computer programs. Their solutions of the Schrödinger equation depend on having all the appropriate parameters for the chemical system under investigation. The second class of electronic structure method is the *ab initio* methods. These methods -unlike the molecular mechanics or semi-empirical methods- use no experimental parameters in their computations. Instead, their computations are based solely on the laws of quantum mechanics (the **first principles** also called ***ab initio***) and on the speed of light, Planck's constant and the masses and charges of electrons and nuclei.

The *ab initio* methods are more computationally cost-effective and accurate than the semi-empirical methods. They provide high quality quantitative predictions of a broad range of

systems. They are not limited to any specific class of system. They can predict structures of molecules having as many as one hundred atoms (Foresman and Frisch, 1996).

Density Functional Methods

A third class of electronic structure methods presently in wide use is the density functional theory (DFT) methods. These DFT methods are similar to the *ab initio* methods in that their calculations take about the same amount of computational resources as the Hartree-Fock (HF) theory, which is the least expensive *ab initio* method.

The DFT methods include effects of energy parameters in the overall functional that accounts for electron correlation (that electrons in a molecular system react to one another's motion and attempt to keep out of one another's way) in the model. The Hartree-Fock method considers this effect only in an average sense (that each electron reacts to an average electron density) while methods including electron correlation account for the instantaneous interactions of pairs of electrons with opposite spin. The approximation causes Hartree-Fock results to be less accurate for some types of systems (Foresman and Frisch, 1996).

Computational Model Chemistries

The implementation of a theoretical model to produce an approximate solution to the Schrödinger equation is termed a theoretical model chemistry or simply model chemistry. Model chemistries are characterised by the combination of theoretical procedure and a basis set. Some model chemistries implemented in the Gaussian program include the Hartree-Fock self-consistent field (SCF) denoted as HF, second order Møller-Plesset Perturbation theory expressed as MP2, fourth order Møller-Plesset theory (including singles, doubles, triples and quadruples) defined by MP4, quadratic correlation interaction (with singles, doubles and triples) as QCSID(T) and the Becke-style-3-parameter DFT method (using the Lee-Yang-Parr correlational functional).

Basis Set

A basis set is a mathematical representation of the molecular orbits within a molecule. It restricts each electron to a particular region of space. Larger basis sets impose fewer constraints on electrons and more accurately approximate exact molecular orbitals. The higher the basis set, the more the computational requirements (Foresman and Frisch, 1996).

High Accuracy Energy Models

A variety of high energy accurate methods developed from a combination of several model chemistries to accurately predict thermochemical quantities are referred to as the compounded methods. They are most important as they combine the accuracies of the various traditional model chemistries in the computation of basic thermochemical results such atomisation energies, ionisation potentials, proton and electron affinities (Foresman and Frisch, 1996). These models include the Gaussian-n methods (such as the G1, G2 and G3) as well as the complete basis set methods (CBS-4 and CBS-QCI).

Compounded ab initio Methods

Improvements in computers, numerical computer programs and the theoretical methods have increased the accuracy of *ab initio* calculations of molecular energies including electron correlation for many small-, medium- and large-molecules (Nyden and Petersson, 1981; Petersson and Al-Laham, 1991; Petersson *et al*, 1991; Montgomery *et al*, 1994; Ochterski *et al*, 1996). The self-consistent field (SCF), multiconfiguration self-consistent-field (MCSCF) and potential energy surface (which are increasingly available for small molecules) have been improved upon by estimating the error resulting from the MCSCF calculation and can provide a more accurate potential energy surface than the *ab initio*

calculations alone (Nyden and Petersson, 1981). For moderately large molecules, the configuration interaction (CI) and many-body perturbation theory (MBPT) have been sufficiently refined that the major error in most *ab initio* calculations of the molecular correlation energies is now the truncation of one-electron basis set. When applied to closed-shell systems, the simple second order Møller-Plesset (MP2) theory recovers over 90 % of the total correlation energy for the basis set used. However, obtaining over 90 % of the exact correlation energy requires the use of a large basis set including the *f* basis functions (Petersson and Al-Laham, 1991). The slow convergence of pair energies with the basis set extrapolation makes a method of extrapolation highly desirable. Hence it could be said that the major source of error in *ab initio* calculations of molecular energies is the truncation of the one-electron basis set. The truncation errors are corrected using a complete basis set (CBS) model chemistry based on the unrestricted Hartree-Fock (UHF) zero-order wave function. The total correlation energy is calculated using the unrestricted Møller-Plesset perturbation theory, the quadratic configuration interaction (QCI) method and the CBS extrapolation (Petersson and Al-Laham, 1991). These models use basis sets ranging from small 6-31G* double zeta plus polarisation (DZ+P) basis sets to very large atomic paired natural orbital (APNO) basis sets. The CBS methods run at more than ten times the computing speed of compounded methods Gaussian-1 (G1) and Gaussian-2 (G2) (Petersson *et al*, 1991). The G1 and G2 have also been used for computing *ab initio* energies due to their high level correction (HLC). They have also been used to calculate thermochemical properties of molecules with additional basis sets such as the atomic natural orbital (ANO) and Dunning correlation consistent basis sets (*cc-p* VTZ and *cc-p* VQZ). In a similar fashion, the CBS was also improved with the addition of a combined configuration interaction/atomic pair natural orbital as (CBS-QCI/APNO) (Montgomery *et al*, 1994).

Evaluating Model Chemistries

The Gaussian Theories

The Gaussian-1 (G1) and Gaussian-2 (G2) theories are two general procedures for computing the total energies of molecules at their equilibrium geometries. Both consist of several component calculations whose results are then combined in a pre-defined way (Foresman and Frisch, 1996).

The G1 procedure for total energy evaluation is:

(a) Produce an initial equilibrium structure at the Hartree-Fock level using the 6-31G(d). Verify that it is a minimum with a frequency calculation and predict the zero-point energy (ZPE).

(b) Beginning with the final optimised structure from step (a), obtain the final equilibrium geometry using the full MP2 method using the 6-31G(d) again. This geometry is used for all subsequent calculations.

(c) Compute a base level energy, E^{base}, using the MP4/6-311G (d,p) at the optimised geometry from step (b). Various corrections will be made to this energy in subsequent steps.

(d) Correct the base energy by including diffuse functions on a second energy calculation by computing the MP4/6-311+G(d,p) energy, then subtracting the base energy, E^{base}, from this energy to obtain ΔE^{+}.

(e) Correct the base energy with higher polarisation functions on heavy atoms by computing the MP4/6-311G(2df,p) energy and subtracting the base energy, E^{base}, from this energy to obtain ΔE^{2df}. If ΔE^{2df} is positive (meaning the additional polarisation function produced a higher energy than resulted without it), set this term to zero.

(f) Correct the base energy for residual correlation effects (to counteract known deficiencies of truncating perturbation theory at fourth order) by computing the QCSID(T)/6-311G(d,p) energy. Subtracting E^{base} from this energy produces ΔE^{QCI}.

(g) Correct the energy from step (f) for remaining basis set deficiencies by empirically estimating the remaining correlation energy between spin-paired electrons with the formula:

$\Delta E^{HLC} = -0.00019 n_\alpha + -0.00595 n_\beta$

where n_α and n_β are the number of alpha (NOA) and beta (NOB) electrons in the molecule, respectively. This energy term is known as the higher level correlation. By convention, n_α is greater than n_β for a system with an odd number of electrons. The energy corrected through this process is the G1 value for the electronic energy, denoted as E^{G1}. The expression for the G1 energy is given as:

$$E^{G1} = E^{base} + \Delta E^{+} + \Delta E^{2df} + \Delta E^{QCI} + \Delta E^{HLC} + ZPE$$

The G2 theory includes some additional corrections to the G1 final result. The major term is a correction at the MP2 level described as step (h):

(h) Perform an MP2/6-311+G(3df,2p) energy calculation and use this energy to correct the G1 energy according to the formula:

$$\Delta^{G2} = (\Delta^{+2df} - \Delta^{+} - \Delta^{2df}) + \Delta^{3d2p}$$

The terms in the parenthesis correct for the G1 energy.

(i) The G2 theory makes a modification to the higher-level correction of G1 theory by adding 0.00114 n_β, into the final energy calculation (which is denoted as ΔE^{HLC}).

The final G2 energy is computed as: $E^{G2} = E^{G1} + \Delta^{G2} + \Delta^{HLC}$

Complete Basis Set Methods

The complete basis set (CBS) methods (as in the G2 theory), compute the total energy from the results of a series of calculations. The component calculations are defined based on principles and observations.

(a) The successive contributions to the total energy generally decrease with order of perturbation theory, while the computational requirement increases rapidly. For example, in order to compute the dissociation energy for O_2 to within $0.64\ kcal\ mol^{-1}$, the self-consistent field (SCF) energy must be corrected to six figures, the MP2 contribution must be corrected to three figures. Lastly the contribution from higher orders of correlation need only be corrected to two figures. The CBS models take advantage of these complementary trends by using progressively smaller basis sets as the level of theory increases.

(b) The CBS models use known convergence of paired natural orbital expansions to extrapolate from calculation using a finite basis set to the estimated *complete basis set limit*.

The CBS models typically include an HF calculation with a very large basis set, followed by an MP2 calculation with a medium-sized basis set and one or more higher-level calculations with a medium-to-modest basis set as given in Table 2-3. The CBS-4 is the less expensive of the two methods. It begins with an HF/3-21G(d) method to compute the geometry optimisation and the zero potential energy. Then, via the same method, using a large basis set, the SCF is computed as a base energy and an MP2/6-31+G calculation with a CBS extrapolation is performed to correct the energy through a second order correlation. An MP4(SQD)/6-31+G(d,p) calculation is used to approximate the higher order contributions. In a similar manner, the CBS-Q is as specified in Table 2-3.

Table 2-3: Components of the complete basis set methods

Energy component	CBS-4	CBS-Q
Optimised geometry	HF/3-21G(d)	HF/6-31G(d)
ZPE (scale factor)	HF/3-21G(d) (0.91671)	HF/6-31G (0.91844)
SCF energy	HF/6-311+G(3d2f,2df,p)	HF/6-311+G(3d2f,2df,2p)
Second order correlation	MP2/6-31+G	MP2/6-311+G(3d2f,2df,2p)
CBS extrapolation	≥5 configurations	≥10 configurations
Higher order correlation	MP4 (SQD)/6-31+G(d,p)	MP4 (SQD)/6-31+G(d(f),d,f) QCISD(T)/6-31+G

Source: Foresman and Frisch (1996)

Analysis of Molecular Configurations of Atmospheric Sulphur

An adequate description of the geometry and electronic properties of sulphur-containing compounds can be obtained from theoretical model calculations (Alkorta, 1994). Since sulphur is commonly found in atmospheric gases and aerosols together with numerous gas-phase oxidants and their precursors, it would be interesting to determine the properties of these compounds using methodologies such as *ab initio*, density functional theory (DFT) and semi-empirical methods. Alkorta 1994 reported the geometric and electronic properties of a number of sulphur derivatives determined using semi-empirical methods carried out at the PM3 level, *ab initio* molecular orbital methods carried out at the Hartree-Fock (HF) and second order Møller-Plesset (MP2) levels and local density functional (LDF) methods. It was observed that the semi-empirical methods yielded a very poor description of the properties, while the *ab initio* methods at the HF and MP2 levels best described the geometries and dipole moments, respectively, and the LDF method was good only for

highly accurate dipole moments. *Ab initio* calculations have been performed on other sulphur-containing compounds (Table 2-4) -such as anions of halosulphites- to describe the geometry optimisation for potential energy surfaces and total energies that are essential for the calculations of reaction enthalpies and free energies (Sapse and Jain, 1985; Schreiner *et al*, 1993; Maulitz *et al*, 1995).

Table 2-4: Structural configuration for sulphur oxide

Compound	Experiment	MP2	HF
$S-O$	1.55[a]	1.51[b]	
$O-S-O$		120[c]	119.1[c]

Sources:* [a,b]*Alkorta, 1994;* [c]*Maulitz* et al*, 1995.

It is possible to obtain an adequate description of the geometric and electronic properties of sulphur-containing compounds (Alkorta, 1994). Since sulphur is commonly found in organic molecules, including numerous inorganic compounds in the atmosphere, it is necessary to have reliable and inexpensive methods to calculate the properties of these compounds. Alkorta, (1994) reported that the semi-empirical (PM3) method poorly describes the geometry and, particularly the electronic properties of sulphur-containing compounds. MP2 calculations yielded improved values generated by the HF method with a basis set of 6-31*. He noted that the local density functional method best predicts the electronic distribution of sulphur-containing compounds while yielding high bond lengths.

Sulphur compounds and, in particular, sulphur-contained radicals play important roles in atmospheric chemistry and environmental science (Sze and Malcom, 1980; Chatgilialoglu and Asmus, 1990; Chatgilialoglu *et al*, 1999; Alfassi, 1999). As a consequence, much attention has been paid to the thermochemistry of these species. Techniques such as calorimetry, mass spectrometry, laser photodetachment, electrochemistry, and pulse radiolysis have provided a wealth of gas-phase and solution data in terms of heats of combustion and formation, bond dissociation energies, electron affinities, ionisation and reduction potentials. Extensive compilation and analysis have been done on these data (Benson 1978; Lias *et al*, 1985; Armstrong, 1999; Chatgilialoglu and Asmus, 1990;

Chatgilialoglu *et al*, 1999; Alfassi, 1999). Despite intensive research in the chemistry of sulphur compounds, no report has appeared to date on the thermochemistry of the numerous intermediate species participating in atmospheric chemical transformations (Calvert *et al*, 1978; Warneck 1988; 1999; Herrmann *et al*, 2000; Grgic and Bercic, 2001; Podkrajsek *et al*, 2004; Brytenbach *et al*, 1984; Pienaar and Helas, 1996; Eggleton and Cox, 1978; Hegg and Hobbs, 1980; Seinfeld and Pandis, 1998; Larsen *et al*, 2001). Quantum-mechanical calculations have shown that the ground state of gaseous and aqueous-phase sulphur dioxide corresponds to an excited state located at significantly higher energy (McKee, 1996).

Overwhelmingly the analyses of chemical reactions for atmospheric sulphur through computation of thermochemical properties, provides other avenue for establishing the speciation of the relevant sulphur compounds. It was also designed to produce an order of importance of the known reactions expected over the study area since chemical reactions are strongly temperature dependent.

To further understand the contributions of chemical transformation on the budget of atmospheric sulphur, horizontal spatial distribution resulting from diffusion is an important step required. In the other sections of this chapter, the relevant literature on air pollution transport required, for the evaluation of atmospheric diffusion will be discussed.

2.12 Transport Models

Air mass trajectories have been used extensively to qualitatively and quantitatively relate atmospheric SO_4^{2-} concentrations to SO_2 emissions (Galvin *et al*, 1978, Husain *et al*, 1984; Husain and Dutkiewicz, 1990; Bari *et al*, 2003b). Emissions from a point-, area- or volume-source in a smoke plume assumes the shape and pattern of an unconfined tubular flow reactor system with horizontal and vertical dispersion, and with advection across the mixed layer height. This is because the concentration variation occurs with air mass transport, transformation and deposition in the along-wind direction.

Acid deposition and photochemical smog are urban air pollution and remain localised as long as sulphur, nitrogen and hydrocarbon emissions are mainly confined to the lower troposphere (below 1 km altitude) where they are short-lived. In this atmospheric sub-layer, the PBL friction with the Earth's surface reduces wind speeds and temperature inversions. This often isolates the air at the top of the PBL from the rest of the troposphere, especially the region that extends from the surface to about 14 km which is essentially where the weather occurs. Some emission sources (volcanoes) allow a rapid vertical transport of air pollutants to the upper troposphere. In this sub-layer, the wind speeds are higher than those of the lower troposphere, thereby increasing pollutants' atmospheric residence times and their influence expands dramatically from local to regional and global atmospheric chemistry problems. Thunderstorms have also been observed as a means of vertical pollutant transport (Dickerson *et al*, 1987). It was observed that some of the effect of acid deposition is ameliorated by vertical transport as atmospheric acids were diluted via thunderstorms. Vertical transport of air pollutants between atmospheric layers is generally slow because the atmosphere is subjected to vertical perturbations (eddy diffusion) under certain conditions (Dickerson *et al*, 1987).

Long-Range Transport Models

An urban air quality simulation model can be used to study the complex relationships between source emissions and ambient concentrations and the dependence of these relationships on the meteorological and urban surface conditions (Shir and Shieh, 1978). The development of such models depends on current knowledge of urban air pollutant transport, on the diffusion mechanism, and on the availability and quality of source emission, meteorological, and surface condition data. The effect on SO_2 concentration in an urban area has been modelled using numerical integration with flexibility for spatial and temporal variation of meteorological variables and surface conditions (Shir and Shieh, 1978). Long-range continental transport of sulphur has been quantified using a simple diffusion trajectory model with fixed mixing height (Szepesi, 1978; Fay and Rosenzweig, 1980; Eliassen and Saltbones, 1983). Also developed is a three-dimensional long-range

Eulerian transport and transformation model to simulate tropospheric sulphur (Carmichael and Peters, 1984a; 1984b; Benkovitz *et al*, 1994).

2.12.1 Air Pollution Dispersion

Industrial effluents from combustion processes are discharged through smoke stacks. Plumes from smoke stacks consist of micron and submicron particles such as fly ash, metallic compounds, and water vapour immersed in flue gas (Emberlin, 1980a; 1980b). The plume from the stack expands and mixes with ambient air which dilutes the effluents. Wind speed affects the rate of mixing. An increase in wind speed will increase the dilution downwind, thereby lowering the concentration, while increasing the volume of the plume. In addition, the increase in wind speed will decrease the plume rise by bending the plume over more rapidly and will increase the horizontal displacement. The volume of the plume depends on the stability of the atmosphere which is a function of the wind speed and the kinematic viscosity of the plume effluent. As the plume effluent temperature decreases downwind, the kinematic viscosity reduces resulting in an increase in the turbulence of the transported plume. The more unstable the atmosphere, the greater the turbulence and increase in the dilution. An increase in the turbulent diffusion causes the pollutants to become more dispersed (Pasquill, 1974; Briggs, 1969). The dispersed plume experiences both horizontal and vertical movement. The horizontal displacement is due to wind speed (horizontal component) while the vertical rise is due to buoyancy, wind speed (vertical component), smoke plume exit velocity and exit temperature.

The buoyancy is the mass fraction ratio of the mass of the exit gas to the mass of the surrounding air. A plume is more buoyant when the mass of the exit gas is less than the mass of the surrounding air. The buoyancy of the plume depends on its exit temperature. When the gas exit temperature is greater than the ambient air temperature, the plume has positive buoyancy which is the common state. Another parameter responsible for the flow pattern of the plume is the gas exit velocity. It is a measure of the vertical inertia. An increase in exit velocity will increase the vertical inertia which leads to higher plume rise (Briggs, 1969).

The understanding and prediction of the impact of emissions from various sources rely essentially on the basic ability to model convective-dispersive transport of air pollutants released from point- and distributed-sources.



Figure 2-10: Two air pollution sources at the Elandsfontein area on the Mpumalanga Highveld

Classification of Emission Sources (Types and Patterns)

The movement of air masses from ground and elevated sources is accompanied by emissions into the atmosphere (Figure 2-10). Atmospheric pollutants are introduced from one or more of line-, point-, area-, or volume-sources (Zib, 1977). These source types are classified by number, size or capacity and configuration. The sources could also be ground-based or elevated and stationary or mobile.

The concentration distribution of a plume from a single elevated or ground source has been well established. However, the phenomena from multiple elevated and ground sources over inhomogeneous surfaces are relatively complex. Thus a systematic study of the concentration distributions under various meteorological and surface conditions is necessary.

Plume Types and Behaviour

Atmospheric stability is a key factor of plume behaviour and dispersion characteristics. The shape of a smoke plume undergoing dispersion, depending on atmospheric stability could assume any of the patterns shown in Figure (2-11). These variations in shape are functions of the wind speed, vertical temperature profile and atmospheric stability (Tyson and Preston-Whyte, 2000).

Looping plumes (Fig. 2-11a), which occurs in unstable air, and fumigating plumes (Fig. 2-11e), that occurs when the air is stable above the emission point, produce the highest ground-level concentration of pollutants. Coning and fanning plumes (Figs. 2-11b and 2-11c) tend to carry pollutants great distances in a relatively undiluted form, while lofting plumes (Fig. 2-11d) disperse emissions both vertically and horizontally since plume is released above the surface inversion (Pretorius *et al*, 1986).

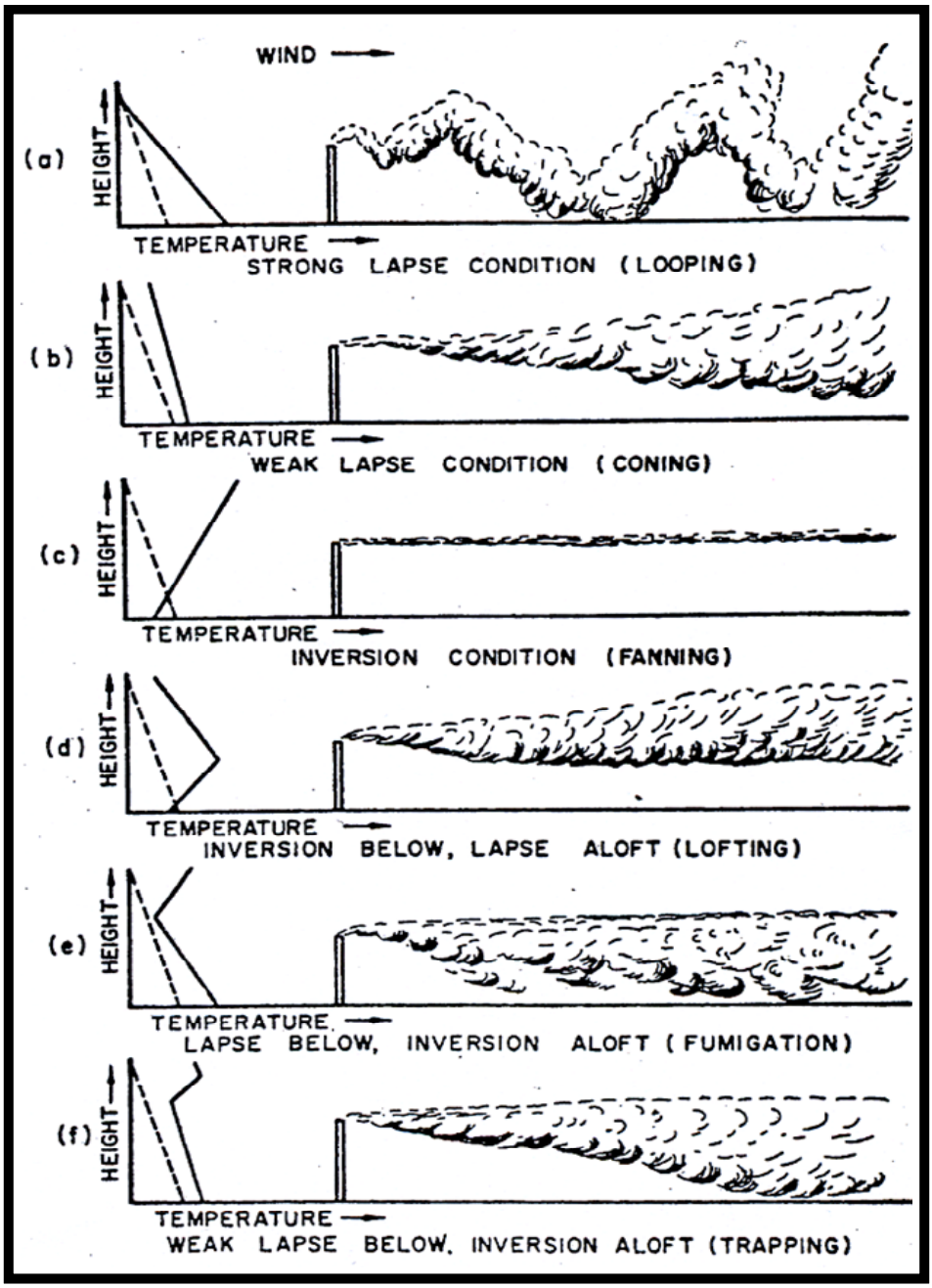

(Source: Pretorius *et al*, 1986)

Figure 2-11: Typical plume shapes with wind and temperature profiles

Determination of Atmospheric Boundary Layer Parameters

The expressions for calculating the PBL parameters for convective (day time) and stable (night time) boundary layers are provided in this section. In the evaluation of the convective boundary layer, the overall heat flux, H, was determined from the heat balance formula (Oke, 1987; Cimorelli *et al*, 2004) simplified as:

$$H = 0.4R_n \tag{2.45}$$

where R_n (W m^{-2}) is the net radiation. Equation (2.45) assumes that the soil heat flux is 10 % of the net radiation (Holtslag and Van Ulden, 1983) and 0.8 for the Bowen ratio for grassland as given by Oke (1987). The frictional velocity u_* (m s^{-1}) and Monin-Obukhov length L (m) are interrelated parameters. For the convective boundary layer, they are calculated with methods described in literature (Holtslag and Van Ulden, 1983; Panofsky and Dutton, 1984; Van Ulden and Holtslag, 1985; Perry, 1992):

$$u_* = \frac{ku_z}{\ln(z/z_0) - \psi_m\{z/L\} + \psi_m\{z_0/L\}} \tag{2.46}$$

where, for $L < 0$ and $0 < -z/L < 30$

$$\psi_m = (1 - 16z/L)^{1/4} - 1 \tag{2.47}$$

And, for $L < 0$ and $-z/L \geq 30$

$$\psi_m\left\{\frac{z}{L}\right\} = 2\ln\left(\frac{1+\mu}{2}\right) + \ln\left(\frac{1+\mu^2}{2}\right) - 2\tan^{-1}\mu + \pi/2 \tag{2.48a}$$

where $\mu = \left(1 - 16\frac{z}{L}\right)^{1/4}$ (2.48b)

$$\psi_m = -5z/L \quad \text{for } L > 0 \tag{2.49}$$

where k is von Karman's constant ($k = 0.41$), and ψ_m and μ are dimensionless quantities. A reference height for wind $z = 10$ m, is conventional for measurements for surface meteorology. Also applicable to dispersion over the South African Highveld (which is dominated by grassland) is roughness height, $z_0 = 0.05$ m, while, for tall grasses, it could range between 0.25 and 1.0 m (Oke, 1987; Seinfeld and Pandis, 1998). u_z is the wind speed at reference height, z. u_* (frictional wind speed) is the speed resulting from shear forces within air stream layers. It is determined by initially assuming a neutral condition with $\psi_m = 0$ and obtaining an initial u_* using equation (2.46). With u_* determined, the Monin-Obukhov length, L^N, was calculated from equation (2.50) (Holtslag and Van Ulden, 1983; Wyngaard, 1988) as:

$$L^N = -324.75\frac{T\mu_*^3}{H} \tag{2.50}$$

where T is ambient temperature in Kelvin at height, z

The calculated L^N was then substituted as L into equation (2.50) and a new friction velocity, u_*^{N+1}, was calculated which was used to calculate the new Monin-Obukhov length, L^{N+1}. This iteration continued until the conditions of equations (2.51) and (2.52) were satisfied.

$$\left|u_*^{N+1} - u_*^N\right| \leq 0.05 \tag{2.51}$$

and

$$\left|L^{N+1} - L^N\right| \leq 0.05 \tag{2.52}$$

The time-dependent convective mixing heights for unstable, h_{us}, and neutral, h_n, conditions were calculated from the combination of a number of energy balance model rate equations discussed in Deardorff *et al (*1980); Venkatram (1980a); Van Ulden and Holtslag (1985); Garratt (1992) and Cimorelli *et al* (2004) utilising morning potential temperature sonding before sunrise as well as the hourly changing surface heat flux. The daytime

mixing height as a function of the changing heat flux and frictional velocity is expressed by equation (2.53) for unstable conditions and equation (2.54) for neutral conditions:

$$h_{us} = \left(2.72x10^{6} u_{*}^{2} \{\psi_{m} = 0\} + \frac{2.68x10^{-2}}{u} \sum_{0}^{t} H \right)^{1/2} \quad \text{if} \quad \left| u_{*} /(fL) \right| \geq 4 \qquad (2.53)$$

$$h_{n} = 2400 u_{*}^{3/2} \quad \text{if} \quad \left| u_{*} /(fL) \right| < 4 \qquad (2.54)$$

Where f is the Coriolis parameter estimated as 1.2×10^{-4} s^{-1} for the grassland area applicable to the Highveld, t (h) is the time of day and u (m s^{-1}) is the mean wind velocity. The convective velocity scale, which is required as a result of turbulent eddies in the vertical dispersion profile, can be evaluated using the expression for the buoyant production of turbulent kinetic energy (Van Ulden and Holtslag, 1985). It is determined using the calculated h_{us}, depending on the L obtained, using equation (2.55) as:

$$w_{*} = 1.96x10^{-1} \left(\frac{h_{us} H}{T} \right)^{1/3} \qquad (2.55)$$

The stable (night time) boundary layer parameters can be evaluated starting with u_{*} based on the works of Venkatram (1980a); (1980b); Panofsky and Dutton (1984); Garratt (1992); Hanna and Chang (1993) and Cimorelli *et al (*2004). Thereafter, the night-time temperature scale, which varies very little, is related to the heat flux by equation (2.56):

$$\theta_{*} = -H / \rho C_{p} u_{*} \qquad (2.56)$$

where C_p is the specific heat of air at constant pressure, given as 1010 J kg^{-1} K^{-1} and ρ is the density of air estimated as 1.2928 kg m^{-3} (Oke, 1987; Seinfeld and Pandis, 1998; Tyson and Preston-Whyte, 2000). Equation (2.56) is simplified by the empirical expression of Van Ulden and Holtslag (1985) to be:

$$\theta_{*} = 0.09(1 - 0.5n^{2}) \qquad (2.56)\ \text{a}$$

where $n \leq 0.25$, $0.25 < n < 0.75$, and $n \geq 0.75$ indicate clear skies, intermediate cloudy skies and cloudy skies, respectively. For the Mpumalanga Highveld subregion, θ_* was estimated to be between 0.08 and 0.09 due to the abundance of clear to partially cloudy days throughout the year. Since stable conditions occur predominantly at night with occasional neutral conditions, the frictional velocity u_* for night-time was simplified as:

$$u_* = 3.78x10^{-2}u \tag{2.57}$$

After verifying the conditions given by Hanna and Paine (1987) and Cimorelli *et al* (2004) on $[(\theta_*)(u_*)]$, the sensible heat flux, H, is calculated from equation (2.58). When $[(\theta_*)(u_*)] > 0.05$ m s^{-1}K, then θ_* was made equal to $0.05/u_*$ and u_* recalculated until $[(\theta_*)(u_*)] \leq 0.05$ m s^{-1}K. With an acceptable u_*, H is determined, using equation (2.58):

$$H = -104.46u_* \tag{2.58}$$

The Monin-Obukhov length, L, is calculated for night-time conditions with known u_* and H using equation (2.58). In a similar pattern, the night-time mixing heights for neutral, h_n, and stable, h_s, conditions were calculated applying Venkatram's (1980a) approximation and Zilitinkevich's (1972) expression given as:

$$h_n \cong 2400u_*^{3/2}\{\psi_m = 0\} \qquad \text{if} \qquad |u_*/(fL)| \geq 4 \tag{2.59}$$

$$h_s = 36.4\left(Lu_*\{\psi_m = 0\}\right)^{1/2} \qquad \text{if} \qquad |u_*/(fL)| < 4 \tag{2.60}$$

2.12.2 Air Quality Dispersion Models

The behaviour of trace species in the atmosphere is commonly described by the mathematics of the horizontal and vertical spatial and temporal distribution of emitted materials (Wayne, 2000). A dispersion model is a computer simulation that uses mathematical equations to predict air pollution concentrations based on weather, topography, and emission data (EPA, 1995a; 1995b). Air pollutants are transported primarily by advection, that is, by the mean or bulk motion of air downwind. Detailed wind

fields (horizontal and vertical) are important variables that indicate the variations in wind which influence the degree of mixing of emissions and, subsequently, advection downwind and dilution (Pasquill, 1974).

A modelling analysis begins with establishing a network of points throughout the air quality modelling area (AQMA) called receptors. This is followed by specifying the available diffusion, boundary layer variables, and transformation mechanisms for the chemically reactive species. Model development for concentration distribution in an air mass has been used for all forms of atmospheric transport processes (EPA 1995a; 1995b; ENVIRON, 1998). A few models concerning the dispersion of atmospheric pollutants are discussed in the next section.

In the work of Eliassen and Saltbones (1983), sulphur dioxide and sulphate depositions were predicted reasonably well using a dispersion model. But the model predicted the seasonal variation less accurately due to the use of constant mixing heights in addition to low reaction rate assumptions for different seasons. In addition no definite mechanism for the exchange of air between the boundary layer and the free troposphere was considered. Benkovitz *et al* (1994) developed a three-dimensional Eulerian transport and transformation model to simulate tropospheric sulphur. The model represents emissions of anthropogenic and biogenic SO_2, sulphate and other sulphur species with horizontal and vertical transport. Also considered were the gas-phase oxidation of SO_2 and dimethyl sulphide; the aqueous-phase oxidation of SO_2, and the wet- and dry-deposition of SO_2, sulphate and methanesulfonic acid. Atmospheric diffusion with chemical reactions and removal mechanisms for sulphur species have also been evaluated and applied to sulphur distribution with advection by Carmichael and Peters (1984a; 1984b).

2.12.3 Atmospheric Diffusion Principles and Mechanisms

Air flow in the atmosphere is predominantly turbulent. Turbulent diffusion (also called dispersion) is proportional to the concentration gradient. The proportionality factor is the coefficient of eddy diffusivity (K) (Seinfeld and Pandis, 1998). The driving force to dispersion is the variation in the diffusivity. It is an important parameter considered in the

development and evaluation of a dispersion models. For more accurate concentration estimation, it designed to account for dispersion in the along-wind, horizontal and vertical wind directions. Atmospheric diffusion is described either using the Lagrangian diffusion models or the Eulerian (mass balance) diffusion model. In the Eulerian model, air pollutants released from a source is considered as undergo chemical transformation together with dispersion. During advection similar materials are introduced from sources other than the original. These additional input sources are accounted for by a total material balance taking the entire mixing zone as the reactor volume. Since both diffusion model systems are the established method, and due to measurement constraints, the Lagrangian method will be considered for the study.

Lagrangian Diffusion Models

The most common form of the Lagrangian model is the Gaussian model. It uses specific input parameters for topographical and meteorological conditions (such as wind speed and direction, atmospheric stability, ambient temperature, and stack gas properties) to estimate the downwind concentration distribution.

Gaussian Theory

Until the development of the Eulerian model (Carmichael and Peters, 1984a; 1984b), atmospheric dispersion modelling of pollutants in the vertical and horizontal (crosswind) directions were commonly solved using the Gaussian models. The Gaussian models are based, in principle on the condition that the atmospheric dispersion of an airborne plume from a point source is typically described by the form shown in Figure (2-12). This model predicts an average concentration under steady- and unsteady-state conditions.

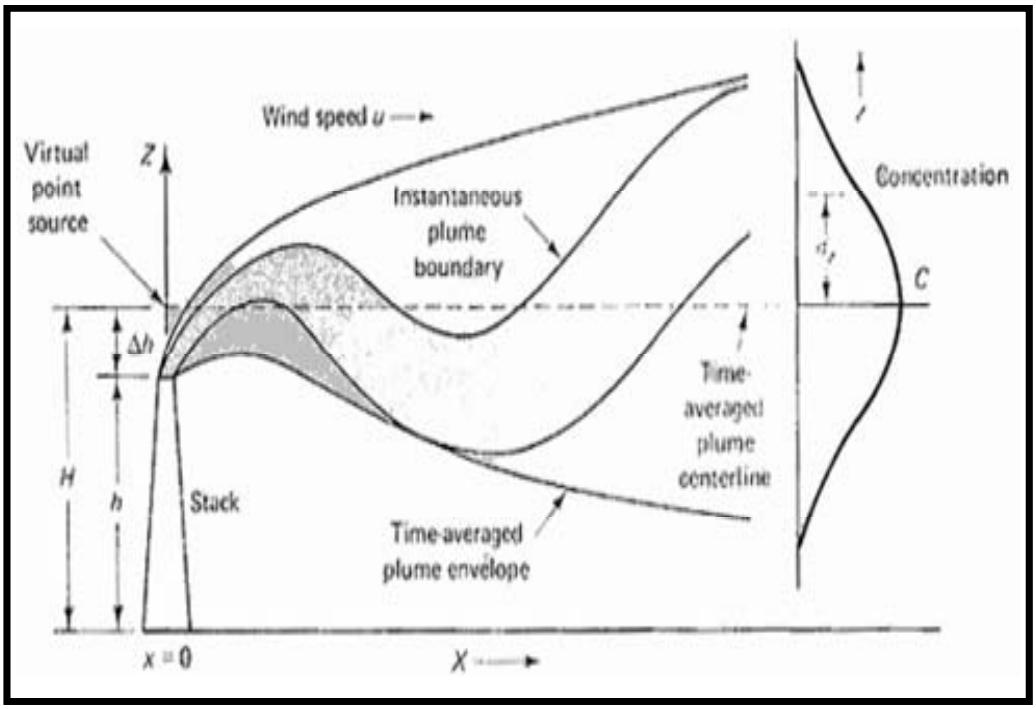

(Source: http://cities.poly.edu/environment/gradedu/ce752/ce752_airmodeling.html)
Figure 2-12: Plume boundary and time-averaged envelope

Gaussian Models

The Gaussian plume model is the most widely used computational approach to calculating the mass concentration of an airborne pollutant from a particular point source (Harrison and McCartney, 1980; Tyson and Preston-Whyte, 2000). This model describes the transport and mixing of the pollutants. It assumes dispersion in the horizontal and vertical direction will take the form of a normal or Gaussian curve with the maximum concentration at the centre of the plume (Figure 2-13).

In Figure (2-13), the orange object is the smoke stack, **A** is the physical stack height and **H** is the effective stack height. The red curves represent dispersion in the horizontal direction and the blue curves represent dispersion in the vertical direction. There are two curves for each colour to illustrate that the Gaussian curve can be narrow or wide, but still have the same area under the curve. That is, curve $(y'y')$ will have same area as curve $(y''y'')$.

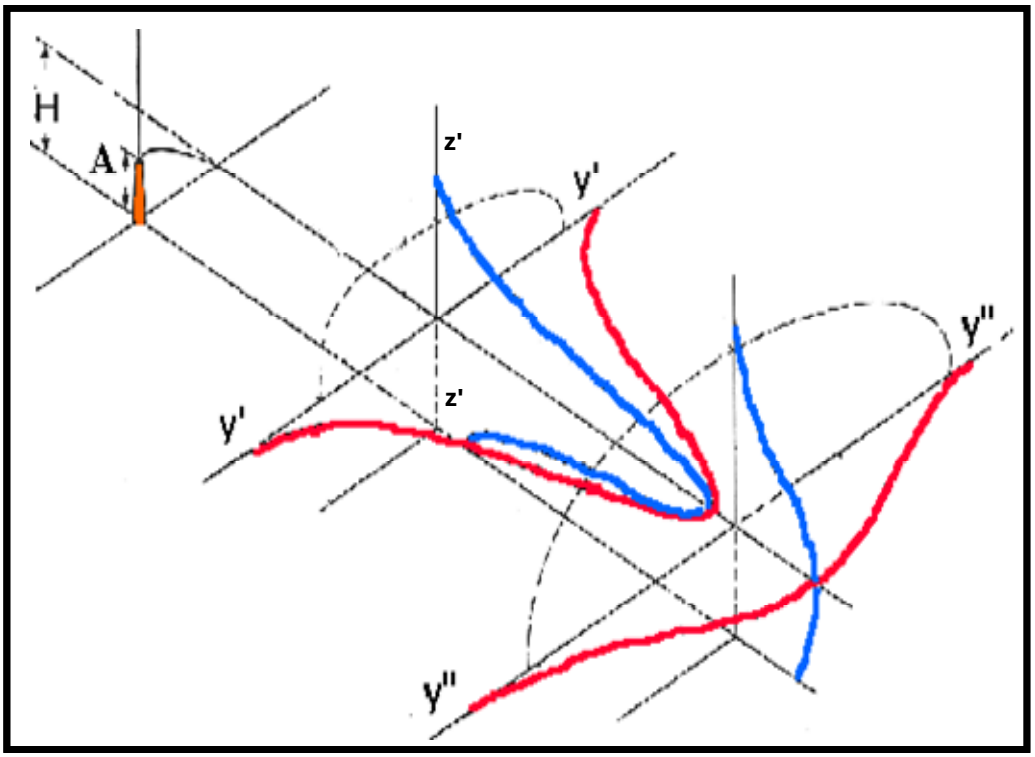

(Source: http://www.rpi.edu/dept/chem-eng/Biotech-Environs/SYSTEMS/plume/plume/html)

Figure 2-13: An aerial view of a plume flow pattern

A typical simplified Gaussian plume equation to calculate the steady-state concentration of an air pollutant resulting from a point source is given by the Pasquill-Gifford model in equation (2.61) as:

$$C(x,y,z) = \frac{Q}{(2\pi)\bar{u}\sigma_y\sigma_z}\left[\exp -\left(\frac{y^2}{2\sigma_y^2}\right)\right]\left\{\exp\left(\frac{-(z-H)^2}{2\sigma_z^2}\right)+\exp\left(\frac{-(z+H)^2}{2\sigma_z^2}\right)\right\} \quad (2.61)$$

and

$$H = h_s + \Delta h \quad (2.62)$$

where

C = Concentration of the pollutant in air at the specified coordinate [mg m^{-3}]

Q = Effluent emission rate [mg s^{-1}]

$\bar{u}$ = Emission height mean wind speed in the downwind direction [m s^{-1}]

σ_y = Horizontal dispersion coefficient function [m]

σ_z = Vertical dispersion coefficient function [m]

y = Crosswind distance [m]

z = Vertical distance above ground (receptor height) [m]

H = Effective stack height [m]

h_s = The physical height of the stack [m]

Δh = The plume rise [m]

Given that: mg = milligram

m = meter

s = second

The steady-state pollutant concentration calculation from a point source could occur either with reflection or without reflection (Pasquill, 1974). A situation with reflection is based on the assumption that a virtual mirror image of an imaginary vertical stack exists releasing a plume simultaneously with an effective height that is the same as that of the real stack, while the situation without reflection ignores that assumption. In most cases, the situation with reflection' is applied due to the presence of the inversion layer. When the situation is that of with reflection, equation (2.61) is applied, while for cases without reflection, equation (2.63) is applied.

$$C(x,y,z) = \frac{Q}{2\pi\bar{u}\sigma_y\sigma_z}\exp\left\{-\frac{1}{2}\left[\frac{y^2}{\sigma_y^2}+\frac{(z-H)^2}{\sigma_z^2}\right]\right\} \qquad (2.63)$$

Equations (2.61) and (2.63) describe the change in the pollutant concentration in a plume as the plume travels downwind and gradually disperse in the vertical and crosswind directions of travel. The horizontal and vertical dispersion coefficient functions depend on the downwind distance and the atmospheric stability class. The Pasquill-Gifford classes of atmospheric stability conditions ranging from A to F are given in Table 2-5. Light winds and lots of sunshine is classified as A; such conditions cause materials to diffuse rapidly. This occurs frequently in the day time.

Table 2-5: Pasquill atmospheric stability classes

Surface wind speed at 10 m ($m\ s^{-1}$)	**Day**			**Night**	
	Incoming solar radiation			Cloud cover	
	Strong	Moderate	Slight	Thinly overcast or ≥4/8 low cloud	≤3/8 or mostly cloudy
<2	A (s = 1)	A-B	B (s = 2)		
2-3	A-B	B	C (s = 3)	E (s = 5)	F (s = 6)
3-5	B	B-C	C	D	E
5-6	C	C-D	D (s = 4)	D	D
>6	C	D	D	D	D

Source: Turner, 1974; Seinfeld and Pandis, 1998.

At night, when winds are light, the classification is either E or F; under these conditions, materials diffuse slowly (Turner, 1974; Draxler, 1981). Equations (2.61) and (2.63) are applicable to emissions for elevated sources. Analogous to equations (2.61) and (2.63), the dispersed concentration from ground-based sources at steady-state is determined using the expression given by:

$$C_{x,y,z,\Delta h} = \frac{Q}{\pi \bar{u} \sigma_y \sigma_z} \exp - \frac{y^2}{2\sigma_z^2} \left[\exp \frac{(z+\Delta h)^2}{2\sigma_z^2} + \exp \frac{(z-\Delta h)^2}{2\sigma_z^2} \right] \qquad (2.64)$$

for the case with reflection and

$$C_{x,y,z,\Delta h} = \frac{Q}{\pi \bar{u} \sigma_y \sigma_z} \exp\left\{-\frac{1}{2}\left[\frac{y^2}{\sigma_z^2} + \frac{(z-\Delta h)^2}{\sigma_z^2}\right]\right\} \quad (2.65)$$

for the case without the inversion layer that is no reflection.

These dispersion coefficients (usually in metres) can also be determined from EPA (1995a) and (1995b) equations as:

$$\sigma_y = 465.11628(x)\tan\left\{0.01745\left(\frac{c}{d} - \ln(x)\right)\right\} \quad (2.66)$$

$$\sigma_z = a\, x^b \quad (2.67)$$

Where, x is the downwind distance and a, b, c, d, e are the stability classes for specific conditions. Dispersion coefficients can also be obtained using Pasquill-Gifford-Turner (PGT) estimates (Turner, 1974; Draxler, 1980) shown in equations (2.68) and (2.69):

$$\sigma_{PGTy}(s,x) = (k_{s,1}x)\left[1 + \left(\frac{x}{k_{s,2}}\right)\right]^{-k_{s,3}} \quad (2.68)$$

$$\sigma_{PGTz}(s,x) = (k_{s,4}x)\left[1 + \left(\frac{x}{k_{s,2}}\right)\right]^{-k_{s,3}} \quad (2.69)$$

where s is an integer [1 to 6] representing the atmospheric stability shown in Table (2-5), while $k_{x,x}$ are empirical constants,
(www.cities.poly.edu/environment/gradedu/ce752/ce752_airmodeling.html , 2006).

A third, and the most conventional, method of estimating the vertical and crosswind dispersion coefficients is the use of a stability class chart. The stability chart is a plot of stability as a function of downwind distance for the six different stability classes (Figures (2-14) and (2-15)).

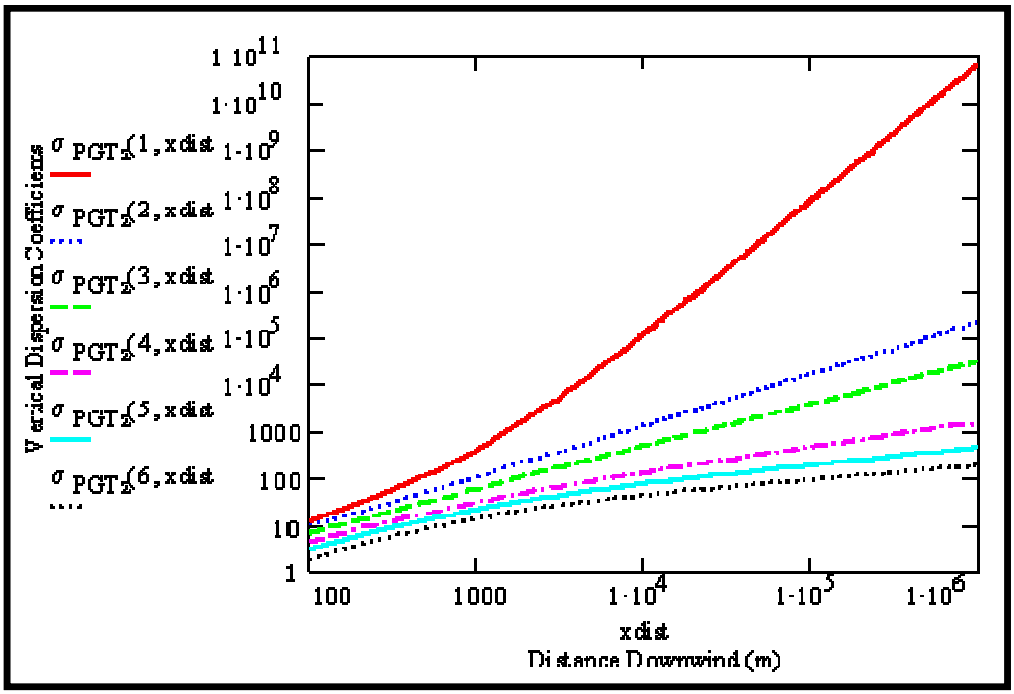

(Source: http://cities.poly.edu/environment/gradedu/ce752/ce752_airmodeling.html)

Figure 2-14: Vertical dispersion coefficient as a function of downwind distance

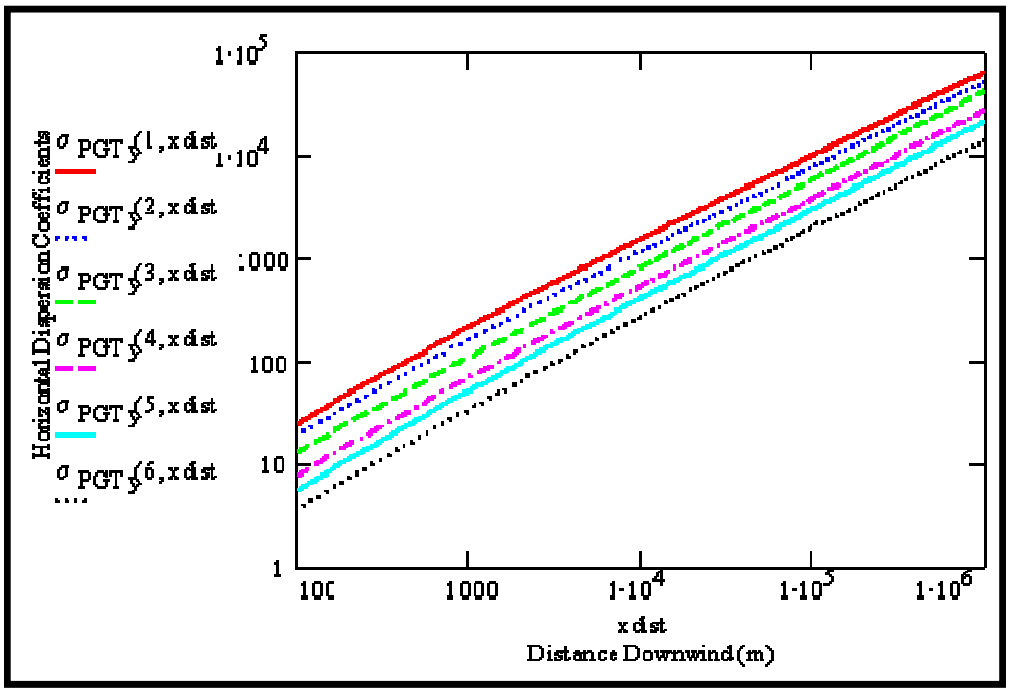

(Source: http://cities.poly.edu/environment/gradedu/ce752/ce752_airmodeling.html)

Figure 2-15: Horizontal dispersion coefficient as a function of downwind distance

Basic General Assumptions of the Gaussian Model

(a) The smoke-stack emission is continuous and constant to allow for steady-state analysis.

(b) The terrain is relatively flat.

(c) The wind speed is constant with time and elevation.

(d) There are no reactions degrading the pollutants. Also, when the pollutants hit the ground, they are reflected and not absorbed.

(e) The concentrations of the pollutants have normal distributions.

(f) The concentration at the edge of the plume is estimated to be one-tenth of the concentration of the centre-line.

Plume Rise

The effective stack height, H, is equal to the physical stack height, h_s, plus the plume rise, Δh. The plume rise point is often assumed to be directly above the stack. Recalling equation (2.62) as equation (2.70), one simplified expression for calculating the plume rise is given by a set of the Briggs' equations (2.71) and (2.72)

$$H = h_s + \Delta h \tag{2.70}$$

$$\Delta h = 1.6\left(\frac{F_b^{1/3} x^{2/3}}{u}\right) \tag{2.71}$$

$$F_b = g\frac{d^2 V}{4}\left(\frac{T_s - T_a}{T_s}\right) \tag{2.72}$$

where

x = Downwind distance [m]

u = Average wind speed at the plume centre-line in the along-wind direction [m s^{-1}]

F_b = Buoyancy flux [m^4 s^{-3}]

g = Acceleration due to gravity [m s^{-2}]

d = Stack top internal diameter [m]

V = Exit gas velocity [m s^{-1}]

T_s = Absolute exit gas temperature [^oC]

T_a = Absolute air temperature [^oC]

The effective height of a stack is the physical height of the exhaust plus any vertical component. It corrects for elevation of the plume due to buoyancy, the exit effluent temperature and velocity (Briggs, 1969).

The plume rise under different conditions can be obtained by empirical equations based on the prevailing conditions at the site. The plume rise is calculated using the Briggs' equations (Briggs, 1969). The wind speed and direction are measured at the anemometer height of the receptor point (conventionally 10 m AGL).

The effective height of the plume does not take into account the relative height of the receptor. The presence of vertical structures -such as buildings, hills or mountains-, disrupt the air flow to varying degrees (Leahey, 1974). In such an environment, there is an air volume of compression on the windward side, and a volume of rarefaction on the leeward side for any situation where the air flow is not completely laminar. Also, depending on the structure, there are stagnation and recirculation volumes (Zib, 1977).

Laminar airflow occurs and it is readily observed within isothermal zones at altitude under highly stable conditions. True laminar flow in the atmosphere near a surface can occur only at low wind speeds across very smooth surfaces, such as a water body, when the conditions are isothermal (Scire *et al*, 2000a; 2000b).

In areas where rolling hills and mountains stand along the plume direction, the ratio of measured downwind concentration, as a function of source release rate, to the calculated value depends on all the usual variables (stability, wind speed, and release height) as well as slope, roundness, and dimensions of the hills. To account for receptors at different elevations, the Gaussian model could be applied to calculate the dispersed concentration using the height differential between the receptor and effective stack height (Zib, 1977; Scire *et al*, 2000b). The simplified coordinate systems used for the development of the Gaussian model are shown in Figure (2-16).

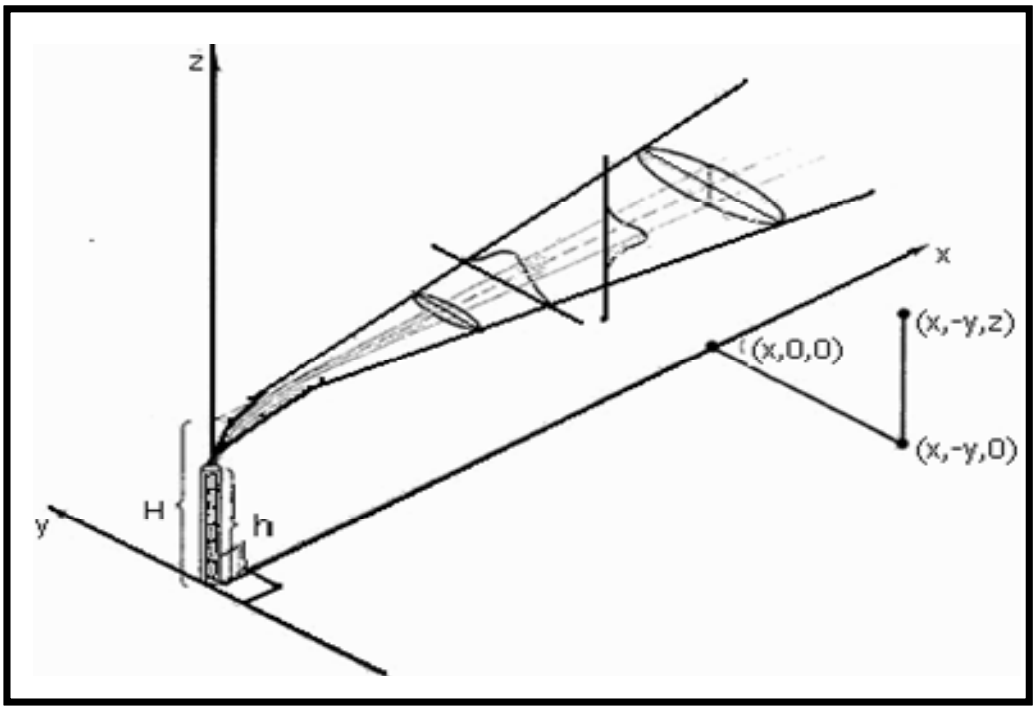

(Source: www.cities.poly.edu/environment/gradedu/ce752/ce752_airmodeling.html)
Figure 2-16: Plume dispersion by Gaussian distribution and coordinate system

Contributions of Stack Physical Height to Dispersion

Lucas (1975) reported that the maximum concentration at any distance decreases steadily with increase in emission height. It was noted that tall chimneys need to be taller for larger

areas of emission as well as to provide effective control of practically measured ground-level concentrations.

The known means of reducing ground level concentrations of gaseous pollutants are:

(a) Reducing the total emission from a given plant without materially reducing its effective performance.

(b) Using stacks whose heights have been evaluated as adequate for the worst pollution situations.

(c) Spacing out sources of emissions so that they are not unduly crowded into particular areas.

In most countries, sulphur dioxide emissions on a large scale, especially from power plants, have been controlled at ground level through the use of the tall stack policies. This tall stack technique is not effective when considering the overall pollution of very large areas. It may lead to unacceptable air quality in adjoining regions despite the huge regional dispersion of the emissions which substantially reduces the pollutant concentrations within the source areas (Lucas, 1975). In addition, tall stacks do not control the formation of sulphate which is dangerous to health; rather they create an accumulation layer of generated secondary pollutants near the temperature inversion layer. These secondary pollutants are, at some stage, dispersed to the ground by dry- or wet-deposition, causing ecological problems (Snyman *et al*, 1990). However Lucas (1975) observed that areas where unacceptable concentrations exist usually have large numbers of low-level emission sources and that any prospect of improving ambient concentrations lies overwhelmingly with the control of these low-level emissions. In the aforesaid situations, the tall stacks are effective even in very large emission areas: partly because for buoyant plumes, emissions raise the critical wind speed and they also limit the possibility of increasing ground-level concentrations as stable layers approach the ground, and partly because in real situations, a large part of the emissions is usually local in origin. High concentrations almost always occur in or near to emission areas. Where emission rates fall appreciably as pollution

travels downwind, so do concentrations fall. Since all pollution effects are closely related to air concentration, adverse effects diminish as the distance increases.

Advanced Lagrangian Models with Chemical Transformations

The environmental protection agency (EPA), in collaboration with air quality research institutes, has recommended some specific dispersion models for the determination of concentration dispersion from stationary and non-stationary source points with high accuracy. The models are designed to account for variability and abrupt change in wind speed and direction, irregular terrain, over-water dispersion and upper-air considerations. The models also account for plume advection as constituting several puffs (pocket of air-mass) aligned in series, as plume models do not accurately describe advection concentrations for long-range transport. The two most applied puff models are MESOPUFF-II and CALPUFF (Scire *et al*, 2000b).

The MESOPUFF-II Dispersion Model

MESOPUFF-II is a Lagrangian variable-trajectory puff superposition model suitable for modelling the transport, diffusion and removal of air pollutants from multiple point- and area-sources at transport distances beyond the range of conventional straight-line Gaussian plume models (that is, beyond 10 to 50 km). MESOPUFF-II is an extensively modified version of the MESOscale PUFF (MESOPUFF) model. MESOPUFF-II uses hourly surface meteorological data and twice daily raw insonde data; separate wind fields (to represent flow within and above the boundary layer); parameterisation of vertical dispersion (in terms of micrometeorological turbulence variables); parameterisation of SO_2 to SO_4^{2-} and NO_x to NO_3 conversion (including the chemical equilibrium of the HNO_3 / NH_3 / NH_4NO_3 system); resistance modelling of dry deposition (including options for source or surface depletion); time- and space-varying wet removal; and a computationally efficient puff-sampling function (Benkley and Bass, 1979). The limitations of the model

are the absence of any complex terrain treatment either in the generation of the meteorological fields or in the dispersion. The model assumes a uniformly mixed puff throughout the depth of the mixed layer. This limitation will overwhelmingly bias the results of this model.

CALPUFF Dispersion Model

CALPUFF is an advanced non-steady-state meteorological and air quality modelling system. It is the most-preferred EPA model for the evaluation of long-range transport of pollutants, visibility assessment, secondary pollutant formation, particulate matter modelling and their impacts. It is a multi-layer, multi-species non-steady-state Lagrangian Gaussian puff dispersion model which can simulate the effects of time- and space-varying meteorological conditions on pollutant transport and transformation. CALPUFF contains modules of complex terrain effects, over-water transport, coastal interaction effects, building downwash, wet and dry removal and simple chemical transformation (Yamartino *et al*, 1992; Scire *et al*, 2000b).

The modelling system includes a meteorological modelling package with both diagnostic and prognostic wind-field generators (CALMET), a Gaussian puff dispersion model with chemical removal, wet- and dry-deposition, complex terrain algorithms, plume fumigation and other effects (CALPUFF). In addition, a photochemical model (CALGRID) was incorporated into the modelling framework to account for both reactive and non-reactive pollutants. A third component of the modelling system is a Lagrangian particle model called the kinematic simulation particle (KSP) model (Scire *et al*, 2000a; Strimaitis *et al*, 1995; Yamartino *et al*, 1996). The modelling system has been used in complex and very unstable environments to predict plume trajectories (Godfrey and Clarkson, 1998; Honaganahalli and Seiber, 2000).

2.13 Conclusion

A review of the available literature on the atmospheric sulphur species that are relevant to the Mpumalanga Highveld has been presented in this chapter. The review is more focused on atmospheric sulphate aerosols -being the end-product of the emitted sulphur compounds- and describes the nature and the state of existence of these species based on the variability of the climate over South Africa. The sulphur species which are of interest in this study, namely: H_2S, SO_2 and sulphate, have been extensively studied around the world in their various forms of existence; the variety of sources from which they are released; their interactions with the various surfaces through which they traverse (land and sea), as well as their mode of distribution, transformation and removal via reactions and depositions in the atmosphere with meteorological influences.

In contrast with studies conducted on these atmospheric sulphur speciation around the world, studies in South Africa have focused on gaseous sulphur species. Of these, only a handful concentrated on sulphate. These few sulphate studies were performed using passive sampling techniques only to determine their concentration distribution which could have been either the result of chemical transformations of smoke plumes -from coal mines, power plants or fuel oil refining plants- or of atmospheric recirculation processes over southern Africa. Since it is the intention in this study to evaluate the overall sulphur budget based on H_2S, SO_2 and sulphate over the Mpumalanga Highveld, a detailed assessment on an *in-situ* basis was devised for the investigation. The investigation is intended to generate from a short-averaging time basis, the temporal concentration distribution of the sulphur species and relationships between the various species (Chapter 4). To understand the chemistry of atmospheric sulphur -that may shed more light on the variations in the gaseous and particulate sulphur distribution since chemical reaction is a factor- the relative importance of the various sulphur reactions were predict. This shows through the most favourable pathways taken during transformations based on the analysis of theoretically generated thermochemical parameters using computational model chemistry (Chapter 5) to assess the expected reactants and products. Finally in order to further comprehend the contributions of chemical transformation on the distribution of the atmospheric sulphur on

a spatial scale; it is necessary to model for dispersion during advection over the sampling site (Chapter 6).

Chapter 3: Experimental

3.1 Introduction

Requirements for an atmospheric sulphur budgetary investigation include the following:

(a) Assessment of the temporal distributions, targeting the source areas and generating a net pollution load with time (dose) in the atmosphere for the sulphur species at Elandsfontein (Chapter 4).

(b) An understanding of all the known possible forms and mechanisms of removal and production of atmospheric sulphur. Hence, in order to justify the values of measured ambient concentrations, it is necessary to investigate all other possible reaction routes (Chapter 5).

(c) The horizontal mode of distribution of the sulphur species (which is dependent on the oxidation rate of SO_2 and, invariably, the production of particulate sulphate) is determined through dispersion during advection (Chapter 6). For simplicity a gas-phase transformation pathway is assumed in the generation of the reaction rates.

This chapter describes the methodology applied for ambient air sampling and tropospheric weather observations, as well as the instruments used for both concentration and meteorological measurements. The site location and its characteristic features are also highlighted. The experiment was designed to obtain an approximation of the sulphur-based pollution distribution on a temporal basis over the Mpumalanga Highveld subregion with Elandsfontein as the reference or sampling site (Figure 2-1).

3.2 Site Description

Elandsfontein is in a strategic location that adequately represents the various types of emissions and their average background levels in ambient air as impacted by all major

pollution sources on the Mpumalanga Highveld. Elandsfontein lies centrally within an area in which various sulphur emission sources on the Highveld are present, such as the coal-fired power stations, hydrocarbon fuel processing industry, open-cast coal mines and vehicular and domestic emissions from townships.

The air quality monitoring station at Elandsfontein is positioned at S26°15'09" E29°25'17". The station is equipped with instruments for measuring ambient air concentrations and meteorological data. Elandsfontein, at a height of 1600 m ASL, is an area that has a relatively flat topographical terrain with few rolling hills and sparse grassland vegetation. It is an open environment that allows for effective diffusion and mixing close to ground level.

The monitoring station is bounded to the north by Duvha power station (≈ 50 km due north); Arnot power station (≈ 50 km north-east), and Hendrina power station (≈ 40 km north-east). To the east of Elandsfontein lies Komati power station (≈ 50 km due east). To the south lies Tutuka power station (≈ 80 km south); Secunda fuel-refining and petrochemical plants (≈ 40 km south-west); New Denmark coal colliery (≈ 20 km south), and Kriel colliery (≈ 15 km south-west). To the west are Kriel and Matla power stations and Matla colliery (≈ 20 km west) and Kendal power station (≈ 50 km north-west) (www.eskom.co.za, 2004; www.angloamerican.co.uk, 2004).

3.3 Sampling Approach for Temporal Analysis

This study intends to quantify the H_2S, SO_2 and particulate sulphate to account for seasonal variations and chemical transformations in the PBL (between the Earth's surface and about 3 km) from immediate industrial emissions and pollutants traversing the Mpumalanga Highveld. Since the quantity of data required is large (due to seasonal variations) coupled with the requirements of a short averaging time of about 10 minutes (to be able to account for chemical transformation rates), a stationary ground-based monitoring station was used to assess the concentrations of the sulphur species. Also, since it was intended to characterise plume behaviours in relation to boundary layer activities, meteorological parameters were included in the sample measurements. This sampling strategy generated a

data set, suitable for providing insights into the relative contribution of different source types to the variety of atmospheric sulphur over Elandsfontein.

3.3.1 Materials and Methods

The materials used for this study included continuous sampling analysers for measuring trace concentrations of hydrogen sulphide, sulphur dioxide and particulate sulphate as well as instruments which measured surface meteorological parameters, all housed in an air quality monitoring station. Hourly data suitable for kinetic studies were obtained from the measurements. The meteorological instruments were used to establish the influence of weather on the observed concentrations, the planetary boundary layer parameters and mixing depth for day- and night-times. Since local meteorology is a good estimation of the microscale diffusion, the meteorological data were also necessary to provide reliable information for targeting source areas of the windborne pollutants traversing Elandsfontein.

To provide information on the effect of the changing atmospheric conditions on the observed pollutants' concentrations, a two-part approach was used in this study. The first part was a twelve-month continuous sampling of ambient air for gas and aerosol concentrations in order to assess the evolution and impact of these sulphur species based on an understanding of the atmospheric sulphur chemistry at Elandsfontein. In addition to concentration measurement, a simultaneous observation of the prevailing meteorological variable which include wind speed and direction, relative humidity, solar radiation, ambient temperature and pressure as well as rainfall. In all these parameters, surface pressure was determine from the particulate sulphate monitor. Measured concentrations were used for the following: quantitative evaluation, emission loading, temporal variation and to propose deposition mechanisms with seasonal variations (Chapter 4); evaluation of the thermochemical properties for the various modes of transformation of atmospheric sulphur over Elandsfontein using theoretical chemistry models (Chapter 5); and the analysis of downwind concentration distribution resulting form SO_2 oxidation during advection (Chapter 6).

3.3.2 Sampling Procedure

The instruments employed for the sampling were a Thermo Environmental Instruments' (now Thermo Electron Corporation) model 43C SO_2 analyser for SO_2 monitoring; a Thermo Environmental Instruments' (now Thermo Electron Corporation) model 450C H_2S-SO_2 analyser for H_2S monitoring, and a Rupprecht and Patashnick Series 8400S ambient particulate sulphate monitor.

The air sampling was conducted on a continuous basis for twelve months from 01 September 2004 to 31 August 2005. This plan was to account for variations in seasonal measurements. Over southern Africa four seasons are observed in the year. These seasons are summer (November to January), autumn (February to April), winter (May to July) and spring (August to October). During the sampling period the gas analysers and the particulate sulphate monitor were calibrated on a monthly basis. Calibration of the instrument was intended to eliminate or reduce bias in the instrument's readings over a range for all continuous values. Reference standards with known values for selected points covering the range of interest were measured with the instrument in question. Then a functional relationship was established between the values of the standards and the corresponding sample measurements.

Model 43C Trace Level Pulsed Fluorescence SO_2 Analyser

The model 43C trace level pulsed fluorescence SO_2 analyser is an environmental protection agency (EPA) recommended instrument for the continuous monitoring of ambient sulphur dioxide concentrations in air. It measures pulse fluorescence signals generated by SO_2 when in an excited state (Dittenhoefer and de Pena, 1978).

The Thermo Environmental Instruments' (now Thermo Electron Corporation) model 43C trace level SO_2 pulse fluorescence analyser is based on the principle that SO_2 molecules absorb ultraviolet (UV) light and become excited at one wavelength, λ_1, then decay to a lower energy state, emitting UV light at a different wavelength, λ_2. This is shown in the reaction:

$$\mathbf{SO_2 + h\nu_1} \longrightarrow \mathbf{SO_2^*} \longrightarrow \mathbf{SO_2 + h\nu_2} \qquad (3.1)\ a$$

The ambient air sample is drawn into the analyser through a sample partition, and flows through a hydrocarbon "kicker", which removes hydrocarbons from the sample by forcing the hydrocarbon molecules to filter through the tube wall. The SO_2 molecules pass through the hydrocarbon "kicker" unaffected. The air sample then flows into the fluorescence chamber, where pulsating UV light excites the SO_2 molecules.

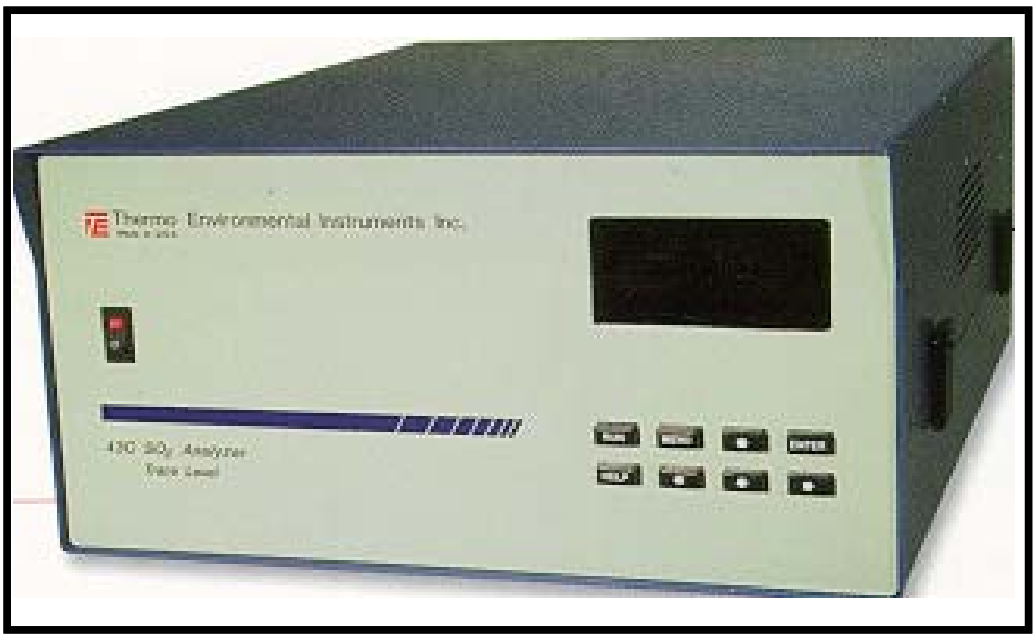

Source: http://www.thermo.com/com/cda/product/detail/1,,14377,00.html
Figure 3-1: Front view of the model 43C trace SO_2 pulse fluorescence analyser

As the excited SO_2 molecules decay to lower energy states they emit UV light, the intensity of which is proportional to the SO_2 concentration. A band-pass filter allows only the wavelengths emitted by the excited SO_2 molecules to reach the photomultiplier tube (PMT). The PMT detects the UV light emitted by the decaying SO_2 molecules. A photo-detector, located behind the fluorescence chamber, continuously monitors the pulsating UV light source and is connected to a circuit that compensates for fluctuations in the UV light. The sample then flows through a flow sensor, a capillary, and the shell side of the hydrocarbon "kicker." The model 43C trace level instrument outputs the SO_2 concentration to the front panel display and the analogue outputs. The instrument is

designed to sample at a flowrate of 1 L min^{-1} with a concentration detection range of 0 to 500 ppb at a response time of 60 seconds. The instrument is designed to operate over a temperature range of 0 °C to 45 °C.

Model 450 Pulsed Fluorescence H_2S-SO_2 Analyser

The Model 450 pulsed fluorescence analyser is an environmental protection agency (EPA) recommended instrument for the continuous monitoring of ambient hydrogen sulphide concentrations in air. The model 450C trace level H2S-SO2 pulse fluorescence analyser measures the total gaseous sulphur comprising H_2S and SO_2 as well as only SO_2 in the air sample. It consists of an H_2S to SO_2 converter coupled to a pulsed fluorescence SO_2 unit.



Source: http://www.thermo.com/com/cda/product/detail/1,,14676,00.html
Figure 3-2: Front view of model 450 H_2S-SO_2 pulse fluorescence analyser

The model 450C H_2S-SO_2 pulse fluorescence analyser uses the same principle to measure SO_2 pulse as the model 43C trace level SO_2 pulse fluorescence analyser. The ambient air sample drawn in through the inlet is divided into two, with one half entering the reaction

chamber where the H_2S present is catalytically converted into SO_2 and the other half bypassing the converter. Continuous H_2S monitoring is accomplished according to the following reaction:

$$\mathbf{H_2S + 3/2\ O_2 \longrightarrow SO_2 + H_2O} \qquad (3.1)\ b$$

Each H_2S molecule is converted to SO_2 so that the output of the SO_2 analyser is equal to the concentration of H_2S entering the converter. This is accomplished when the pulse generated from the two flow lines is transmitted through the analyser and the electronics subtract the SO_2 result from the total signal of sample passing through the converter to give an H_2S reading.

Ambient Particulate Sulphate Monitor

The Rupprecht and Patashnick Series 8400S ambient particulate sulphate monitor measures the mass concentration of ambient particulate sulphate contained in fine particulate matter less than or equal to 2.5 μm size in near real time (Rupprecht and Patashnick, 2001). The monitor consists of an SO_2 pulse generator and a pulse analyser (Figure 3-3). In the pulse generator, air samples that contain particles of size less than or equal to 2.5 μm, pass through a humidifier to a reaction chamber (Drewnick *et al*, 2003).

The monitor measures total particle sulphur comprised overwhelmingly of particulate sulphate using a flash volatilisation technique. Flash volatilisation occurs at about 600 °C when a high resistance current is passed through a platinum flash strip for approximately 0.01 seconds, producing an SO_2 pulse which is interpreted by a pulse analyser and computed and displayed as particulate sulphate concentration in $\mu g\ m^{-3}$ present in the sampled air over a given time.



Source: Rupprecht and Patashnick (2001)
(Legend: Pulse analyser (left) and Pulse generator (right))
Figure 3-3: Series 8400S ambient particulate sulphate monitor

Series 8400S Particulate Sulphate Monitor Operating Principle

Ambient aerosol samples are pulled through a sharp cut cyclone at a flow rate of 5 L min^{-1} to remove particles above 2.5 µm (Figure 3-4). From this initial flow, a sub-flow of 1 L min^{-1} is channelled through a second Teflon tube to be used for the sulphate analysis.

The 1 L min^{-1} stream of air is passed through a carbon honeycomb denuder to remove any existing SO_2 or H_2S. The presence of these gases produces artefacts in the total sulphate concentration. Particles are first wetted through a humidifier and subsequently collected by impaction onto a platinum strip mounted in a collection and vaporisation cell. The collection efficiency of this impactor is greater than 95 % for particles in the range 0.1 to 0.8 µm (Stolzenburg and Hering, 2000; Drewnick *et al*, 2003).

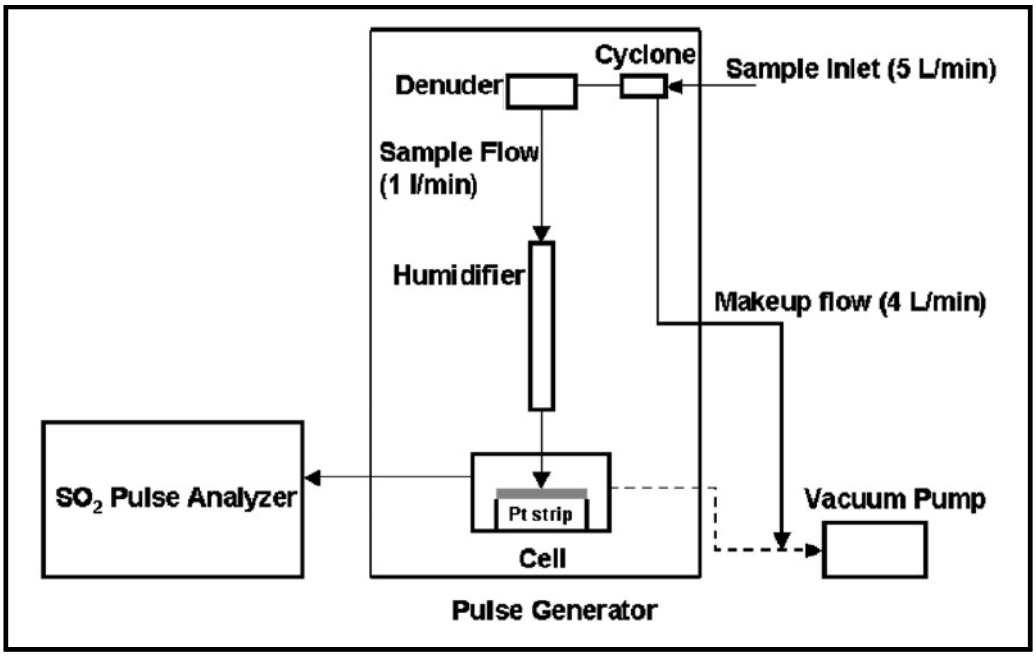

Source: Rupprecht and Patashnick (2001)
Figure 3-4: Schematic of the Rupprecht and Patashnick Series 8400S monitor consisting of a pulse generator and pulse analyser

Samples are typically collected over an 8-minute sampling interval, after which the instrument switches to analysing mode. A complete sampling cycle is 10 minutes, made up of 8 minutes of sampling time and 2 minutes of analysis time. During analysis, the sampling flow bypasses the collection cell. During the analysing mode of the operation, the sampling cell is purged with zero-air (approximately 97 % pure air) obtained from a cylinder. Particles smaller than 2.5 μm are accumulated on a metallic strip in the pulse generator after which it is flash-vaporised at about 600 °C (generated through resistive heating) to produce a pulse fluorescence of SO_2. The fluorescence pulse generated is transmitted to the pulse analyser (same as the model 43C trace level SO_2 pulse fluorescence analyser) which evaluates the amount of SO_2 produced during the vaporisation of the particulate matter within 120 seconds after an 8 minutes batch-sample.

The SO_2 is measured using standard pulsed fluorescence technology (Dittenhoefer and de Pena, 1978). The analyser output is integrated over the signal real-time, and then

converted using the ambient pressure, temperature and calibration factors, yielding a 10-minute average sulphate concentration for each sample batch. The baseline of the SO_2 analyser is constantly monitored between pulse analysis modes. The signal from the pulse analyser is passed to the data acquisition system where it is converted to the appropriate concentration of sulphate measured and displayed in $\mu g\ m^{-3}$ (Drewnick *et al*, 2003).

Quality assurance of the instrument is maintained automatically by the instrument through a range of internal audits. The system was calibrated manually every month with aqueous standards applied directly to the collection strip. Field blanks were measured monthly by placing a Teflon filter between the cyclone and the denuder. A constant watch on the cylinder pressures attached to the equipment was maintained to ensure that the data measured were reliable.

The sulphate mass concentration is automatically calculated from the SO_2 analyser reading, using the sample flow rate and sampling time as well as the conversion efficiency determined during aqueous standard calibration (Figure 3-5). These data are manually corrected for variations in the automatic analyser calibrations and the manual liquid standards calibrations, as well as for the field blank readings (Drewnick *et al*, 2003).

A series of tests conducted to evaluate the accuracy of the Rupprecht and Patashnick Series 8400S ambient particulate sulphate monitor against the analyses made with filter samples and conducted by Drewnick and co-workers. The agreement between these two methods, as well as three other methods, yielded a correlation coefficient of more than 0.9 (Drewnick *et al*, 2003).

The monitor was calibrated monthly using 96 % pure ammonium sulphate solution for the pulse generator and 1 ppm SO_2 in zero-air for the pulse analyser. The response times for the analysers are 120 seconds for the H_2S and SO_2 analysers and 10 minutes for the particulate sulphate monitor.

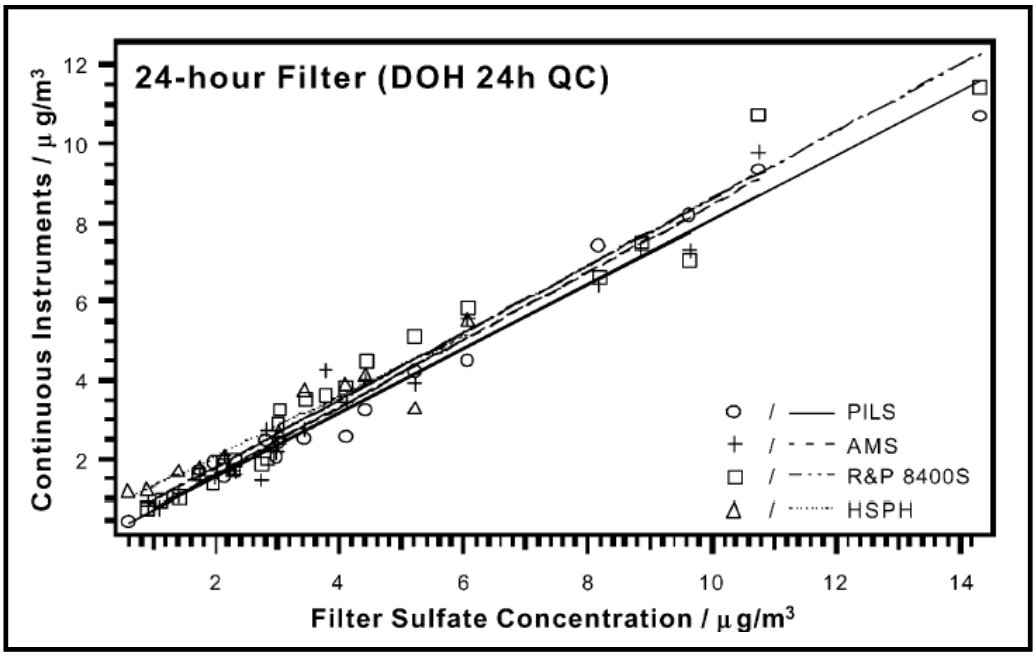

Source: Drewnick *et al* (2003)

Figure 3-5: Correlations between the semi-continuous sulphate concentrations and the 24-h filter data, collected at the Queens College site

In this study the field observations generated a twelve-month experimental data set using the continuous monitoring analysers on hourly average measurements at Elandsfontein in the Mpumalanga Highveld. This period was structured to provide for seasonal variations in the measured parameters.

Determination Meteorological Parameters

The various meterological parameters determined during the field campaign were wind speed and direction, relative humidity, solar radiation and ambient temperature and rainfall, while the surface pressure was obtained from one of the concentration analysers designed with such in-built facility.

05305-L R. M. Young Wind Monitor-AQ

The wind speed and direction were measured using the model 05305 Wind Monitor-AQ. It is a high-performance with lightweight instrument designed specifically for air-quality

measurements and is an accredited EPA instrument for the measurements of wind speed and direction. It is made out of rigid, UV-stabilized thermoplastic with stainless-steel and anodized-aluminum fittings. The thermoplastic material resists corrosion from sea-air environments and atmospheric pollutants.



[Source: http://www. www.campbellsci.com/05305-l]
Figure 3-6: Model 05305-L R. M. Young Wind Monitor-AQ

The wind monitors use stainless-steel, precision-grade ball bearings for the propeller shaft and vertical shaft bearings. It provides a lower starting threshold, faster response, and higher accuracy. The instrument has a wind speed range of 0-40 m/s, accuracy of ±0.2 m/s, threshold of 0.4 m/s and a wind direction range of 0-360°, accuracy of ±3°and threshold of 10°. The output of the instrument is retrieved trough a data logger at 10 minute interval (http://www.campbellsci.com/05305-l).

41003-5 Plate Gill Radiation Shield

The 41003-5 Plate Gill Radiation Shield was used to analyse solar radiation, ambient temperature and relative humidity. It is a naturally aspirated 10-plate radiation shield. Its louvered construction allows air to pass freely through the shield, keeping the probe at or near ambient temperature. The shield's white colour reflects solar radiation. Temperature

probes that are exposed to sunlight should be housed in a radiation shield to reduce the effects of solar loading on the temperature measurement.



[Source:http://www.campbellsci.com/documents/lit/b_mounts.pdf]
Figure 3-7: The model 41003-5 10-Plate Gill Radiation Shield

Within the Gill radiation shields are the ambient temperature and relative humidity probes. The probe fits into the bottom of the shield and is held into place with screws. A U-bolt attaches the radiation shield to the mast on which the wind instrument was placed. The output of the instrument is retrieved trough a data logger at 10 minute interval (www.campbellsci.com/documents/lit/b_mounts.pdf).

Tipping Bucket Rain gauge

RG600 Tipping Bucket was the instrument used for monitoring total rainfall. It has an 8"; orifice with mounting brackets. The tipping bucket sensor mechanism activates a sealed reed switch that produces a contact closure for each 0.01" or 0.2 mm of rainfall. The tipping bucket rain gauge can be pole mounted or bolted to a level plate. A datalogger connects to the tipping bucket's pulse output to record data.

(http://www.globalw.com/downloads/RG/RG200B.pdf)

3.4 Computational Chemistry Approach to Modelling Atmospheric Transformations

To further understand the nature and forms of existence of atmospheric sulphur during and after oxidation requires very expensive analyses and instrumentations. But several questions relating to the variability in the state of existence could be answered using thermochemical analyses of the chemical reaction. These include evaluating -using thermochemical properties- the equilibrium constants and conversions as ambient temperature changes.

The important role of various sulphur species in the chemistry of the atmosphere has been extensively studied and detailed information (especially for gas-phase reactions) are available. In contrast, for aqueous-phase reactions only few the published data exist on thermochemical properties for the species. The available properties were derived from a variety of experimental techniques. With advancements in the computational chemistry, the thermochemical energies can be computed from the electronic structures of the various species and enthalpies evaluated for isodesmic reactions. Since atmospheric reactions are complex, involving several reactions occurring at the same time for same species, computational chemical models are a very useful tool.

The computational model chemistry applied in this study was seven high-energy accuracy methods built into the Gaussian 03 model chemistry package.

3.4.1 Computational Method for Thermochemical Analyses

All calculations were performed using *ab initio* and density functional theory methods (Hirst, 1990; Grant and Richards, 1995; Jensen, 1999) for the various species involved in the reactions as implemented in the Gaussian 03 (G-03) quantum chemistry package (Frisch *et al*, 2004). Energy computations were done at the B3LYP/6-311+G (2d,p) level

for the purpose of comparison; calculations were done using four high-energy accuracy levels. These are compounded computational methods, that is, the Gaussian-1 (G1), Gaussian-2 (G2), Gaussian-3 (G3), complete basis set (CBS-4) and quadratic configuration interaction (CBS-Q) theoretical levels. Each molecular structure and molecular geometry for a particular molecule was obtained using the GuassView chemistry package and structures were fully optimised at HF/3-21G* level to obtain an optimised molecular geometry for each potential energy surface. The Cartesian coordinates of the optimised molecular geometry, together with the charge and multiplicity of the compound and the computational method, were used as input for the G-03 simulation package.

3.5 Data Evaluation for Kinetic and Dispersion Modelling

The oxidation of SO_2 has been described as a very slow process (Calvert *et al* 1978; Forney and Giz, 1980; Newman, 1981; Seinfeld and Pandis, 1998) and is the rate-controlling step in the formation of sulphate (Pienaar and Helas, 1996), while the reaction between the trioxide and water vapour is a faster reaction (Pienaar and Helas, 1996). It may then be assumed that the transformation into trioxide and sulphate are negligible at the emission source. Hence, in addition to the model development, field measurements were conducted for the deduction of SO_2 disappearance rates with advection.

3.5.1 Materials and Method

The materials required for the development and evaluation of the kinetic and the dispersion models are similar to that in used for the temporal analyses (section 3.3). The data used for the kinetic model development were systematically extracted from air pollution episodes in the Elandsfontein area undertaken between 01 September 2004 and 31 August 2005 (section 3.3). This was possible due to the close proximity (about 20 km apart) of Elandsfontein to Kriel where two coal-fired power stations are located.

3.5.2 Sampling Description

The sampling processes had been described previously (section 3.3) for concentration measurement and for meteorological variables of the PBL at the sampling area. The surface meteorological variables were assumed to be a fairly good estimation for the micro scale dispersion, especially over Elandsfontein.

Based on the mean wind velocities of advecting air mass to the sampling site, the travelling time was estimated. It was assumed for transformation purposes that all SO_2 and sulphates emerged from the industrial emission source area since only data from the wind directional sector towards the industrial part of the town were considered.

In conclusion, it is to be noted that the detailed methodology adopted for the computational chemistry and dispersion with reaction modelling parts of this study are reported in the various chapters dealing with the model development and evaluation.

Chapter 4: Analysis of Temporal Variations of Atmospheric Sulphur over Elandsfontein

4.1 Introduction to Total Sulphur Evaluation

An essential programme of activity of industries in South Africa is to incorporate, as part of their production plan, compliance and adherence to the air quality standards (RSA, 2005) of the country. An awareness of the nature and composition of the secondary pollutants that may result from the industrial emissions is also an underlying problem to be investigated by the industries. Since the 1990s, the emphasis on environmental consciousness, with particular reference to the atmospheric environment, has lead to several advances in air quality monitoring methodology, instrumentation and abatement or control strategies, especially in developed countries. In the case of the United States of America, these technological improvements include the evaluation of specific atmospheric pollution problems at particular sites by determining the overall distribution of the pollutants in their primary and secondary forms with the change in meteorology. In the past, in South Africa only criteria pollutants have been assessed from an air quality point of view to provide a foundation for establishing compliance monitoring air quality guidelines and, to some extent, for research purposes. But, with recent changes in legislation, studies in atmospheric science are advancing such that research questions have become increasingly more involved, requiring the need for source identification, quantification and characterisation of pollutants. In addition, studies have included speciation investigation of reactive and non-reactive pollutants in their different phases of existence. In this study, the concentration distributions of gaseous and particulate sulphur were evaluated to ascertain the gas-to-particle ratio as well as the sulphur loading in the PBL with meteorological changes for the different seasons of the year over Elandsfontein. An air quality research facility, strategically located at Elandsfontein would provide appropriate data to answer the questions in this study.

The priority of this study is to address questions on the chemistry of H_2S, SO_2 and particulate sulphate, which are the predominant sulphur species over the Mpumalanga Highveld region. Another priority was to ascertain the contributions of regional transported air masses to particulate sulphate at Elandsfontein. This is due to the understanding that the sulphate which constitute a significant percentage of the fine particulate matter in the atmosphere over the Mpumalanga Highveld results from long-range transport from countries north of South Africa (D'Abreton, 1996; Piketh 2000; Dlamini, 2005).

The presence of submicron particulate matter in the atmosphere has been observed to exhibit deleterious effects on humans compared to the presence of its precursor sulphur species and other chemically inactive particulate matter (Newman *et al*, 1975a). Hence, its mitigation via a reduction of its precursors is essential. Over an extensive episode, the serious concern regarding the release of pollutant species into the atmosphere was caused by the high density of large industries on the Mpumalanga Highveld. Several approaches, with the view to reducing the source emissions, have been applied. These include the use of bag-filters for particulate matter reduction, steam quenches in furnaces for NO_x reduction and tall stacks for higher level dispersion of released pollutants, resulting in long-range pollutant transport. In spite of these reduction mechanisms, emitted species undergo chemical transformations with advection and, due to the atmospheric stability from lapse and inversion as well as air mass circulation processes over southern Africa, atmospheric pollutants are constantly accumulating within the boundary layer, whilst simultaneously recirculating over the region. The particulate matter is known to exhibit radiative forcing potential as well as permitting a greenhouse effect on the heat absorbed by the Earth's surface. This chapter deals with the atmospheric chemistry and synergistic effect of gaseous sulphur to particulate sulphate at Elandsfontein on the Mpumalanga Highveld.

A temporal scale analysis of H_2S, SO_2 and particulate sulphate over the Mpumalanga Highveld is presented in this section. The sulphur species are assessed relative to one another at varying meteorological conditions. The diurnal and seasonal variations are used to describe the pollution loadings exhibited by the compounds over the study area. The

presence of ambient particulate sulphate was shown to result from chemical interactions during long-range aerosol transport coupled to the variations in the removal rate as a result of changing meteorological conditions from one season to another. Finally, statistical regression on the meteorological variables is used to predict the presence of particulate sulphate in the planetary boundary layer.

4.2 Evaluations of Measured Concentrations

The outcomes of the field campaign at Elandsfontein on the Mpumalanga Highveld between 01 September 2004 and 31 August 2005 are discussed in this section. These results are discussed based on targeting between the source and sink for the major contributors of the observed sulphur species within the sampling area; diurnal and seasonal characteristics of the effects of meteorology on changes in concentration and finally the mathematical relationship between the particulate sulphate and the meteorological variables.

H_2S and SO_2 data were measured in ppb and, for cases of comparison with the particulate sulphate measurements, the concentrations of the gases were converted to $\mu g\, m^{-3}$ as described in Seinfeld and Pandis (1998) and were simplified at an average surface pressure of 84×10^3 N m^{-2} as follows:

$$[H_2S](\mu g\ m^{-3}) = 344.3083 * \frac{H_2S(ppb)}{T(K)} \qquad (4.1)$$

where $[H_2S]$ and H_2S are the concentration and mixing ratio and $T(K)$ is the average ambient temperature at Elandsfontein. Similarly, for the same pressure condition, SO_2 is expressed as:

$$[SO_2](\mu g\ m^{-3}) = 647.0934 * \frac{SO_2(ppb)}{T(K)} \qquad (4.2)$$

4.3 Analyses of Measured Concentrations

4.3.1 The Effect of Wind on Concentration Distribution

The determination of the concentration distribution and magnitude of the major sources of pollutants is an important step towards a meaningful interpretation of the surface sampling data. Concentration distribution with wind direction provides a basis for source targeting. Considerable amounts of basic data were measured from which fairly reasonable source targeting could be done. Since only ground-based sampling was conducted, pollutants could be attributed only the major contributing sources nearest the sampling site.

This is illustrated in the wind and pollution roses of H_2S, SO_2 and particulate sulphate (Figures 4-1 to 4-4). Wind and pollution roses for the sulphur species were obtained for 10-minute average data collected over the 12-month sampling period at Elandsfontein.

In a wind rose, the length and thickness of the straight lines indicates the frequency of occurrence and speed of wind, respectively, in a particular wind direction, while the dotted lines indicate the average wind speeds with their corresponding directions for the period.

Throughout the sampling period, the average wind speeds at Elandsfontein were predominantly between 6.0 and 12.0 m s^{-1} (Figure 4-1), while wind speeds of <6.0 and >12 m s^{-1} occurred <10 % in all wind directions. However, the average wind speeds in all directions except for the south-east and north-west are approximately equal. The wind direction was predominant from the north-westerly and easterly sectors.

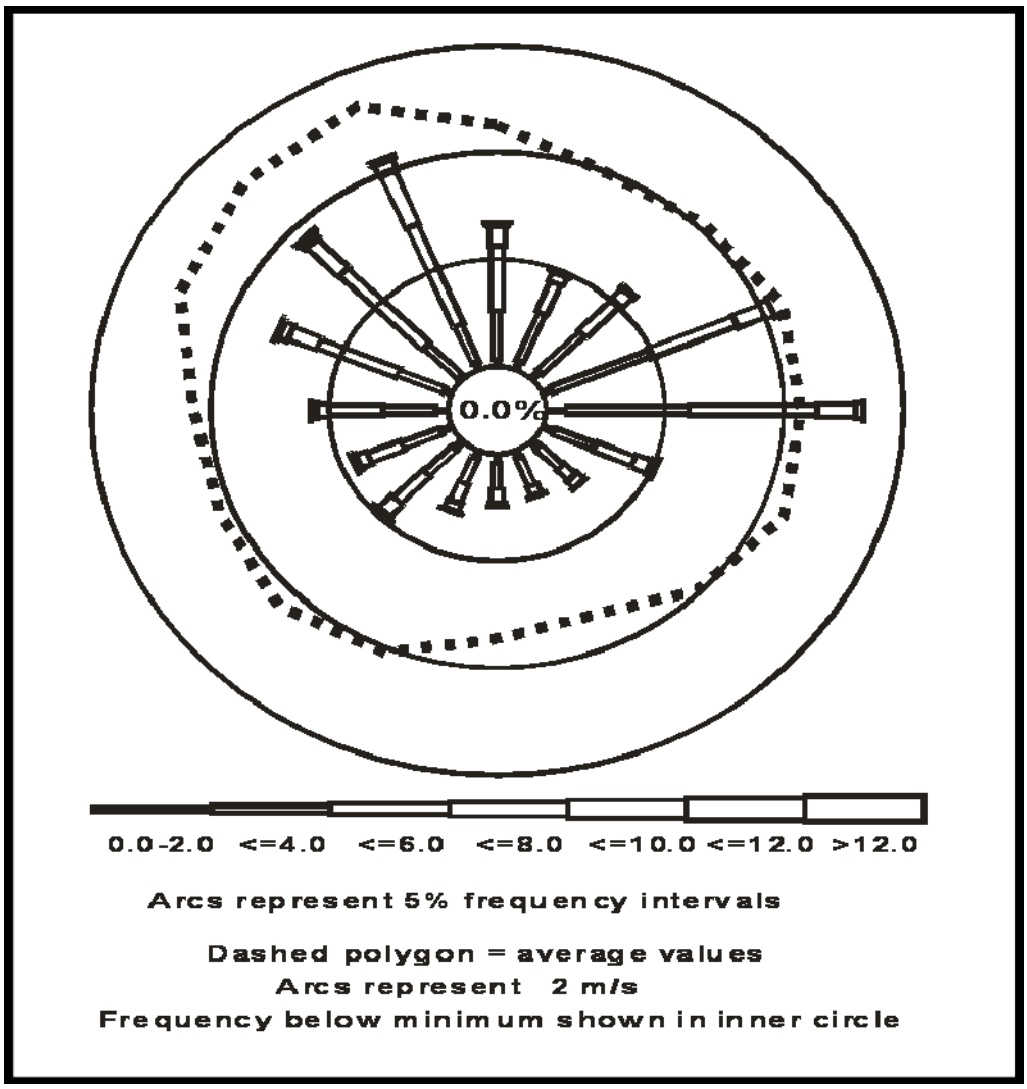

Figure 4-1: Wind rose for Elandsfontein between September 2004 and August 2005

In a pollution rose the length of the straight lines indicates the frequency of wind from a particular direction and the thickness of the lines shows the concentration intensities at fixed intervals along a particular wind direction, while the dotted lines indicate the average pollutant concentrations during the sampling period in relation to the wind direction.

The major contributors of H_2S into the planetary boundary layer over Elandsfontein are in the south-westerly and north-westerly directions (Figure 4-2). These directions are

indicative of the presence of synthetic fuel oil refineries and open-cast coal mines (Figure 2-1).

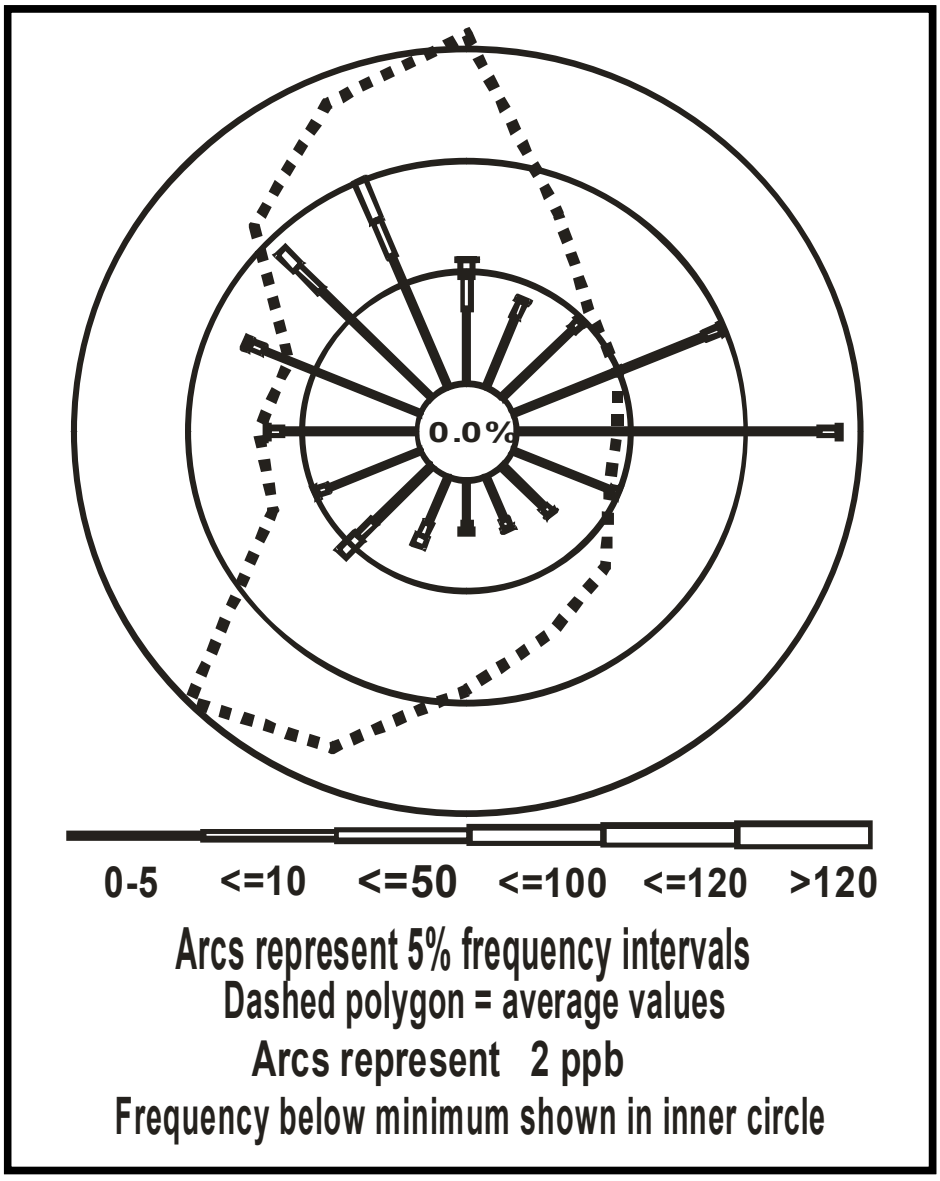

Figure 4-2: Mean H_2S concentration distribution at Elandsfontein between September 2004 and August 2005

SO_2 contributions to the area are predominantly from the westerly and north-westerly directions (Figure 4-3). This is due to the presence of power plants adjacent to the study area.

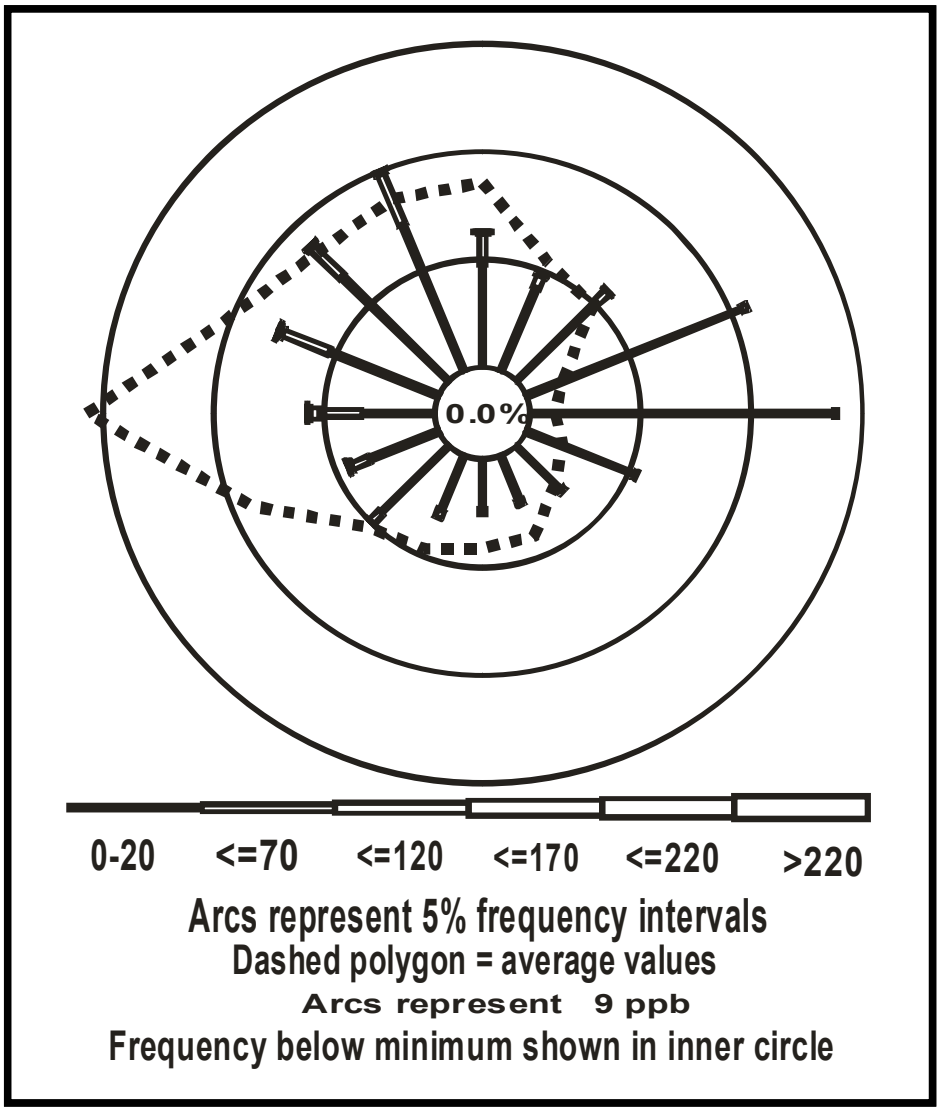

Figure 4-3: Mean SO_2 concentration distribution at Elandsfontein between September 2004 and August 2005

Particulate sulphate appears to be uniformly distributed in all directions (Figure 4-4). Particulate sulphate is known to accompany windborne aerosols during long-range air-mass transport (Benkovitz *et al*, 1994; Husain *et al*, 1984). On the Highveld aerosol transport occurs via air mass recirculation over southern Africa (Piketh *et al*, 1999; Piketh, 2000; Tyson and Preston-Whyte, 2000). Although north-westerly and easterly winds predominate, the distribution remains uniform from all wind directions (Figure 4-4). This

suggests that sulphate measured at Elandsfontein results not only from local sulphur emissions, but is also due to long-range transport of sulphate aerosols. Consequently, the observed values are the result of well-mixed advecting concentrations.

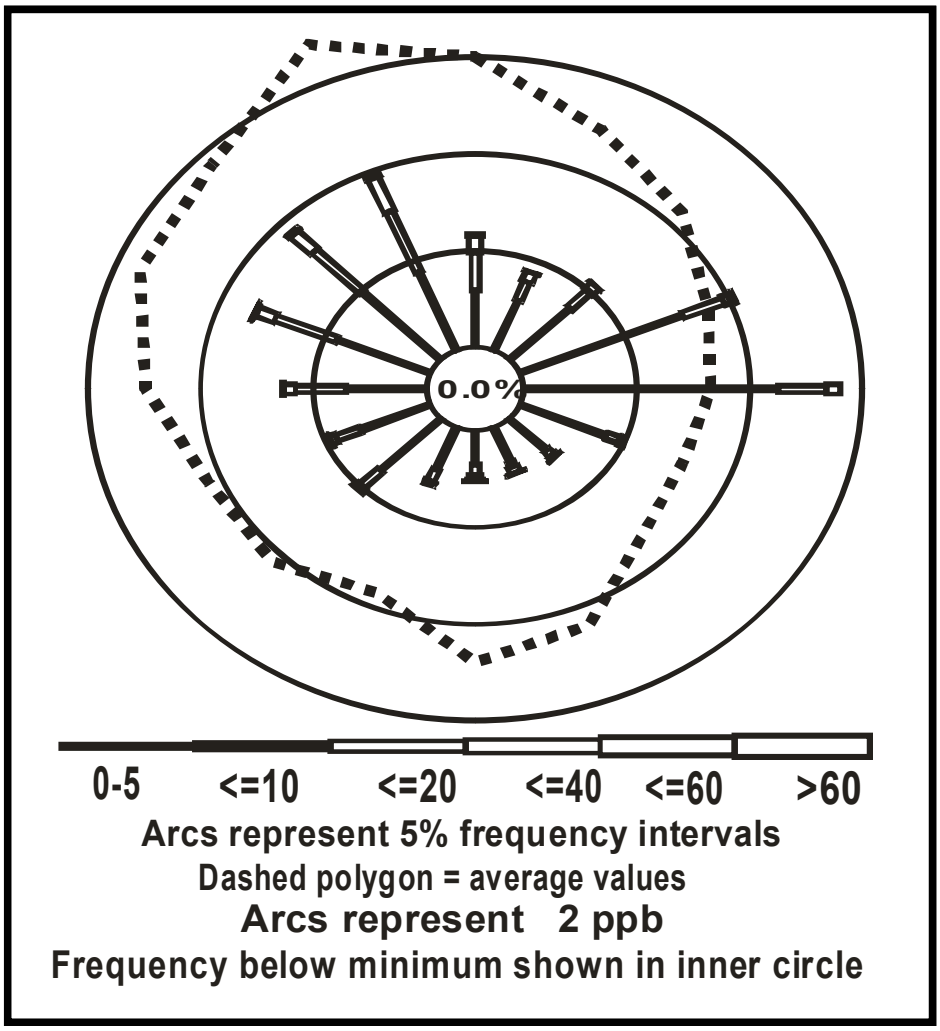

Figure 4-4: Mean particulate sulphate concentration distribution at Elandsfontein between September 2004 and August 2005

Observations from the wind rose (Figure 4-1) reveal that pollution concentrations reaching Elandsfontein are effectively a mixture of all sampled gases and particulate matter, emitted and evolved from both ground- and elevated-sources. The coal-fired power stations were

seen to be the major contributors to sulphur dioxide and particulate sulphate in the atmosphere, while the hydrogen sulphide emission source areas were fairly close to the coal-fired power plants and, hence, may be attributed to the nearby open-cast coal mines that feed the power-plants' boilers.

4.3.2 Temporal Variations of Atmospheric Sulphur at Elandsfontein

Temporal variations have been used to describe concentration distributions of sulphurous compounds in the planetary boundary layer (Bari *et al*, 2003a). A significant amount of particulate sulphate traverses the Highveld region annually (Tables 4-1 and 4-2). In order to ascertain the probable sulphur pollution load over the Mpumalanga Highveld, an hourly temporal scale of up to a year's dosage of H_2S, SO_2 and sulphate was estimated for Elandsfontein (Table 4-1).

Table 4-1: Estimation of sulphur dosage in the planetary boundary layer at Elandsfontein

	Temporal scale dosage as a percentage of total sulphur			
Compound / Duration	**1 h [10^3] (mg m^{-3})**	**1 day (mg m^{-3})**	**1 month (mg m^{-3})**	**1 year (mg m^{-3})**
Hydrogen sulphide	6.89 ± 1.1	0.17 ± 0.1	3.04 ± 0.1	62 ± 0.001
Sulphur dioxide	24.16 ± 9.2	0.58 ± 1.2	17.93 ± 1.2	216 ± 0.01
Particulate sulphate	5.24 ± 0.4	0.13 ± 0.1	3.39 ± 0.1	47 ± 0.001

The dosage, expressed as the mass concentration of the species per unit time (Drufuca *et al*, 1980), indicated exceptionally high values of SO_2 compared with values obtained for either H_2S or sulphate. On average, the values obtained for either H_2S or sulphate were about 25 % of the values obtained for SO_2 over the same time scales. Further, the amount of SO_2 that is released yearly from the power plants near Elandsfontein, about 216 mg m^{-3}, is significant. Hence, the large SO_2 level is most likely to be partly deposited on the surface and partly traverse over Elandsfontein (Figure 2-1).

Table 4-2: Monthly mean ambient total sulphur, gaseous sulphur and particulate sulphate concentrations at Elandsfontein

Time (Month)	$S_P = SO_4^{2-}$ /µg m^{-3}	$S_g = H_2S + SO_2$ /µg m^{-3}	$S_T = SO_4^{2-} + H_2S + SO_2$ / µg m^{-3}	$[S_P / S_T]$ %
Sep-04	4.42 ± 3.9	21.48 ± 30.1	25.89 ± 12.1	17.05
Oct-04	7.62 ± 4.2	26.75 ± 37.5	34.37 ± 13.5	22.18
Nov-04	7.28 ± 4.1	26.24 ± 35.3	33.52 ± 13.4	21.73
Dec-04	4.29 ± 3.3	18.43 ± 28.3	22.72 ± 10.0	18.87
Jan-05	4.26 ± 3.4	20.96 ± 28.0	25.23 ± 11.8	16.89
Feb-05	4.13 ± 3.1	23.09 ± 46.2	27.22 ± 13.4	15.18
Mar-05	3.04 ± 2.9	24.25 ± 39.9	27.28 ± 15.0	11.12
Apr-05	2.35 ± 1.7	22.82 ± 37.7	25.17 ± 14.5	9.32
May-05	4.33 ± 5.3	34.94 ± 48.2	39.27 ± 21.6	11.04
Jun-05	5.76 ± 5.6	36.52 ± 43.0	42.27 ± 21.8	13.62
Jul-05	5.77 ± 5.2	29.47 ± 35.8	35.24 ± 16.8	16.36
Aug-05	4.66 ± 3.9	35.96 ± 55.4	40.62 ± 22.1	11.48

The H_2S yearly dose, of about 62 mg m^{-3}, is low. Consequently its characteristic malodorous form is masked by dilution. Particulate sulphate present over the Mpumalanga Highveld is also low at about 47 mg m^{-3} per year, yet it is significant since it is known to be a more harmful aerosol than its acid precursors (Newman *et al*, 1975b; Carmichael and Peters, 1984a). With this level of particulate sulphate observed within one year in the planetary boundary layer over Elandsfontein, the Mpumalanga Highveld subregion and adjacent communities will be likely to experience the pollution problems associated with sulphate aerosols.

The form of temporal distribution illustrating the amount of sulphate relative to the total amount of sulphur in air is the mass percent of sulphate (Table 4-2). These mass percentages were based on the assumption that the total sulphur compounds over the Highveld consist of H_2S, SO_2 (as reactants) and particulate sulphate (as final product), while any other sulphur compounds are intermediates within the reaction for the production of particulate sulphate and are thus always assumed to be present at very low

concentrations (Figure 4-5). The particulate sulphate relative to total observed sulphur ranged between 9.32 and 22.18 %.

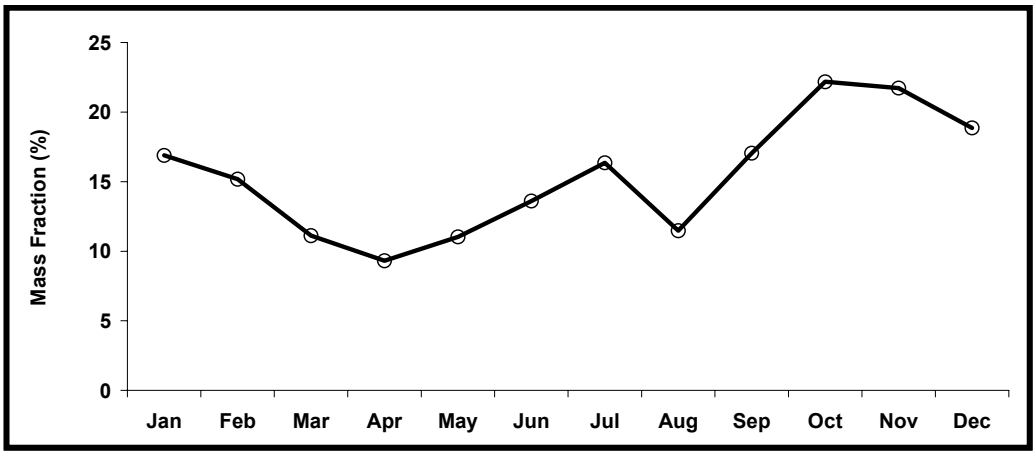

Figure 4-5: Monthly mass fraction distributions of particulate sulphate relative to total sulphur at Elandsfontein between September 2004 and August 2005

The highest mass fraction of particulate sulphate was observed in October (indicating a high accumulation and low removal rate) and the reverse in April. Since the intention of this study did not include the investigation of the deposition mechanisms, the behaviour differences in accumulation and removal rates were attributed to variations in either deposition rates or oxidation rate or by the combination of both processes. Therefore, for air quality purposes, particulate sulphate observations in October and April are essential over the Mpumalanga Highveld.

Diurnal Characteristics of Sulphur Species

The different patterns exhibited by H_2S are characteristic of emissions occurring from a variety of sources and at varying source strengths (Figure 4-6). There was apparently no definite diurnal variation observed for H_2S in summer and autumn. This may be due to possible rapid thermal oxidation, together with diffusion, reducing the concentration of H_2S to the background level between the source areas and the monitoring station. The

summer and autumn observations were the lowest, with approximately equal day- and night-time values. Consequently, the observed H_2S concentrations at the monitoring station were most likely the background concentrations.

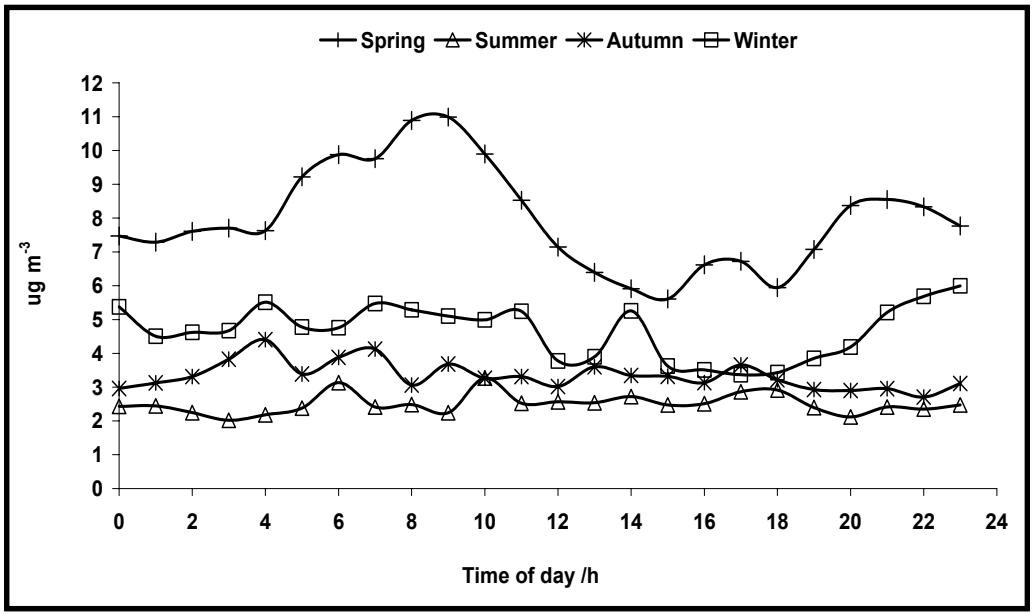

Figure 4-6: Diurnal variations of mean H_2S concentrations at Elandsfontein for the various seasons observed over southern Africa

In winter and spring there was a consistent concentration reduction in the daytime, while at night there was concentration accumulation. This accumulation may be attributed to low-level emissions below the surface inversion which only breaks in the daytime. This is more pronounced in spring than in winter. In spring there was a distinct diurnal pattern, with very high concentrations of H_2S occurring between 08:00 and 10:00 and between 20:00 and 22:00. The night-time increase was similar to winter observations. During the day oxidation would occur, while at night emitted H_2S would accumulate in the planetary boundary layer. Whereas in the mornings, as the boundary layer height increases, the gases tend to occupy the added volume until a particular temperature (at midday) is reached, leading to the occurrence of thermal oxidation, -hence the increased H_2S advecting across the monitoring site. Also there is the possibility that the observed H_2S was evolving from

surface emissions since morning plume fumigation characteristics with boundary layer effects were not observed even with observations in spring. The order of increasing H_2S distribution for the four seasons was summer, autumn, winter and spring.

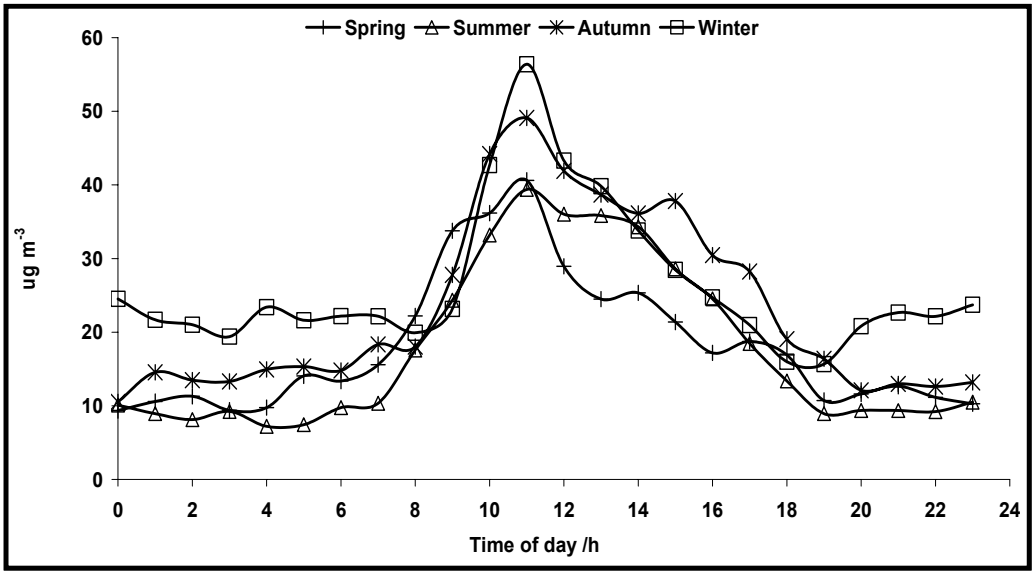

Figure 4-7: Diurnal variations of mean SO_2 concentrations at Elandsfontein for the various seasons observed over southern Africa

A consistent diurnal variation was observed for SO_2 concentrations over Elandsfontein but with slight variations in the levels (Figure 4-7) in all four seasons with maximum at about 11:00. The diurnal pattern shows that the SO_2 emissions were most likely from elevated smoke plumes since concentrations increase in the daytime and decrease at night. This variation is attributed to downwash of morning plume fumigation resulting from the transition from an inversion to a lapse temperature profile.

The gradation in properties between spring, summer, autumn and winter variations can be seen as the mean concentration rises and the diurnal peak becomes more pronounced and narrower from spring to winter. The maximum observed SO_2 concentration was in winter while summer recorded the lowest. In winter, increased demand for energy is associated with more coal combustion (Terblanche *et al*, 1993) as well as low oxidation rate (Moller,

1980), whereas the reverse is the case in summer. The difference in the diurnal behaviour for winter confirms that coal combustion processes, coupled with low mixed layer heights, are the principal causes of higher night-time and daytime peaks.

In all four seasons the concentration decreased in a similar manner after reaching the maximum with a sudden drop between 11:00 and 12:00, followed by a gentle reduction which terminated at 19:00. The decrease in SO_2 from 11:00 is due to boundary layer effects which include the changing of plume shape from fumigation to coning and reduction in the mixed layer height coupled with photochemical reactions. Since the intensity of gas concentration is a function of the volume of the mixing height, the differences in the day- and night-time mixed layer heights for the seasons may be deduced. Based on the degree of concentration differences, an empirical estimation of the mixed layer height, h_{us}, is that in summer the depth was larger than winter by a factor of about 1.5 in the daytime and by about 3.0 at night-time.

The diurnal variation of particulate sulphate shows unique behaviour in all seasons (Figure 4-8). This may be ascribed partly to atmospheric aerosol recirculation activities over southern Africa and partly to chemical transformation of hydrogen sulphide and sulphur dioxide (Piketh *et al*, 1999; Dlamini, 2005; Eggleton and Cox, 1978; Benkovitz *et al*, 1994; Husain *et al*, 1984). For summer, autumn and spring, maximum concentrations occurred between 11:00 and 18:00, while in winter the maximum occurred between 08:00 and 11:00. It can be seen that the overall curve is a combination between nocturnal accumulations with rapid dissipation after sunrise, with a regular diurnal pattern showing a maximum at midday. The pattern shows that the sulphate was possibly from elevated advecting smoke plumes since morning plume fumigation patterns, together with a variation in boundary layer mixing heights, were observed (Djolov *et al*, 1987).

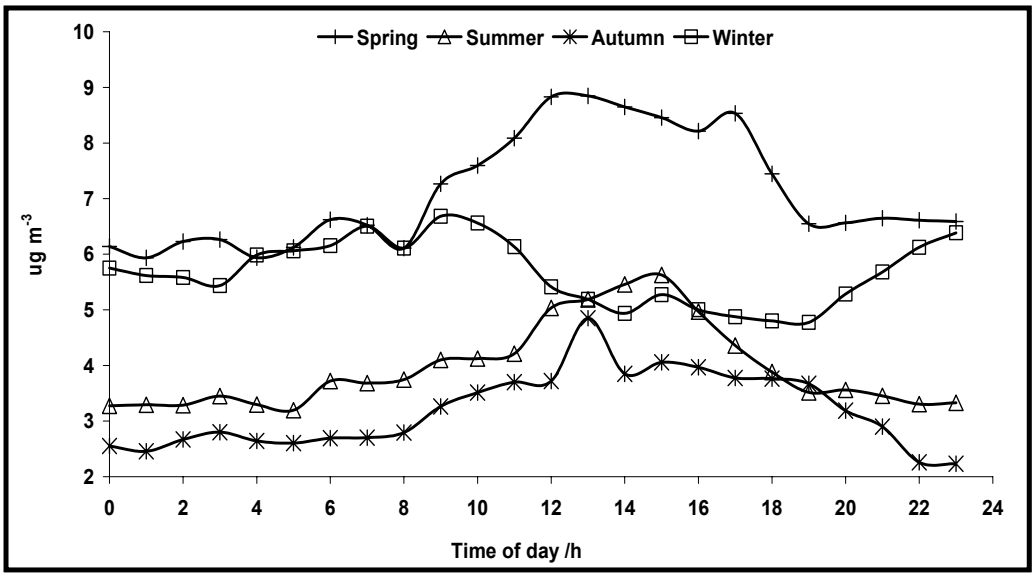

Figure 4-8: Diurnal variations of mean particulate sulphate concentrations at Elandsfontein for the various seasons observed over southern Africa

In addition summer has been characterised by frequent episodes of sulphate (Husain *et al*, 1984; Rahn and Lowenthal, 1984; Tuncel *et al*, 1985) as a result of air masses traversing industrial areas where heavy coal users are located (Bari *et al*, 2003b).

With the exception of winter, the daytime particulate sulphate concentrations approached maxima about two hours after the maximum observed daytime SO_2 concentration. This implies that SO_2 may be partly responsible for sulphate formation with a two-hour residence time. In addition, on winter mornings, surface inversion occurs strongly which results in accumulation close to the Earth's surface. Also, winter is characterised by low temperatures, low relative humidity and, consequently, low water vapour content which does not favour aqueous-phase reactions. Therefore, transformation would probably be principally through gas-phase reactions. The winter diurnal variation showed that less particulate sulphate was present in the daytime compared to night-time. This may be attributed to increased wind, low mixing height as well as reduced daytime SO_2 photochemical oxidation (Moller, 1980). In addition, almost no rainfall in winter means that dry deposition will dominantly contribute to daytime concentration reduction as well

as surface absorption when particles make contact with the Earth's surface, while, at night-time, mist will dominantly scavenge the particles to the surface.

During the study period, the summer, autumn and spring rainfall patterns were erratic, hence both wet- and dry-deposition mechanisms contributed to particulate matter removal over the Mpumalanga Highveld. The maximum sulphate concentration occurred in spring, while the minimum was recorded during autumn. The maximum spring sulphate concentrations were larger than the autumn maximum by a factor of about 2.25 for daytime and by a factor of about 2.40 for night-time.

Although not all the three sulphur species exhibited consistent diurnal behaviour, the explanation to their variations was easily obtained from the effects of meteorological parameters on the planetary boundary layer. Daytime temperature lapse and night-time temperature inversion processes are notably evident from the diurnal signature of the measured SO_2 concentrations and, to some extent, with particulate sulphate concentration distribution (Figures 4-7 and 4-8).

Seasonal Characteristics of Sulphur Species

A combination of the monthly characteristics of the three sulphur species observed over Elandsfontein is shown in Figures (4-9) to (4-11). Throughout the 12-months sampling period, the averages of the measurements for SO_2, H_2S and particulate sulphate levels ranged between 16 and 32 μg m^{-3}, 2.5 and 8 μg m^{-3} and 3.0 and 7.5 μg m^{-3}, respectively (Figure 4-9). SO_2 dominated, with its concentration reaching 450 μg m^{-3}, while observed H_2S and sulphate reached a maximum of about 130 μg m^{-3} and 32 μg m^{-3}, respectively (Figure 4-10).

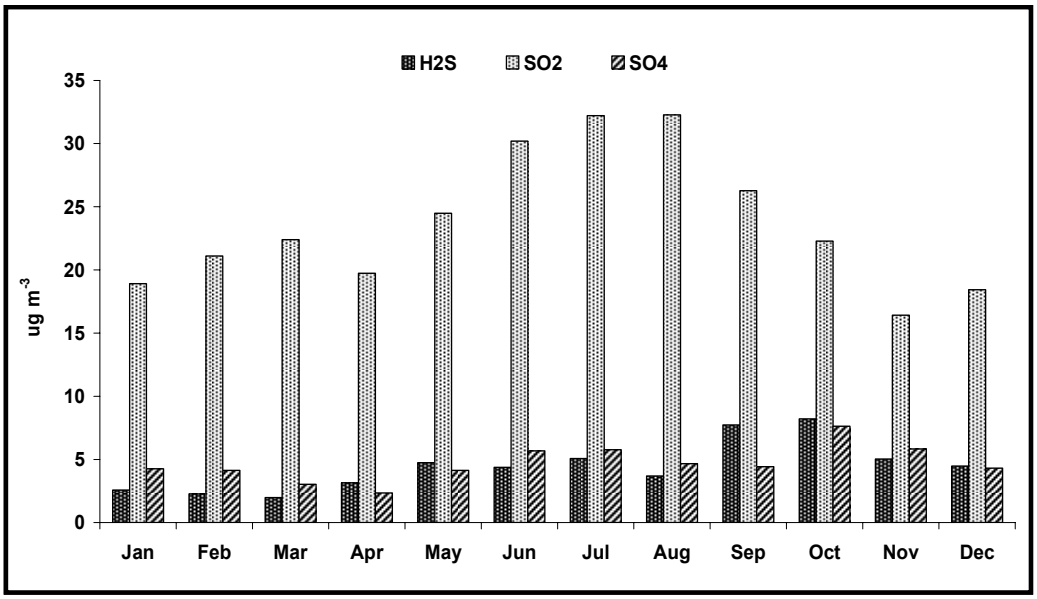

Figure 4-9: Seasonal variations of mean concentrations of the observed sulphur species at Elandsfontein between September 2004 and August 2005

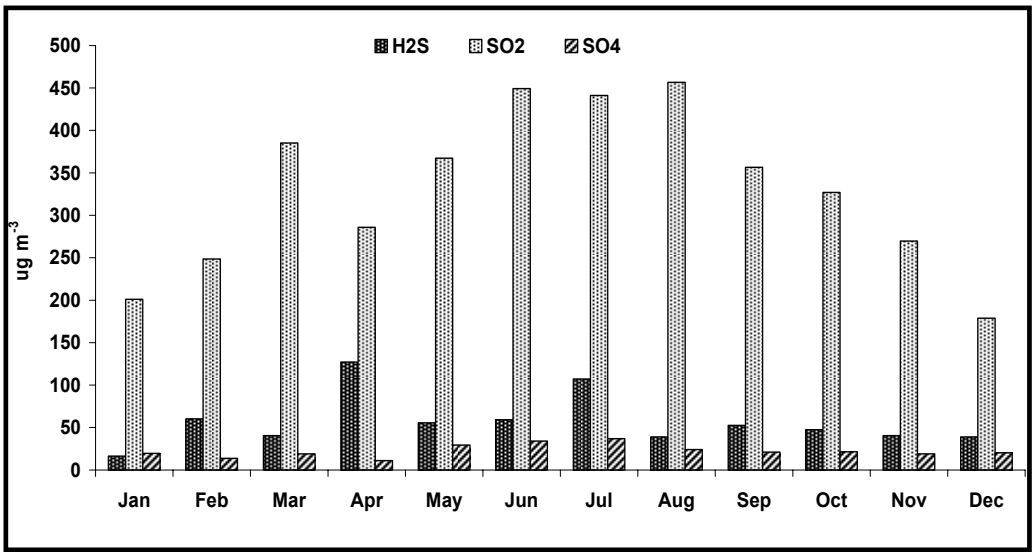

Figure 4-10: Seasonal variations of maximum concentrations of the observed sulphur species at Elandsfontein between September 2004 and August 2005

The minimum observed ambient SO_2 concentration decreased to almost zero for some months during the year (Figure 4-11). With the exception of the March data, a direct

proportional relationship is evident for SO_2 between the monthly averages and monthly maxima, as seen between April and November (Figure 4-9 and 4-10).

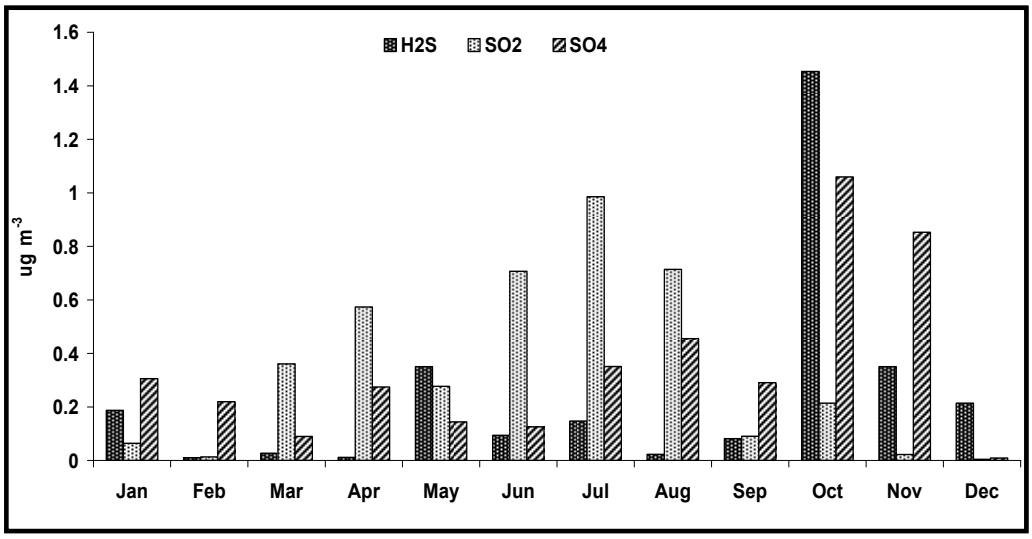

Figure 4-11: Seasonal variations of minimum concentrations of the observed sulphur species at Elandsfontein between September 2004 and August 2005

This is an indication that the average values are a true reflection of all the sampled data. It stands to substantiate the explanations for the seasonal variations of SO_2 concentration over the study area illustrated with average values. There are clear indications of higher concentrations for SO_2 during winter (June to August), while the highest concentrations of H_2S and sulphate occur during spring (September to November). The high SO_2 levels could be attributed to an increase in energy demand during winter (Snyman *et al*, 1990), coupled with the reduction in atmospheric water droplets that have been known to enhance SO_2 oxidation (Moller, 1980). In contrast, during spring, the high concentrations of H_2S and sulphate are attributed to the substantially lower mixing heights -which are dependent on the temperature- during these months than in autumn and summer. Similar observation for SO_2 had been reported (Annegarn *et al*, 1996).

A distinct seasonality is seen with SO_2 variations between January and December, varying by a factor of about two between the lowest month (November) and the highest (July and August). The monthly variation in H_2S and SO_2 concentrations is most likely due to a difference in oxidation rates influenced by the prevailing meteorological conditions at the time of occurrence. In comparison, sulphate variations may be attributed to varying deposition mechanisms and rates (Granat, 1978), coupled with atmospheric aerosol recirculation in southern Africa (D'Abreton, 1996; Tyson and D'Abreton, 1995; Sampson, 1980). In summary, the pollution loading over the Mpumalanga Highveld subregion of the various observed sulphur species was the result of direct emissions, meteorological variations, boundary layer characteristics and air circulation within the troposphere (Oke, 1987; Annegarn *et al*, 1996).

Based on the mean seasonal observations, H_2S, though not present in concentrations comparable with ambient SO_2 concentrations, cannot be ignored as contributing to the ambient SO_2 levels. Also, a linear relationship is evident (Figure 4-9) between H_2S and sulphate with their maximum in spring and minimum in summer and, to some extent, SO_2. These may be attributed to variations in transport, transformation and removal rates and mechanism for different seasons. The summer (December to February) and autumn (March to May) months are unfavourable for the presence of H_2S, SO_2 and particulate sulphate. This is due to the increased thermal oxidation rate of H_2S (Eggleton and Cox, 1978) and SO_2 photochemical oxidation (Moller 1980; Warneck, 1999; Herrmann *et al*, 2000; Grgic and Bercic, 2001) as well as the high removal rate of particulate sulphate due to wet deposition (Granat, 1978). The extent of removal via wet deposition is obvious with the rainfall observed during the aforementioned periods (Table 4-3). The climatology of the area has also shown that wet deposition is imminent during the said periods of concentration drop (Figure 4-12).The variations in monthly concentrations reveal a simple approach for the quick estimation of particle removal rate as well as the predominant deposition mechanism during transition from one season to another. These variations are most noticed with observations shown in Figure (4-10). It can deduced that either the accumulation of particulate sulphate is at a maximum in spring and minimum in autumn or the deposition rate is lowest in spring and highest in autumn.

Table 4-3: Rainfall data over Mpumalanga (September 2004 and August 2005)

Months	Rainfall range (mm)
September, 2004	0 – 10
October, 2004	25 – 50
November, 2004	50 – 100
December, 2004	300 – 500
January, 2005	100 – 300
February, 2005	50 – 100
March, 2005	50 – 100
April, 2005	25 – 50
May, 2005	0 – 10
June, 2005	0 – 10
July, 2005	0 – 10
August, 2005	0 – 10

Source: www.weathersa.co.za/RainfallMaps/RainMaps.jsp

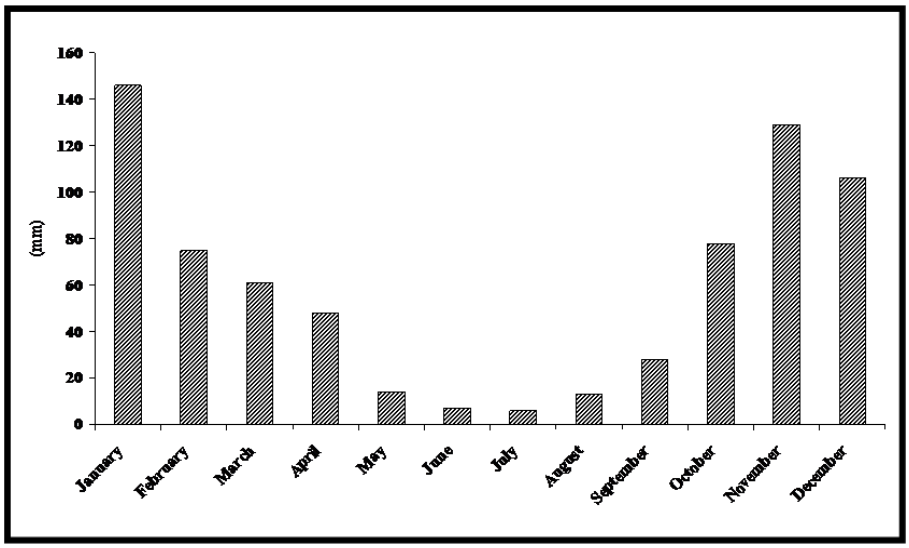

Figure 4-12: Climatological information according to World Meteorological Organization (WMO) on the seasonal rainfall variation in over Mpumalanga (GPS: 26° 27' S, 29° 29' E; Height: 1663m) between 1961 and 1990 from South African Weather Service Records.

4.3.3 Relationships between SO_2 and Particulate Sulphate in the Atmosphere

Until recently there has not been a known very short averaging time (10-minute) relationship between sulphur dioxide and sulphate over the Mpumalanga Highveld, since

sampling and analyses for sulphate have been done by passive methods. This was because SO_2 in the atmosphere is well known to undergo transformation during long-range transport of pollutants. Now that it is possible to observe these sulphur species through continuous monitoring with short averaging time, it has been noted that a linear trend exist between SO_2 and sulphate during summer, autumn and spring (Figures 4-13a to 4-13c). This implies that during summer, autumn and spring higher SO_2 results in more particulate sulphate formation. In contrast, for winter, there were large scatterings of the data (Figure 4-13d) with no apparent direct proportionality due to a reduction in SO_2 oxidation rates (which is enhanced by high relative humidity).

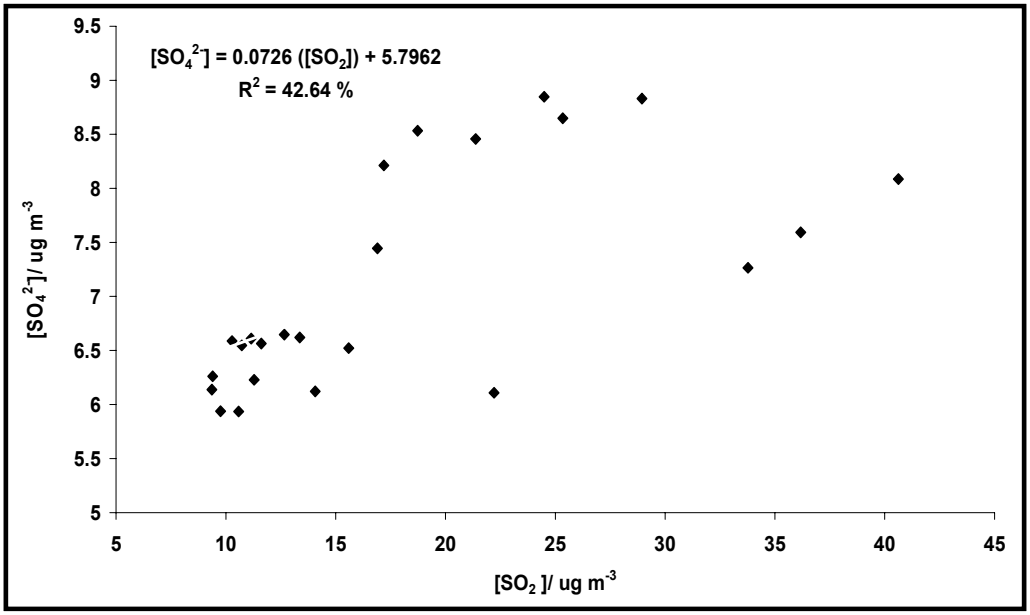

Figure 4-13a: Regression correlation between SO_2 and particulate sulphate in spring from measurements at Elandsfontein

The best correlation is seen in the summer observations (Figure 4-13b). This could be attributed to the high rate of chemical reactions between the released SO_2 and the generated sulphate.

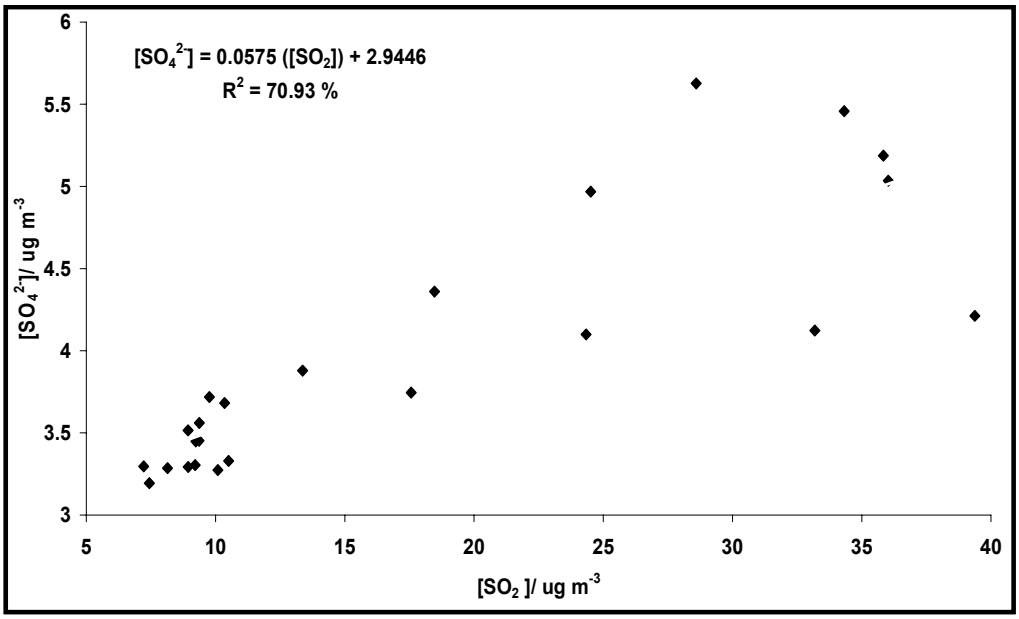

Figure 4-13b: Regression correlation between SO_2 and particulate sulphate in summer from measurements at Elandsfontein

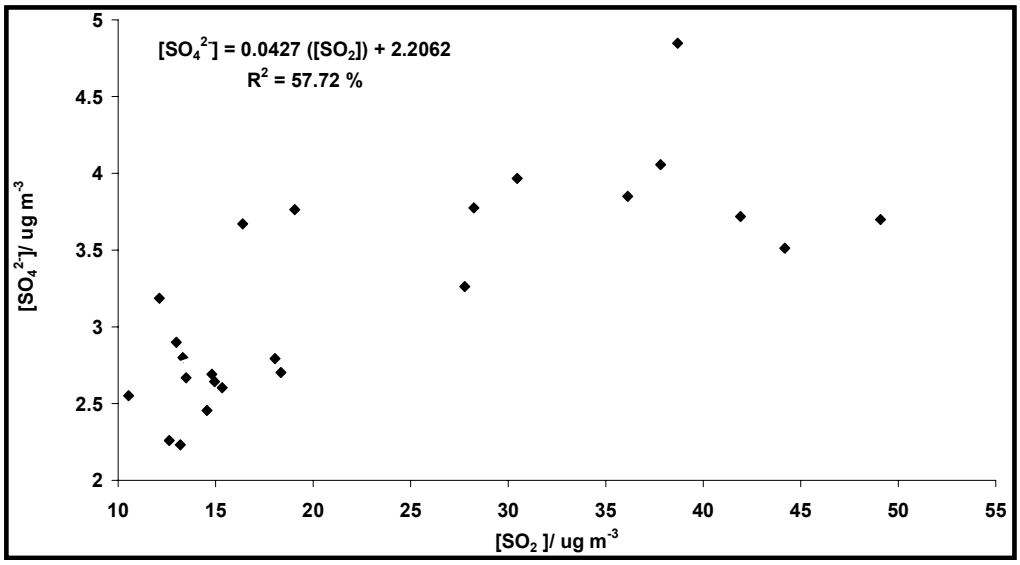

Figure 4-13c: Regression correlation between SO_2 and particulate sulphate in autumn from measurements at Elandsfontein

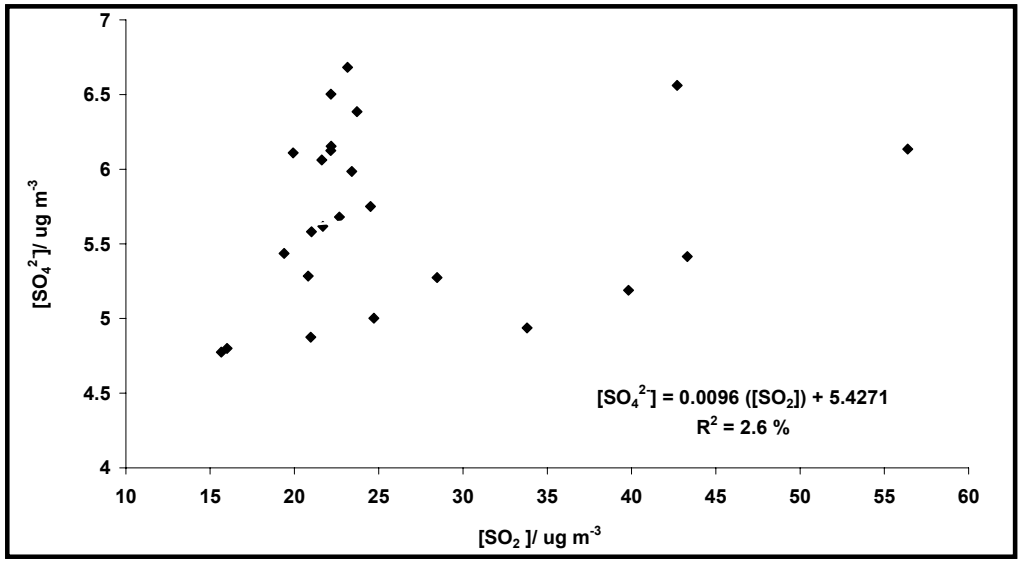

Figure 4-13d: Regression correlation between SO_2 and particulate sulphate in winter from measurements at Elandsfontein

To compare in-plume and well-mixed ambient concentrations, the summer observations were used. The data were extracted for two wind directional sectors, for the purpose of separating in-plume and background concentrations (Figure 4-14).

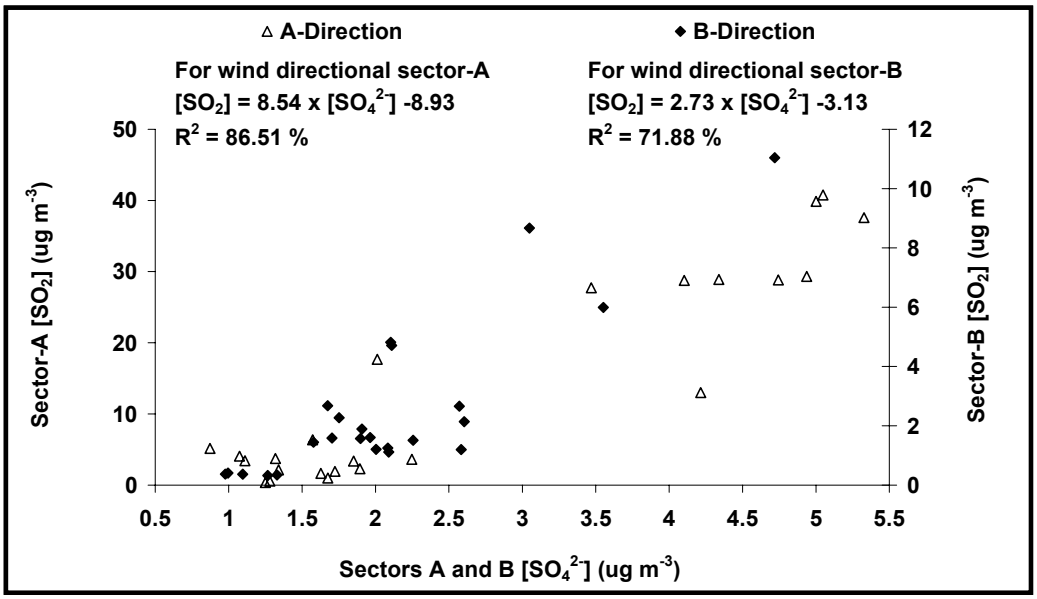

(Legend: Sector A (210 to 300°) and Sector B (68 to 110°))

Figure 4-14: Relationship between SO_2 and particulate sulphate obtained as an average of all measured data at Elandsfontein, from wind directional sectors A and B.

Wind directional sector A refers to the vicinity where the major pollution source to Elandsfontein is located (Figure 2-1), while pollutants from the wind directional sector B were assumed to be well-mixed ambient concentrations from all significant pollution sources in the area. The concentrations from the wind directional sector B were assumed to be of the same magnitude as the pollutants' background levels. In both wind directional sectors, the degree of agreement of the formulated correlations was about 87 % and 72 % for sectors A and B, respectively, hence the SO_2 and sulphate concentrations are also substantially controlled by chemical reactions.

4.3.4 Meteorological Contributions to Particulate Sulphate Distribution

Over the southern African sub-continental region particulate sulphate is known to accompany long-range aerosol transport across the Highveld (Piketh *et al*, 1999; Piketh, 2000). From the field measurements, two case studies are used to describe the effects of meteorology on transport of particulate sulphate. The episodes of 02 and 15 July 2004 recorded the maximum observed sulphate concentrations at Elandsfontein.

In the case of the episode of 02 July, the daytime convective boundary effects were not influencing the concentration since at steady low wind speed, concentration growth occurred between 03:00 and 09:00, reaching a peak at 06:00 (Figure 4-15). In contrast, the variation in the day- and night-time boundary layer parameters is likely to occur between 09:00 and 20:00. However the decrease in sulphate concentration was complete before this time.

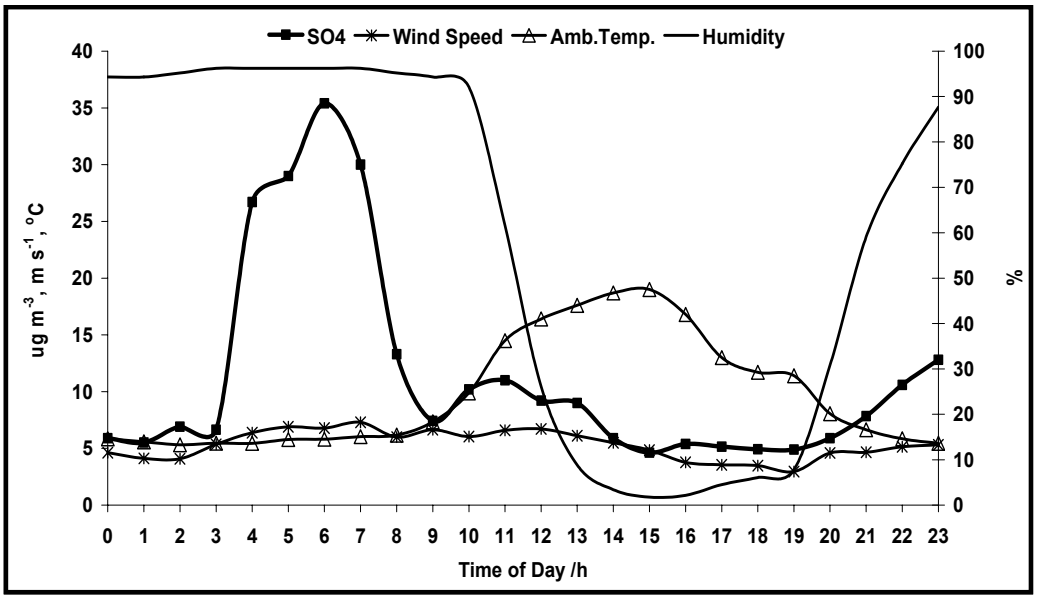

Figure 4-15: A diurnal episode on 02 July 2005 indicating the first observed maximum particulate sulphate concentration at Elandsfontein

The episode of 15 July is almost certainly as a result of morning convective eddies mixing the elevated nocturnal effluent concentrate towards the ground (Figure 4-16). It is a combination of nocturnal accumulation with rapid dissipation and regular diurnal behaviour with the maximum observed shortly after 11:00. Despite the influence of convective boundary layer parameters, the peak concentration is very steep rather than gentle, with the night-time temperature inversion reducing ground-level sulphate concentrations. It is thus evident from the observations on 02 and 15 July 2004 that long-range atmospheric aerosol recirculation was partly responsible for sulphate concentrations measured over the Mpumalanga Highveld.

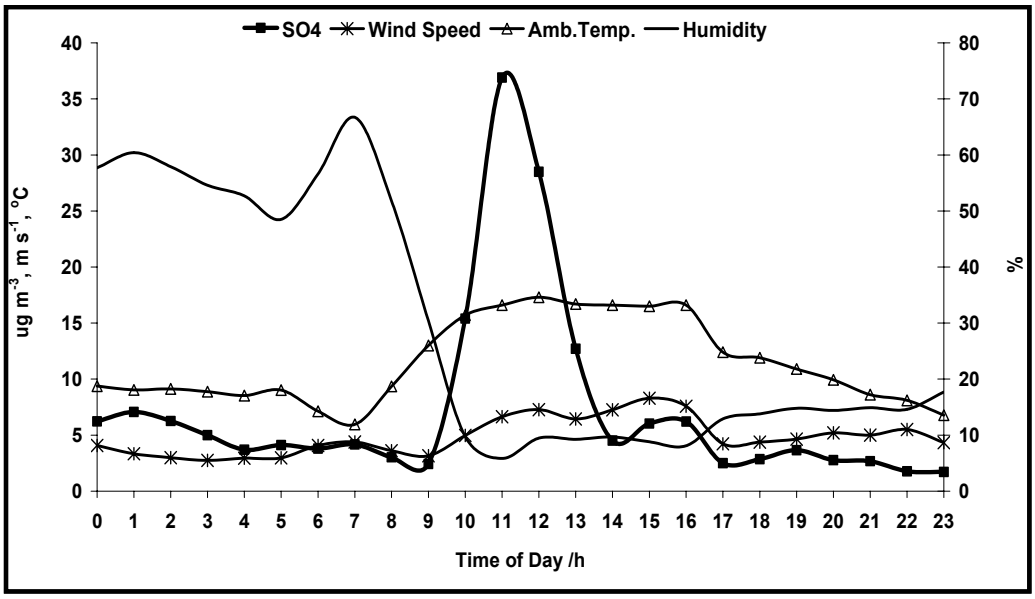

Figure 4-16: A diurnal episode on 15 July 2005 indicating the second observed maximum particulate sulphate concentration at Elandsfontein

These two episodes, especially that of 02 July (Figure 4-15), where the maximum observed concentration occurred at 06:00, exhibit a characteristic event influenced by the synoptic air circulation on regional aerosol transport within southern Africa. To further exemplify the 02 and 15 July episodes backward air trajectories at different elevations were used (Figures 4-17 and 4-18).

Back trajectories have been used in several case studies for evaluating air pollutant transport in the United Kingdom (Bari *et al*, 2003b). Similar to the method of Bari *et al* (2003b), a three-day NOAA HYSPLIT model back trajectory (Figures 4-17 and 4-18) of the episodes of the 02 and 15 July have indicated that sulphate aerosols are introduced through long-range transport. The trajectories show that air mass transport at about 500 hPa on 02 July and 700 hPa on 15 July originated from the mid-latitudes around Namibia which is not known to be a major source of sulphate (Piketh, 2000).

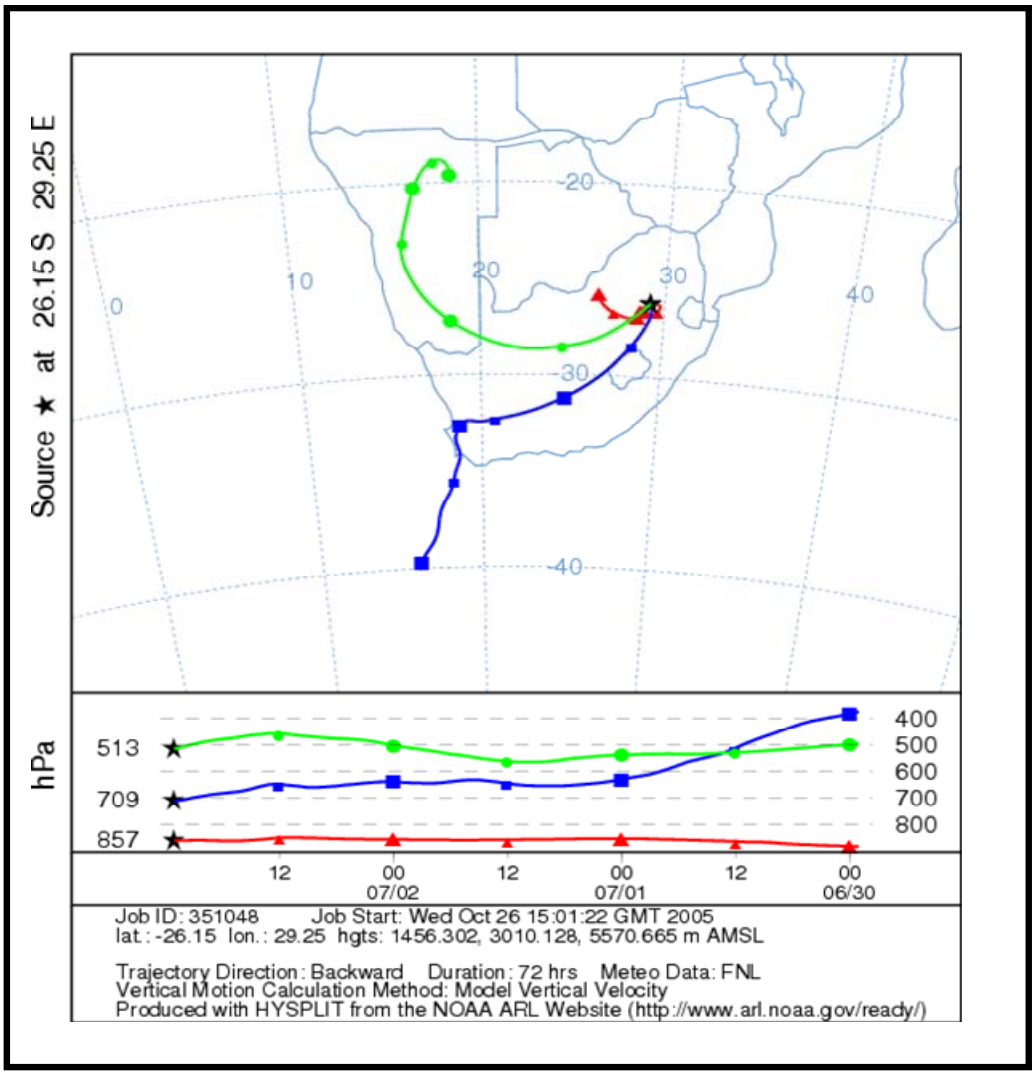

Figure 4-17: NOAA HYSPLIT backward trajectories ending at 23:00 UTC for 02 July 2005 from Elandsfontein

Between 30 June and 03 July the trajectory at 400 hPa drops to 709 hPa altitude, thereby bringing entrained particles towards the surface. This trajectory, being that originating from the Atlantic Ocean towards in-land, would most likely be transporting sulphates of sea salt. But, at that altitude, sea salts are most likely absent in the circulating air mass. The trajectory at 500 hPa, which originates from Namibia decreased slightly to 580 hPa before 02 July, then progressively gains height which results in a vertical transport of particles reaching an altitude of 513 hPa.

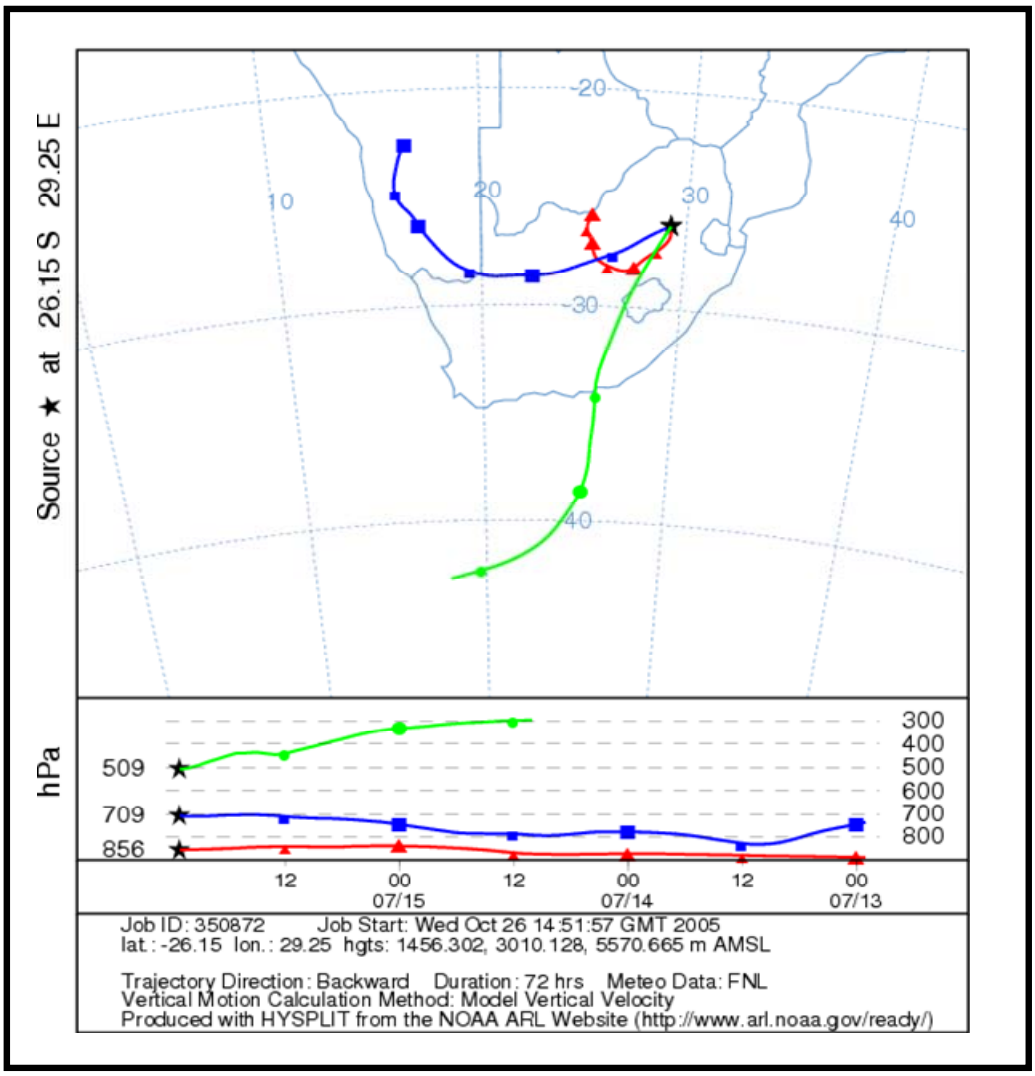

Figure 4-18: NOAA HYSPLIT backward trajectories ending at 23:00 UTC for 15 July 2005 from Elandsfontein

The third trajectory, which increases very gentle between the ground and 857 hPa, was transporting particles from the North of South Africa to Elandsfontein. All three trajectories have produced no evidence that air mass circulation over the region was responsible for the sulphate level observed. In contrast, during these days (in July) air flow is slow and, with fairly stagnated air, accumulation of sulphate occurs as well as SO_2 that

may oxidise to sulphate (Piketh, 2000). This could be the result of the accumulation of sulphate.

In the second episode (Figure 4-18), an upper tropospheric trajectory well below 300 hPa drops to 509 hPa from 13 to 16 July, thereby resulting in downward movement of particles towards the surface. This trajectory is also from the Atlantic Ocean, hence the accompanied sulphates are of the sea salts, while the in-land trajectory from Namibia decreased slightly and progressively gained height reaching 709 hPa. The third trajectory, of the 15 July episode, exhibited the same behaviour as that of the 02 July at Elandsfontein. Therefore, the episodes of 02 and 15 July may be attributed to the accumulation of sulphate due to the presence of stagnant air over the three-day period.

Characterising Atmospheric Particulate Sulphate Using Liquid Water Content

Atmospheric particulate sulphate has been characterised by using deliquescence relative humidity (DRH) and crystallisation relative humidity (CRH) (Tang, 1980; Tang and Munkelwitz, 1993). A distinction between two particulate sulphate types at Elandsfontein with seasonal variations is shown in the degrees of exceedances of deliquescence and crystallisation relative humidities (Figure 4-19). These two sulphate types were deduced by extracting for each seasonal sulphate measurement the DRH and CRH values of $(NH_4)_2SO_4$ and NH_4HSO_4 as given by Tang (1980); Tang and Munkelwitz (1993); Tang and Munkelwitz (1994), in section 2.9.5. Spring is dominated by aqueous-phase NH_4HSO_4 and solid $(NH_4)_2SO_4$, with the latter accounting for about 73.7 % of the NH_4HSO_4. The NH_4HSO_4 occurs more in solution than in the solid phase by a factor of about 2.7, while $(NH_4)_2SO_4$ occurs more in the solid phase than in solution by a factor of about 3.5.

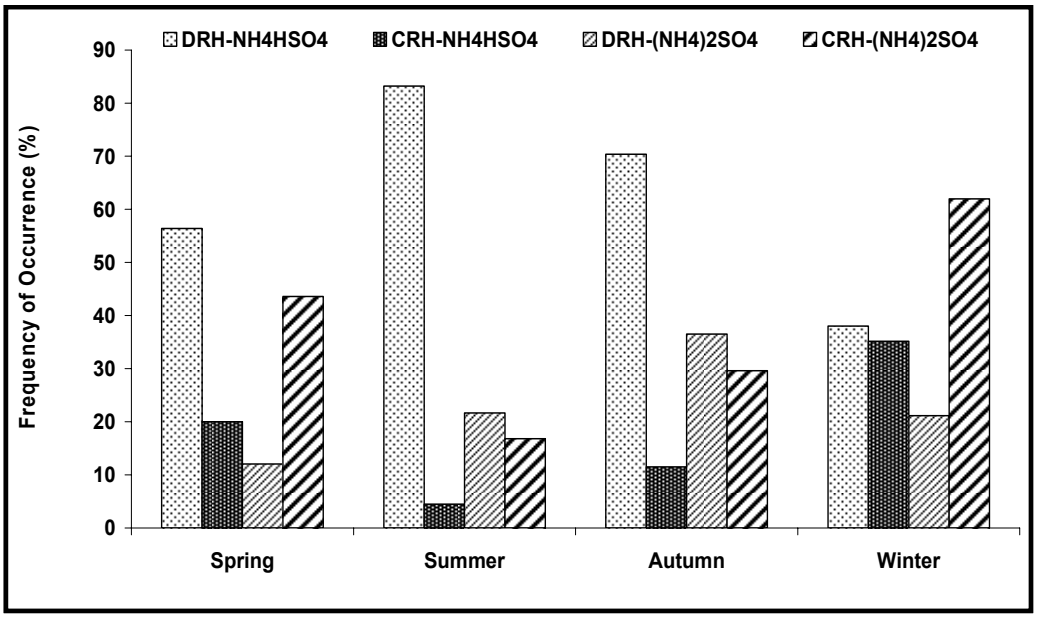

Figure 4-19: Frequency distribution of deliquescence and crystallisation relative humidities for particulate NH_4HSO_4 and $(NH_4)_2SO_4$ at Elandsfontein

In summer, NH_4HSO_4 solution occurs more frequently -amounting to about 60 % of the total sulphate. In the same observation, $(NH_4)_2SO_4$ solution occurred more than solid $(NH_4)_2SO_4$ by about 8 %. NH_4HSO_4 occurred more in the aqueous-phase than as a solid by a factor of about 80. A similar observation to summer occurrences of solution phases of NH_4HSO_4 and $(NH_4)_2SO_4$ dominating both species, but to different extents, was made in autumn. Aqueous NH_4HSO_4 occurs more frequently than solid NH_4HSO_4 by a factor of about 7.0 and $(NH_4)_2SO_4$ by about 1.2. The winter pattern is similar to that of spring but with higher values observed for solution NH_4HSO_4 and solid $(NH_4)_2SO_4$ occurring frequently, but it is slightly different in the sense that the largest occurrence is solid $(NH_4)_2SO_4$. The solid $(NH_4)_2SO_4$ is greater than aqueous $(NH_4)_2SO_4$, aqueous NH_4HSO_4 and solid NH_4HSO_4 by factors of 3.3, 1.8 and 1.7, respectively. Therefore, sampling specifically for NH_4HSO_4 is recommended in summer or autumn, while winter is the most appropriate period to sample for $(NH_4)_2SO_4$. Sampling in spring would results in aqueous NH_4HSO_4 competing against solid $(NH_4)_2SO_4$ since both forms of the sulphate occur frequently than the others.

4.3.5 Statistical Analyses for Total Atmospheric Sulphur Distribution

With a view to establishing the background levels of the sulphur species, frequency distributions of each 10-minute measured data set for the entire 12-month sampling period were produced (Figures 4-20 to 4-22).

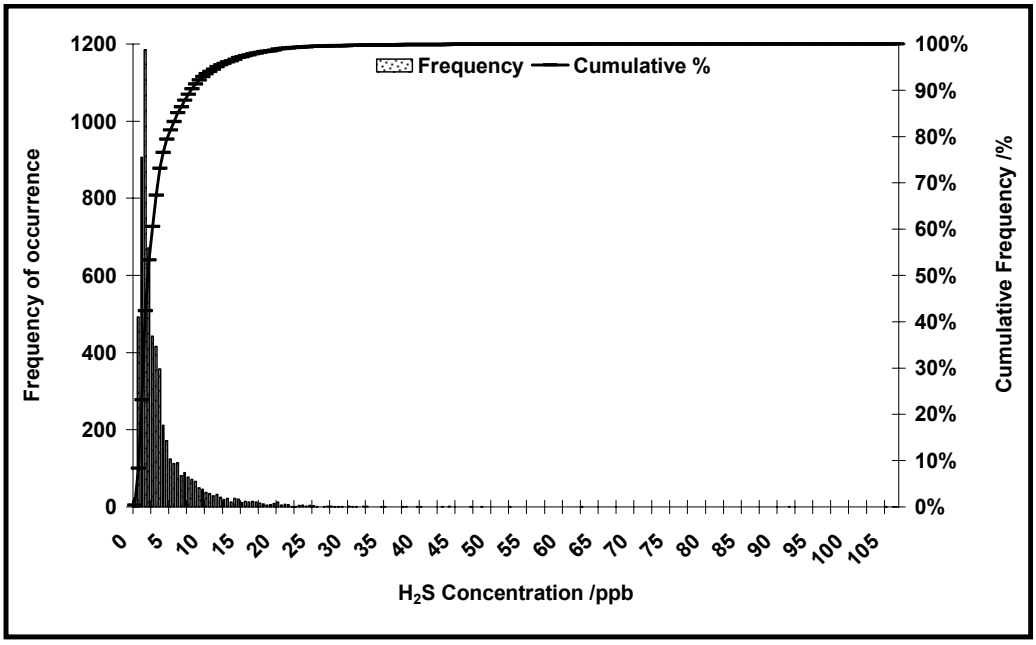

Figure 4-20: Frequency distribution of H_2S concentrations from September 2004 to August 2005 at Elandsfontein

These histograms were generated using two columns of sample size (H_2S between 0 and 110 ppb; SO_2 between 0 and 220 ppb; sulphate between 0 and 40 μg m^{-3}) and the corresponding measured values in Microsoft excel data analysis tool options. The dominant concentration occurrences which are representative of the background level for H_2S, SO_2 and particulate sulphate were 2.5 ppb, 3.0 ppb and 1.5 μg m^{-3}, respectively. These estimated background concentrations are independent of diurnal and seasonal variations for the various sulphur species over Elandsfontein.

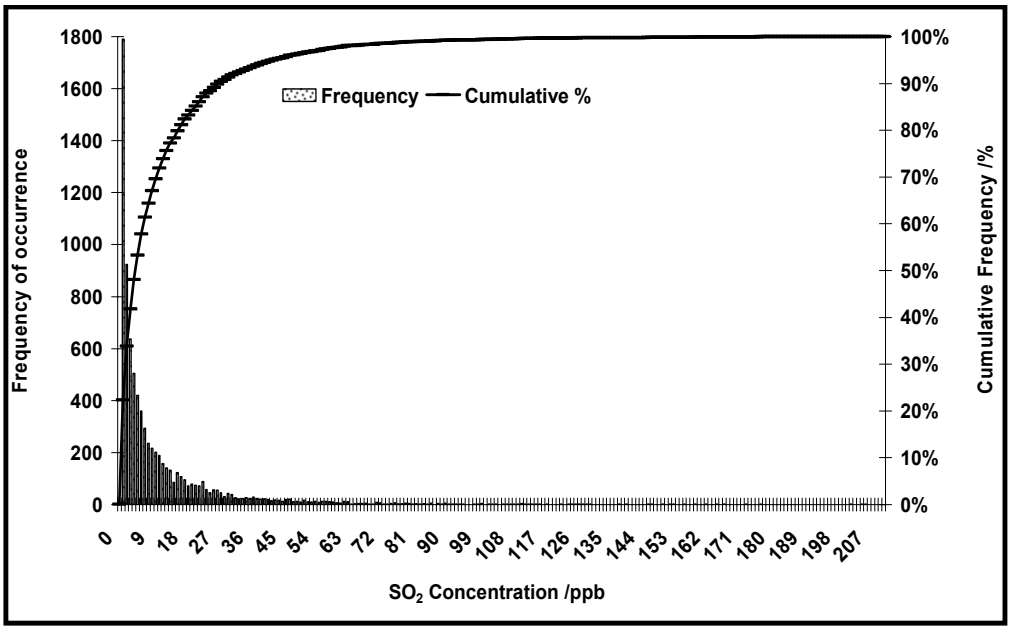

Figure 4-21: Frequency distribution of SO_2 concentrations from September 2004 to August 2005 at Elandsfontein

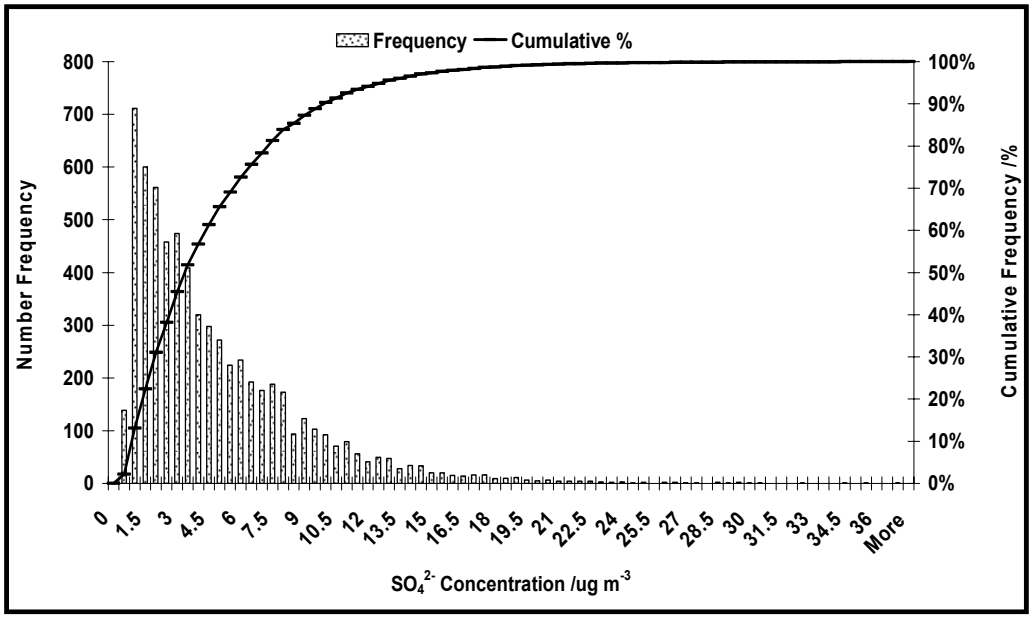

Figure 4-22: Frequency distribution of particulate sulphate concentrations from September 2004 to August 2005 at Elandsfontein

Large differences were observed between the mean, median and mode of H_2S, SO_2 and sulphate (Table 4-4), or, in other words, the distribution of the raw data is skewed. The raw data for all three sulphur species have been replotted in Figure 4-23 to emphasize this point.

Table 4-4: Summary data of the central tendency of the sulphur species

	Untransformed Values			Log. Transformed Values		
	H_2S	**SO_2**	**SO_4^{2-}**	**H_2S**	**SO_2**	**SO_4^{2-}**
Mean (µg m^{-3})	5.5	23.9	4.6	2.5	8.6	3.2
Median (µg m^{-3})	2.1	10.1	3.4	2.1	10.1	3.4
Mode (µg m^{-3})	1.5	24.2	1.5	1.5	24.2	1.5
Standard deviations (µg m^{-3})	13.2	38.6	4.0	3.7	10.8	2.5

This observation is expected of most raw environmental data (Ott, 1995; Patil and Rao, 1993). In order to justify the measures of central tendency of the data, to produce a 95 % confidence in mean, median and mode, a data transformation is required (Datez and Pantel, 1974; Ott, 1995).

These sets of raw concentration data for the three sulphur species throughout the 12-month sampling period have skewed frequency distributions (Figure 4-23) and, after transformation, yielded a normal distribution (Figure 4-24). This transformation included outliers that are regarded as spurious data but, from atmospheric studies, may represent several episodes that occurred during sampling.

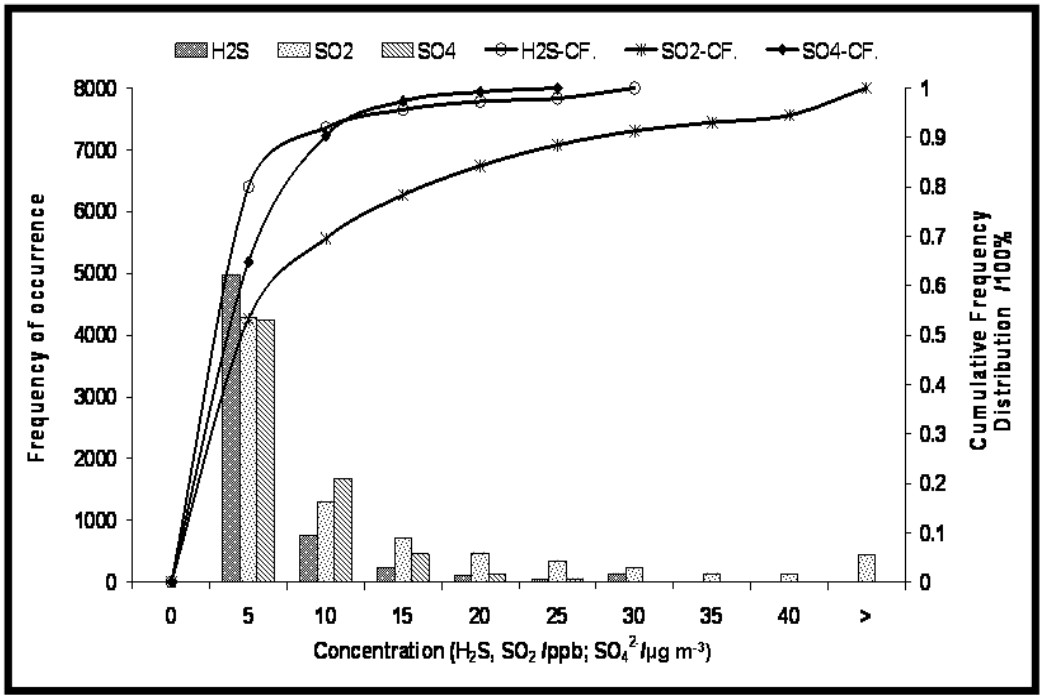

Figure 4-23: Frequency and cumulative distribution of raw measured H_2S, SO_2 and particulate sulphate concentrations from September 2004 to August 2005 at Elandsfontein

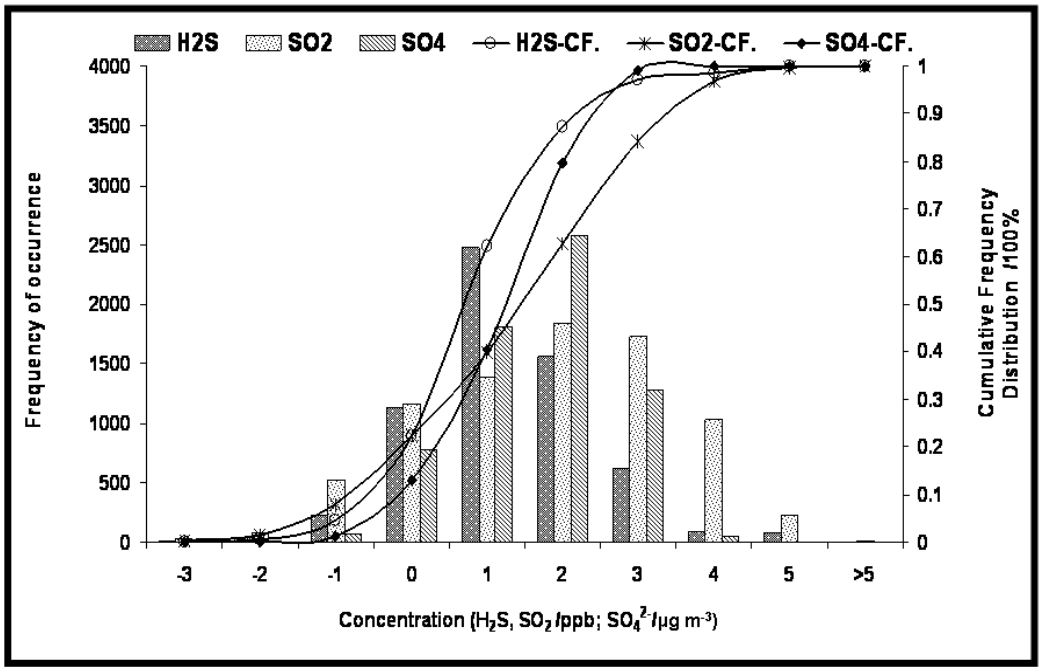

Figure 4-24: Frequency and cumulative distribution of the natural logarithmic transformed H_2S, SO_2 and particulate sulphate concentrations from September 2004 to August 2005 at Elandsfontein

For all three sulphur species, the natural logarithmic transformation (Ott, 1995) generated the best normalised data set compared with the other two generally applied transformation modes, namely; square root and inverse transformations (Figures 4-25 and 4-26). The latter transformation modes did not mitigate positive skewness of the data since there were still significant heavy tails, especially on the positive side (Patil and Rao, 1994). Subsequently, the actual concentrations of the natural logarithmic transformation are obtained by evaluating the antilogarithm of the values. This logarithmic transformation yielded mean averages and standard deviations of 2.5± 3.7 µg m^{-3}, 8.6 ± 10.8 µg m^{-3} and 3.2 ± 2.5 µg m^{-3}

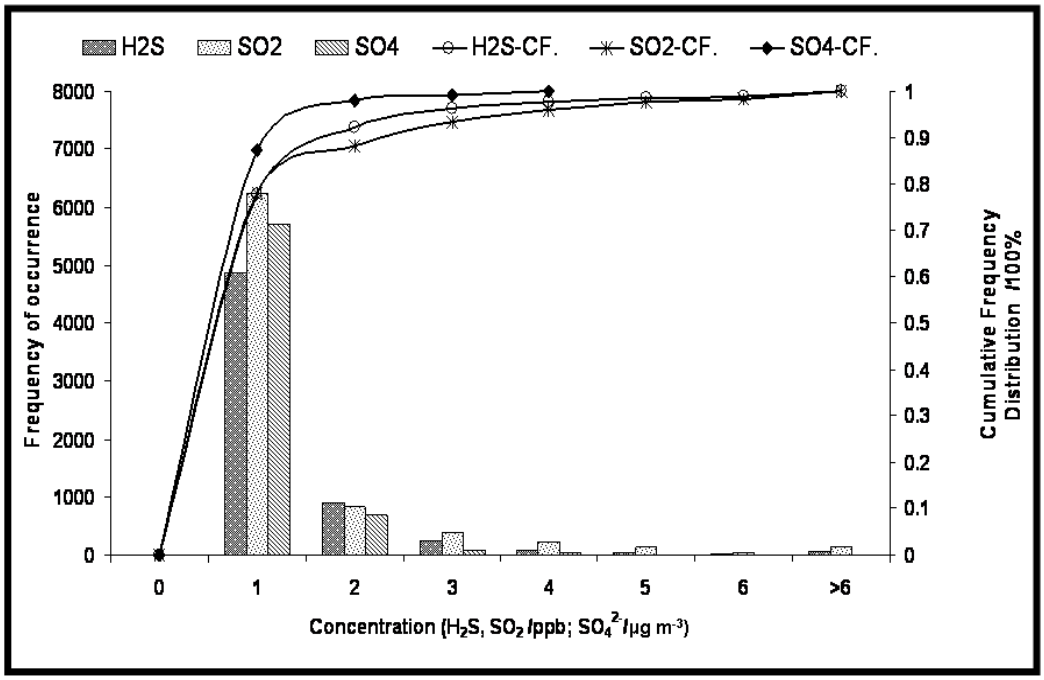

Figure 4-25: Frequency and cumulative distribution of the inverse transformed H_2S, SO_2 and particulate sulphate concentrations from September 2004 to August 2005 at Elandsfontein

for H_2S, SO_2 and particulate sulphate, respectively. In contrast, prior to the transformation, H_2S, SO_2 and particulate sulphate were 5.5 ± 13.2 µg m^{-3}, 23.9 ± 38.6 µg m^{-3} and 4.6 ± 4.0 µg m^{-3}, respectively.

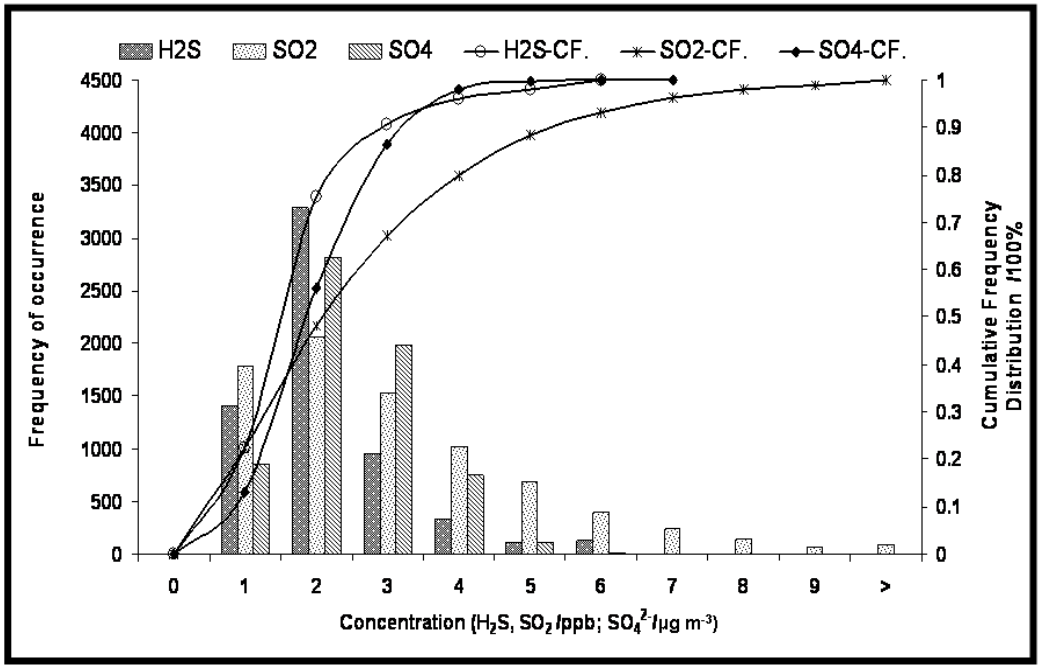

Figure 4-26: Frequency and cumulative distribution of the square root transformed H_2S, SO_2 and particulate sulphate concentrations from September 2004 to August 2005 at Elandsfontein

Also medians and modes that closely reflect normally distributed data were obtained as compared to the large values and deviations observed with raw data (Table 4-4). As a result, the standard deviations are smaller and there was a reduction in the errors that may arise from non-normality (Datez and Pantel, 1974). This normally distributed data formed a suitable data set for the development of a statistical model.

Air Quality Evaluation over Elandsfontein

The state of air quality over a region is evaluated using the standard of the local, provincial or national standards in comparison with the average values of the measured pollutants. As mentioned in section 2.7.2, the South African ambient air quality standard for sulphur states that the ambient concentrations of SO_2 at 25°C and 1 normal atmosphere may not exceed: a 10-minute average instant peak of 191 ppb, a 24-hour average of 125 µg m^{-3} or

48 ppb, an annual average of 50 μg m^{-3} or 19 ppb. While for particulate matter, it states that ambient PM_{10} may not exceed: a 24-hour average of 180 μg m^{-3} and that the 24-hour limit may not be exceeded more than three times in one year, an annual average of 60 μg m^{-3} (RSA, 2005). Since there are no standards for particulate sulphate as well as $PM_{2.5}$, and that sulphate exist within particles of size 2.5 μm (Lestari *et al*, 2003). The standard for PM_{10} was used to evaluate the extent of pollution resulting from particulate sulphate. At Elandsfontein the annual average for SO_2 and sulphate were 24 and 5 μg m^{-3}, respectively. These standards which were derived from the WHO, European Union and USA air quality standards (Scorgie *et al*, 2003), indicated high values compared to those measured at Elandsfontein during the study period. In the case of hydrogen sulphide, there are very few countries with regulatory standards these include the Bay Area Air Quality Management District in the United State of America (Collins and Lewis, 2000), which specifies ambient ground level H_2S concentrations may not exceed 60 ppb averaged over 3 consecutive minutes. Also in Indonesia, 42000 μg m^{-3} or 3ppb is applied on a 30-minute averaging time (www.worldbank.org/html/fpd/em/power/standards/airqstd.stm). Comparing the aforementioned level to an annual average of 6 μg m^{-3} or 0.0052 ppb determined at Elandsfontein show a considerable low H_2S level. Hence, over the subregion, the means levels of all three measured sulphur species were well within the new South African air quality guidelines (RSA, 2005) for the species under observation. This may be due the rapid diffusion and dilution as Elandsfontein is on a very high spot consequently frequently occurring high winds and also any low-level jet over the region aid to diffuse surface pollution.

Forecasting of Particulate Sulphate with Multivariate Regression

Like other aerosols, the distribution of particulate sulphate is overwhelmingly affected by meteorology, therefore in the absence of a sulphate analyser, a quick estimation of the sulphate distribution over an area may be predicted using observed meteorological variables. For this reason the presence of particulate sulphate over Elandsfontein was predicted using three meteorological variables, namely wind speed, relative humidity and ambient temperature.

The distributions of particulate sulphate values obtained from measurement as against those predicted are shown in Figures (4-27) to (4-30). The combined effect of relative humidity and temperature was determined by considering the atmospheric water vapour content. Multivariate regression models for predicting the distributions of particulate sulphate as a function of atmospheric water vapour content and wind speed (the driving force of atmospheric transport), in the planetary boundary layer over Elandsfontein are given by equations (4.3) to (4.6). The concentration variations were established on a seasonal basis to ascertain the expected concentrations of particulate sulphate in ambient air under different meteorological conditions. In spring the predicted particulate sulphate concentration relative to wind speed and water vapour concentration, evaluated over a range of tropospheric temperatures of between –50 °C and +50 °C, is expressed by equation (4.3) as:

$$y_{SO_4} = 0.46\upsilon - 0.45\psi + 8.06 \qquad (4.3)$$

Where, y_{SO_4} (μg m^{-3}), is the sulphate mass concentration at a given time, t, υ (m s^{-1}) is the wind speed at the same time, t, and ψ (hPa), is the water vapour partial pressure in the atmosphere also at the same time, t. The water vapour content was determined by equation (2.9). The model prediction is given by Figure 4-27

In a similar form, the summer particulate sulphate concentration over the same tropospheric temperature range is expressed by equation (4.4) as:

$$y_{SO_4} = 0.65\upsilon - 0.38\psi + 6.16 \qquad (4.4)$$

In like manner, the autumn particulate sulphate concentration was described by equation (4.5) as:

$$y_{SO_4} = 0.74\upsilon - 0.19\psi + 1.89 \qquad (4.5)$$

These summer and autumn model predictions are shown in Figures 4-28 and 4-29, respectively.

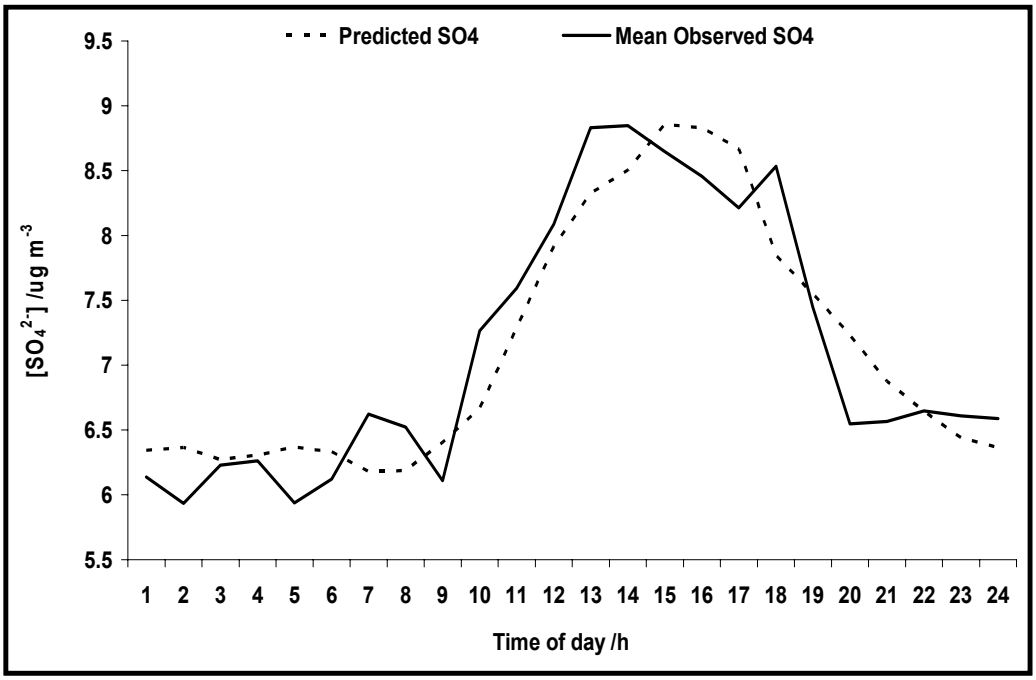

Figure 4-27: Diurnal characteristics of observed and predicted particulate sulphate in spring at Elandsfontein

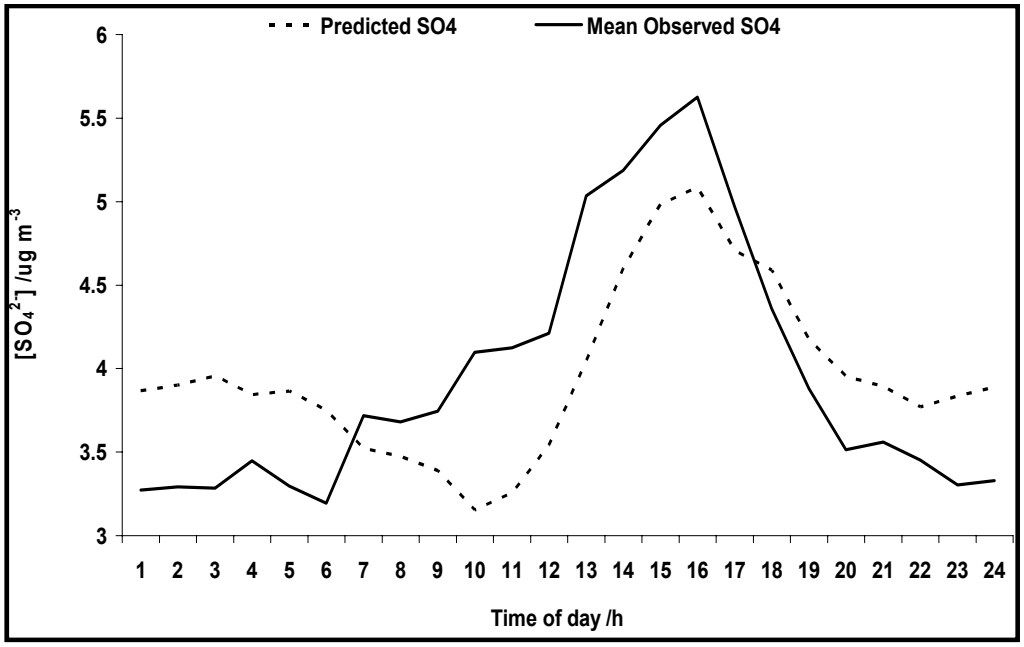

Figure 4-28: Diurnal characteristics of observed and predicted particulate sulphate in summer at Elandsfontein

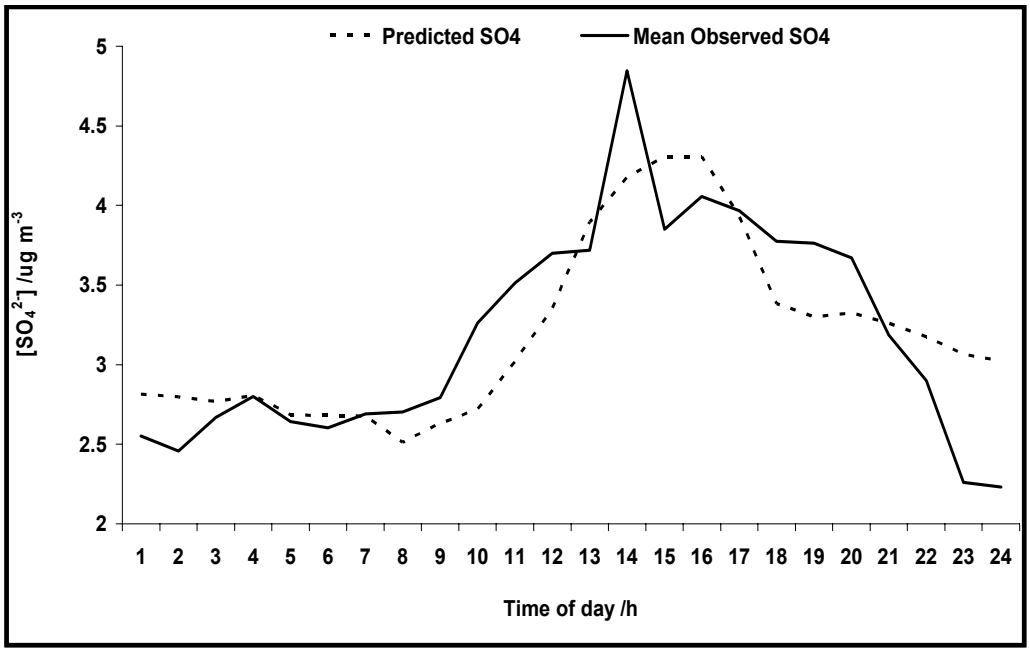

Figure 4-29: Diurnal characteristics of observed and predicted particulate sulphate in autumn at Elandsfontein

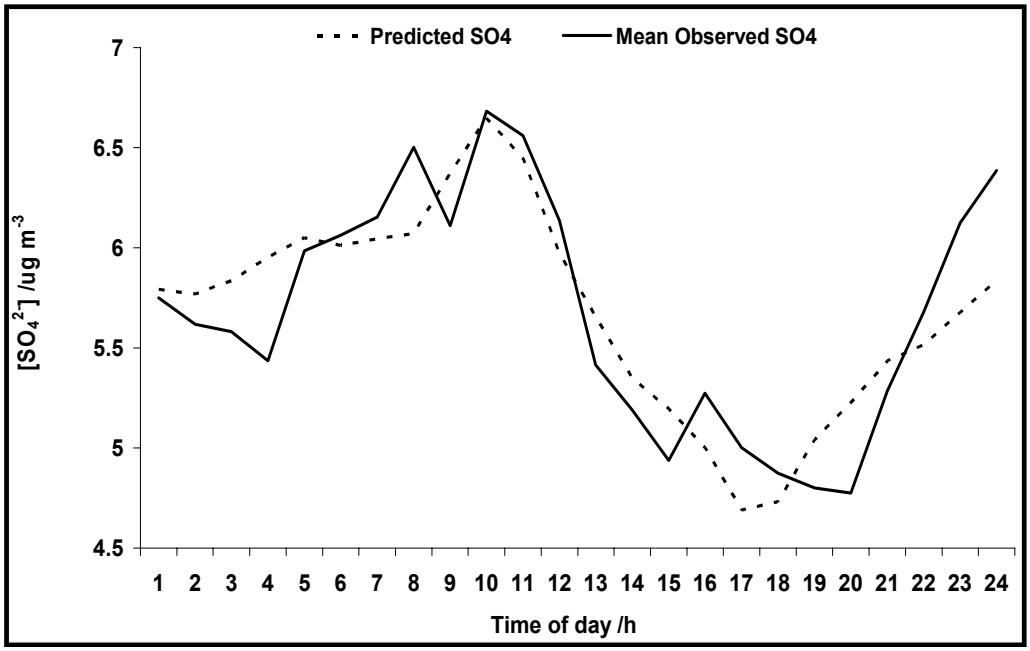

Figure 4-30: Diurnal characteristics of observed and predicted particulate sulphate in winter at Elandsfontein

And that of winter is given by equation (4.6) as:

$$y_{SO_4} = 0.58\upsilon + 0.54\psi + 0.67 \quad (4.6)$$

While it's predicted sulphate concentrations are displayed in Figure 4-30.

Interpretation of Coefficient of Determination

In multiple regression analysis, such as the type shown in equation (4.7), the following terms are applied in resolving the extent of prediction produced by the predictors.

$$y = \{\beta_0 + \beta_1 x_1 + \beta_2 x_2\} + \Im \quad (4.7)$$

The multiple R (which is applied for multiple variable regression), expresses the degree to which the two or more dependent variables, x, are related to the independent variable, y. This correlation coefficient is commonly expressed in a rationalised form as fractions ranging between 0 and 1, known as the coefficient of determination, R-square. Another regression value used for multiple regressions is the adjusted R-square. The parameter modifies the R-square when a new dependent variable is introduced into the model. This adjusted R-square is always less than or equal to the R-square and may increase if the new variable improves the model. The error term is the last term considered for the assessment of the predictor. It is expresses as:

$$\Im = y_{measured} - y_{predicted} \quad (4.8)$$

It accounts for the other parameters apart from the dependent x-variable that might affect the model to deviate from the measured values. It is the deviation between the observed data and the predicted data.

Table 4-5: Summary output of regression analysis

Variables	Spring	Summer	Autumn	Winter	Overall
Multiple R	0.9298	0.8431	0.8172	0.8782	0.8237
R Square	0.8645	0.5644	0.6678	0.7713	0.7170
Adjusted R Square	0.8516	0.4982	0.6361	0.7495	0.6582

Standard Error	0.3921	0.6435	0.4098	0.2947	0.4217

The models appear to predict on average about 72 % (Table 4-5) of the expected measurements of particulate sulphate. From the standard error values, there appears to be some parameters (possibly of meteorology) that were absent from the model that prevented the model from completely predicting the measured values.

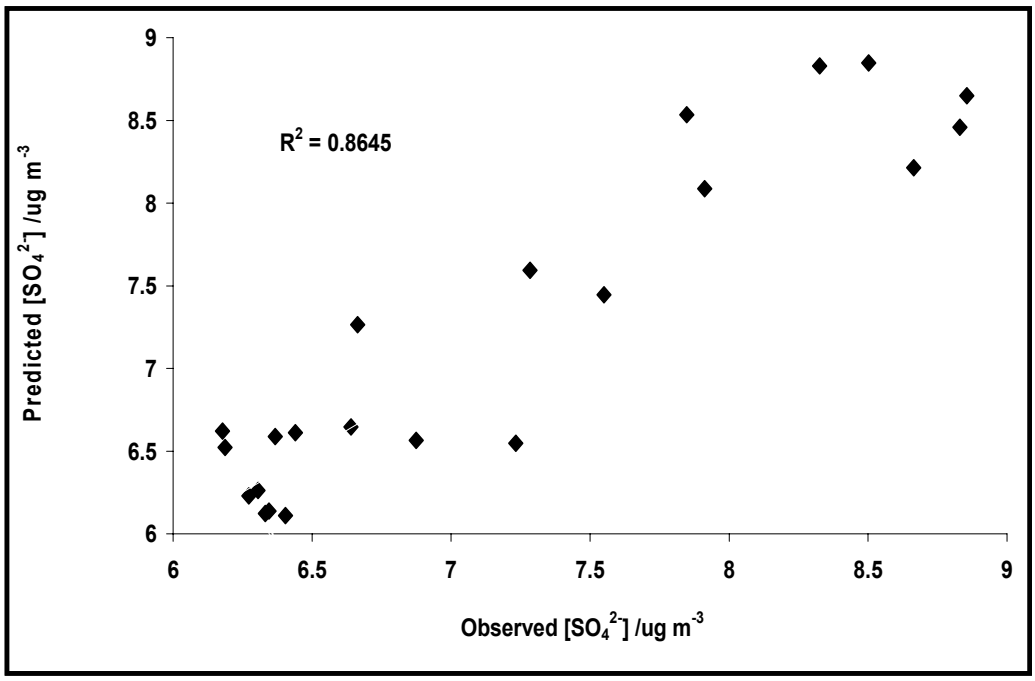

Figure 4-31: Comparison of the predicted against the mean observed particulate sulphate in spring at Elandsfontein

In comparison with the predicted against observed concentrations, the following regression coefficients were obtained: R^2 of 86.5 % for spring, 56.4 % for summer, 66.8 % for autumn and 77.1 % for winter (Figures 4-31 to 4-34).

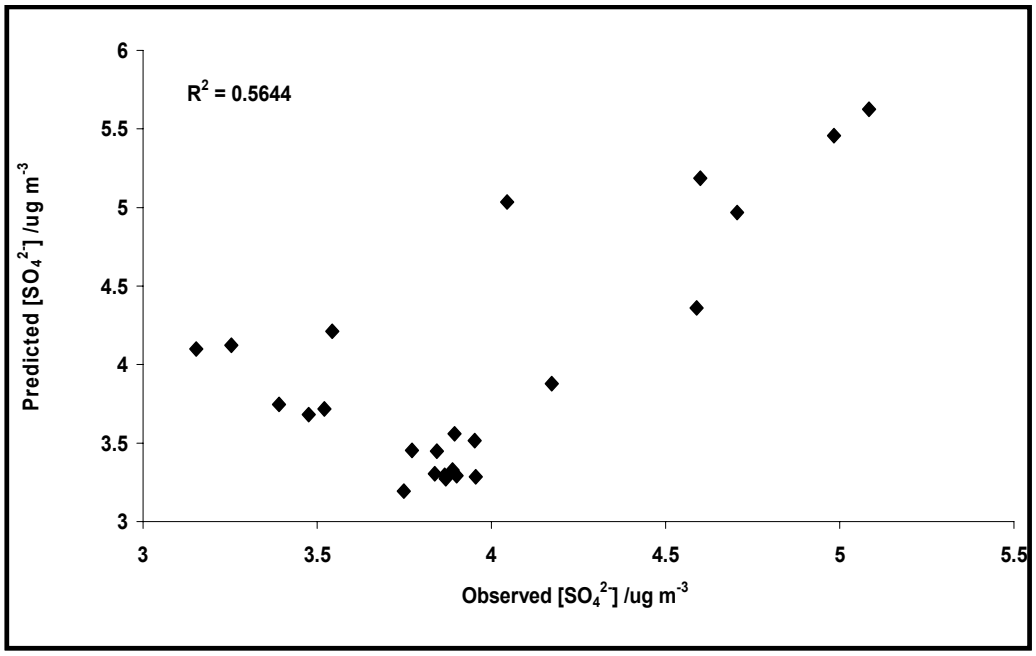

Figure 4-32: Comparison of the predicted against the mean observed particulate sulphate in summer at Elandsfontein

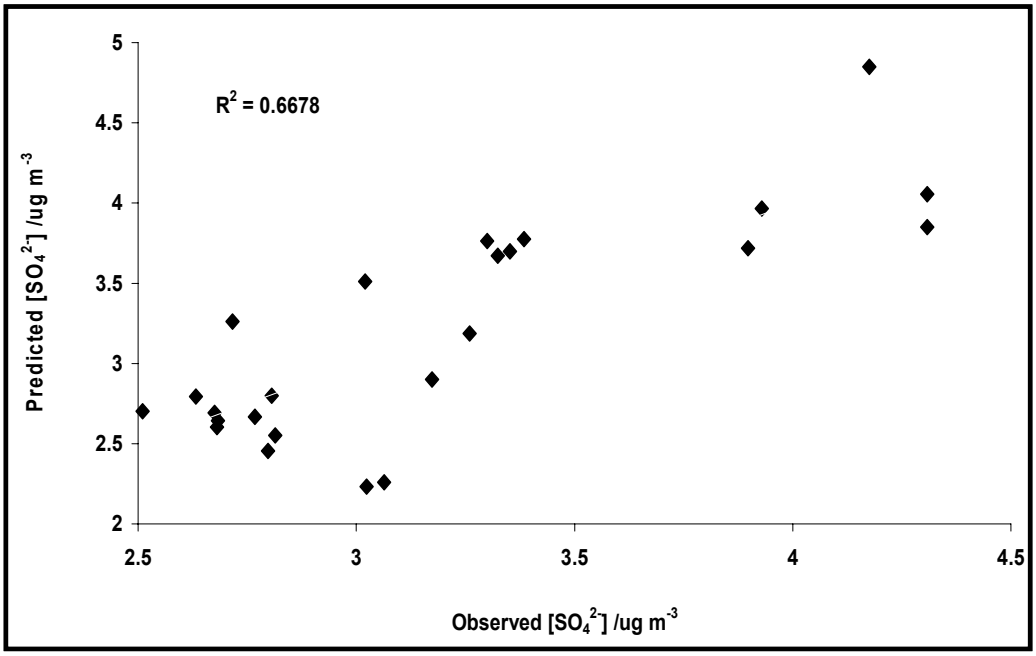

Figure 4-33: Comparison of the predicted against the mean observed particulate sulphate in autumn at Elandsfontein

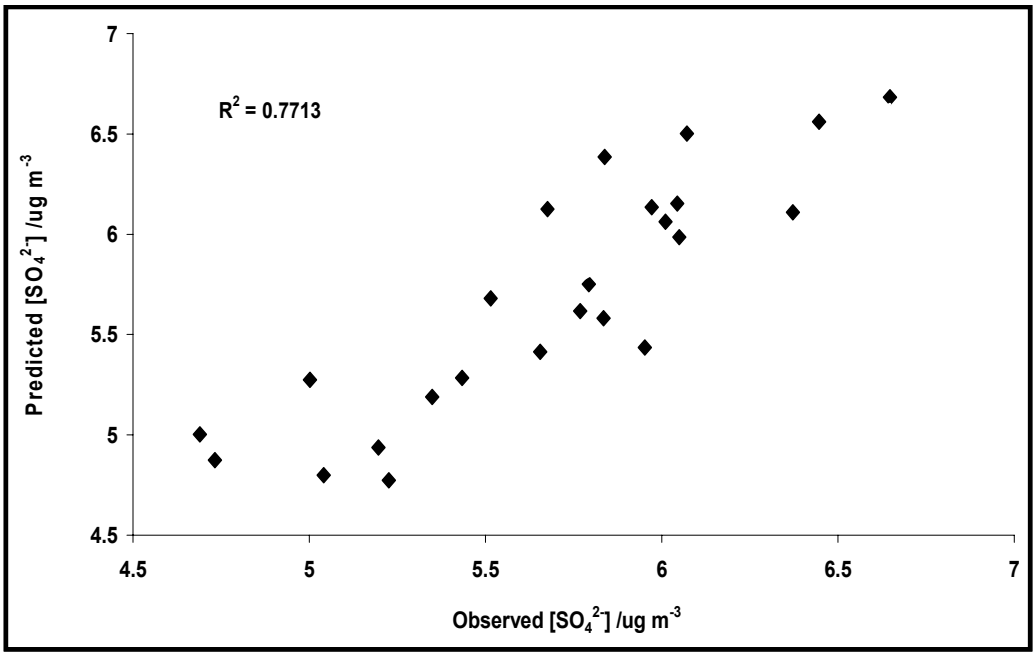

Figure 4-34: Comparison of the predicted against the mean observed particulate sulphate in winter at Elandsfontein

When the data for solar radiation were included in the multivariate data analysis, the R^2 reduced slightly, indicating that it does not significantly influence the presence of particulate sulphate or that its impact had overwhelmingly been accounted for by temperature.

4.4 Conclusion

This study has shown the variations of total atmospheric sulphur observed over the Mpumalanga Highveld. It has shown for the first time on a 10-minute average continuous measurement for twelve months, the outcome of total sulphur distribution comprising H_2S, SO_2 and particulate sulphate concentrations with simultaneously observing the prevailing meteorological parameters at Elandsfontein. It is evident from this study that the three prominent sulphur compounds: H_2S, SO_2 and sulphate observed at Elandsfontein exist at significant concentrations above background levels over the Mpumalanga Highveld subregion at certain times of the day and of the year. These observations were shown from

pollution roses. Also these sulphur compounds vary in amount and characteristic pattern with time of day and seasonal changes controlled by the prevailing meteorology.

With regards to the *in situ* temporal behaviours, the diurnal variation has shown that H_2S might possibly be released from surface emission sources consisting of open-cast coal mines and fugitive emissions from hydrocarbon fuel processing plants. Hydrogen sulphide levels in summer, autumn and winter were ascribed to possible rapid thermal oxidation, while in spring high advection and convective boundary layer dispersion created the daytime trough-like concentration pattern; with stable night-time conditions, accumulation occurs.

Over Elandsfontein, SO_2 is released from several sources, some of which include coal-fired power plants, spontaneous combustion in open-cast coal mines and, to some extent, fuel processing plants. The diurnal variations supported by the pollution rose suggest that SO_2 released was mainly from elevated power station plumes.

In the planetary boundary layer over Elandsfontein, the concentration of particulate sulphate varies significantly for different conditions and times of the year. The variation depends predominantly on the meteorology, with long-range pollutant transport within the southern Africa subcontinent contributing occasionally to episodes of very high concentrations. However, industrial activities, taking into account variations in meteorological parameters, are largely responsible for the concentration build-up and distribution of gaseous sulphur compounds at Elandsfontein.

This study has confirm that SO_2, H_2S and particulate sulphate traverse over the Mpumalanga Highveld subregion at consistently very high to moderately high doses all through the year. This is as a result, not only of chemical transformations between reactive sulphur species, but also due to atmospheric aerosol transport activities. It has also been shown from diurnal patterns that the most likely form of removal mechanism of atmospheric particulate is by wet deposition controlled by rainfall during summer, while in other seasons dry deposition, mist and dew (since aerosols accumulate as CCN) when the water vapour content in the atmosphere is high.

The characteristics of particulate sulphate aerosols over the Mpumalanga industrial Highveld are significantly influenced by variations in atmospheric liquid water content, which, consequently, affect ground- and surface-water. The concentrations of this sulphur species (which scatters incoming solar radiation, and thereby alters the surface radiation budget as well as contributing to cloud formation) have been predicted using meteorological variables. The presence of particulate sulphate has been related to wind speed and the partial pressure of atmospheric water vapour, since they alter the temporal distribution considerably. The multivariate correlation relationships defined by equations (4.3) to (4.6) were shown to predict with accuracy the diurnal variation of ambient particulate sulphate on a seasonal basis in the planetary boundary layer of the Mpumalanga Highveld. The confidence of the multivariate correlations was deduced from the regression coefficients (R^2), which ranged between 69 % and 87 %, obtained from the plot of observed against predicted sulphate concentrations as a function of the applied meteorological variables. This study closely predicts the gas-to-particle distribution of atmospheric sulphur over the Mpumalanga Highveld.

The 12-month sample measurements provided emission values suitable for evaluation of temporal trends to ascertain the predominant removal mode (reaction and fallout), source targeting (major emission area), evaluation of air recirculation (transport effect) and the multivariate model (sulphate aerosol quantification).

Chapter 5: Theoretical Analyses of Thermochemical Properties of Atmospheric Sulphur

5.1 Introduction to Theoretical Analyses for Atmospheric Sulphur Reactions

Sulphur compounds emitted from both anthropogenic and biogenic activities into the atmosphere undergo chemical transformation under the influence of the meteorological conditions (Ahlberg *et al*, 1978; Tang *et al*, 1981; Eliassen and Saltbones, 1983; Tuncel *et al*, 1985; Stockwell, 1986; Walcek *et al*, 1986; Benkovitz *et al*, 1994). These compounds end up generating submicron particulates, acidic and neutral sulphate salts in advection plumes away from the source area (Latimer and Samuelsen, 1978; Gillani and Wilson, 1983; Terblanche *et al*, 1993; Seinfeld and Pandis, 1998). The troposphere has significant potential for chemical reactions, which has motivated studies such as smog-chamber simulated atmospheric experiments of the oxidation of trace gaseous sulphur species (Carmichael and Peters, 1984a; Warneck, 1999).

This chapter provides insight into concentration distribution of the atmospheric sulphur species determined by the analyses of the thermochemically favourable reactions at tropospheric conditions. It shows the effects of different phases on the relative importance of a reaction over another. It also affirms the most dominant phase through which the SO_2 oxidation occurs in the atmosphere. In this chapter, a computational approach is used to evaluate some of the energies generated and consumed during chemical reactions for several well-known atmospheric sulphur transformations taking place in the troposphere. It highlights the thermodynamic potential of these sulphur transformations in the planetary boundary layer.

Combustion and thermal processes are generally recognised as the major activities of H_2S and SO_2 production in the atmospheric environment (Eggleton and Cox, 1978). Previous studies (Calvert *et al*, 1978; Sze and Ko, 1980; Breytenbach *et al*, 1994; Pienaar and Helas, 1996; Warneck, 1999; Herrmann *et al*, 2000; Grgic and Bercic, 2001; Podkrajsek *et al*,

2004) have shown from experimental observations that gas-phase, aqueous-phase and radical reactions are some of the pathways taken by atmospheric sulphur during transformation. The important role of various sulphur species in the chemistry of the atmosphere is well established and detailed information is available on the various thermochemical properties for these species (Calvert *et al*, 1978). These properties had been derived from a variety of experimental techniques, such as calorimetry, mass spectrometry and pulse radiolysis (Larsen *et al*, 2001). Despite several detailed studies on atmospheric transformation of sulphur-based compounds (Calvert *et al*, 1978; Warneck, 1999; Herrmann *et al*, 2000; Somnitz *et al*, 2003), a large fraction of the proposed reacting species and reaction mechanisms of sulphur had not been studied with a view to examining the thermodynamic favourability which is indicative of the potential of these species to react in the atmosphere. The establishment of definite thermodynamic conditions for these species in the atmosphere would aid modelling of the atmospheric reaction types for different environmental conditions.

A number of atmospheric sulphur transformations is expected over the Mpumalanga Highveld subregion due to the presence of power-generating and hydrocarbon fuel-processing plants as well as the vast open-cast coal mines within the area. The predominant sulphur species observed in the area are hydrogen sulphide and sulphur dioxide. In deciding the relative importance of the various reaction pathways by which certain common atmospheric transformations occur, some forty-six gas-phase and forty-six aqueous-phase atmospheric sulphur reactions involving H_2S and SO_2 disappearances that were obtained from the literature (Beilke and Gravenhorst, 1978; Calvert *et al*, 1978; Eggleton and Cox, 1978; Hegg and Hobbs, 1980; Britton and Clarke, 1980; Moller, 1980; Viggiano *et al*, 1980; 1982; Breytenbach *et al*, 1984; Barnes *et al*, 1986; Warneck, 1988; Eisele and Tanner, 1991; Herrmann *et al*, 2000; Pienaar and Helas, 1996; Seinfeld and Pandis, 1998; Warneck, 1999; Grgic and Bercic, 2001; Somnitz *et al*, 2003), have been considered in this study (Table 5-1).

Table 5-1: Gas-phase and aqueous-phase atmospheric sulphur reactions considered in this study

S/N	Gas-phase Reactions	Aqueous-phase Reactions
1	$H_2S + OH^* \rightarrow H_2O + SH^*$	$SO_2 + H_2O \rightarrow H_2SO_3$
2	$HS^* + O_2 \rightarrow SO^* + OH^*$	$SO_3^{2-} + O_3 \rightarrow O_2 + SO_4^{2-}$
3	$HS^* + O_2 \rightarrow SO_2 + H^*$	$SO_3^{2-} + O_2 \rightarrow O^* + SO_4^{2-}$
4	$HS^* + O_3 \rightarrow HSO + O_2$	$HSO_3^- + OH^* \rightarrow OH^- + HSO_3^*$
5	$HS^* + O_3 \rightarrow OH^* + SO^* + O^*$	$HSO_3^* + O_2 \rightarrow HSO_5^*$
6	$HSO^* + O_2 \rightarrow HO_2^* + SO^*$	$HSO_3^- + HSO_5^* \rightarrow HSO_3^* + HSO_5^-$
7	$HSO^* + O_3 \rightarrow OH^* + SO^* + O_2$	$HSO_3^- + HSO_5^- + H^+ \rightarrow 2SO_4^{2-} + 3H^+$
8	$SO_2 + O^* \rightarrow SO_3$	$HSO_3^- + H_2O \rightarrow SO_3^{2-} + H_3O^+$
9	$SO_2 + OH^* \rightarrow HOSO_2^*$	$HCHO + HSO_3^- \rightarrow HOCH_2SO_3^-$
10	$HOSO_2^* + O_2 \rightarrow HO_2^* + SO_3$	$HCHO + SO_3^{2-} + H^+ \rightarrow HOCH_2SO_3^-$
11	$SO_2 + HO_2^* \rightarrow OH^* + SO_3$	$HOCH_2SO_3^- + OH^- \rightarrow CH_2(OH)_2 + SO_3^{2-}$
12	$SO_2 + HO_2^* \rightarrow HO_2SO_2^*$	$OH^* + HOCH_2SO_3^- \rightarrow HOCHSO_3^- + H_2O$
13	$HO_2SO_2^* \rightarrow HO^* + SO_3$	$HOCHSO_3^- + O_2 + H_2O \rightarrow HCOOH + HSO_3^- + HO_2^*$
14	$SO_2 + CH_3O^* \rightarrow CH_3OSO_2^*$	$O_3 + HSO_3^- \rightarrow HSO_4^- + O_2$
15	$SO_2 + CH_3O_2^* \rightarrow CH_3O^* + SO_3$	$O_3 + SO_2 + H_2O \rightarrow HSO_4^- + O_2 + H^+$
16	$SO_2 + CH_3CHOO^* \rightarrow CH_3CHO^* + SO_3$	$HSO_3^- + H_2O_2 \rightarrow HSO_4^- + H_2O$
17	$SO_2 + (CH_3)_3CO_2^* \rightarrow (CH_3)_3CO^* + SO_3$	$HSO_3^- + CH_3OOH \rightarrow HSO_4^- + CH_3OH$
18	$SO_2 + CH_3COO_2^* \rightarrow CH_3CO_2^* + SO_3$	$HSO_3^- + HOONO_2 \rightarrow HSO_4^- + NO_3^- + H^+$
19	$SO_2 + CH_3COO_2^* \rightarrow CH_3COO_2SO_2^*$	$HSO_3^- + HOONO \rightarrow HSO_4^- + HNO_2$
20	$SO_2 + O_3 \rightarrow O_2 + SO_3$	$HSO_3^- + HSO_5^- \rightarrow 2HSO_4^-$
21	$SO_2 + NO_2 \rightarrow NO + SO_3$	$HSO_3^{2-} + Cl_2 \rightarrow SO_3^- + 2Cl^- + H^+$
22	$SO_2 + NO_3 \rightarrow NO_2 + SO_3$	$OH^* + HSO_3^- \rightarrow SO_3^- + H_2O$
23	$SO_2 + N_2O_5 \rightarrow N_2O_4 + SO_3$	$OH^* + SO_3^{2-} \rightarrow SO_3^- + OH^-$
24	$OCS + O^* \rightarrow CO + SO$	$OH^* + HSO_5^- \rightarrow SO_5^- + H_2O$
25	$OCS + OH^* \rightarrow CO_2 + HS$	$OH^* + HSO_4^- \rightarrow SO_4^- + H_2O$

S/N	Gas-phase Reactions	Aqueous-phase Reactions
26	$SO^* + O^* \rightarrow SO_2$	$SO_3^- + O_2 \rightarrow SO_5^-$
27	$SO^* + SO^* \rightarrow S + SO_2$	$SO_5^- + HSO_3^- \rightarrow HSO_5^- + SO_3^-$
28	$SO^* + OH^* \rightarrow H + SO_2$	$SO_5^- + HSO_3^- \rightarrow SO_4^{2-} + SO_4^- + H^+$
29	$SO^* + SO_3 \rightarrow SO_2 + SO_2$	$SO_5^- + SO_3^{2-} + H^+ \rightarrow HSO_5^- + SO_3^-$
30	$SO^* + NO_2 \rightarrow NO + SO_2$	$SO_5^- + SO_3^{2-} \rightarrow SO_4^{2-} + SO_4^-$
31	$SO^* + O_2 \rightarrow O^* + SO_2$	$SO_5^- + SO_5^- \rightarrow 2SO_4^- + O_2$
32	$SO^* + O_2 \rightarrow SO_3$	$SO_5^- + HO_2^* \rightarrow HSO_5^- + O_2$
33	$SO^* + O_3 \rightarrow O^* + SO_3$	$SO_5^- + O_2^- + H^+ \rightarrow HSO_5^- + O_2$
34	$SO^* + O_3 \rightarrow SO_2 + O_2$	$SO_4^- + HSO_3^- \rightarrow HSO_4^- + SO_3^-$
35	$HOSO_2^* + O_2 \rightarrow HOSO_2OO^*$	$SO_4^- + O_2^- \rightarrow SO_4^{2-} + O_2$
36	$HOSO_2OO^* + NO \rightarrow HOSO_2O^* + NO_2$	$SO_4^- + SO_3^{2-} \rightarrow SO_4^{2-} + SO_3^-$
37	$HOSO_2OO^* + NO_2 \rightarrow HOSO_2O^* + NO_3$	$SO_4^- + NO_3^- \rightarrow SO_4^{2-} + NO_3$
38	$HOSO_2OO^* + HO_2 \rightarrow HOSO_2O_2H + O_2$	$SO_4^- + OH^- \rightarrow SO_4^{2-} + OH^*$
39	$2HOSO_2OO^* \rightarrow 2HOSO_2O^* + O_2$	$SO_4^- + H_2O \rightarrow SO_4^{2-} + H^+ + OH^*$
40	$HOSO_2O^* + NO \rightarrow HOSO_2ONO^*$	$SO_4^- + H_2O_2 \rightarrow HSO_4^- + HO_2^*$
41	$HOSO_2O^* + NO_2 \rightarrow HOSO_2ONO_2^*$	$SO_4^- + HCOOH \rightarrow HSO_4^- + H^+ + COO^-$
42	$HOSO_2O^* + HO_2 \rightarrow HOSO_2OH + O_2$	$SO_4^- + HCOO^- \rightarrow HSO_4^- + COO^-$
43	$HOSO_2ONO^* + H_2O \rightarrow H_2SO_4 + HNO_2$	$SO_4^- + CH_2(OH)_2 + O_2 \rightarrow HSO_4^- + HO_2^* + HCOOH$
44	$HOSO_2ONO_2^* + H_2O \rightarrow H_2SO_4 + HNO_3$	$SO_4^- + CH_2(OH)_2 + O_2 \rightarrow HSO_4^- + HO_2^* + HCHO + O^*$
45	$SO_3 + O^* \rightarrow SO_2 + O_2$	$SO_4^- + Cl^- \rightarrow SO_4^{2-} + Cl$
46	$SO_3 + H_2O \rightarrow H_2SO_4$	$H_2SO_4 + NO_3^- \rightarrow HSO_4^- + HNO_3$

In the literature there have been some theoretical studies of reactions involving sulphur systems using empirical, *ab initio* (Markham and Bock, 1993; Alkorta, 1994; Bachrach and Mulhearn, 1996; Maulitz *et al*, 1995; Çakmak and Srivastava, 1999) and high-level molecular orbital methods (Yang *et al*, 1995; McKee, 1996; Morgan *et al*, 1997), but there

seems to be no reported energy computation for isodesmic reactions, which are chemical reactions (actual or hypothetical) in which the types of bonds that are made in forming the products, are the same as those which are broken in the reactants, they are often used as hypothetical reactions in thermochemistry -involving atmospheric reactions with compounded methods, while, for atmospheric chemistry applications, very few information based on molecular orbital theory have been recorded (Parthiban *et al*, 2003).

Many gas- and aqueous-phase reactions have been proposed (Table 5-1) for the chemical transformation of atmospheric H_2S and SO_2, in addition to establishing the relative importance of the various reactions with respect to each other, based on how fast the reaction occurs, that is, the rate of reaction (Calvert *et al*, 1978; Pienaar and Helas, 1996; Warneck, 1999). Also their aqueous-phase reactions involving these species are known to be more favourable than the gas-phase reactions (Moller, 1980; Herrmann *et al*, 2000).

In this study, the tool of chemical thermodynamics was applied to predict the favourability and feasibility of these reactions, in order to arrive at the common reaction path(s) taken by H_2S and SO_2 over a large temperature range of between -100 °C and +100 °C. It should be noted that although this temperature range is not practicable in the troposphere at its extremes, this range is useful for understanding the transformation of atmospheric species. The equilibrium conversion allows one to predict the temperature at which the reaction yields more of the products than the reactants. The analyses were achieved using the electronic model theories of computational chemistry. The computational methodology has been described in Chapter 3. The computational package consists of a number of built-in model chemistry solutions to evaluating the thermochemical properties at 0 and 298 K.

5.2 Analyses of Computational Energies

The enthalpies and free energies of formation for the 95 species participating in both the gas- and aqueous-phase transformations are reported in Tables (B-3a) and (B-3b) respectively of Appendix B-3. The computation was performed using five *ab initio* and DFT chemistry models in order to examine the degree of accuracy of each method and to deduce the most accurate of the methods. The methods applied in this computation are the

most advanced chemistry models that evaluate the approximation to the Schrödinger equation that produces the thermochemical energies with minimum error. These errors are generated because the approximation efficiency of some of the computational methods is less rigorous than others.

Energy values for the enthalpies and free energies are computed in units of Hartree by the various methods. These values can only be converted into kilo-Joules only when evaluating the overall enthalpy of free energy of transformation for each reaction. It may be observed that the values obtained for a particular specie appears approximately equal from the results of the five computing method, this is only true when expressed in the Hartree. However, when these energies are combined to give the energy of a particular reaction, the difference widens. In a comparison with past studies, calculated energies in Morgan *et al* (1997) and Maulitz *et al* (1995) for some simple anions for water and some carbon-based molecules in Dunbar and Petrie (2005), and calculations for some radical species in Khachatryan *et al* (2004) yielded values which closely agreed with the values of the calculated energies obtained in Tables (B-3a) and (B-3b).

The computed enthalpies for gas- and aqueous-phase reactions at 298K are shown in Tables (B-3c) and (B-3d) respectively of Appendix B-3. In addition enthalpies from experimental measurements for gas- and aqueous-phase reactions from literature are included in the Tables. These enthalpies were included for the purpose of comparison in order to ascertain the best method to apply for evaluating the enthalpies of the reactions for which no data is available. About 80 % of the enthalpies from experimental observations correspond approximately to values obtained using the model chemistry packages (Table B-3c). Due to insufficient literature data, only few aqueous enthalpies were available for comparison (Table B-3d). Some of the electronic energies in Hartree for diatomic sulphur molecules have been computed at the B3LYP level (McKee, 1996). Similar to the aforementioned precision of computation, in the energies obtained for this study closely agree with computed values for the diatomic sulphur molecules.

Analogous to the enthalpy of reaction evaluated from the computed energies using the model chemistry package, the Gibbs free energy of reaction has been calculated. The

energies for the gas-phase reactions are given in Table (B-3e), while those for the aqueous-phase reactions are shown in Table (B-3f) of Appendix B-3. In comparison with enthalpies of reaction, just less than 20 % of the data were available from literature for the comparison of the Gibbs free energy of reaction for the sulphur species.

5.3 Analyses of Computational Methods

The level of accuracy of the various molecular orbital computational model chemistries in relation to experimentally determined values (where these are available) was determined (Figure 5-1) for calculated energies of reaction. The energies from the model chemistry computations were compared against those measured experimentally to determine the method that most accurately predicts the values derived from experimental measurements. This comparison was performed using two criteria. This first was based on the frequency of occurrences of computed energies that coincides relatively close to those derived from experimental values.

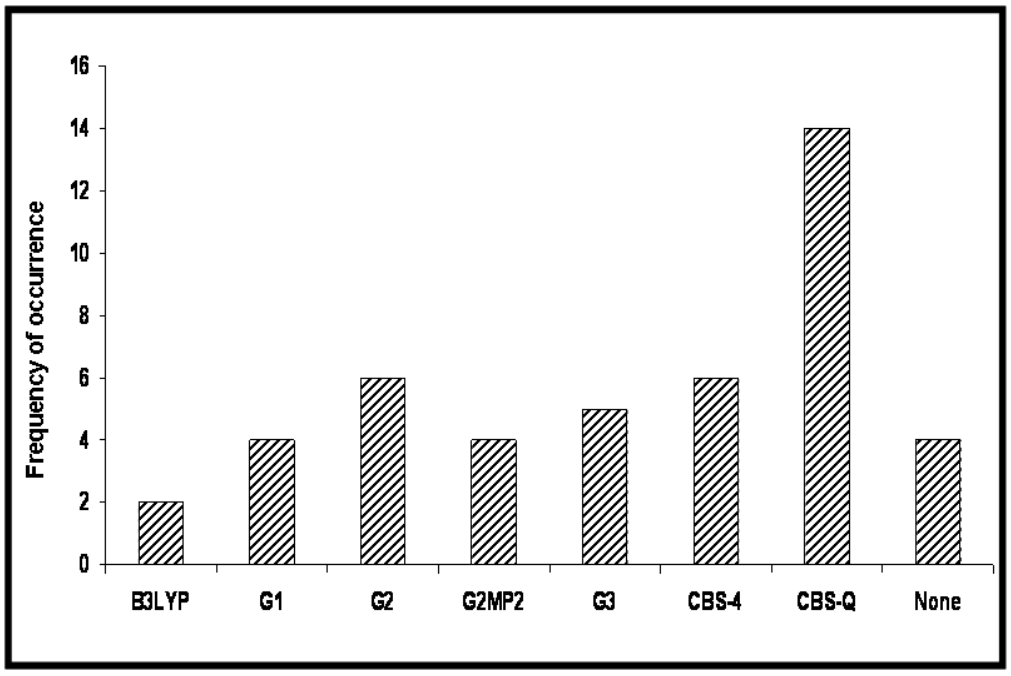

Figure 5-1: Comparison of the level of accuracy for the various compounded and density functional methods from calculated enthalpies of reactions

And the second was based on the degree of mean absolute deviation (MAD) for the enthalpies of reaction. Since only the enthalpies provided sufficient data for comparison.

The CBS-Q method produced the highest fraction of computed energies of reaction that closely approximate the experimentally determined energies of reaction with a mean absolute deviation of 1.08 %. The mean absolute deviation is the mean difference between the standard deviation of energies computed from that of energies obtained from experimental data. This closely agrees with the expected mean absolute deviation for the CBS-Q method as described in Foresman and Frisch (1996) and hence confirmed the use of the CBS-Q calculated energies in the computation of the chemical equilibrium parameters for all the reactions. The term "NA" was used to denote instances where the computed energies deviated from the experimental energies by about ±5 %, Tables (B-3c to B-3f).

5.4 Effect of Temperature on Equilibrium Constant

The equilibrium constants were calculated to provide a criterion for thermodynamically characterising an order or preference of occurrence of one reaction against another reaction over a particular temperature range (Figures 5-2a to 5-5d). The higher the equilibrium constant, the less stable the reacting species for the reaction as written, that is, the more likely its transformation and the more its equilibrium conversion tends to unity leaving no provision for reversibility.

Figures (5-2a) to (5-3d) show the temperature dependencies for the various gas-phase and aqueous-phase sulphur reactions. A number of the equilibrium constant are observed to be consistently decreasing with increasing temperature, while some of the set of reactions was increasing with temperature rise. Also similar reactants involved with the same co-reactants, yielding different products, respond to temperature changes at different rates. This behaviour is more pronounced for the gas-phase reactions than for the aqueous-phase reactions.

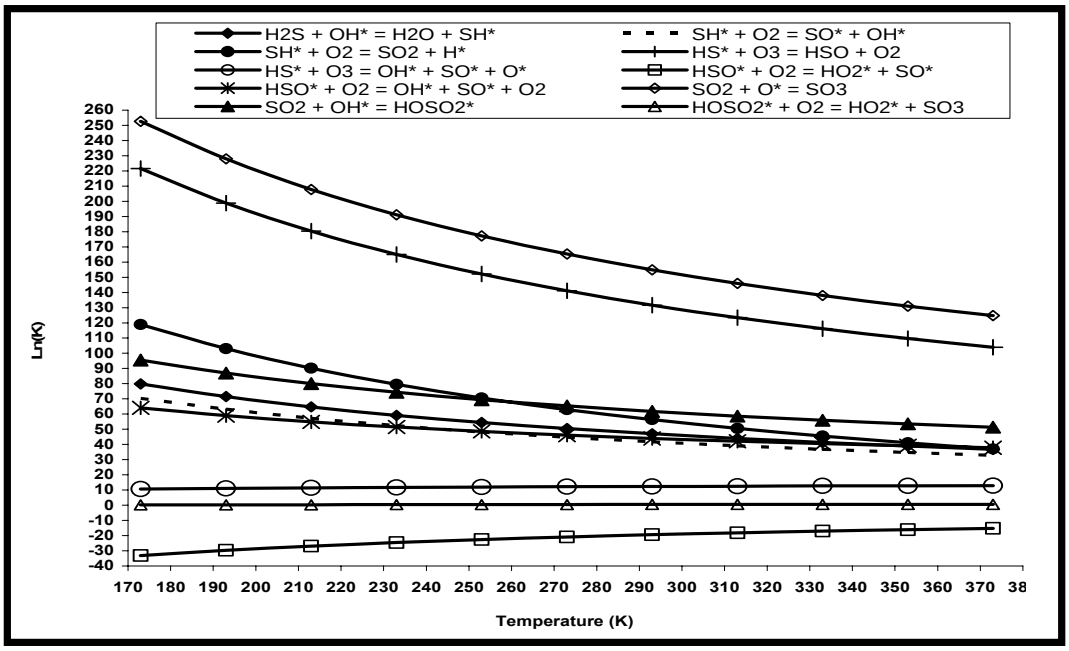

Figure 5-2a: The effects of ambient temperature on equilibrium constants at atmospheric pressure for the gas-phase sulphur reactions shown in the legend

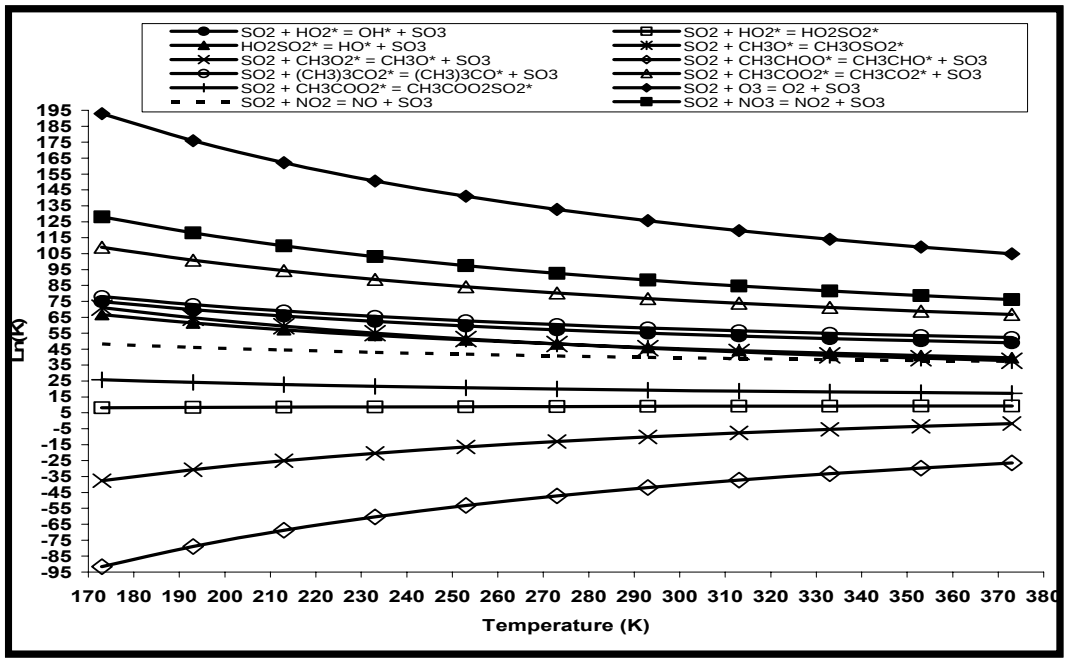

Figure 5-2b: The effects of ambient temperature on equilibrium constants at atmospheric pressure for the gas-phase sulphur reactions shown in the legend

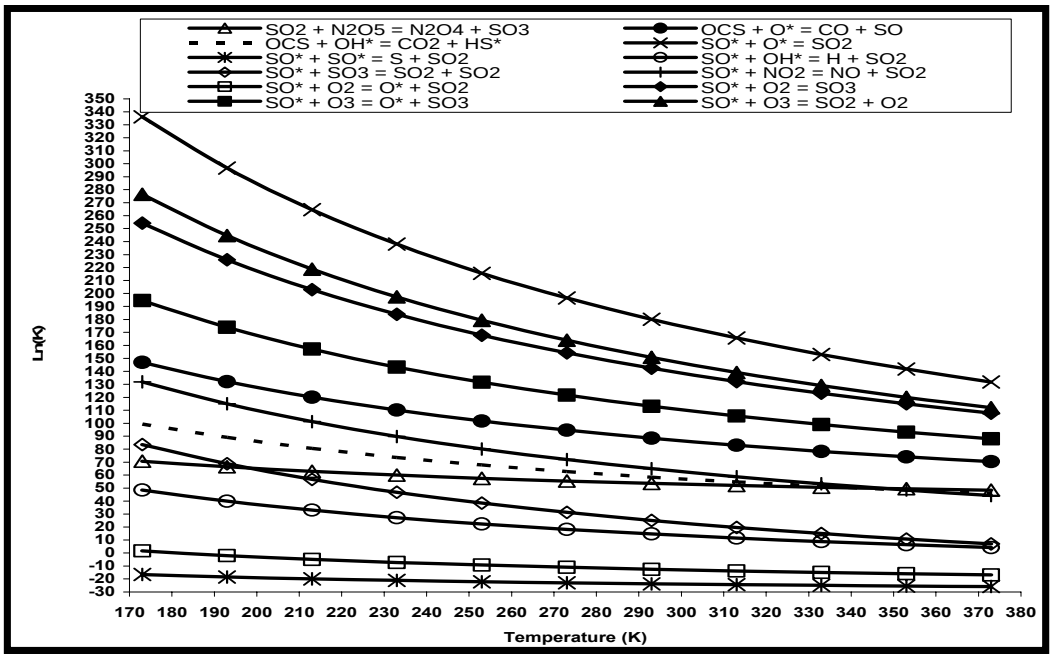

Figure 5-2c: The effects of ambient temperature on equilibrium constants at atmospheric pressure for the gas-phase sulphur reactions shown in the legend

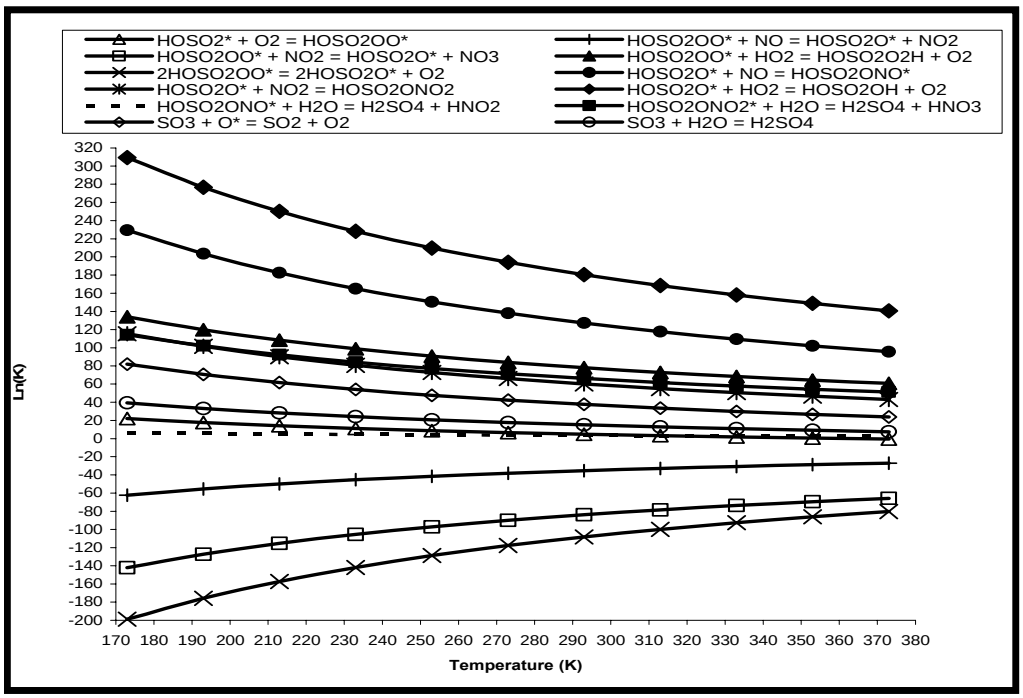

Figure 5-2d: The effects of ambient temperature on equilibrium constants at atmospheric pressure for the gas-phase sulphur reactions shown in the legend

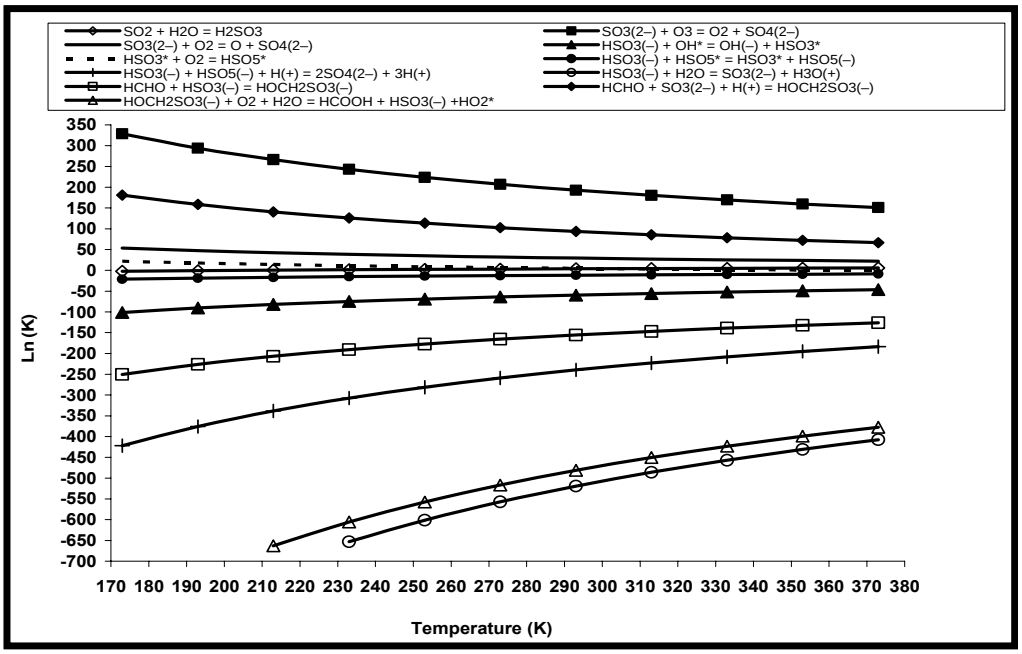

Figure 5-3a: The effects of ambient temperature on equilibrium constants at atmospheric pressure for the aqueous-phase sulphur reactions shown in the legend

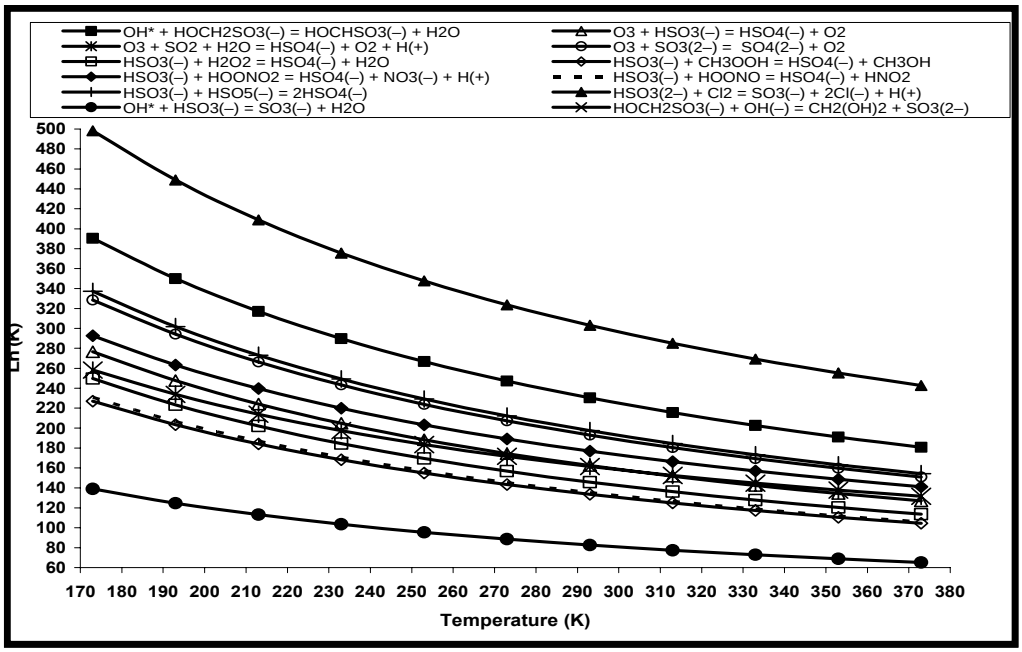

Figure 5-3b: The effects of ambient temperature on equilibrium constants at atmospheric pressure for the aqueous-phase sulphur reactions shown in the legend

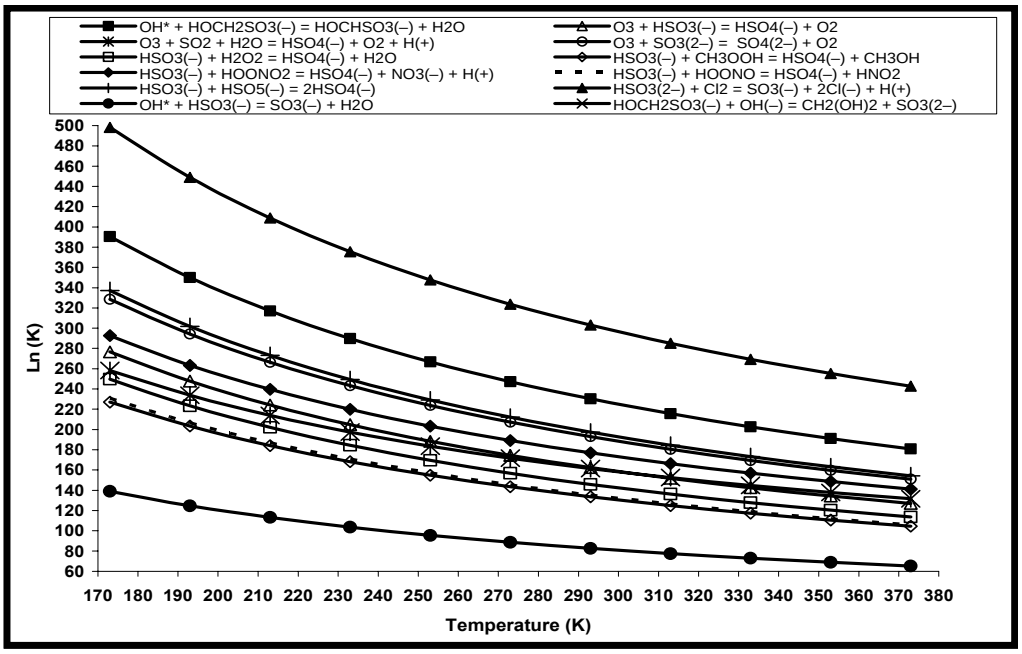

Figure 5-3c: The effects of ambient temperature on equilibrium constants at atmospheric pressure for the aqueous-phase sulphur reactions shown in the legend

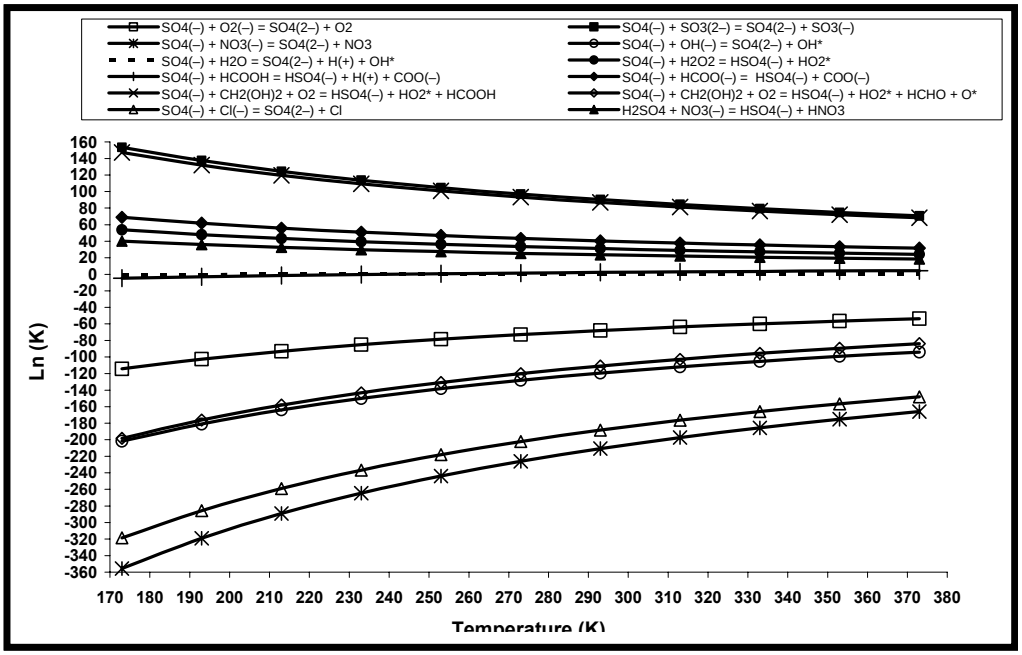

Figure 5-3d: The effects of ambient temperature on equilibrium constants at atmospheric pressure for the aqueous-phase sulphur reactions shown in the legend

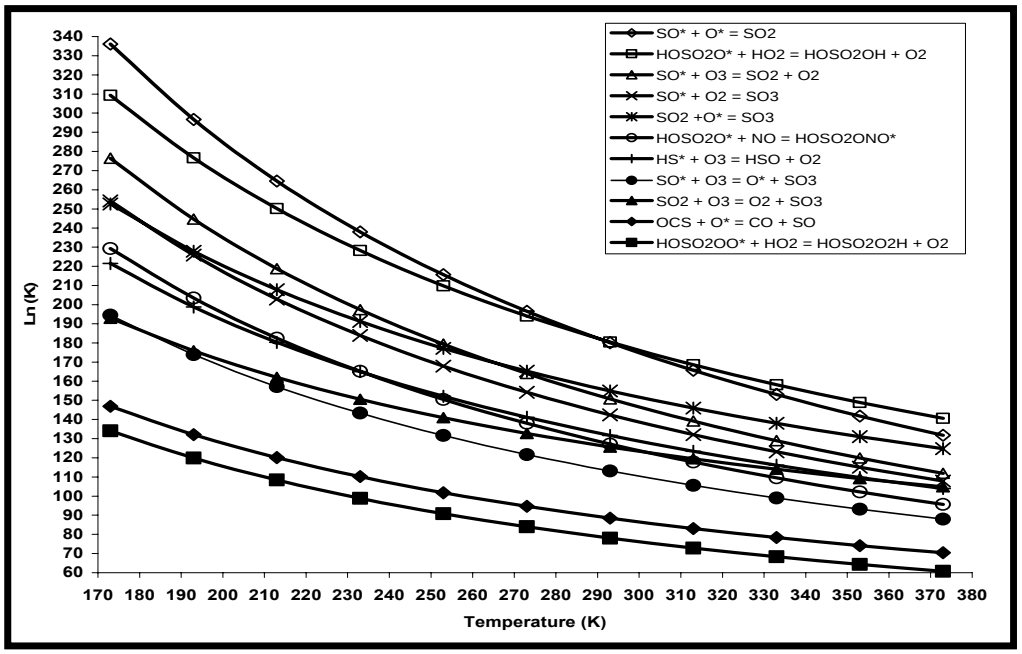

Figure 5-4a: The degree of importance of the gas-phase atmospheric sulphur reactions shown in the legend from thermochemical analyses arranged from the most relevant (top plot) to the least (bottom plot)

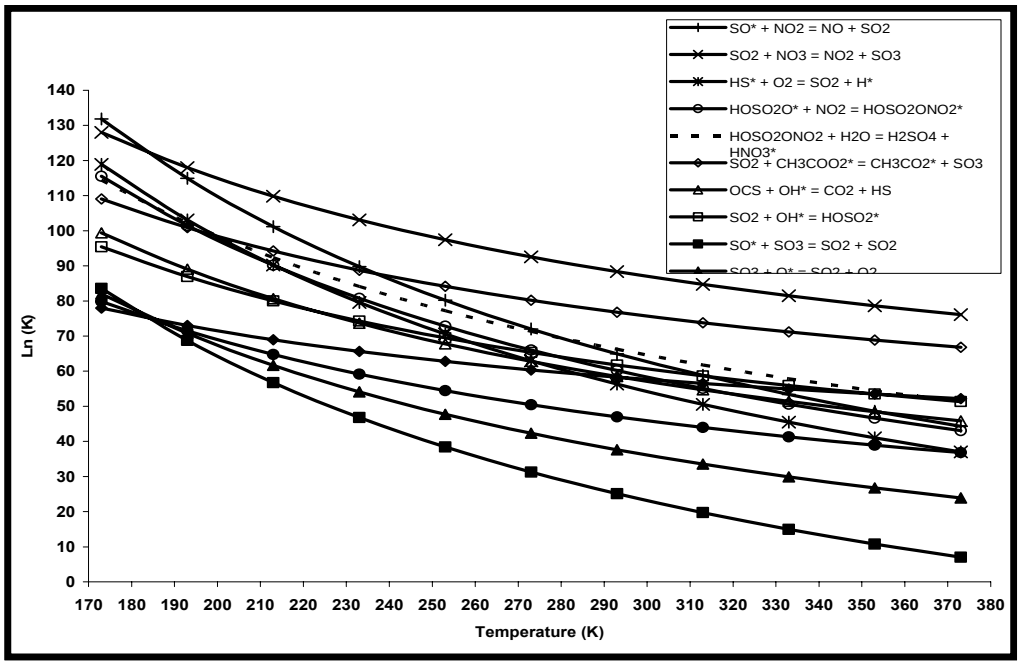

Figure 5-4b: The degree of importance of the gas-phase atmospheric sulphur reactions shown in the legend from thermochemical analyses arranged from the most relevant (top plot) to the least (bottom plot)

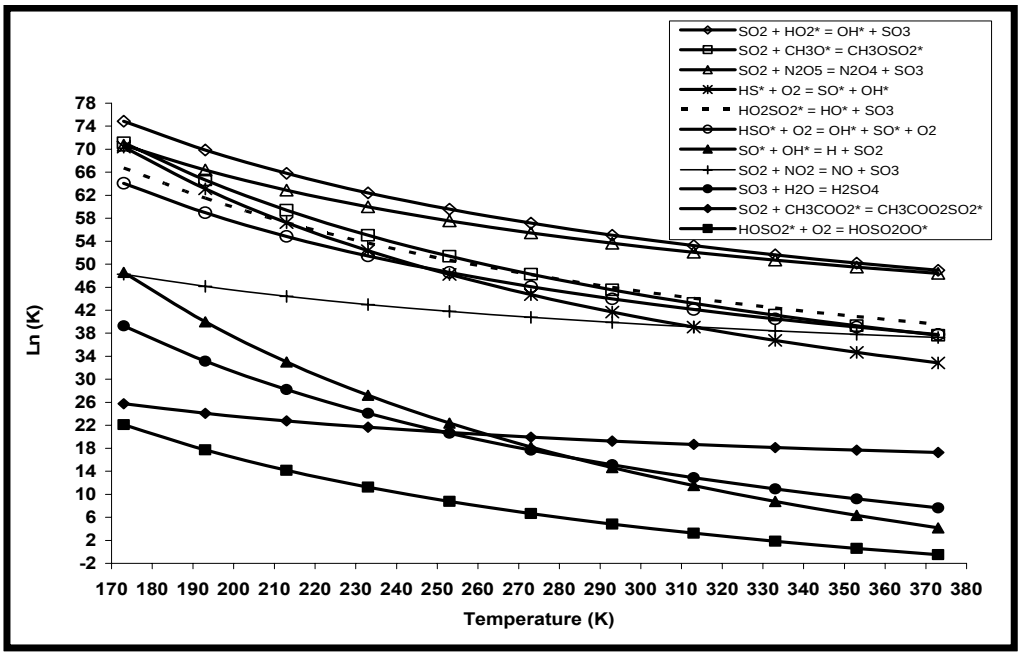

Figure 5-4c: The degree of importance of the gas-phase atmospheric sulphur reactions shown in the legend from thermochemical analyses arranged from the most relevant (top plot) to the least (bottom plot)

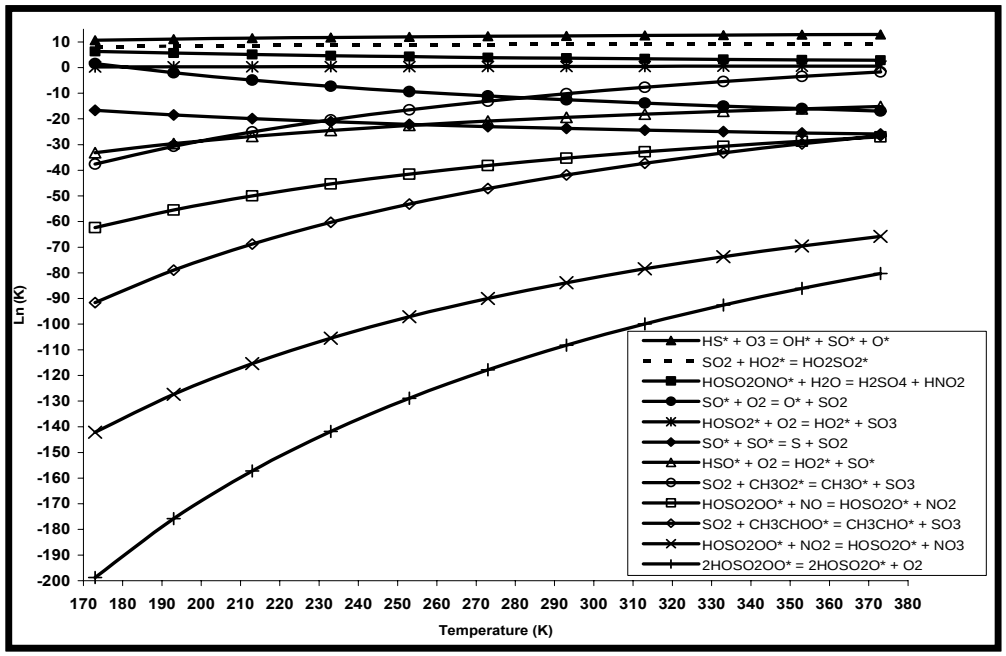

Figure 5-4d: The degree of importance of the gas-phase atmospheric sulphur reactions shown in the legend from thermochemical analyses arranged from the most relevant (top plot) to the least (bottom plot)

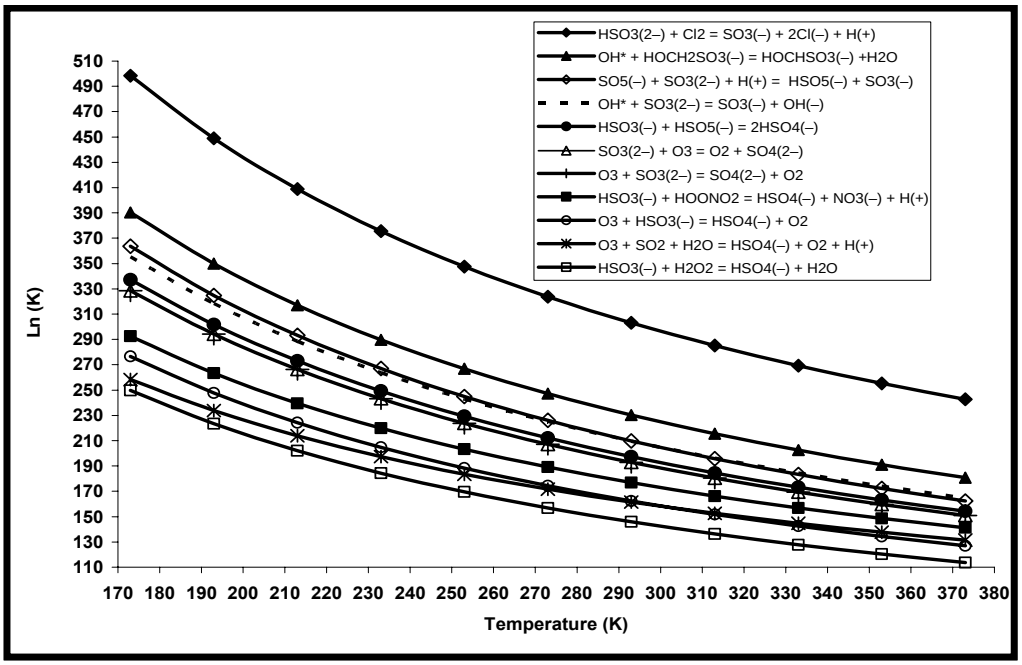

Figure 5-5a: The degree of importance of the aqueous -phase atmospheric sulphur reactions shown in the legend from thermochemical analyses arranged from the most relevant (top plot) to the least (bottom plot)

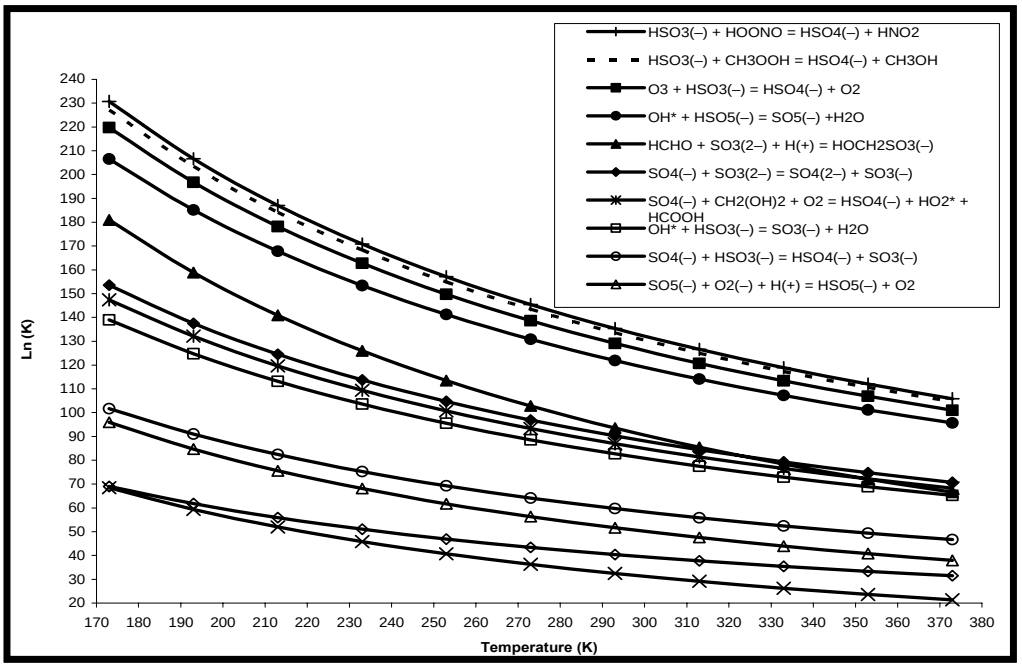

Figure 5-5b: The degree of importance of the aqueous -phase atmospheric sulphur reactions shown in the legend from thermochemical analyses arranged from the most relevant (top plot) to the least (bottom plot)

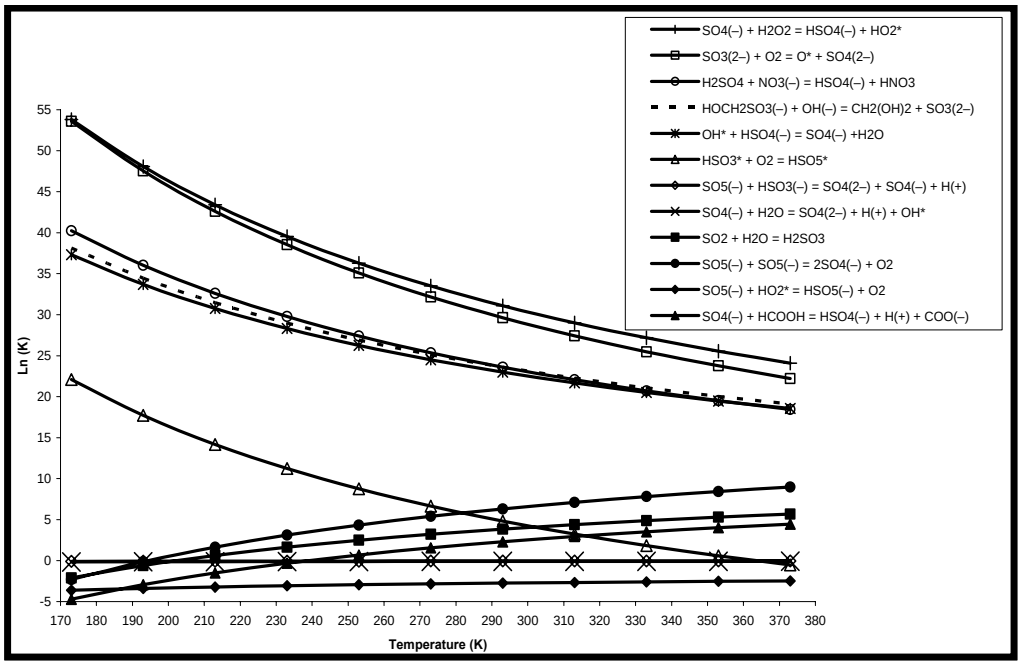

Figure 5-5c: The degree of importance of the aqueous -phase atmospheric sulphur reactions shown in the legend from thermochemical analyses arranged from the most relevant (top plot) to the least (bottom plot)

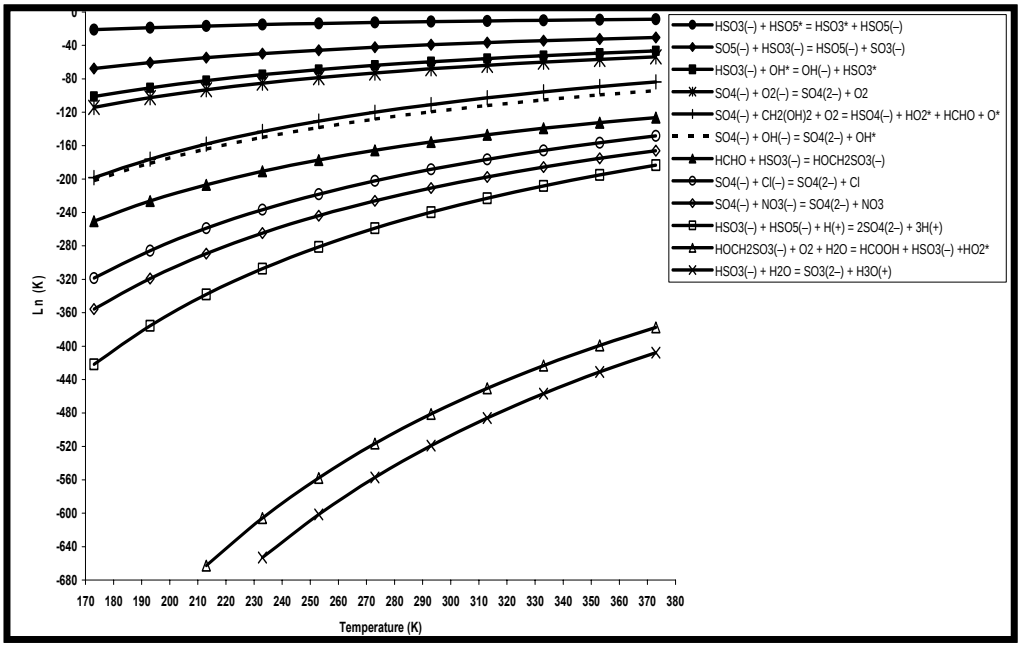

Figure 5-5d: The degree of importance of the aqueous-phase atmospheric sulphur reactions shown in the legend from thermochemical analyses arranged from the most relevant (top plot) to the least (bottom plot)

5.5 Equilibrium Conversion over Tropospheric Temperature Range

Over the temperature range –100 °C to +100 °C proposed for extreme situations of ambient tropospheric temperatures, about 80 % and 65 % of the gas-phase and aqueous-phase reactions in Table (5-1), are favoured by the forward reactions. This means that they are likely to attain equilibrium since their equilibrium conversion, $X_{RE} > 1$ over the specified temperature range. Consequently their products of transformation should constitute only those of the forward reaction. About 15 % and 23 % of the gas-phase and aqueous-phase reactions respectively will attain equilibrium such that both reactant and product species will be present in moderate concentrations. The balance of about 5 % and 12 % of the gas-phase and aqueous-phase reactions may attain equilibrium at higher temperatures that is, above 20 ^{o}C. This implies that at certain ambient temperatures the forward reaction dominates while at other temperatures the reverse is the case. With these forms of reactions any slight variation in ambient temperature will alter the sulphur distribution over the area substantially.

All the reactions with positively large equilibrium constant, K, are favoured by the forward reactions and are most likely irreversible throughout the given temperature range. While those reactions with negative K-values, are favoured in the reverse direction. Winter (which is characterised by very low ambient temperatures) will most likely favour only the forward reactions shown in Figures (5-4a) to (5-4c) for gas-phase and those in Figures (5-5a), (5-5b) and about seven reactions in Figure (5-5c) for the aqueous-phase reactions. This is because their equilibrium conversion is far from reaching unity at between –100 ^{o}C and 0 ^{o}C.

For the gas-phase processes, $HOSO_2^* + O_2 \rightarrow HO_2^* + SO_3$ and $SO^* + O_2 \rightarrow O^* + SO_2$ are favourable at low temperatures in the forward direction while reverse direction dominates at high temperature since its equilibrium conversion, $X_{RE} = 1$. And $HOSO_2^* + O_2 \rightarrow HOSO_2OO^*$ is favoured by the forward reaction only up till 80 ^{o}C as $X_{RE} > 1$ after which the reverse reaction occurs since $X_{RE} < 1$. For $HOSO_2ONO^* + H_2O \rightarrow H_2SO_4 + HNO_2$ the forward reaction is favoured between -100 ^{o}C and -60 ^{o}C and between 0 ^{o}C and 100 ^{o}C, while between -60 ^{o}C and 0 ^{o}C the reverse reaction is favoured. And for the aqueous-phase

reactions over the temperature range, $HSO_3^{2-} + Cl_2 \rightarrow SO_3^{-} + 2Cl^{-} + H^{+}$ is favoured in the forward direction between -100 °C and -90 °C, while between -90 °C and +100 °C it is favoured in the reverse direction. Also $OH^{*} + HSO_3^{2-} \rightarrow SO_5^{-} + H_2O$ is partially favoured in the forward direction throughout the temperature range.

5.6 The Most Significant Atmosphere Sulphur Transformations

In order to ascertain the most relevant atmospheric sulphur reactions, the equilibrium constant temperature relationships were arranged in descending order as in Figures (5-4a) to (5-5d). This arrangement shows the highest to lowest thermodynamically favourable reactions over extreme cases of tropospheric temperature ranges (-100 °C to +100 °C) which are possibly attained in the Antarctic region and Dead Valley of the United States of America, respectively.

In Figures (5-4a) and (5-5a), the largest gas-phase and aqueous-phase equilibrium constants with temperatures are shown. This was to clearly distinguish the most dominant pathway taken by the released gaseous sulphur during oxidation and to indicate the most significant sulphur transformation. In the gas-phase, $SO^{*} + O^{*} \rightarrow SO_2$ topped the group, while for the aqueous-phase $HSO_3^{2-} + Cl_2 \rightarrow SO_3^{-} + 2Cl^{-} + H^{+}$ was the most favoured. But on an overall rating, the aqueous-phase reaction was about 35 % higher in the equilibrium constant values than the first of the gas-phase reaction. In a decreasing order, the most favourable atmospheric sulphur species likely to be participating in chemical transformation in summer, autumn, winter and spring at Elandsfontein are HSO_3^{2-}, $HOCH_2SO_3^{-}$, SO_5^{-} and SO_3^{2-} in the aqueous-phase and SO^{*} in the gas-phase. This is due to the aqueous-phase species having larger equilibrium constants than the gas-phase (Figure 5-3a), hence indicating that the aqueous-phase plays a more important role in SO_2 oxidation than gas-phase. Similar observations have been made by various researches (Moller, 1980; Pienaar and Helas, 1996; Warneck, 1999), that aqueous-phase reactions predominate and provide the essential atmospheric reaction mechanisms of SO_2 oxidation.

A number of gas-phase transformations involving atmospheric sulphur have been classified important in the troposphere by previous workers. Out of all the reactions, four sets of

reaction were classified the most important, based on their rates of reaction. These reactions presented in the descending order of relevancy (Calvert *et al*, 1978; Pienaar and Helas, 1996) are:

$$SO_2 + O^* \rightarrow SO_3, \qquad (A)$$

$$SO_2 + OH^* \rightarrow HOSO_2^* \qquad (B)$$

$$SO_2 + HO_2^* \rightarrow OH^* + SO_3 \qquad (C)$$

and

$$SO_2 + CH_3O_2^* \rightarrow CH_3O^* + SO_3 \qquad (D)$$

In this study, the relative importance of a reaction was evaluated on the basis of its ability to occur relative to other competing reactions rather than by how fast it occurs. Since the thermodynamic conditions of the atmosphere dictate the likelihood of the occurrence of a particular reaction, it was thus reasonable to express the importance of the reactions (A), (B), (C) and (D) in relation to their thermodynamic favourability. From the thermochemical analysis reactions (C) was observed to be more favourable to reaction (D), but the situation was different for reactions (A) and (B). Reaction (B) [Fig. 5-4b] was more favoured according to the thermochemical analysis than reaction (A) [Fig. 5-4a]. Therefore applying chemical thermodynamics of reaction as a basis for the evaluation of the degree of importance for the four atmospheric sulphur oxidation, produced a descending order of importance of the form (B), (A), (C) and (D).

5.7 Conclusion

Analysis of atmospheric chemical reactions that may otherwise be experimentally difficult to investigate can be achieved through the use of computational model theories. It is complex to effectively determine actual reaction kinetics and thermochemical properties of the reaction species of atmospheric transformations. The latter has been achieved for a total of 92 homogeneous gas-phase and aqueous-phase sulphur reactions with the use of molecular orbital model theories of computational chemistry to calculate electronic energies. This electronic energy is computed based on the geometrical configuration of the

species and the electronic properties, consisting of its electronic charge and spin multiplicity. Several relevant pathways for both gas-phase and aqueous-phase reactions were established, as well as the equilibrium constants. The predicted reactions have been characterised in order of increasing significance of favourability between –100 °C and +100 °C. The aqueous-phase processes emerge as the dominant favourable reaction routes. This demonstrates the reactions for SO_2 oxidation, over an extensive ambient temperature range of -100 °C to +100 °C is, to a significant extent, enhanced by the variation in atmospheric water vapour content. Although equilibrium constant values indicate thermodynamic favourability, for the favoured reactions, the values may be very large. However, if the concentrations of the reacting species present are very small, this reaction will only have a very small or no contribution to the expected product overall ambient levels.

Over the Mpumalanga Highveld area, it is most possible to predict that during the months October to April (summer and autumn) due to the fairly consistent rainfall, the most likely the expected sulphur and associated species are HSO_3^{2-}, $HOCH_2SO_3^-$, SO_5^- and SO_3^{2-} undergoing aqueous-phase reactions and their corresponding products such as HCOOH, H_2O, $CH_2(OH)_2$, H_2SO_3, H_2SO_4, whereas during the other months (winter and spring), SO^* (which is formed from a sulphide) and its products SO_2 would dominate. On the other hand all the SO_2 present are most likely associated with the products of the reduced SO_3 (such as H_2SO_4) resulting from the presence of OH^* that gave rise to $HOSO_2^*$.

Chapter 6: Analyses of SO_2 Oxidation during Dispersion over Elandsfontein

6.1 Introduction

The ultimate fate of gaseous emitted sulphur species is their transformation into particulate sulphate. In Chapter 4 it was shown that despite the influence from atmospheric transport activities of air masses over southern Africa, particulate sulphate over Elandsfontein can also occur due to chemical transformation. While in Chapter 5, thermodynamic analyses have shown that aqueous phase reactions are the most favourable for the transformation of SO_2. This may only be occasional since the weather pattern throughout the year over the Elandsfontein is dominated by dry conditions. Therefore in this chapter, it is thus necessary to evaluate the atmospheric sulphur (SO_2 and sulphate) distribution during advection since dispersion, transformation and deposition processes alter the gas-particle ratio.

When SO_2 is emitted from point- or area-sources within an industrial area advecting over adjoining communities where synergistic effects among pollutants are of considerable consequence, chemical transformation rates may be of concern. In such an environment, models are applied primarily for regional evaluations of the combination of line-, point-, area- and volume-sources over the entire region. Atmospheric sulphur gases undergo transformation and removal occurs during air mass transport away from an emission source area along the wind direction. Their vertical and horizontal distribution is controlled by variations in meteorological parameters. The various mechanisms of chemical transformation of atmospheric sulphur include photochemical, gas- and aqueous-phase and heterogeneous reactions. Sulphur transformation is terminated either after the formation of particulate sulphate or after deposition to the surface.

In the atmosphere, chemical reactions do not occur according to any specific reaction pattern due to the many variations in atmospheric conditions, composition of reacting mixture, reactant concentration and meteorological conditions which cannot be controlled.

Also most of the conversion rates for atmospheric SO_2 reported in the literature were deduced from laboratory experiments or from theoretical computations yielding results of SO_2 having longer atmospheric lifetimes (Junkermann and Roedel, 1983). These rate equations vary as a result of the reaction type and the mechanism investigated, which include photochemical, gas-phase, aqueous-phase and heterogeneous reactions proposed for the kinetic rate of transformation.

Therefore it was necessary to develop a model using direct measured field data. In this chapter, a kinetic model is described, developed and simulated using an unsteady state Gaussian puff model with the mixed layer height limited by the inversion layer at the top and, at the bottom, by the Earth's surface. The model was formulated to predict the kinetic episodes of SO_2 oxidation to sulphate through mathematical derivations similar to the works of Alkezweeny and Powell (1977) and Ronneau and Snappe-Jacob (1978) and applied to the air dispersion model according to Lusis and Phillips (1977). The difference in this study was that the order of reaction used was a second order (which had been proposed in literature) rather than the first order used in previous studies.

6.2 Model Development

The kinetic model was based on the conservation of mass for the total sulphur in air present as sulphur dioxide and sulphate traversing the monitoring station from two nearby coal-fired power plants. Both power stations smoke stacks are fairly close to each other; about 200 m apart. The combined capacity of the coal-fired power plants is 5400 MW with four smoke stacks consisting of three chimneys in one stack-casing arrangement. Each stack is about 3 m inner-diameter and about 250 m in physical height.

The diffusion was assumed to follow the pattern of a Gaussian distribution. The dispersed material was assumed to occur as "puffs" in order to account for the unsteady-state variation of concentration with wind direction. Mixing heights for the boundary layers were determined, starting with a simple energy balance approach similar to that described by Oke (1987). The heat flux, H, was calculated followed by the friction velocity, u^*, and

the Monin-Obukhov length, L. These parameters were used to determine the mixing heights.

The kinetic and diffusion models were proposed based on the following assumptions:

(a) The atmospheric diffusion rates of all gases and submicron particles (such as sulphates) are equal.

(b) The rate of reaction is second order (Freiberg, 1975; Calvert *et al*, 1978; Eggleton and Cox, 1978; Pienaar and Helas, 1996; Warneck, 1999; Seinfeld and Pandis, 1998; Grgic and Bercic, 2001) and the deposition rate is first order (Alkezweeny and Powell, 1977; Ronneau and Snappe-Jacob, 1978; Sehmel, 1980).

(c) The vertical distribution of reactant and product concentrations is of the Gaussian pattern throughout the mixing layer.

(d) The sulphates are formed as a result of the transformation of emitted sulphur dioxide in the puff.

(e) The background concentrations have a negligible effect on the emitted sulphur concentration and are insignificant compared to the total sulphur at source point.

(f) Concentration changes due to diffusion exceed those due to chemical reactions.

(g) Wind directions at ground level are considered to be fairly good indicators of the origin of polluted air masses. Boundary layer wind speed was estimated from surface winds based on the power exponents' law (Stern *et al*, 1973; Seinfeld and Pandis, 1998; Wayne, 2000; Tyson and Preston-Whyte, 2000).

(h) From defined source points, the sojourn (between source and monitoring station) times of air advecting through the sampling site depend on the surface winds and mixing heights.

6.2.1 Estimation of SO_2 Concentration at the Source

One of the most essential parameter for the evaluation of a rate constant for a second order reaction is the reactant concentration at source. The source concentration (also known as stack's emission strength) is equally important in the evaluation of the Lagrangian dispersion model. For the case of SO_2 oxidation, the source concentration may be estimated as follows:

If S % of sulphur is present in the coal-feed to the stack heater, and for every mole of sulphur combusted, 1 mole of SO_2 is formed, since sulphur has a molecular weight of 32g/gmol and combines with O_2 with a molecular weight of 32g/gmol, then for every 32 grams of sulphur burned, 64 grams of SO_2 is produced. Therefore, the initial reactant concentration (stack's emission strength), Q_{SO_2}, for SO_2 released is given by:

$$Q_{SO_2}(kg/h) = x_0 = Q_{Coal}(kg/h)\left(\frac{S}{100}\right)\left(\frac{64g/gmol}{32g/gmol}\right)\left(\frac{SO_2}{S}\right) \qquad (6.1)$$

In equation (6.1) from Turner (1974), Q_{Coal} is the emission source strength (kg h^{-1}), while Q_{SO_2} is the amount of gaseous sulphur released during the combustion (kg h^{-1}) and S (%) is the sulphur content in the coal. The average sulphur content of South African coal ranges from 0.75 to 1.2 %. The Kriel and Matla power plants use coal from the same seams which are estimated to have an average sulphur content of 0.9 %. Therefore, equation (6.1) reduces to:

$$Q_{SO_2}(kg/h) = x_0 = (0.018)Q_{Coal}(kg/h) \qquad (6.2)$$

Where Q_{SO_2} also designated as x_0 is the initial concentration of SO_2 at the source area. From equation (6.2), the SO_2 concentration at the source area can be estimated.

6.2.2 Chemical Sub-models

A number of chemical transformations of atmospheric SO_2 have been proposed under varying atmospheric conditions (Moller, 1980; Carmichael and Peters, 1984a; 1984b;

Warneck, 1999). The oxidation of SO_2 has been described as a very slow process in the formation of sulphate and, as a result, it is the rate-controlling step for the several numbers of participating consecutive reactions. This stage is followed by a faster reaction between the sulphur trioxide formed from SO_2 oxidation and water vapour (Calvert *et al*, 1978; Pienaar and Helas, 1996; Warneck, 1999; Herrmann *et al*, 2000). It can be assumed that the rate of transformation into trioxide and sulphate are negligible at the emission source. In this chapter, for the development of this chemical sub-model (which is tagged *model type-1*), the assumptions mentioned above are used and the reaction is taken as a second order type and deposition as first order both at the source area and the sampling site where plume fumigation allows airborne concentrations to approach the Earth's surface.

For the purpose of comparison, overall rate constants for SO_2 oxidation of two kinetic models were applied. The rates of these models were developed from atmospherically simulated smog-chamber experiments (Carmichael and Peters, 1984b) and from the combination of several published rates of reaction (Moller, 1980). The rate expression from the simulated smog-chamber study was designated *model type-2A*, while that obtained from the combination of several published rates was tagged *model type-2B*.

Determination of an Overall Rate Constant for Model Type-1

The degree of transformation applied for the development of the chemical sub-model is given by equation (6.3). This simplify chemical model has been applied in Alkezweeny and Powell (1977) and Ronneau and Snappe-Jacob (1978) for first order SO_2 oxidation. For the overall reaction pattern given in terms of elemental sulphur mass balance as:

$$SO_2 \quad \rightarrow \quad SO_4^{2-} \tag{6.3}$$

The change of the reacting species in the mixture is expressed as the ratio of the reactant SO_2 to the total product mixture of SO_2 and SO_4^{2-} given by:

$$r(t) = \left[\frac{[SO_2]}{[SO_2] + [SO_4]} \right] = \left[\frac{[SO_2]}{[S_T]} \right] \tag{6.4}$$

where $[SO_2]$ and $[SO_4^{2-}]$ represent the concentration of gaseous sulphur present as sulphur dioxide and the concentration of sulphate, while $[S_T]$ is the numeric sum of the concentrations of sulphur dioxide and sulphate.

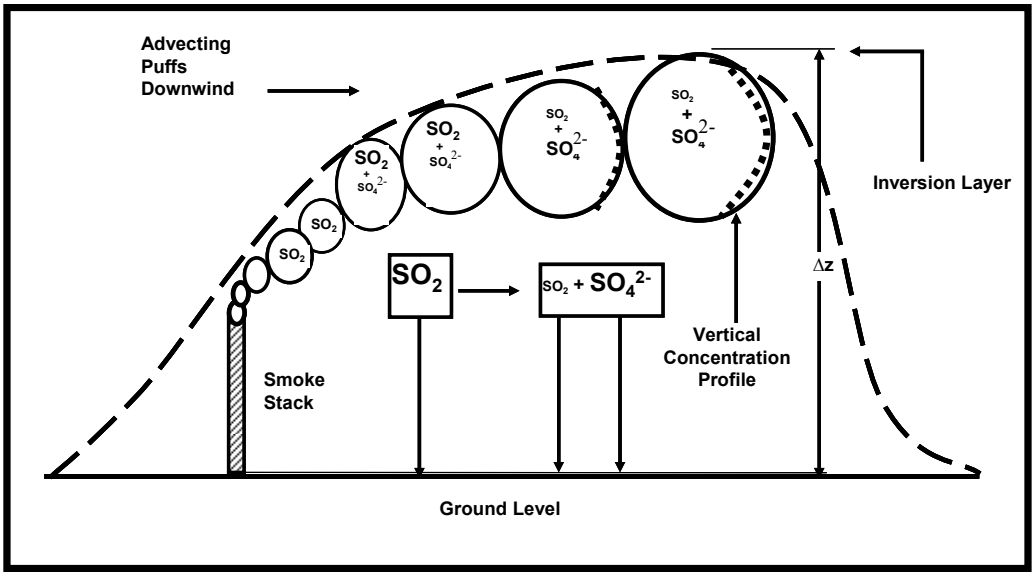

Figure 6-1: A diffusion model pattern for the disappearance of SO_2 to sulphate

Figure (6-1) gives a schematic illustration of the transformation pattern used in the kinetic development. It shows the various processes considered for the transformation and deposition as well as the mixing height that account for the estimated reactor fluid volume. Given that $[SO_2](t)$ is the mass concentration of sulphur dioxide in an advecting air parcel ($\mu g\ m^{-3}$) and $[SO_4^{2-}](t)$ is the mass concentration of sulphate in an advecting air parcel ($\mu g\ m^{-3}$), the mass of the reacting sulphur species in a particular fluid volume, $V(t)$, is given as:

$$x(t) = [SO_2](t) * V(t) \tag{6.5}$$

and

$$y(t) = [SO_2](t) * V(t) + [SO_4^{2-}](t) * V(t) \tag{6.6}$$

where *x(t)* is the mass of sulphur present as sulphur dioxide in the given air parcel (μg), *y(t)* is the mass of total sulphur present as the numeric sum of sulphur dioxide and sulphate in the given air parcel (μg). If $k_d^{SO_2}$ is the dry deposition rate constant for sulphur dioxide at the source area up to the sampling site (h^{-1}), $k_d^{SO_4}$ is the dry removal rate constant for sulphate downwind at the sampling site (h^{-1}), k is the reaction rate constant of sulphur dioxide oxidation ($\mu g^{-1}\ h^{-1}$), the rate of disappearance of sulphur dioxide in a transported air mass in the PBL, η_{SO_2}, is expressed as:

$$\eta_{SO_2} = \frac{d[x(t)]}{dt} = -k[x(t)]^2 - k_d^{SO_2}[x(t)] \tag{6.7}$$

and

$$\frac{d[y(t)]}{dt} = -k_d^{SO_2}[x(t)] - k_d^{SO_4}\{[y(t)] - [x(t)]\} \tag{6.8}$$

It should be noted that a chemical reaction rate is usually defined in terms of the concentration, but in this case it is more convenient to use the mass of the reacting species. Solving equation (6.7) gives the along-wind SO_2 concentration at any given time, t_2, after a sampling start time, t_1, with known initial concentration as a result of chemical reaction and deposition, and is expressed as:

$$\frac{1}{[x(t)]} = \left(\frac{1}{x_0} + \frac{k}{k_d^{SO_2}}\right)\exp(k_d^{SO_2}t) - \frac{k}{k_d^{SO_2}} \tag{6.9}$$

where x_0 is the initial SO_2 concentration released at the source (stack's emission strength). Substituting the time-dependent SO_2 concentration expression (equation 6.9) into equation (6.8), rearranging and integrating gives:

$$[y(t)] = \ell^{-k_d^{SO_4}t}\left\{x_0 + j\left(\sum_{l=1}^{5}\nabla_l\right)\right\} \tag{6.10}$$

where

$$\nabla_1 = \ln(\ell^{k_d^{SO_2}t} - h) - \ln(1-h) = \ln\left\{\frac{\ell^{k_d^{SO_2}t} - h}{1-h}\right\} \quad (6.10)\ \text{a}$$

$$\nabla_2 = \frac{a_1[(\ell^{k_d^{SO_2}t} - h) - (1-h)]}{h} = \frac{a_1(\ell^{k_d^{SO_2}t} - 1)}{h} \quad (6.10)\ \text{b}$$

$$\nabla_3 = \frac{a_2[(\ell^{k_d^{SO_2}t} - h)^2 - (1-h)^2]}{4h^2} \quad (6.10)\ \text{c}$$

$$\nabla_4 = \frac{a_3[(\ell^{k_d^{SO_2}t} - h)^3 - (1-h)^3]}{18h^3} \quad (6.10)\ \text{d}$$

$$\nabla_5 = \frac{a_4[(\ell^{k_d^{SO_2}t} - h)^4 - (1-h)^4]}{96h^4} \quad (6.10)\ \text{e}$$

Also,

$$j = \frac{ih^{\left(\frac{k_d^{SO_4}}{k_d^{SO_2}} - 1\right)}}{k_d^{SO_2}} \quad (6.10)\ \text{f}$$

$$i = \left(\frac{k_d^{SO_4} - k_d^{SO_2}}{1/x_0 + k/k_d^{SO_2}}\right) \quad (6.10)\ \text{g}$$

$$h = \left(\frac{kx_0}{kx_0 + k_d^{SO_2}}\right) \quad (6.10)\ \text{h}$$

$$1-h = \left(\frac{k_d^{SO_2}}{k_d^{SO_2} + kx_0}\right) \quad (6.10)\ \text{i}$$

Furthermore,

$$a_1 = \frac{k_d^{SO_4}}{k_d^{SO_2}} - 1 \quad (6.10)\ \text{j}$$

$$a_2 = a_1\left(\frac{k_d^{SO_4}}{k_d^{SO_2}} - 2\right) \qquad (6.10)\ \text{k}$$

$$a_3 = a_2\left(\frac{k_d^{SO_4}}{k_d^{SO_2}} - 3\right) \qquad (6.10)\ \text{l}$$

and

$$a_4 = a_3\left(\frac{k_d^{SO_4}}{k_d^{SO_2}} - 4\right) \qquad (6.10)\ \text{m}$$

When equations (6.9) and (6.10) are combined, $r(t)$ which is expressed as $x(t)/y(t)$ is produced. Then rearranging and evaluating $r(t)$ over the travel time, τ, gives:

$$\frac{1}{r(\tau)} = \sum_{p=1}^{6} \Delta_p \qquad (6.11)$$

where,

$$\Delta_1 = \left(b_1 \exp[(k_d^{SO_2} - k_d^{SO_4})\tau]\right) - \left(b_0 \exp[(-k_d^{SO_4})\tau]\right) \qquad (6.11)\ \text{a}$$

$$\Delta_2 = \ln\left(h[\exp(k_d^{SO_2}\tau) - h]\right)\left\{\left(b_2 \exp[(k_d^{SO_2} - k_d^{SO_4})\tau]\right) - \left(b_3 \exp[(-k_d^{SO_4})\tau]\right)\right\} \qquad (6.11)\ \text{b}$$

$$\Delta_3 = \left[\frac{a_1}{h}\left([\exp(k_d^{SO_2}\tau) - h] + [1-h]\right)\right]\left\{\left(b_2 \exp[(k_d^{SO_2} - k_d^{SO_4})\tau]\right) - \left(b_3 \exp[(-k_d^{SO_2})\tau]\right)\right\} \qquad (6.11)\ \text{c}$$

$$\Delta_4 = \left[\frac{a_2}{4h^2}\left([\exp(k_d^{SO_2}\tau) - h]^2 + [1-h]^2\right)\right]\left\{\left(b_2 \exp[(k_d^{SO_2} - k_d^{SO_4})\tau]\right) - \left(b_3 \exp[(-k_d^{SO_2})\tau]\right)\right\} \qquad (6.11)\ \text{d}$$

$$\Delta_5 = \left[\frac{a_3}{18h^3}\left([\exp(k_d^{SO_2}\tau) - h]^3 + [1-h]^3\right)\right]\left\{\left(b_2 \exp[(k_d^{SO_2} - k_d^{SO_4})\tau]\right) - \left(b_3 \exp[(-k_d^{SO_4})\tau]\right)\right\} \qquad (6.11)\ \text{e}$$

$$\Delta_6 = \left[\frac{a_4}{96h^4}\left([\exp(k_d^{SO_2}\tau) - h]^4 + [1-h]^4\right)\right]\left\{\left(b_2 \exp[(k_d^{SO_2} - k_d^{SO_4})\tau]\right) - \left(b_3 \exp[(-k_d^{SO_4})\tau]\right)\right\} \qquad (6.11)\ \text{f}$$

and

$$b_0 = x_0 \frac{k}{k_d^{SO_2}} \qquad (6.12)\ a$$

$$b_1 = x_0 \frac{k}{k_d^{SO_2}} + 1 \qquad (6.12)\ b$$

$$b_2 = \frac{k_d^{SO_4} - k_d^{SO_2}}{k} \left(\frac{k_d^{SO_2} + kx_0}{k_d^{SO_2} x_0} \right) \left(\frac{kx_0}{k_d^{SO_2} + kx_0} \right)^{\frac{k_d^{SO_4}}{k_d^{SO_2}}} \qquad (6.12)\ c$$

$$b_3 = \frac{k_d^{SO_4} - k_d^{SO_2}}{k_d^{SO_2}} \left(\frac{kx_0}{k_d^{SO_2} + kx_0} \right)^{\frac{k_d^{SO_4}}{k_d^{SO_2}}} \qquad (6.12)\ d$$

where $r(\tau)$ is the mass fraction of sulphur dioxide present in the total sulphur at any given time, τ, downwind in a particular air mass. It represents the changes in the reactant gas with change in time during advection. A plot of $1/r(\tau)$ against τ should generate a straight line, with an intercept equal to $1/x_0$ and a slope equal to the rate constant, k, for sulphur dioxide removal in the troposphere.

In order to evaluate $1/r(\tau)$ using equation (6.12), the dry deposition rate constants $k_d^{SO_2}$ (SO_2) and $k_d^{SO_4}$ (sulphate) are required. These dry deposition rate constants can be determined using the dry deposition velocities, $v_d^{SO_2}$ (cm s^{-1}) and $v_d^{SO_4}$ (cm s^{-1}) together with the mixing height, *h*, given as:

$$k_d^{SO_2} = \frac{v_d^{SO_2}}{h} \qquad (6.13)$$

and

$$k_d^{SO_4} = \frac{v_d^{SO_4}}{h} \qquad (6.14)$$

Table 6-1: Meteorological conditions during sampling period

Meteorological Parameters	Mean ± SD	Max	Min
Solar Radiation (W m^{-2})	413 ± 179	1097	-0.4
Ambient Temperature (^oC)	19.4 ± 2.7	33.7	-0.4
Relative Humidity (%)	35.7 ± 14.4	100.0	0.0
Wind Speed (m s^{-1}) @ Wind Directional Sector 230° to 289°	4.7 ± 0.2	14.7	0.3

The mixed layer height, *h*, was evaluated using equations (2-45) to (2-60) using meteorological parameters whose mean values are shown in Table (6-1). The weather pattern shows fairly dry but either partly cloudy or very low sunshine conditions with relative humidity, radiation and temperature of about 36 %, 400 W m^{-2} and 20 ^oC, respectively. It also appears that stable to neutral conditions would predominate over the region as wind is low coupled with the degree of solar radiation (Table 6-1). The dry deposition velocities can be determined from the aerodynamics of the diffusing gases and particles coupled with Stokes' effect on the quasi-laminar layer and the canopy resistances (Wesley, 1989; Seinfeld and Pandis, 1998). For gases and particles the velocities may be determined as follows:

$$\left(v_d^{SO_2}\right)^{-1} = r_a^{SO_2} + r_b^{SO_2} + r_c^{SO_2} \tag{6.15}$$

and

$$\left(v_d^{SO_4}\right)^{-1} = r_a^{SO_4} + r_b^{SO_4} + r_c^{SO_4} \tag{6.16}$$

Where r_a, r_b and r_c are the dry deposition resistances in the aerodynamic layer, quasi-laminar layer and the vegetation canopy layer, respectively.

The dry deposition velocity for SO_2, $v_d^{SO_2}$, on grassland has been estimated as 1.1 cm s^{-1} at a mean frictional velocity, $u_* = 0.4$ m s^{-1} (Garland, 1978; Omstedt and Rodhe, 1978; Sehmel, 1980). And that for sulphate, $v_d^{SO_4}$, for grassland was 0.21 cm s^{-1} (Omstedt and Rodhe, 1978; Eliassen, 1978; Garland, 1978; Carmichael and Peters, 1984a; 1984b;

Walcek *et al*, 1986). These values were applicable to Elandsfontein since the vegetation is also grassland.

Therefore with known deposition velocities across the mixed layer height, h, equations (6.13) and (6.14) simplifies to

$$k_d^{SO_2} = 1.1/h \tag{6.17}$$

and

$$k_d^{SO_4} = 0.21/h \tag{6.18}$$

Then with known deposition rate constants, $k_d^{SO_2}$ and $k_d^{SO_4}$, as well as the estimated SO_2 source concentration, x_0, using equation (6.10) the reaction rate constant, k, can be determined. The oxidation rate constants for the various months of the year are evaluated are shown in (Tables 6-2).

Table 6-2: Monthly rate constant for SO_2 disappearances between the source power station and Elandsfontein

Time τ **(Month)**	$[SO_2]$ from Source $x_0(\tau)$ **(µg m^{-3})**	Mean Ambient Temp. **(K)**	Reaction Rate Constant k x 10^6 **(µg m^{-3} s^{-1})**	Mean Observed Downwind $[SO_2]$ $x(\tau)$ **(µg m^{-3})**
Jan	22132.72	299.10	4.98	78.82
Feb	22132.84	298.03	3.08	103.41
Mar	22301.86	297.51	3.46	102.10
Apr	22458.23	293.07	3.42	100.33
May	22557.98	294.54	3.68	103.01
Jun	22666.04	290.81	2.94	134.96
Jul	22746.30	288.72	1.77	193.03
Aug	22541.91	289.34	3.87	119.17

Sep	22542.53	295.18	3.88	105.04
Oct	22298.72	298.45	4.54	99.12
Nov	22123.74	299.91	3.18	76.89
Dec	22195.45	298.76	6.15	68.85

Based on the estimated source concentration, $x_0 = [SO_2]_{t=0}$, reaction rate constant, k, was obtained using equation (6.10) on a monthly basis to reveal the seasonal variations (Table 6-2). These rate constants (which ranged between 1.77 x 10^{-6} and 6.15 x 10^{-6} μg m^{-3} s^{-1}) appear to accurately calculate downwind SO_2 concentrations, $x(\tau) = [SO_2]_{t=\tau}$, which at any particular time, τ, are approximately equal to the mean observed values.

In order to establish the transformation rate while considering atmospheric deposition as given in equations (6.17) and (6.18), over the Elandsfontein area, the rate model will be expressed as follows:

If the rate of disappearance through oxidation of SO_2 is given as:

$$\frac{d[SO_2]}{dt} = -k[SO_2]^2 - k_d^{SO_2}[SO_2] \qquad (6.19)$$

The % loss per hour is expressed as:

$$-\frac{d[SO_2]}{[SO_2]dt} = \left(k[SO_2]_0 + k_d^{SO_2}\right)\left(3.6 \times 10^5\right) \qquad (6.20)$$

where k, $k_d^{SO_2}$ and $[SO_2]_0$ are the reaction rate constant, dry deposition rate constant and the SO_2 concentration at the source respectively. Equation (6.20) expresses the oxidation rate as % h^{-1} loss of SO_2.

Outcomes of Model Type-1 Evaluations

The seasonal outcome of the effects of variations in oxidation and deposition rate constants on atmospheric SO_2 oxidation are presented in Table 6-3.

Table 6-3: Rate constants of SO_2 disappearances with seasonal variations obtained from *model type-1*

Season	Temperature Range (K)	k x 10^6 $m^3\,(\mu g\ s)^{-1}$	$k_d^{SO_2}$ x 10^5 s^{-1}	Rate % h^{-1}	Estimated Mixing Height (m)
Summer	298 to 309	4.920	1.137	10.90	967.14
Autumn	293 to 298	3.939	1.567	8.83	702.01
Winter	288 to 292	2.896	2.198	6.56	500.52
Spring	295 to 303	4.821	1.750	10.80	628.42
Overall	288 to 309	4.288	1.571	9.60	700.00

The disappearances of SO_2 due to oxidation for the different seasons vary at rate ranging from 8.83 and 10.9 % h^{-1} (Table 6-3). The oxidation rate is a minimum in winter and a maximum in summer this is obvious since aqueous phase reactions which have been observed as more favourable to SO_2 oxidation (Chapter 5) occur in summer. The computed reaction rate appears to decrease with increasing ambient temperature. Hence, an increase in the mixing height would most likely decrease the reaction rate of sulphur dioxide since in the daytime the mixed layer height increases with increasing ambient temperature. An overall estimated oxidation rate relevant to Elandsfontein area is 9.6 % h^{-1} provided the atmospheric conditions observed are similar to those in Table 6-1.

Table 6-4: Rate constants of SO_2 disappearances with seasonal variations obtained from *model type-1* from observations against least squares fitted values

Season	Temperature Range (K)	Calculated from Observations		Fitted with the Arrhenius Equation	
		k_0 $m^3\,(\mu g\ s)^{-1}$	$\frac{E_A}{R}$ (K)	k_0 $m^3\,(\mu g\ s)^{-1}$	$\frac{E_A}{R}$ (K)
Summer	298 to 309	9.569	4394.9	9.565	4394.87
Autumn	293 to 298	2.258 x 10^2	5278.9	2.258 x 10^2	5278.87

Winter	288 to 292	1.997×10^{15}	13915.0	1.997×10^{15}	13914.8
Spring	295 to 303	1.760×10^{2}	5206.5	1.759×10^{2}	5206.47
Overall	288 to 309	4.325	4126.5	9.937×10^{-1}	3692.75

Evaluation of other relevant kinetic model Parameters

The temperature dependent kinetic parameters required for reaction purposes are given by the Arrhenius equation. These parameters are the pre-exponential rate constant, k_0, and the activation energy of reaction, E_A. These parameters are evaluated using equation (2.96a). In Table 6-4, larger activation energies are required during winter to enable SO_2 oxidation than in other seasons. This is due to the low temperature range coupled with dry conditions so that only a few aqueous-phase reactions are favoured. Hence only gas-phase oxidation, that requires a high energy of activation can occur and so the overall rate is small. In order to minimise errors due to computations, the calculated preexponential factor and activation energies were fitted to the Arrhenius equation (Appendix A-2). The activation energies are calculated to be 36.5 kJ for summer, 43.9 kJ for autumn, 115.7 kJ for winter, and 43.2 kJ for spring.

Determination of an Overall Rate Constant for Model Type-2A

From the smog-chamber studies, simplified gas- and aqueous-phase kinetic models based on several reactions with major species including NO, NO_2, SO_2, O_3, HNO_2, HNO_3, NO_3, H_2O_2, CO, CO_2, SO_3 and HSO_3 are presented (Carmichael and Peters, 1984b). The gas- and aqueous-phase rate expressions are given by:

$$\frac{d[SO_2]}{dt} = -1.85 \times 10^{-4}[SO_2] \qquad (6.21)\ a$$

$$\frac{d[SO_2]}{dt} = -3.69 \times 10^{-5}[SO_2] \qquad (6.21)\ b$$

Combining equations (6.21a) and (6.21b) gives the overall rate of SO_2 disappearance in the smog-chamber studies for the advection with reaction model. The overall rate expression is given as:

$$\eta_{SO_2} = \frac{d[SO_2]}{dt} = -2.22 \times 10^{-4}[SO_2] \qquad (6.22)$$

In equation (6.22), the overall oxidation rate constant, *k*, is a first order with a value of 2.22×10^{-4} s^{-1}.

Determination of an Overall Rate Constant for Model Type-2B

A kinetic model of developed from published data was applied as model type-2. The mechanisms considered included photochemical oxidation, homogeneous gas-phase oxidation, liquid-phase oxidation and gas-to-particle conversion. For the photochemical oxidation, the mechanism obtained was defined by the rate expression:

$$-\left(\frac{d[SO_2]}{dt}\right)_{hv} \approx 10^{-7}[SO_2] \qquad (6.23)\ a$$

while the derived rate expression for the homogeneous gas-phase reaction was:

$$-\left(\frac{d[SO_2]}{dt}\right)_{\text{hom}} \approx 1.2 \times 10^{-6}[SO_2] \qquad (6.23)\ b$$

and aqueous-phase oxidations, which are predominantly as a result of SO_2 oxidation with water droplets of clouds or rain or the catalytic contribution of other gases and/or metals is expressed as:

$$-\left(\frac{d[SO_2]}{dt}\right)_{aq} \geq 5x10^{-5}[SO_2] \qquad (6.23)\ c$$

and, finally, the SO_2-to-particle derived model was based on the adsorption capacity of atmospheric particles is given by:

$$-\left(\frac{d[SO_2]}{dt}\right)_{particle} \geq 5 \times 10^{-6}[SO_2] \qquad (6.23)\ \text{d}$$

The resulting overall kinetic equation is given by:

$$\eta_{SO_2} = -\frac{d[SO_2]}{dt} \geq 5.63 \times 10^{-5}[SO_2] \qquad (6.24)$$

In a similar fashion to equation (6.22), the overall oxidation rate constant, *k*, for *model type-2* from equation (6.24) is 5.63 x 10^{-5} s^{-1}.

6.2.3 Comparison of the Three Predicted Rate Constants

The *model type-1* rate constants are lower than those from the smog-chamber studies *(model type-2A)* and the theoretical model rate *(model type-2B)*. Since *model type-1* and *model type-2A* considered deposition during transformation, the reason for reduced oxidation rate of *model type-1* may be attributed to variations in atmospheric stability that may result in rapidly occurring diffusion. The *model type-2B* indicates a rapid disappearance of SO_2 during oxidation, and hence a reduced residence time. This characteristic behaviour could be attributed to contributions of the catalysed heterogeneous rate expression.

In order to establish the atmospheric diffusion effects on transformation, equations (6.19), (6.22) and (6.24) are incorporated into the trajectory model for advection.

6.2.4 Application of Transformation Rates to Atmospheric Diffusion

The transformation mechanism proposed for the atmospheric diffusion modelling is similar to that established by Lusis and Phillips (1977), where the value of the developed rate constant derived from equation (6.10) and estimated SO_2 deposition constant are substituted into equation (6.5), the expression for the chemical sub-model. In reaction kinetics the rate of a chemical reaction is expressed either as a function of the disappearances of the reactants or the formations of the products. Since the chains of chemical reactions involved in the formation of particulate sulphate are very complex and

not well understood, it is more convenient to express the transformation only in terms of the disappearance of SO_2 by oxidation and deposition. The formulated rate expressions of equations (6.5), (6.19) and (6.21) are incorporated into a diffusion-with-advection model.

For stationary situations and homogeneous turbulence, the common atmospheric diffusion formula for the mean concentration of a species emitted from a continuous, elevated point source is the Gaussian formula (Seinfeld and Pandis, 1998). Based on the mean wind speed ($\overline{u}$) in the along-wind direction, coupled with the assumption that the mean crosswind speed ($\overline{v}$) and mean vertical wind speed ($\overline{w}$) equals zero, the equation for the contribution of a puff at a receptor point from a continuous point source for real-time atmospheric application of partial absorption at $z = 0$ and the presence of an impermeable upper boundary with $0 \le z \le H$ (that is, an inversion layer), is given by equation (6.25). In equation (6.25) the mean concentration, $\overline{c}$ (μg m^{-3}), at the receptor point, (x, y, z), at time, *t*, expressed in terms of the emission rate, q, at the source point, (x_0, y_0, z_0), at time, t_0, is given as:

$$\overline{c}(t) = \frac{q(t)}{2\pi\sqrt{\overline{K}_{xx}\overline{K}_{yy}}}\, g \exp\left[-\frac{(x - x_0 - \overline{u}(t - t_0))^2}{4\overline{K}_{xx}} - \frac{(y - y_0)^2}{4\overline{K}_{yy}} \right] \qquad (6.25)$$

where

$$g = \sum_{n=1}^{\infty} \frac{(\lambda_n^2 + \beta^2)\cos[\lambda_n(H - z_0)]\cos[\lambda_n(H - z)]}{H(\lambda_n^2 + \beta^2) + \beta} \exp(-\lambda_n^2 \overline{K}_{zz}) \qquad (6.25)\ a$$

where

$$\lambda_n \tan \lambda_n H = \beta \qquad (6.25)\ b$$

$$\lambda_n = \frac{n\pi}{H} \qquad (6.25)\ c$$

$$K_{xx} = \frac{1}{2}\frac{d\sigma_x^2}{dt} \qquad (6.25)\ d$$

$$K_{yy} = \frac{1}{2}\frac{d\sigma_y^2}{dt} \qquad (6.25)\ \text{e}$$

$$K_{zz} = \frac{1}{2}\frac{d\sigma_z^2}{dt} \qquad (6.25)\ \text{f}$$

Given the following boundary conditions that:

$$\bar{c} = 0 \qquad \text{as} \qquad \left.\begin{matrix} x \\ y \end{matrix}\right\} = \infty \qquad (6.26)\text{a}$$

and $$\frac{d\bar{c}}{dz} = 0 \qquad \text{as} \qquad z = H \qquad (6.26)\text{b}$$

also $$\frac{d\bar{c}}{dz} = \frac{v_d}{K_{zz}} = \beta \qquad \text{as} \qquad z = 0 \qquad (6.26)\text{c}$$

where v_d is the deposition velocity that measures the degree of absorption of the Earth's surface, while K_{zz} is the vertical eddy diffusivity. At steady state it is convenient to assumed that $\overline{K}_{xx} \cong \sigma_x^2/2$, $\overline{K}_{yy} \cong \sigma_y^2/2$ and $\overline{K}_{zz} \cong \sigma_z^2/2$ (Seinfeld and Pandis, 1998). Where $\overline{K}$ is the diffusivity of the pollutant in the atmosphere. Replacing the diffusivities with dispersion coefficients and simplifying equation (6.25) gives:

$$\bar{c}(t) = \frac{q(t)}{\pi\sigma_x\sigma_y} g \exp\left[-\frac{(x - x_0 - \bar{u}(t - t_0))^2}{2\sigma_x^2}\right]\exp\left[-\frac{(y - y_0)^2}{2\sigma_y^2}\right] \qquad (6.27)$$

$$g = \sum_{n=1}^{\infty} \frac{(\lambda_n^2 + \beta^2)}{H(\lambda_n^2 + \beta^2) + \beta} \exp - \left(\frac{\lambda_n^2\sigma_z^2}{2}\right)\cos(n\pi - \lambda_n z_0)\cos(n\pi - \lambda_n z) \qquad (6.27)\ \text{a}$$

where σ_x, σ_y and σ_z are the along-wind, crosswind and vertical dispersion coefficients, respectively.

With the conservation of mass for an unsteady state emission from a continuous point source, the variation of the source strength, q, is related to the reaction rate, η (Lusis and Phillips, 1977), according to equation:

$$\frac{1}{\bar{u}}\frac{dq(t)}{dt} = \int_0^H \int_{-\infty}^{\infty} \int_{-\infty}^{\infty} \eta_{SO_2}(\bar{c},t)dxdydz \tag{6.28}$$

Combining equations (6.7) and (6.27) into equation (6.28) for *model type-1*; equations (6.22) and (6.27) into equation (6.28) for *model type-2A* and equations (6.24) and (6.27) into equation (6.28) for *model type-2B* gives:

$$\frac{1}{\bar{u}}\frac{dq(t)}{dt} = -1.42x10^{-7}\int_0^H \int_{-\infty}^{\infty} \int_{-\infty}^{\infty} \bar{c}^2 dxdydz - 2.65x10^{-4}\int_0^H \int_{-\infty}^{\infty} \int_{-\infty}^{\infty} \bar{c}\,dxdydz \tag{6.29}$$

$$\frac{1}{\bar{u}}\frac{dq(t)}{dt} \cong -3.69x10^{-6}\int_0^H \int_{-\infty}^{\infty} \int_{-\infty}^{\infty} \bar{c}\,dxdydz \tag{6.30}$$

$$\frac{1}{\bar{u}}\frac{dq(t)}{dt} \cong -5.64x10^{-5}\int_0^H \int_{-\infty}^{\infty} \int_{-\infty}^{\infty} \bar{c}\,dxdydz \tag{6.31}$$

Integrating equations (6.29) to (6.31) for x-, y-, z- distances travelled by the reacting fluid yields the following:

From equation (6.29) for *model type-1*:

$$dq(t) = -4.52x10^{-8}\bar{u}q(t)^2\int_{t_1}^{t_2}\left[\frac{1}{\sigma_x\sigma_y}\int_0^H g^2 dz\right]dt - 5.30x10^{-4}\bar{u}q(t)\int_{t_1}^{t_2}\sum_{n=1}^{\infty} w_n\left[\exp-\left(\frac{\lambda_n^2\sigma_z^2}{2}\right)\right]dt \tag{6.32}$$

where

$$w_n = \left(\frac{(\lambda_n^2+\beta^2)}{H(\lambda_n^2+\beta^2)+\beta}\right)\frac{\sin n\pi}{\lambda_n}\cos(n\pi - \lambda_n z_0) \tag{6.32 a}$$

and from equation (6.30) for *model type-2A*:

$$dq(t) = -7.38x10^{-6}\,\bar{u}q(t)\int_{t_1}^{t_2}\sum_{n=1}^{\infty} w_n\left[\exp-\left(\frac{\lambda_n^2\sigma_z^2}{2}\right)\right]dt \qquad (6.33)$$

and from equation (6.31) for *model type-2B*:

$$dq(t) = -1.13x10^{-4}\,\bar{u}q(t)\int_{t_1}^{t_2}\sum_{n=1}^{\infty} w_n\left[\exp-\left(\frac{\lambda_n^2\sigma_z^2}{2}\right)\right]dt \qquad (6.34)$$

In equations (6.32) to (6.34), the summation term was truncated at $n = 15$, because beyond this value of n, the exponential terms were approximately zero. And assuming that for horizontally symmetric puffs with $\sigma_x = \sigma_y$, equation (6.32) for *model type-1* reduces to:

$$\frac{dq(t)}{dt} = -4.52x10^{-8}\,\frac{\bar{u}q(t)^2}{\sigma_v^2}\left[\frac{1}{f_{ly}^2t^2}\int_0^H g^2dz\right] - 5.30x10^{-4}\,\bar{u}q(t)\sum_{n=1}^{15} w_n\left[\exp-\left(\frac{\lambda_n^2\sigma_{w.}^2 f_{lz}^2t^2}{2}\right)\right] \qquad (6.35)$$

where

$$\int_0^H g^2dz = \sum_{n=1}^{15}\frac{\varepsilon_n^2}{2}\left(\frac{\sin(2n\pi)}{2\lambda_n} + H\right) + \sum_{m=1}^{m=14}\sum_{n=m+1}^{n=15}\varepsilon_m\varepsilon_n\left(\frac{\sin(m+n)\pi}{\lambda_m+\lambda_n} + \frac{\sin(m-n)\pi}{\lambda_m-\lambda_n}\right) \qquad (6.35)\text{ a}$$

and

$$\varepsilon_n = \frac{(\lambda_n^2+\beta^2)}{H(\lambda_n^2+\beta^2)+\beta}\exp-\left(\frac{\lambda_n^2\sigma_z^2}{2}\right)\cos\left(n\pi - \lambda_n z_0\right) \qquad (6.35)\text{ b}$$

while equation (6.33) for *model type-2B* simplifies into:

$$\frac{dq(t)}{dt} = -7.38x10^{-6}\,\bar{u}q(t)\sum_{n=1}^{15} w_n\left[\exp-\left(\frac{\lambda_n^2\sigma_{w.}^2 f_{lz}^2t^2}{2}\right)\right] \qquad (6.36)$$

and equation (6.34) for *model type-2B* becomes:

$$\frac{dq(t)}{dt} = -1.13x10^{-4}\,\bar{u}q(t)\sum_{n=1}^{15} w_n\left[\exp-\left(\frac{\lambda_n^2\sigma_{w.}^2 f_{lz}^2t^2}{2}\right)\right] \qquad (6.37)$$

In this study, the dispersion model conducted for SO_2 transport with regard to the Highveld region, was calculated for $z/L < 0$, the deviations of wind velocities in the crosswind and vertical directions are given in Seinfeld and Pandis (1998) as:

$$\sigma_y(t) = \sigma_v f_{ly} t \qquad (6.38)\ a$$

$$\sigma_z(t) = \sigma_w f_{lz} t \qquad (6.38)\ b$$

where

$$\sigma_v = 1.78 u_* [1 + 0.059(-h_{us}/L)]^{1/3} \qquad (6.38)\ c$$

and

$$\sigma_w = 2.891 w_* h_{us}^{-0.333} \qquad (6.38)\ d$$

where f is the Lagrangian time scale that specifies the characteristics of the atmospheric boundary layer. Simplifying equations (6.35) to (6.37) for the convective and stable boundary layer conditions gives the dispersed concentration at the receptor point in relation to the emission area. These receptor point concentrations for the three different rate models are given in the following sections.

Diffusion Evaluations for Model Type-1

The developed rate expression referred to as *model type-1* from equation (6.32) is reduced to:

$$\left.\frac{1}{q(t)}\right|_{(Q_S/Q_S^0)_1}^{(Q_S/Q_S^0)_2} = e^{j(t)}.i(t) \qquad (6.39)$$

where

$$i(t) = \left(\int_{t_1}^{t_2} e^{-j(t)} Q(t) dt \right) \qquad (6.39)\ a$$

$$Q(t) = \alpha\left[\sum_{n=1}^{15} V_n \exp\left(-\frac{\lambda_n^2\sigma_w^2 t^2}{(1+0.9t^{0.5})^2}\right) + \sum_{m=1}^{m=14}\sum_{n=m+1}^{n=15} U_{mn}\exp\left(-\frac{(\lambda_m^2+\lambda_n^2)\sigma_w^2 t^2}{2(1+0.9t^{0.5})^2}\right)\right] \quad (6.39)\text{ b}$$

$$V_n = \left[\frac{(\lambda_n^2+\beta^2)}{H(\lambda_n^2+\beta^2)+\beta}\cos\left(n\pi-\lambda_n z_0\right)\right]^2\left(\frac{\sin(2n\pi)}{4\lambda_n}+\frac{H}{2}\right) \quad (6.39)\text{ c}$$

$$U_{mn} = \Gamma_{mn}\left(\frac{\sin(m+n)\pi}{\lambda_m+\lambda_n}+\frac{\sin(m-n)\pi}{\lambda_m-\lambda_n}\right) \quad (6.39)\text{ d}$$

$$\Gamma_{mn} = \left[\frac{(\lambda_n^2+\beta^2)}{H(\lambda_n^2+\beta^2)+\beta}\cos\left(n\pi-\lambda_n z_0\right)\right]\left[\frac{(\lambda_m^2+\beta^2)}{H(\lambda_m^2+\beta^2)+\beta}\cos\left(m\pi-\lambda_m z_0\right)\right] \quad (6.39)\text{ e}$$

$$j(t) = 5.30x10^{-4}\,\delta(t) \quad (6.40)\text{ a}$$

$$\delta(t) = \overline{u}\int_{t_1}^{t_2}\sum_{n=1}^{15} w_n\left[\exp-\left(\frac{\lambda_n^2\sigma_w^2 t^2}{2(1+0.9t^{0.5})^2}\right)\right] \quad (6.40)\text{ b}$$

$$\alpha = -\frac{4.52x10^{-8}\,\overline{u}}{\sigma_v^2}\left(\frac{(T_i^{0.5}+t^{0.5})^2}{T_i t^2}\right) \quad (6.41)$$

$$T_i = 50u_*\left(1+0.0013\left(-h_{us}/L\right)\right)^{-1/3} \quad (6.42)$$

The detailed mathematical evaluations of the concentration distribution of *model type-1* are given in Appendix A-1.

Diffusion Evaluations for Model Type-2A

Incorporating the rate expression for *model type-2A* into equation (6.36) and simplifying gives equation (6.43)

$$\ln q(t)\Big|_{(Q_S/Q_S^0)_1}^{(Q_S/Q_S^0)_2} = -7.38x10^{-6}\overline{u}\int_{t_1}^{t_2}\sum_{n=1}^{15} w_n\left[\exp-\left(\frac{\lambda_n^2\sigma_w^2 t^2}{2(1+0.9t^{0.5})^2}\right)\right]dt \quad (6.43)$$

Equation (6.43) can be further simplified to:

$$q(t)\Big|_{(Q_S/Q_S^0)_1}^{(Q_S/Q_S^0)_2} = \ell^{-7.38x10^{-6}\delta(t)} \qquad (6.43)\text{ a}$$

The complete derivations of the concentration distribution for *model type-2A* are given in Appendix A-1.

Diffusion Evaluations for Model Type-2B

Substituting the reaction rate constant for model *type-2B* (Moller, 1980) into equation (6.37) gives

$$\ln q(t)\Big|_{(Q_S/Q_S^0)_1}^{(Q_S/Q_S^0)_2} = -1.13x10^{-4}\overline{u}\int_{t_1}^{t_2}\sum_{n=1}^{15} w_n\left[\exp-\left(\frac{\lambda_n^2\sigma_w^2 t^2}{2(1+0.9t^{0.5})^2}\right)\right]dt \qquad (6.44)$$

In a similar manner equation (6.44) is simplified as:

$$q(t)\Big|_{(Q_S/Q_S^0)_1}^{(Q_S/Q_S^0)_2} = \ell^{-1.13x10^{-4}\delta(t)} \qquad (6.44)\text{ a}$$

The complete derivations of the concentration distribution of *model type-2B* are given in Appendix A-1. Equations (6.39), (6.43) and (6.44) represent the contribution of atmospheric stability on emission rate variations. These equations were developed for change in the daytime emission rate within the convective boundary layer for unstable conditions at z <50 m.

$$I = \int_{t_1}^{t_2} H(t) \cong \frac{\Delta t}{3}\left\{\left[\Psi(t_1)+\Psi(t_2)\right]+2\sum_{\substack{i=2\\ j=i+1}}^{\substack{i=q-2\\ j=q-1}}\left[2\Psi(t_i)+\Psi(t_j)\right]\right\} \qquad (6.45)$$

where $\Psi(t)$ represents functions such as $j(t)$, $i(t)$ or $\delta(t)$.

Integrating equations (6.39), (6.43) and (6.44) numerically using Simpson's formula defined in equation (6.45), for t_1 to t_2, yielded the mass fraction of SO_2 $(Q_s / Q^0_s)_2$ present in an air parcel in a puff at location 2 with a known plume age, t_2, in relation to the fraction of SO_2 $(Q_s / Q^0_s)_1$ remaining at an earlier plume location 1 and age, t_1, within the day. If s_q is a downwind distance at any fixed point, q, from the emission source between location 1 and 2, then, t_q, the travelling time is evaluated by:

$$t_q = \frac{s_q}{\bar{u}} \tag{6.46}$$

The time interval is expressed as:

$$\Delta t = \frac{t_{q+1} - t_q}{\kappa} \tag{6.47}$$

where Δt is the time interval, t_1 and t_2 are the start and finish times, respectively, while κ is an even number of divisions between the start and finish times, and q are equidistant locations generated from the κ-divisions. The emission rate change of the SO_2 content downwind, $(Q_s / Q^0_s)_2$, with reference to the stack emission rate, $(Q_s / Q^0_s)_1$, over the travelled time, t (h), after emission at the Elandsfontein area was estimated from equations (6.39), (6.43) and (6.44) and shown in Figure (6-2) with the deviations from the observed given in Table (6-5).

Table 6-5: Differences resulting from all three model predictions

Time (Month)	Monthly Mean Wind Speed ($m\ s^{-1}$)	Observed Mean SO_2 ($\mu g\ m^{-3}$)	SO_2 deviation ***Type-1*** **($\mu g\ m^{-3}$)**	***Type-2*****A** **($\mu g\ m^{-3}$)**	***Type-2*****B** **($\mu g\ m^{-3}$)**
January	6.88	78.82	31.53	52.82	55.99
February	5.62	103.42	34.03	72.39	82.74
March	6.22	102.11	26.36	71.48	81.69
April	6.04	100.34	36.2	80.27	90.31
May	6.66	103.02	38.12	80.36	80.87
June	6.96	134.97	49.49	99.48	106.64
July	6.04	193.03	77.21	146.6	150.6
August	8.07	119.17	31.94	95.34	95.63

September	7.14	105.04	40.9	72.42	77.73
October	7.87	99.12	41.58	64.37	74.74
November	4.35	76.89	22.83	51.52	54.62
December	7.41	68.85	27.54	46.14	48.9

6.3 Outcomes of the Dispersion Modelled with Transformations

The advection model was tested with aircraft-sampled data for sulphur in the form of sulphur dioxide at various distances downwind of the emission source up to the sampling site. Using the concentration closest to the source as a starting point, the concentrations at farther-out locations were predicted as shown in Figure (6-2).

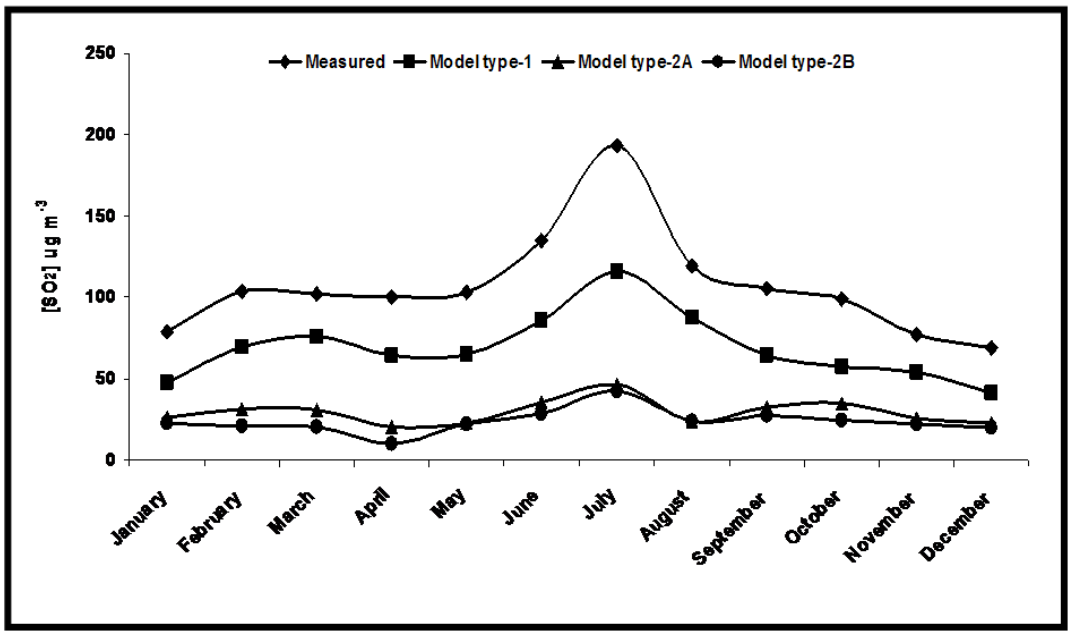

Figure 6-2: Comparison of the mean monthly SO_2 observations to the corresponding monthly predicted model outcomes

These downwind concentrations were determined using equations (6.39), (6.43) and (6.44) that define the various model patterns for changing concentration of sulphur dioxide during

advection with oxidation from a smoke stack in the PBL. A better prediction was achieved from using the *model type-1* oxidation and deposition rate constants compared to the other two models without deposition rate constant used. The *model type-1* appears to have predicted about 65 % of the average measured data, while *models type-2* and *type-3* were only able to predict the observation to about 28 % and 23 %, respectively. The mean standard deviations of the predictions from the mean observed concentrations were 14.3 with *model type-1*, 27.1 with *model type-2* and 27.2 with *model type-3*.

6.4 Conclusion

The rate of disappearance of sulphur dioxide and the formation of submicron particulate sulphate in the PBL over Elandsfontein have been predicted from mathematically developed diffusion with transformation models. The data used were ground-level sulphur concentrations at the sampling station from episodes of industrial emissions adjacent to Elandsfontein on the Mpumalanga Highveld. For reasons of comparison, the SO_2 oxidation was modelled using the reaction rate constant in a Lagrangian atmospheric diffusion puff expression under the influence of the surface meteorology. The diffusion model was developed as a time-dependent (non-steady state) expression accounting only for dry deposition as the removal mechanism during advection over Elandsfontein. The model was parametised for a wide range of meteorological variations obtainable on the Highveld. A chemical (Kinetic) sub-model was developed for the evaluation of oxidation rate constants of SO_2 disappearances and the rate was compared with results of other existing rate constants (Moller, 1980; Carmichael and Peters, 1984b).

The transformation rate sub-models were tested against two other existing overall reaction rate constants for SO_2 oxidation. The first, defined as *model type-1*, has a second order rate constant developed (in this work) mathematically while considering the deposition of SO_2 and sulphate during advection. The second, *model type-2A*, has a first order rate constant obtained from a smog chamber study and the third, *model type-2B*, has a first order rate constant obtained from a theoretically modelled overall rate via photochemical, homogeneous, aqueous and heterogeneous phase oxidation of SO_2.

The estimated conversions for the three models were 0.65 % h^{-1} for *model type-1*, 0.08 % h^{-1} for *model type-2A* and 0.25 % h^{-1} for *model type-2B* with average meteorological variables of 35.7 % relative humidity, 19.4 °C ambient temperature, 413 W m^{-2} net solar radiation and 4.7 m s^{-1} wind speed. The developed oxidation rate constant when incorporated into the diffusion model predicts transformation with advection to an accuracy of about 65 % of observed values (Table 6-2). In contrast, *models type-2* and *type-3* were only able to predict the observation to about 28 % and 23 %, respectively. The mean standard deviations of the predictions from the mean observed concentrations were 14.3 with *model type-1*, 27.1 with *model type-2* and 27.2 with *model type-3*.

Thus, it is preferable to model atmospheric SO_2 oxidation considering the reaction as a second order type, in addition to incorporation of the deposition factor during advection, because it yields a more accurate prediction when compared to those predictions that assumed a first order reaction rate with or without deposition. With the best prediction generated by *model type-1*, the kinetic properties: rate constant and activation energy obtained were 4.92 x 10^{-6} µg m^{-3} s^{-1} and 36.54 kJ kg^{-1} for summer; 3.939 x 10^{-6} µg m^{-3} s^{-1} and 43.89 kJ kg^{-1} for autumn; 2.90 x 10^{-6} µg m^{-3} s^{-1} and 115.69 kJ kg^{-1} for winter; 4.82 x 10^{-6} µg m^{-3} s^{-1} and 43.29 kJ kg^{-1} for spring, while for the year 4.29 x 10^{-6} µg m^{-3} s^{-1} and 34.31 kJ kg^{-1}.

Chapter 7: Overall Conclusion

As a part of the attainment of clean air in South Africa, in line with the air quality standards of the country, the nature and composition of the atmospheric sulphur species resulting from the industrial activities have been investigated. This study focussed on the Mpumalanga industrial Highveld region which is an integral area where most of the potentially polluting industries are located due to the nearness to the coal mines.

Over the Mpumalanga industrial Highveld subregion substantial sulphur emissions occur from anthropogenic sources. These overwhelmingly consist of emissions from industries and open-cast coal mines. These industries include coal-fired power plants, fuel refineries and iron smelting factories.

- This study has shown from a twelve-month continuous measurement of ambient concentrations and meteorological parameters the incessant presence of hydrogen sulphide, sulphur dioxide and particulate sulphate throughout the year at an average ratio of 1.3:4.6:1.0 respectively.

- Source profiles by pollution rose plots has been used to apportion source areas contributing to the sulphur loading at Elandsfontein. On an average, air pollution reaching Elandsfontein originating from the east and north-west directions predominate those from other directions.

- On an *in situ* evaluation of temporal behaviours, the diurnal variation supported by the pollution rose has shown that H_2S and SO_2 might possibly be released from a variety of sources which include surface and elevated emission sources consisting of open-cast coal mines and fugitive emissions from hydrocarbon fuel processing plants and coal-fired power plants smoke plumes. The seasonal variations suggest that levels in summer, autumn and winter were ascribed to possible rapid thermal oxidation for H_2S, while in spring high advection and convective boundary layer dispersion created the daytime trough-like concentration pattern; with stable night-

time conditions, accumulation occurs. While SO_2 level shows an indication of the contributions from boundary layer effects and photochemical process in summer and autumn and low inversion layer effects in winter and spring.

- In the lower troposphere, the concentration of particulate sulphate varies significantly for different conditions and times of the year over Elandsfontein. The variation depends predominantly on the meteorology, with long-range pollutant transport within the southern Africa subcontinent contributing occasionally to episodes of very high concentrations. However, industrial activities and meteorology are largely responsible for the concentration accumulation, distribution an removal.

- Annual average dosages of about 62 mg m^{-3} of H_2S, 216 mg m^{-3} of SO_2 and 47 mg m^{-3} of particulate sulphate traverse the study area thereby altering the atmospheric sulphur loading over Mpumalanga Highveld yearly.

- Over the four seasons of the year, the formation and or accumulation is predominant in October while the removal of sulphate occurs more in April as shown by changing meteorology over Elandsfontein.

- Information has been given on the transport pattern to and from the Elandsfontein area with seasonal variation as well as on the temporal profiles of both trace sulphur gases and particulate sulphate. This indicates that in the different seasons, particulate sulphate is removed at different rates at noticeably high concentrations within the PBL.

- Contrary to usual findings, ambient SO_2 is related to sulphate. Normally it has not been related from the view of transformation rate because of the time-lag resulting from the rate limiting step. The findings suggested that the overall mass balance of both species is equal.

- From back trajectory analysis, the contribution of aerosols from the sea and neighbouring countries to South Africa, have been shown to be insignificant to the

particulate sulphate loading at Elandsfontein when compared to those generated from local sources.

- Statistical analysis has been used to model the distribution of sulphate with meteorological parameters as the dependent variables. The model predicted the observed values to an accuracy of 86.5 % for spring, 56.4 % for summer, 66.8 % for autumn and 77.1 % for winter.

Furthermore to comprehend the reasons for the variations in the concentration with time of day and seasons in the year, a study of the favourability that certain sulphur reactions had over others, was evaluated. Thermochemical properties of known gaseous atmospheric sulphur species present over Elandsfontein, including the intermediate- and end-products of their transformation, are reported. These properties were obtained from the approximation of the Schrödinger equation (Grant and Richards, 1995; Jensen, 1999) as applied in the Gaussian 03 (G-03) model chemistry package.

- Analyses of the chemical reaction equilibrium for a variety of atmospheric sulphur transformations was used to establish the thermodynamically favourable reaction pathways over a temperature range of between -100 °C and +100 °C to consider for extremes of tropospheric temperature.

- Seven high energy accuracy model chemistries in G-03 comprising several *ab initio* methods and density functional theory (DFT) methods were applied. The methods were tested with a number of basis sets to yield values approximating those of experimental observations. Of all chosen methods, the complete basis set (CBS-Q) method was observed to most closely approximate the experimentally determined thermodynamic enthalpies and Gibbs free energies of reactions.

- The CBS-Q produced a mean absolute deviation (MAD) of 1.08 %. Equilibrium conversions obtained indicated that 90 % of the reactions are irreversible over the chosen tropospheric temperature range.

The theoretical chemistry model was able to predict the most feasible pathways taken by gaseous sulphur during oxidation. The predicted reactions were characterised in order of increasing significance of favourability between –100 °C and +100 °C. The aqueous-phase SO_2 oxidations which are enhanced by the variation in atmospheric water vapour content appeared as the dominant favourable reaction routes. Although the atmospheric reaction concentrations are often minimal, the contribution from the resulting products of the reaction to the overall ambient sulphur budget cannot be ignored.

The aqueous phase reactions dominated in the atmosphere based on the equilibrium constants of HSO_3^{2-}, $HOCH_2SO_3^-$, SO_5^- and SO_3^{2-} of aqueous-phase reactions compared to SO^* of the gas-phase reactions, but since Elandsfontein is climatologically in a region with predominantly dry conditions, products of gas-phase reactions are expected. Hence, the unique concentration distribution observed for the ambient gaseous and particulate sulphur. Therefore in the absence of measurements, it is very possible to predict the state of the atmosphere relative to the presence of the atmospheric sulphur species that are relevant to the Mpumalanga Highveld.

The resolution of the atmospheric sulphur budget in this study (which is the evaluation of the net total sulphur distribution over Elandsfontein area) depends on the combination of the chemistry and physics of the atmosphere to both the primary and secondary pollutants. For this reason the effects of sulphur oxidation during diffusion of an advecting air over the entire area was investigated.

In order to further assess the behaviour of sulphur emission interactions with the atmosphere over the Mpumalanga Highveld region, the measured data were used in mathematically derived kinetic and diffusion models. The gas-to-particle sulphur transformation was modelled for SO_2 emission from an elevated source point using a puff model expression with vertical inversion and surface absorption taken into account. Dry deposition as assumed to be the predominant removal mechanism during advection over Elandsfontein. The chemical sub-model was determined for a gas-phase SO_2-to-sulphate process based on a second order reaction rate and a first order dry deposition rate.

- The rate model generated kinetic parameters of oxidation rates, rate constants and activation energies of 10.90 % h^{-1}, 4.920 m^3 ($\mu g\ s^{-1}$) and 36.5 kJ for summer; 8.83 % h^{-1}, 3.939 m^3 ($\mu g\ s^{-1}$) and 43.9 kJ for autumn; 6.56 % h^{-1}, 2.896 m^3 ($\mu g\ s^{-1}$) and 115.7 kJ for winter and 10.80 % h^{-1}, 4.821 m^3 ($\mu g\ s^{-1}$) and 43.2 kJ for spring.

- Conversions for the three models were 0.65 % h^{-1} for *model type-1*, 0.08 % h^{-1} for *model type-2A* and 0.25 % h^{-1} for *model type-2B*.

- The developed model predicted dispersion during advection for the different seasons to about 65 % accuracy when compared to measured values, whilst, *models type-2* and *type-3* predicted about 28 % and 23 %, respectively of the observation. The kinetic properties that gave rise to the best prediction were pre-exponential constant and energy of activation, E_A/R, of 5.18 x 10^{-9} $\mu g^{-1}\ s^{-1}$ and 976K, respectively.

In this study, the source assessment, temporal-scale quantification and statistical evaluation in addition to the theoretical molecular chemistry predictions utilised computational approach to yield qualitative information on the speciation of both the reactant and product species of atmospheric sulphur expected over Elandsfontein at any given tropospheric temperature. And the developed diffusion model formulated mathematically predicted sulphur concentrations during advection significantly. Then it is most essential that the combination of the temporal scale analyses of the field measured data together with the outcomes of the thermodynamic analyses and diffusion with transformation model sufficiently disclose qualitatively (types) and quantitatively (levels), the atmospheric sulphur present over Elandsfontein. This total sulphur evaluation is only applicable to horizontal concentration distribution of the sulphur species in the along wind direction.

Recommendation for Future work

A weekly field campaign using the various qualitative and quantitative approaches for determining all the known sulphur species as well as ammonia with meteorological parameters in the different season in the year within and around the Mpumalanga Highveld is essential. The purpose of the campaign will be to provide emission inventory of the detailed speciation of all the detectable atmospheric sulphur and sulphate of ammonia (being the common alkali) over land, within the PBL over the Mpumalanga Highveld Industrial region. The data measured will be analysed to interpret the nature of emitted and evolved sulphur species as well as the dominating reaction pathway via the most dominant product observed as well as the conditions favouring such transformation. This first study would form a basis for developing the reaction and reactor or dispersion model for the proposed reactions relevant to the South African environment.

Also further works to determine the possible reaction rate constant for the most favourable reaction using the computational model chemistry approach to evaluate the enthalpies of the transition state species of the reaction. This approach will produce a value independent of any measurement pattern but from an atomic / molecular approach. Hence the value stands to be representative over any atmospheric environment.

An air craft monthly field campaign in smoke plumes at different elevations for the different season in the year within and around the Mpumalanga Highveld region is essential. The purpose of the campaign will be to measure horizontal and vertical concentration distribution with variations in meteorological parameters as a result of transformation and diffusion of sulphur dioxide and sulphate both at Elandsfontein and the boundaries of the Mpumalanga Highveld region. The data measured will be analysed in conjunction with the ground base measurements at to evaluate the emitted SO_2 from all sources in the area and evolved sulphate concentration distribution with prevailing meteorology which can be simulated in the diffusion model. In addition a comprehensive combine Lagrangian-Eulerian model can be applied to the SO_2 oxidation for the Highveld

environment, to enable one model correct the deficiencies of the other. There are most likely improvement in models when parameters are determined compared to estimated over the advection region due to the huge variations in meteorological impact rates, hence over Elansdontein the works of Zunckel and co-workers, are recommended values for seasonal dry deposition velocities.

References

Ahlberg, M. S., Leslie, A. C. D. and Winchester, J. W. (1978): Characteristics of Sulfur Aerosol in Florida as Determined by PIXE Analysis, *Atmospheric Environment*, Vol. 12, No. 1-3, pp. 773 - 777.

Air Pollution Transport Teaching Modelling, Environmental Science and Engineering, http://cities.poly.edu/environment/gradedu/ce752/ce752_airmodeling.html, Website accessed date: 14-12-2004.

Alfassi, Z. B. (Ed.) (1999): S-Centered Radicals (The Chemistry of Free Radicals), John Wiley and Sons, New York, 371p.

Alkezweeny, A. J. and Powell, D. C. (1977): Estimation of Transformation Rate of SO_2 to SO_4 from Atmospheric Concentration Data, *Atmospheric Environment*, Vol. 11, No. 2, pp. 179 - 182.

Alkorta, I. (1994): Comparison of Methods to Estimate Geometric and Electronic Properties on Sulphur Containing Compounds, *Theoretica Chimica Acta*, Vol. 89, pp. 1-12.

Allen, A. G., Harrison, R. M. and Erisman, J. W. (1989): Field Measurements of the Dissociation of Ammonium Nitrate and Ammonium Chloride Aerosols, *Atmospheric Environment*, Vol. 23, No. 7, pp. 1591 - 1599.

Amdur, M. O. (1971): Aerosols Formed by Oxidation of Sulfur dioxide, Review of Their Toxicology, *Archives of Environmental Health*, Vol. 23, pp. 459 - 468.

Annegarn, H. J., Turner, C. R., Helas, G., Tosen, G. R. and Rorich, R. P. (1996): Gaseous Pollutants. In: Air Pollution and its Impacts on the South African Highveld (Eds:

Held, G., Gore, B. J., Surridge, A. D., Tosen, G. R., Turner, C. R. and Walmsley, R. D.), *Environmental Scientific Association*, Cleveland, South Africa, pp. 25 - 33.

Armstrong, D. A. (1999): Thermochemistry of Sulfur Radicals. In: Alfassi, Z. B. (Ed.), S-Centered Radicals, John Wiley and Sons, New York, pp. 27 - 61.

Bachrach, S. M. and Mulhearn, D. C. (1996): Nucleophilic Substitution at Sulphur: S_N2 or Addition – Elimination? *Journal of Physical Chemistry*, Vol. 100, pp. 3535 - 3540.

Balmes, J. R., Fine, J. M., Gordon, T. and Sheppard, D. (1989): Potential Bronchoconstrictor Stimuli in Acid Fog, *Environmental Health Perspectives*, Vol. 79, pp. 163 - 166.

Bari, A., Ferraro, V., Wilson, L. R., Luttinger, D. and Husain, L. (2003a): Measurements of Gaseous HONO, HNO_3, SO_2, HCl, NH_3, Particulate Sulphate and $PM_{2.5}$ in New York, *Atmospheric Environment*, Vol. 37, No. 20, pp. 2825 - 2835.

Bari, A., Dutkiewicz, V. A., Judd, C. D., Wilson, L. R., Luttinger, D. and Husain, L. (2003b): Regional Sources of Particulate Sulphate, SO_2, $PM_{2.5}$, HCl, and HNO_3, in New York, *Atmospheric Environment*, Vol. 37, No. 20, pp. 2837 - 2844.

Barker and Associates (1985): Coalfields of South Africa, Johannesburg, South Africa.

Barnes, I., Bastian, V., Becker, K. H., Fink, E. H. and Nelsen, W. (1986): Oxidation of Sulphur Compounds In the Atmosphere: I. Rate Constants of OH Radical Reactions with Sulphur Dioxide, Hydrogen Sulphide, Aliphatic Thiols and Thiophenol, *Journal Atmospheric Chemistry*, Vol. 4, No. 4, pp. 445 - 466.

Bassett, M. E. and Seinfeld, J. H. (1983): Atmospheric equilibrium model of sulfate and nitrate aerosol, *Atmospheric Environment*, Vol. 17, pp. 2237 - 2252.

Bates, D. V. and Sizto, R. (1987): Air Pollution and Hospital Admissions in Southern Ontario: The Acid Summer Haze Effect, *Environmental Research*, Vol. 43, pp. 317 - 331.

Becker, S. (2004): Analysis and Modelling of Atmospheric Boundary Layer Characteristics and the Near Ground Sulphur dioxide Pollution Levels over the South African Mpumalanga Highveld, Dissertation Habilitationsarbeit am institut für Geographie, Fachbereich 07: Mathematik, Informatik, Physic und Geographie, Justus-Liebig-Universität Giessen, Germany, 283p.

Beilke, S. and Gravenhorst, G. (1978): Heterogeneous SO_2 – Oxidation in the Droplet Phase, *Atmospheric Environment*, Vol. 12, No. 1-3, pp. 231 - 239.

Benkley, C. W. and Bass, A. (1979): Development of Mesoscale Air Quality Simulation Model: Volume 3 User's Guide to MESOPUFF. EPA-600/7-80-058. U.S. Environmental Protection Agency, Atmospheric Research and Exposure Assessment Laboratory, Research Triangle Park, North Carolina.

Benkovitz, C. M., Berkowitz, C. M., Easter, R. C., Nemesure, S., Wagener, R. and Schwartz, S. E. (1994): Sulphate over the North Atlantic and Adjacent Continental Regions: Evaluation for October and November 1986 Using a Three-Dimensional Model Driven by Observation – Derived Meteorology, *Journal of Geographical Research*, Vol. 99, No. D10, pp. 20725 - 20756.

Benson, S. W. (1978): Thermochemistry and Kinetics of Sulfur-Containing Molecules and Radicals, *Chemical Review*, Vol. 78, pp. 23 - 35.

Bigg, E. K. (1980): Comparison of Aerosol at Four Baseline Atmospheric Monitoring Stations, *Journal of Applied Meteorology*, Vol. 19, pp. 521 - 533.

Blanchet, J. -P. (1995): Mechanism of Direct and Indirect Climate Forcing by Aerosols, Report of the Dahlem Workshop on Aerosol Forcing of Climate, Berlin 1994, pp. 109 - 121.

Blanchet, J. -P. and Girard, E. (1994): Arctic Greenhouse Cooling, *Nature*, Vol. 371, p. 383.

Blanchet J.-P. and List, R. (1987): On Radiative Effects of Anthropogenic Aerosol Components in Arctic Haze and Snow, *Tellus*, Vol. 39B, pp. 293 - 317.

Bocola, W. and Cirillo, M. C. (1989): Air Pollutant Emissions by Combustion Processes in Italy, *Atmospheric Environment*, Vol. 23, No. 1, pp. 17 - 24.

Bohren, C. F. (1985): Comment on "Cloud Optical Thickness Feedbacks in the CO_2 Climate Problem" by R. Somerville and L. A. Remer, *Journal of Geophysical Research*, Vol. 90, No. D3, pp. 5867 - 5867.

Bolin, B. and Rodhe, H. (1973): Note on Concepts of Age Distribution and Transit time in Natural Reservoirs, *Tellus*, Vol. 25, pp. 58 - 62.

Bouland, D., Bricard, J. and Madelaine, G. (1978): Aerosol Growth Kinetics during SO_2 Oxidation, *Atmospheric Environment*, Vol. 12, No. 1-3, pp. 171 - 177.

Breytenbach, L., Pareen, W. V., Pienaar, J. J. and Eldik, R. V. (1994): The Influence of Organic Acids and Metal Ions on the Kinetics of the Oxidation of Sulphur (IV) by Hydrogen Peroxide, *Atmospheric Environment*, Vol. 28, No. 15, pp. 2451 - 2459.

Briggs, G. A. (1969): Plume Rise, U.S. Atomic Energy Commission Division of Technical Information Pub., Tennessee, U.S.A, 81p.

Britton, L. G. and Clarke, A. G. (1980): Heterogeneous Reactions of Sulphur Dioxide and SO_2/NO_2 Mixtures with a Carbon Soot Aerosol, *Atmospheric Environment*, Vol. 14, No. 7, pp. 829 - 839.

Brosset, C. (1978): Watersoluble Sulphur Compounds in Aerosols, *Atmospheric Environment*, Vol. 12, No. 1-3, pp. 25 - 38.

Çakmak, M. and Srivastava, G. P. (1999): Ab-initio study of the adsorption of H_2S onto the Si (001) Surface, *Surface Science*, Vol. 433-435, pp. 420 - 424.

Calvert, J. G., Su, F., Bottenheim, W. J. and Strausz, O. P. (1978): Mechanism of the Homogeneous Oxidation of Sulphur Dioxide in the Troposphere, *Atmospheric Environment*, Vol. 12, No. 1-3, pp. 197 - 226.

Calvert, J. G. and Stockwell, W. R. (1983): Acid Generation in the Troposphere by Gas-Phase Chemistry, *Environmental Science and Technology*, Vol. 17, No. 9, pp. 428A - 433A.

Cant, N. W., Chambers, D. C. and Liu, I. O. Y. (2003): The Reduction of NO by CO in the Presence of Water Vapour on Supported Platinum Catalysts: Formation of Isocyanic Acid (HNCO) and Ammonia, *Applied Catalysis: Environment*, Vol. 46, No. 3, pp. 551 - 559.

Carlson, T. N. and Benjamin, S. G. (1980): Radiative Heating Rates for Saharan Dust, *Journal of Atmospheric Science*, Vol. 37, pp. 193 - 213.

Carmichael, G. R. and Peters, L. K. (1984a): An Eulerian Transport/Transformation /Removal Model for SO_2 and Sulfate-I. Model Development, *Atmospheric Environment*, Vol. 18, No. 5, pp. 937 - 951.

Carmichael, G. R. and Peters, L. K. (1984b): An Eulerian Transport/Transformation /Removal Model for SO_2 and Sulfate-II. Model Calculation of SO_x Transport in the Eastern United States, *Atmospheric Environment*, Vol. 18, No. 5, pp. 953 - 967.

Carrico, C. M., Koloutsou-Vakakis, S. and Rood, M. J. (1995): Development of an Aerosol Sampling System for Controlled Relative Humidity Light Scattering of Laboratory and Ambient Aerosols at a Northern Hemispheric Mid-Latitude Continental Site, Proceedings of the 88th Annual Meeting and Exhibition of the Air and Waste Management Association, San Antonio, Texas, June 18 - 23.

Cass, G. R. (1979): On the Relationship between Sulfate in Air Quality and Visibility with Examples in Los Angeles, *Atmospheric Environment*, Vol. 13, No. 8, pp. 1069 - 1084.

Chagger, H. K., Jones, J. M., Pourkashanian, M., Williams, A., Owen, A. and Fynes, G. (1999): Emission of Volatile Organic Compounds from Coal Combustion, *Fuel*, Vol. 78, pp. 1527 - 1538.

Chan, W. H., Vet, R. J., Lusis, M. A., Hunt, J. E. and Stevens, R. D. S. (1980): Airborne Sulfur Dioxide to Sulfate Oxidation Studies of the INCO 381M Chimney Plume, *Atmospheric Environment*, Vol. 14, No. 10, pp. 1159 - 1170.

Charlock, T. P. (1982): Cloud Optical Feedback and Climate Stability in a Radiative-Convective Model, *Tellus*, Vol. 24, pp. 245 - 254.

Charlson, R. J., Langer, J., Rodhe, H., Leovy, C. B and Warren, S. G. (1991): Perturbation of the Northern Hemisphere Radiative Balance by Backscattering from Anthropogenic Sulphate Aerosols, *Tellus*, Vol. 43A, pp. 152 - 163.

Charlson, R. J., Lovelock, J. E., Andreae, M. O. and Warren, S. G. (1987): Oceanic Phytoplankton, Atmospheric Sulphur, Cloud Albedo and Climate: A Geophysiological Feedback, *Nature*, Vol. 326, pp. 655 - 661.

Chatgilialoglu, C. and Asmus, K. -D. (1990): Sulfur-Centered Reactive Intermediates in Chemistry and Biology, Proceedings of a NATO Advanced Study Institute Series A, Life Sciences, Vol. 197, Plenum Press, New York, pp. 367 - 376.

Chatgilialoglu, C., Bertrand, M. P. and Ferreri, C. (1999): Sulfur-Centered Radicals in Organic Synthesis. In: Alfassi, Z. B. (Ed.), S-Centered Radicals, John Wiley and Sons, New York, pp. 311 - 354.

Cheng, M. -D., Hopke, P. K. and Zeng, Y. (1993a): A Receptor-Oriented Methodology for Determining Source Regions of Particulate Sulphate at Dorset, Ontario, *Journal of Geophysical Research*, Vol. 98, pp. 16839 - 16849.

Cheng, M. -D., Hopke, P. K., Barrie, L., Rippe, A., Olson, M. and Landsberger, S. (1993b): Quantitative Determination of Source Regions of Aerosol in Canadian High Arctic, *Environmental Science and Technology*, Vol. 27, pp. 2063 - 2071.

Chimka, C. T., Galloway, J. N. and Cosby, B. J. (1997): Ammonia and the Chesapeake Bay Airshed, *STAC Publication No. 97-1*, Department of Environmental Sciences, University of Virginia, U. S. A., 29p.

Chisaka, F. (1984): HC-NO_x Type Photochemical Air Pollution with Advection, *Bulletin of the Japanese Society of Mechanical Engineers*, Vol. 27, No. 228, pp. 1 - 22.

Chy'lek, P., Ramaswamy, V., Ashkin, A. and Dziedzic, J. M. (1983): Simultaneous Determination of Refractive Index and Size of Spherical Dielectric Particles from Light Scattering Data, *Applied Optics*, Vol. 22, No. 15, pp. 2302 - 2307.

Cimorelli, A. J., Perry, S. G., Venkatram, A., Weil, J. C., Paine, R. J., Wilson, R. B., Lee, R. F., Peters, W. D., Brode, R.W. and Paumier, J. O. (2004) : AERMOD: Description of Model Formulation, *US EPA Office of Air Quality Planning and Standards Emission Monitoring and Analysis Division*, North Carolina, 91p.

Cogbill, C.V and Likens, G.E. (1974): Acid Precipitation in the North-Eastern United States, *Water Resources Research*, Vol. 10, pp. 1133 - 1137.

Collins, J. and Lewis, D. (2000): Hydrogen Sulfide: Evaluation of Current California Air Quality Standards with Respect to Protection of Children Report prepared for California air resources board California office of environmental health hazard assessment September 1, California, USA.

Cox, R. A. and Sandalls, F. J. (1974): The Photo-Oxidation of Hydrogen Sulphide and Dimethyl Sulphide in Air, *Atmospheric Environment*, Vol. 8, No. 12, pp. 1269 - 1271.

CTMR (1988): National State of Environmental Report: Climate and Atmospheric Change, *Cape Town Metropolitan Report*, pp. 1 - 3.

Cullis, C. F. and Hirschler, M. M. (1980): Atmospheric Sulphur: Natural and Man-Made Sources, *Atmosphere Environment*, Vol. 14, No. 11, pp. 1263 - 1278.

Cuong, Nguyen B. A, Bonsang, B. and Lambert, G. (1974): The Atmospheric Concentration of Sulphur Dioxide and Sulphate Aerosol over Antarctic and Subantarctic areas and Oceans, *Tellus*, Vol. 26, pp. 241 - 249.

Cuong, Nguyen B. A., Bonsang, B., Lambert, G and Pasqueir, J. L. (1975): Residence Time of Sulfur Dioxide in the Marine Atmosphere, *Journal of Pure and Applied Geophysics*, Vol. 113, No. 1, pp. 489 - 500.

D'Abreton, P. C. (1996): Lagrangian Kinematic and Isentropic Trajectory Models for Aerosol and Trace Gas Transport Studies in Southern Africa, *South African Journal of Science*, 92, pp. 157 - 160.

D'Abreton, P.C., Zunckel, M. and Gondwe, P.M. (1998): Estimating Mixing Heights over Southern Africa using Surface Based Measurements, *South African Journal of Science*, Vol. 94, pp. 375 - 380.

Datez, D. and Pantel, R. H. (1974): Environmental Modelling: Analysis and Management, Dowden, Hutchinson and Ross, Pennsylvania, 407p.

Davison, G. and Hewitt, C. N. (1997): Air Pollution in the United Kingdom, the Royal Society of Chemistry, London, 147p.

Deardorff, J. W., Villis, G. E. and Stockton, G. H. (1980): Laboratory Studies of the Entrainment Zone of a Convectively Mixed Layer, *Journal of Fluid Mechanics*, Vol. 100, pp. 41 - 64.

DeBary, E. and Junge, C. E. (1963): Distribution of Sulphur and Chlorine over Europe, *Tellus*, Vol. 15, pp. 370 - 381.

Denbigh, K. (1981): The Principles of Chemical Equilibrium, 4th Edition: Cambridge University Press, Cambridge, United Kingdom, 516p.

DePuy, C. H., Grabowski, J. J., Bierbaum, V. M. (1982): Chemical Reactions of Anions in the Gas Phase, *Science*, Vol. 218, No. 4576, pp. 955 - 960.

Diab, R. D. (1975): Stability and Mixing Layer Characteristics over the South Africa, M.A. Thesis, University of Natal, Durban, South Africa, 203p.

Dickerson, R. R., Huffman, G. J., Luke, W. T., Nunnermacker, L. J., Pickering, K. E., Leslie, A. C. D., Linsay, C. G., Slinn, W. G. N., Kelly, T. J., Daum, P. H., Delany, A. C., Greenberg, J. P., Zimmerman, P. R., Boatman, J. F., Ray, J. D. and Stedman, D. H. (1987): Thunderstorms: An Important Mechanism in the Transport of Air Pollution, *Science*, Vol. 235, pp. 460 - 465.

Dittenhoefer, A. C. and de Pena, R. G. (1978): A Study of Production and Growth of Sulfate Particles in Plumes from a Coal-Fired Power Plant, *Atmospheric Environment*, Vol. 12, No. 1-3, pp. 297 - 306.

Djolov, G. D., Yordanov, D. L. and Syrakov, D. E. (1987): Modelling the-Long-Range Transport of Air Pollutants with Atmospheric Boundary Layer Chemistry, *Boundary Layer Meteorology*, Vol. 41, pp. 407 - 416.

Dlamini, S. (2005): Transboundary Transport of Pollutants from the Zambia Copperbelt over Southern Africa, M Sc Thesis, University of the Witwatersrand, Johannesburg, South Africa, 91p.

Dockery, D. W. and Pope, C. A. (1994): Acute Respiratory Effects of Particulate Air Pollution, *Annual Review of Public Health*, Vol. 15, pp. 107 - 132.

Dockery, D. W., Pope, C. A., Xu, X., Spengler, J. D., Ware, J. H., Fay, M. E., Ferris, B. G. Jr, and Speizer, F. E. (1993): An Association between Air Pollution and Mortality in Six U.S. Cities, *New England Journal of Medicine*, Vol. 329, No. 24, pp. 1753 - 1759.

Draxler, R. R. (1980): An Approved Gaussian Model for Long-Term Average Air Concentration Estimates, *Atmospheric Environment*, Vol. 14, No. 5, pp. 597 - 601.

Draxler, R. R. (1981): Forty-Eight Hour Atmospheric Dispersion Forecast at Selected Locations in the United States, *NOAA Technical Memorandum ERL ARL-100*, pp. 1 - 12.

Drewnick, F., Schwab, J. J., Hogrefe, O., Peters, S., Husain, L., Diamond, D., Weber, R. and Demerjian, K. L. (2003): Intercomparison and Evaluation of Four Semi-Continuous $PM_{2.5}$ Sulphate Instruments, *Atmospheric Environment*, Vol. 37, pp. 3335 - 3350.

Drufuca, G., Gingliano, M and Torlaschi, E. (1980): SO_2 Dosage in an Urban Area, *Atmospheric Environment*, Vol. 14, pp. 11 - 17.

Duce, R. A. and Hoffman, E. J. (1976): Chemical Fractionation at the Air/Sea Interface**,** *Annual Review of Earth and Planetary Sciences*, Vol. 4, pp. 187 - 228.

Dunbar, B. C. and Petrie, S. (2005): Magnesium Monocationic Complexes: A Theoretical Study of Metal Ion Binding Energies and Gas-Phase Associated Kinetics, *Journal of Physical Chemistry A*, Vol. 109, pp. 1411 - 1419.

Eatough, D. T., Eatough, M., Hansen, L. D., Lewis, E. A., Eatough, N. L., Gordon, J. K., Gobson, C., Conger, L., Tomlinson, E. M. and Missen, R. (1991): Apportioning of Sulphur Oxides and Canyon Lands During the Winter of 1990 Based on SAS Particle of Fluoride As Endemic Tracers of Coal Fired Power Plants Emissions, *Air and Waste Management Association*, 84th Annual Meeting and Exhibition Vancouver, British Colombia, No. 91-52.6, pp. 1 - 16.

Eatough, D. J., Caka, F. M. and Farber, R. J. (1994): The Conversion of SO_2 to Sulphate in the Atmosphere, *Israel Journal of Chemistry*, Vol. 34, pp. 301 - 314.

Edna, P. (1957): Coal in Southern Africa, University Press, University of the Witwatersrand, Johannesburg, South Africa, 24p.

Eggleton, A. E. J. (1969): The Chemical Composition of Atmospheric Aerosols on Tees-side and its Relation to Visibility, *Atmospheric Environment*, Vol. 3, pp. 355 - 372.

Eggleton, A. E. J. and Cox, R. A. (1978): Homogeneous Oxidation of Sulphur Compounds in the Atmosphere, *Atmospheric Environment*, Vol. 12, No. 1-3, pp. 227 - 230.

Eisele, F. L. and Tanner, D. J. (1991): Ion Assisted Tropospheric OH Measurement, *Journal of Geographical Research*, Vol. 96, No. D5, pp. 9295 - 9308.

Eliassen, A. (1978): The OECD Study of Long Range Transport of Air Pollutants: Long-Range Transport Modelling, *Atmospheric Environment*, Vol. 12, pp. 479 - 487.

Eliassen, A. and Saltbones, J. (1975): Decay and Transformation Rates of SO_2, as Estimated from Emission Data, Trajectories and Measured Concentrations, *Atmospheric Environment*, Vol. 9, pp. 425 - 430.

Eliassen, A. and Saltbones, J. (1983): Modelling of Long-Range Transport of Sulphur over Europe: A Two-Year Model Run and Some Model Experiments, *Atmospheric Environment*, Vol. 17, pp. 1457 - 1473.

Elliott, J. R. and Carl, T. L. (1999): Introductory Chemical Engineering Thermodynamics, 1st Edition, Published by Prentice Hall, New York, 560p.

Emberlin, J. C. (1980a): Smoke and Sulphur Dioxide in a Rural Area of Central Southern England, *Atmospheric Environment*, Vol. 14, pp. 1371 - 1380.

Emberlin, J. C. (1980b): Smoke and Sulphur Dioxide Concentrations in Relation to Topography in a Rural Area of Central Southern England, *Atmospheric Environment*, Vol. 14, pp. 1381 - 1390.

Endow, N., Doyle, G. J. and J. L. Jones (1963): The Nature of Some Model Photochemical Aerosols, *Journal of Air Pollution Control Association*, Vol. 13, pp. 141 - 147.

ENVIRON (1998): Environ International Corporation User's Guide: Comprehensive Air Quality Model with Extension (CAMx) – ver 2.00, http://www.camx.com, 251p. Website accessed date: 20-04-2005.

EPA (1974): Health Consequences of Sulfur Oxides: A Report from CHESS 1970 – 1971, Environmental Protection Agency, EPA-650/1-74-004, Research Triangle Park, North Carolina, Vol 2, pp 75 - 91.

EPA (1995a): User's Guide for the Industrial Source (ISC3) Dispersion Model. Vol. I, User instructions, EPA-454/B-95-003a, U.S. Environmental Protection Agency [NTIS PB95-222741], 320 p.

EPA (1995b): User's Guide for the Industrial Source (ISC3) Dispersion Model. Vol. II, Description of model algorithms, EPA-454/B-95-003b, U.S. Environmental Protection Agency [NTIS PB95 - 222758], 120 p.

Eriksson, E. (1963): The Yearly Circulation of Sulfur in Nature, *Journal of Geophysical Research*, Vol. 68, pp. 4001 - 4008.

Fay, J. A. and Rosenzweig, J. J. (1980): An Analytical Diffusion Model for Long Distance Transport of Air Pollutants, *Atmospheric Environment*, Vol. 14, pp. 355 - 365.

Fernandez-Martinez, G., Lopez-Mahia, P., Muniategui-Lorenzo, S., Prada-Rodriguez, D. P. and Fernandez-Fernandez, E. F. (2001): Distribution of Volatile Organic Compounds during the Combustion Process in Coal-Fired Power Stations, *Atmospheric Environment*, Vol. 35, pp. 5823 - 5831.

Ferraris, G., Fierro, G., Lo Jacono, M., Inversi, M. and Dragone, R. (2003): Catalytic Activity of Copper-Zinc Manganites for the Reduction of NO and N_2O by Hydrocarbons, *Applied Catalysis B: Environmental*, Vol. 45, No. 2, pp. 91 - 101.

Fisher, G. L., Prentice, B. A., Silberman, D., Ondov, J. M., Biermann, A. H., Ragaini, R. C. and McFarland, A. R. (1978): Physical and Morphological-Studies of Size-

Classified Coal Fly-Ash, *Environmental Science and Technology*, Vol. 12, No. 4, pp. 447 - 451.

Flyger, H., Fenger, J., Lund Thomsen, E., Lewin, E., Gryning, S. E. and Lyck, E. (1978): Conversion of Sulphur Dioxide in the Atmosphere, *Fresenius' Journal of Analytical Chemistry*, Vol. 282, No. 4, pp. 297 - 300.

Foresman, J. B. and Frisch, Æ. (1996): Exploring Chemistry with Electronic Structure Methods, 2nd Edition, Gaussian, Inc., Carnegie, Pittsburgh, USA, 302p.

Forney, L. J. and Giz, Z. G. (1980): Slow Chemical Reactions in Power Plant Plumes: Applications to Sulfates, *Atmospheric Environment*, Vol. 14, pp. 533 - 541.

Forrest, J. and Newman, L. (1977): Further Studies on the Oxidation of Sulfur Dioxide in Coal-Fired Power Plant Plumes, *Atmospheric Environment*, Vol. 11, pp. 465 - 477.

Freiberg, J. (1975): The Iron Catalyzed Oxidation of SO_2 to Sulphates Mist in Dispersing Plumes, *Atmospheric Environment*, Vol. 10, pp. 121 - 130.

Freiberg, J. (1976): The Iron Catalyzed Oxidation of SO_2 to Acid Sulphate Mist in Dispersing Plumes, *Atmospheric Environment*, Vol. 10, No. 2, pp. 121 - 130.

Freiberg, J. (1978): Conversion Limit and Characteristic Time of SO_2 Oxidation in Plumes, *Atmospheric Environment*, Vol. 12, pp. 339 - 347.

Frenzel, A. and Arnold, F. (1994): Sulfuric Acid Cluster Ion Formation by Jet Engines: Implications for Sulfuric Acid Formation and Nucleation, DLR-Mitt. 94-06, Deutsches Zentrum Für Luft-und Raumfahrt, Köln, Germany, pp. 106 - 112.

Friend, J. P. (1973): The Global Sulfur Cycle. In: S. I. Rasool (Ed.), Chemistry of the Lower Atmosphere, Plenum Press, New York, pp. 177 - 201.

Frisch, M. J., G. W. Trucks, H. B. Schlegel, G. E. Scuseria, M. A. Robb, J. R. Cheeseman, J. A. Montgomery, Jr., T. Vreven, K. N. Kudin, J. C. Burant, J. M. Millam, S. S. Iyengar, J. Tomasi, V. Barone, B. Mennucci, M. Cossi, G. Scalmani, N. Rega, G. A. Petersson, H. Nakatsuji, M. Hada, M. Ehara, K. Toyota, R. Fukuda, J. Hasegawa, M. Ishida, T. Nakajima, Y. Honda, O. Kitao, H. Nakai, M. Klene, X. Li, J. E. Knox, H. P. Hratchian, J. B. Cross, C. Adamo, J. Jaramillo, R. Gomperts, R. E. Stratmann, O. Yazyev, A. J. Austin, R. Cammi, C. Pomelli, J. W. Ochterski, P. Y. Ayala, K. Morokuma, G. A. Voth, P. Salvador, J. J. Dannenberg, V. G. Zakrzewski, S. Dapprich, A. D. Daniels, M. C. Strain, O. Farkas, D. K. Malick, A. D. Rabuck, K. Raghavachari, J. B. Foresman, J. V. Ortiz, Q. Cui, A. G. Baboul, S. Clifford, J. Cioslowski, B. B. Stefanov, G. Liu, A. Liashenko, P. Piskorz, I. Komaromi, R. L. Martin, D. J. Fox, T. Keith, M. A. Al-Laham, C. Y. Peng, A. Nanayakkara, M. Challacombe, P. M. W. Gill, B. Johnson, W. Chen, M. W. Wong, C. Gonzalez, and J. A. Pople (2004): Gaussian 03, Revision C.02,Gaussian, Inc., Wallingford CT.

Fugas, M. and Gentilizza, M. (1978): The Relationship between Sulphate and Sulphur Dioxide in the Air, *Atmospheric Environment*, Vol. 12, pp. 335 - 337.

Gabruk, R. S., Sykes, R. I., Seigneur, C., Pai, P., Gillespie, P., Bergstrom, R. W. and Saxena, P. (1999): Evaluation of the Reactive and Optical Model of Emissions (ROME), *Atmospheric Environment*, Vol. 33, pp. 383 - 399.

Galloway, J. N. and Whelpdale, D. M. (1980): An Atmospheric Sulfur Budget for Eastern North America, *Atmospheric Environment*, Vol. 14, pp. 409 - 418.

Galloway, J. N., Likens, E. G. and Edgerton, E. S. (1976): Acid Precipitation in the North-eastern United States, pH and Acidity, *Science*, Vol. 194, pp. 722 - 723.

Galvin, P. J., Samson, P. J., Peter, E. C. and Romano, D. (1978): Transport of Sulfate to

New York State, *Atmospheric Environment*, Vol. 9, pp. 643 - 659.

Garland, J. A. (1978): Dry and Wet Removal of Sulphur from the Atmosphere, *Atmospheric Environment*, Vol. 12, No. 1-3, pp. 349 - 362.

Garratt, J. R. (1992): The Atmospheric Boundary Layer, Cambridge University Press, Cambridge, 316p.

Garstang, M., Tyson, P. D., Swap, R., Edwards, M., Kallberg, P. and Lindesay, J. A. (1996): Horizontal and Vertical Transport of Air over Southern Africa, *Journal of Geophysical Research*, Vol. 101, No. D10, pp. 23721 - 23736.

Gassan-zedeh, G. Z. and Seyidbayova, S. F. (2003): The Heterogeneous Catalytic Reduction of NO and N_2O Mixture by Carbon Monoxide, *Applied Catalysis: Environment*, Vol. 42, No. 4, pp. 359 - 367.

Gayer, R. and Harris, I. (Ed.) (1996): Coalbed Methane and Coal Geology, *Geological Society*, Special Publication, London, No. 109, 344p.

Georgii, H. W. (1970): Contributions to the Atmospheric Sulfur Budget, *Journal of Geophysical Research*, Vol. 75, pp. 2365 - 2371.

Gerhard, E. R. and Johnstone, H. F. (1955): Photochemical Oxidation of Sulfur Dioxide in Air, *Industrial Engineering and Chemistry*, Vol. 47, pp. 972 - 974.

Gillani, V. N., Husar, R. B., Husar, J. D., Petterson, D. E. and Wilson Jr., W. E. (1978): Project Mistt: Kinetics of Particulate Sulphur Formation in a Power Plant Plume Out to 300 km, *Atmospheric Environment*, Vol. 12, pp. 589 - 598.

Gillani, N.V. and Wilson, W. E. (1983): Gas-to-Particle Conversion of Sulphur in Power Plant Plumes-II. Observations of Liquid-Phase Conversions, *Atmospheric Environment*, Vol. 17, No. 9, pp. 1739 - 1752.

Gillani, N.V., Colby, J. A. and Wilson, W. E. (1983): Gas-to-Particle Conversion of Sulphur in Power Plant Plumes-III. Parameterization of Plume Cloud Interactions, *Atmospheric Environment*, Vol. 17, No. 9, pp. 1753 - 1763.

Godfrey, J. J. and Clarkson, T. S. (1998): Air Quality Modelling in a Stable Polar Environment - Ross Island, Antartica, *Atmospheric Environment*, Vol. 32, No. 17, pp. 2899 - 2911.

Gordon, G. E. (1980): Receptor Models, *Environmental Science and Technology*, Vol. 14, pp. 792 - 800.

Graedel, T. E. (1979): Reduced Sulfur Emission from the Open Oceans, *Geophysical Research Letters*, Vol. 6, pp. 329 - 331.

Granat, L. (1972): On the Relationship between pH and the Chemical Composition of Atmospheric Precipitation, *Tellus*, Vol. 24, pp. 550 - 560.

Granat, L. (1978): Sulphate in Precipitation as observed by European Atmospheric Chemistry Network, *Atmospheric Environment*, Vol. 12, No. 1-3, pp. 413 - 424.

Granat, L., Rodhe, H. and Hallberg, R. U. (1976): The Global Sulfur Cycle. In: Nitrogen, Phosphorus and Sulfur-Global Cycles, B. H. Svensson and R. Soderlund, (Eds.), *Ecological Bulletins*, Stockholm, Vol. 22, pp. 89 - 134.

Grant, G. H. and Richards, W. G. (1995): Computational Chemistry, Oxford University Press, New York, 90p.

Grgic, I. and Bercic, G. (2001): A Simple Kinetic Model for Autoxidation of S(IV) Oxides Catalyzed by Iron and/or Manganese Ions, *Atmospheric Chemistry*, Vol. 39, pp. 155 - 170.

Groblicki, P. J. and Nebel, G. J. (1971): Chemical Reactions in Urban Atmospheres" [Tuesday, C. S. (Ed.)], American Elsevier, New York, 263p.

Guise-Bagley, L., Hoff, R. M., Wiebe, H. A. and Sakayama, S. (1994): The Pacific'93 Experiment: Aerosol Speciation Measurements in the Vancouver Urban Area and the Development of Hydroscopic Index. Proceedings AGU/AWMA Radiation in the Atmosphere Speciality Conference, Snowbird, Utah, pp. 429 - 436.

Hall, F. P., Duchon, C. E., Lee, L. G. and Hagan, R. R. (1975): Long-Range Transport of Air Pollution: A Case Study, August 1970, *Monthly Weather Review*, Vol. 101, pp. 404 - 411.

Hallquist, M., Stewart, D. J., Baker, J. and Cox, R. A. (2000): Hydrolysis of N_2O_5 on Submicron Sulfuric Acid Aerosols, *Journal Physical Chemistry*, Vol. 104, pp. 3984 - 3990.

Hallquist, M., Stewart, D. J., Stephenson, S. K. and Cox, R. A. (2003): Hydrolysis of N_2O_5 on Submicron Sulfate Aerosols, *Physical Chemistry Chemical Physics*, Vol. 5, No. 16, pp. 3453 - 3463.

Hanna, S. R. and Chang, J. C. (1993): Hybrid Plume Dispersion Model (HPDM), Improvements and Testing at Three Field Sites, *Atmospheric Environment*, Vol. 27A, No. 9, pp. 1491 - 1508.

Hanna, S. R. and Paine, R. J. (1987): Convective Scaling Applied to Diffusion of Buoyant Plumes from Tall Stacks, *Atmospheric Environment*, Vol. 21, No. 10, pp. 2153 - 2162.

Harrison, M. S. J. (1993): Elevated Inversion over Southern Africa: Climatological Properties and Relationships with Rainfall, *South African Geographical Journal*, Vol. 75, pp. 1 - 8.

Harrison, R. M. and McCartney, H. A. (1980): A Comparison of the Predictions of a Simple Gaussian Plume Dispersion Model with Measurements of Pollutants Concentration at Ground-level and Aloft, *Atmospheric Environment*, Vol. 14, pp. 589 - 596.

Harrison, R. M. and McKenzie, A.R. (1990): A Numerical Simulation of Kinetic Constraints upon Achievement of the Ammonium Nitrate Dissociation Equilibrium in the Troposphere, *Atmospheric Environment*, Vol. 24, pp. 91 - 102.

Harrison, R. M., Sturges, W. T., Kitto, A. -M. N. and Li, Y. (1990): Kinetics of Evaporation of Ammonium Chloride and Ammonium Nitrate Aerosols, *Atmospheric Environment*, Vol. 24, pp. 1883 - 1888.

Hegg, D. A. and Hobbs, P. V. (1980): Measurements of Gas-to-Particle Conversion in the Plumes from Five Coal-Fired Electric Power Plants, *Atmospheric Environment*, Vol. 14, No. 1, pp. 99 - 116.

Held, G., Snyman, G. M. and Scheifinger, H. (1993): Seasonal Variations and Trends of Atmospheric Particulate on the South African Highveld, *The Clean Air Journal*, Vol. 8, No. 8, pp. 4 - 11.

Held, G., Pienaar, J. J., Turner, C. R., Snyman, G. M., van Schalkwyk, B. and Osborne, J. (1994): Vertical Distribution of Pollutants in the Atmosphere over the South-Eastern Transvaal (Methods and Preliminary Results), *Proceedings of the 25th Annual Clean Air Conference of NACA*, Cape Town, 8p.

Held, G., Scheifinger, H. Synman, G. M., Tosen, G. R. and Zunckel, M. (1996): The Climatology and Meteorology of the Highveld. In: Air Pollution and its Impacts on the South African Highveld (Eds: Held, G., Gore, B. J., Surridge, A. D., Tosen, G. R., Turner, C. R. and Walmsley, R. D.), Environmental Scientific Association, Cleveland, South Africa, pp. 60 - 71.

Henmi, T. and Reiter, E. R. (1978): Regional Residence Time of Sulfur Dioxide over the Eastern United States, *Atmospheric Environment*, Vol. 12, pp. 1489 - 1495.

Herrmann, H., Ervens, B., Jacobi, H. W., Wolke, R., Nowacki, P. and Zellner, R. (2000): CAPRAM2.3: A Chemical Aqueous Phase Radical Mechanism for Tropospheric Chemistry, *Journal of Atmospheric Chemistry*, Vol. 36, pp. 231 - 284.

Hewitt, C. N. (2000): The Atmospheric Chemistry of Sulphur and Nitrogen in Power Station Plumes, *Atmospheric Environment*, Vol. 35, pp. 1155 - 1170.

Hidy, G. M., Katz, J. L. and Mirabel, P. (1978a): Sulfate Aerosol Formation and Growth in the Stratosphere, *Atmospheric Environment*, Vol. 12, pp. 887 - 892.

Hidy, G. M., Muelter, P. K. and Tong, E. Y. (1978b): Spatial and Temporal Distribution of Airborne Sulphate in Parts of the United States, *Atmospheric Environment*, Vol. 12, pp. 735 - 752.

Hirst, D. M. (1990): A Computational Approach to Chemistry, Blackwell Scientific, London, 444p.

Hobbs, P. V., Harrison, H. and Robinson, E. (1974): Atmospheric Effects of Pollutants, *Science*, Vol. 183, pp. 909 - 915.

Holtslag, A. A. M. and Van Ulden, A. P. (1983): A Simple Scheme for Daytime Estimates of the Surface Fluxes from Routine Weather Data, *Journal of Climate and Applied Meteorology*, Vol. 22, No. 4, pp. 517 - 529.

Honaganahalli, P. S. and Seiber, J. N. (2000): Measured and Predicted Airshed Concentrations of Methyl-bromide in an Agriculture Valley and Applications to Exposure Assessment, *Atmospheric Environment*, Vol. 34, pp. 3511 - 3523.

Husain, L. and Dutkiewicz, V. A. (1990): A Long-term (1975-1988) Study of Atmospheric SO_4^{2-}: Regional Contributions and Concentration Trends, *Atmospheric Environment*, Vol. 24A, pp. 1175 - 1187.

Husain, L., Webber, J. S., Canelli, E., Dutkiewicz, V. A. and Halstead, J. A. (1984): Mn/V Ratio as a Tracer of Aerosol Sulphate Transport, *Atmospheric Environment*, Vol. 18, No. 6, pp. 1059 - 1071.

Husar, R. B., Peterson, D. E., Husar, J. D., Gillani, N. V. and Wilson, W. E. (1978): Sulphur Budget of a Power Plant Plume, *Atmospheric Environment*, Vol. 12, No. 1-3, pp. 549 - 568.

Igbafe, A. I., Jewell, L. L., Piketh, S. J. and Dlamini, T. S. (2006): A Wintertime Impact of Dilution on Transformation Rate in the Planetary Boundary Layer, *Journal of Environmental Informatics*, Vol. 8, No. 1, pp. 34 – 48.

Isodesmic Reactions, http://en.wikipedia.org/wiki/Isodesmic_reaction, 2006,

Website accessed date: 20-04-2006

Jacobson, M. Z. (1997a): Development and Application of a New Air Pollution Modelling System - II: Aerosol Module Structure and Design, *Atmospheric Environment*, Vol. 31, pp. 131 - 144.

Jacobson, M. Z. (1997b): Development and Application of a New Air Pollution Modelling System - III: Aerosol-phase Simulation, *Atmospheric Environment*, Vol. 31, pp. 587 - 608.

Jensen, F. (1999): Introduction to Computational Chemistry, John Wiley and Sons, Ltd., Chichester, 429p.

John, W., Wall, S. M., Ondo, J. L. and Winklmayr, W. (1990): Modes in the Size Distribution of Atmospheric Inorganic Aerosol, *Atmospheric Environment*, Vol. 24A, pp. 2349 - 2359.

Junge, C. E. (1960): Sulphur in the Atmosphere, *Journal of Geophysical Research*, Vol. 65, pp. 227 - 237.

Junkermann, W. and Roedel, W. (1983): Evidence for Short SO_2 Lifetimes in the Atmosphere: An In-situ Measurement of Atmospheric SO_2 Lifetime Using Cosmic Ray Produced Sulphur-38, *Atmospheric Environment*, Vol. 17, No. 12, pp. 2549 - 2554.

Jury, M. R. and Tosen, G. R. (1989): Characteristics of the Winter Boundary Layer Over the African Plateau: 26 ° S, *Boundary-layer meteorology*, Vol. 48, No. 1-2, pp. 53 - 76.

Kadowaki, S. (1976): Size Distribution of Atmospheric Total Aerosols, Sulfate, Ammonium and Nitrate Particulates in the Nagoya Area, *Atmospheric Environment*, Vol. 10, pp. 39 - 43.

Karamchandani, P., Santos, L., Sykes, I., Zhang, Y., Tonne, C. and Seigneur, C. (2000): Development and Evaluation of a State-of-the-Science Reactive Plume Model, *Environmental Science and Technology*, Vol. 34, pp. 870 - 880.

Karcher, B. (1996): Aircraft-generated Aerosols and Visible Contrails, *Geophysical Research Letters*, Vol. 23, pp. 1933 - 1936.

Katsoulis, B. D. and Whelpdale, D. M. (1990): Atmospheric Sulfur and Nitrogen Budgets for Southeast Europe, *Atmospheric Environment*, Vol. 24A, pp. 2959 - 2970.

Katz, J. L. and Mirabel, P. (1974): The Generation of Aerosols by Binary Homogeneous Nucleation, *Water*, *Air and Soil Pollution*, Vol. 3, No. 4, pp. 507 - 513.

Kellogg, W. W., Cadle, R. D., Allen, E. R., Lazrus, A. L. and Martell, E. A. (1972): The Sulphur Cycle, *Science*, Vol. 175, pp. 587 - 596.

Khachatryan, L., Asatryan, R. and Dellinger, B. (2004): An Elementary Reaction Kinetic Model of the Gas-Phase Formation of Polychlorinated Dibenzofurans from Chlorinated Phenols, *Journal of Physical Chemistry A*, Vol. 108, pp. 9567 - 9572.

Kim, Y. P., Seinfeld, J. H. and Saxena, P. (1993a): Atmospheric Gas-Aerosol Equilibrium I. Thermodynamic Model, *Aerosol Science and Technology*, Vol. 19, pp. 157 - 181.

Kim, Y. P., Seinfeld, J. H. and Saxena, P. (1993b): Atmospheric Gas-Aerosol Equilibrium II. Analysis of Common Approximations and Activity Coefficient Calculation Methods, *Aerosol Science and Technology*, Vol. 19, pp. 182 - 198.

Kitagawa, T. (1984): Cause Analysis of the Yokkaichi Asthma Episode in Japan, *Journal of the Air Pollution Control Association*, Vol. 34, No. 7, pp. 743 - 746.

Koch, E. (1977): Non-Isothermal Reaction Analysis, Academic Press Inc, London, 500p.

Koenig, J. Q., Larson, T. V., Hanley, Q. S., Rebbolledo, V., Dumler, K., Checkoway, H., Wang, S. -Z., Lin, D. and Pierson, W. E. (1993): Pulmonary Function Changes in Children Associated with Particulate Matter, *Environmental Research*, Vol. 63, pp. 26 - 38.

Korhonen, H., Napari, I., Timmreck, C., Vehkamäki, H., Pirjola, L., Lehtinen, K. E. J., Lauri, A. and Kulmala, M. (2003): Heterogeneous Nucleation as a Potential Sulphate-Coated Mechanism of Atmospheric Mineral Dust Particles and Implications of Coated Dust on New Particle Formation, *Journal of Geophysical Research*, Vol. 108, No. D17, pp. 4546 - 4554.

Lagrange, J., Pallares, G., Wenger, G. and Lagrange, P. (1993): Electrolyte Effects on Aqueous Atmospheric Oxidation of Sulphur Dioxide by Hydrogen Peroxide. *Atmospheric Environment*, Vol. 27A, pp. 129–137.

Larsen, A. G., Holm, A. H., Roberson, M. and Daasbjerg, K. (2001): Substituent Effects on the Oxidation and Reduction Potentials of Phenylthiyl Radicals in Acetonitrile, *Journal of the American Chemical Society*, Vol. 123, pp. 1723 - 1729.

Latimer, D. A. and Samuelsen, G. S. (1978): Visual Impact of Plumes from Power Plants: A Theoretical Model, *Atmospheric Environment*, Vol. 12, pp. 1455 - 1465.

Leahey, D. M. (1974): A Study of Air Flow over Irregular Terrain, *Atmospheric Environment*, Vol. 8, pp. 738 - 791.

Lee, D. S. and Kingdon, R. D. (2001): Modelling Long-Term Trends in UK Sulphur Deposition, *Physical Chemistry: Earth. B*, Vol. 26, No. 10, pp. 813 - 817.

Lestari, P., Oskouie, A. K. and Noll, K. E. (2003): Size Distribution and Dry Deposition of Particulate Mass, Sulfate and Nitrate in an Urban Area, *Atmospheric Environment*, Vol. 37, No. 18, pp. 2507 - 2516.

Levenspiel, O. (1999): Chemical Reaction Engineering, 3rd Edition, John Wiley and Sons, New York, 668p.

Lias, S., Karpas, Z., Liebman, J. (1985): Halomethylenes: Effects of Halogen Substitution on Absolute Heats of Formation, *Journal of the American Chemical Society*, Vol. 107, pp. 6089 - 6096.

Liberti, A., Brocco, D. and M. Possanzini (1978): Adsorption and Oxidation of Sulfur Dioxide on Particles, *Atmospheric Environment*, Vol. 12, pp. 255 - 261.

Lide, D. R. [Ed.] (2002): CRC Handbook of Chemistry and Physics, 82nd Edition, Chemical Rubber Co. Press, Florida, 2514p.

Likens, G. E. (1976): Acid Precipitation, *Chemical Engineering News*, November 22, pp. 44 - 99.

Likens, G. E., Bormann, F. H., Pierce, R. S., Eaton, J. S. and Munn, R. E. (1984): Long-Term Trends in Precipitation Chemistry at Hubbard Brook, New Hampshire, *Atmospheric Environment*, Vol. 18, pp. 2641 - 2647.

Linder, P. D., Duan, X. and Page, M. (1995): Ab-initio Variational Transition State Theory Calculations for the $H + NH_2 \leftrightarrow H_2 + NH$ Hydrogen Abstraction Reaction on the Triplet Potential Energy Surface, *Journal of Physical Chemistry*, Vol. 99, pp. 11458 - 11463.

Lovelock, J. E., Maggs, R. J. and Rasmussen, R. A. (1972): Atmospheric Dimethylsulfide and the Global Sulfur Cycle, *Nature*, Vol. 237, pp. 452 - 453.

Lucas, D. H. (1975): The Effect of Emission Height in Very Large Areas of Emission, *Atmospheric Environment*, Vol. 9, pp. 607 - 622.

Lundgren, D. A. (1970): Atmospheric Aerosol Composition and Concentration as a Function of Particle Size and of Time, *Journal of Air Pollution Control Association*, Vol. 20, pp. 603 - 608.

Lurmann, F. W., Wexler, A. S., Pandis, S. N., Musarra, S. P., Kumar, N. and Seinfeld, J. H. (1997): Modelling Urban and Regional Aerosols - II. Application to California's South Coast Air Basin, *Atmospheric Environment*, Vol. 31, pp. 2695 – 2715.

Lusis, M. A. and Phillips, C. R. (1977): The Oxidation of SO_2 to Sulphates in Dispersing Plumes, *Atmospheric Environment*, Vol. 11, No. 3, pp. 239 - 241.

Macias, E. S., Wicker, J. O. and White, W. H. (1981): Regional Haze Case Studies in the South-western U.S. - II. Source Contributions, *Atmospheric Environment*, Vol. 15, pp. 1987 - 1997.

Mage, D., Ozolins, G., Peterson, P., Webster, A., Orthofer, R., Vandeweerd, V. and Gwynne, M. (1996): Urban Air Pollution in Megacities of the World, *Atmospheric Environment*, Vol. 30, No. 5, pp. 681- 686.

Malm, W. C., Sisler, J. F., Huffman, D., Eldred, R. A and Cahill, T. A. (1994): Spatial and Seasonal Trends in Particle Concentration and Optical Extinction in the United States, *Journal of Geophysical Research*, Vol. 99, No. D1, pp. 1347 - 1370.

Manahan, S. E. (1991): Environmental Chemistry, 5th Edition, Lewis Pub. Michigan, 583p.

Markham, G. D. and Bock, C. W. (1993): Structural and Thermodynamic Properties of Sulfonium Ions - An Ab-initio Molecular Orbital Study, *Journal Physical Chemistry*, Vol. 97, pp. 5562 - 5569.

Martin, A. and Barber, F. R. (1981): Sulphur Dioxide, Oxides of Nitrogen and Ozone, Measured Continuously for 2 Years at a Rural Site, *Atmospheric Environment*, Vol. 15, pp. 567 - 578.

Martin, L. R. and Damschen, D. E. (1981): Aqueous Oxidation of Sulfur Dioxide by Hydrogen Peroxides at Low pH, *Atmospheric Environment*, Vol. 9, pp. 1615 - 1621.

Maul, P. R., Barber, F. R. and Martin, A. (1980): Some Observations of the Mesoscale Transport of Sulphur Compounds in the Rural East Midlands, *Atmospheric Environment*, Vol. 14, pp. 339 - 354.

Maulitz, A. H., Boese, R. and Kuhn, N. (1995): Ab-initio Studies on Halosulphite Ions, *Journal of Molecular Structure (Theochem)*, Vol. 333, pp. 227 - 232.

Mayer, H. (1999): Air Pollution in Cities, *Atmospheric Environment*, Vol. 33, pp. 4029 - 4037.

McArdle, J. V. and Hoffmann, M. R. (1983): Kinetics and Mechanism of the Oxidation of Aquated Sulfur Dioxide by Hydrogen Peroxide at Low pH, *Journal of Physical Chemistry*, Vol. 87, pp. 5425 - 5429.

McCracken, M. C., Cess, R. D. and Potter, G. L. (1986): Climatic Effects of Anthropogenic Arctic Aerosols: An Illustration of Climatic Feedback Mechanisms with One- and Two-Dimensional Climate Models, *Journal of Geophysical Research*, Vol. 91, pp. 14450 - 14455.

McGonigle, A. J. S., Thomson, C. L., Tsanev, V. I. and Oppenheimer, C. (2004): A Simple Technique for Measuring Power Station SO_2 and NO_2 Emissions, *Atmospheric Environment*, Vol. 38, pp. 21 - 25.

McJilton, E. E., Frank, N. T. and Charlston, R. (1973): Role of Relative Humidity in the Synergistic Effect of a Sulfur Dioxide-Aerosol Mixture in the Lung, *Science*, Vol. 82, pp. 503 - 504.

McKee, M. (1996): Computational Study of the Mono- and Dianions of SO_2, SO_3, SO_4, S_2O_3, S_2O_4, S_2O_6, S_2O_8, *Journal of Physical Chemistry*, Vol. 100, pp. 3473 - 3481.

McMurry, P. H. and Friedlander, S. K. (1978): Aerosol Formation in Reacting Gases: Relation of Surface Area to Rate of Gas-to-Particle Conversion, *Journal of Colloidal and Interface Science*, Vol. 64, No. 2, pp. 248 - 257.

McMurry, P. H. and Stolzenburg, M. R. (1989): On the Sensitivity of Particle Size to Relative Humidity for Los Angeles Aerosols, *Atmospheric Environment*, Vol. 23, pp. 497 - 507.

Mdluli, T. (2007): Indoor household evaluation for PM_7, PhD Thesis, University of the Witwatersrand, Johannesburg, South Africa.

Meagher, J. F., Bailey, E. M. and Luria, M. (1983): The Seasonal Variation of the Atmospheric SO_2 to SO_4 Conversion Rate, *Journal of Geophysical Research*, Vol. 15, pp. 567 - 578.

Meetham, A. R. (1950): Natural Removal of Pollution from the Atmosphere, *Quarterly Journal of the Royal Meteorological Society*, Vol. 76, pp. 359 - 371.

Meng, Z. and Seinfeld, J. H. (1996): Time Scales to Achieve Atmospheric Gas-Aerosol Equilibrium for Volatile Species, *Atmospheric Environment*, Vol. 30, pp. 2889 - 2900.

Miller, D. F. (1978): Precursor Effects on SO_2 Oxidation, *Atmospheric Environment*, Vol. 12, No. (1-3), pp. 273 - 280.

Moller, D. (1980): Kinetic Model of Atmospheric SO_2 Oxidation Based on Published Data, *Atmospheric Environment*, Vol. 14, pp. 1067 - 1076.

Montgomery, J. A. Jr., Ochterski, J. W. and Petersson, G. A. (1994): A Complete Basis Set Model Chemistry, IV. An Improved Atomic Pair Natural Orbital Method, *Journal of Chemical Physics*, Vol. 101, pp. 5900 - 5909.

Morgan, N. H., Linnert, H. V. and Riveros, J. M. (1995): Experimental and Theoretical Characterisation of the Gas Phase NSO_2^- Ion, *Journal of Physical Chemistry*, Vol. 99, pp. 11667 - 11672.

Morgan, N. H., Linnert, H. V., de Souza, L. A. G. and Riveros, J. M. (1997): Gas-Phase Nucleophilic Reactions in SO_2F_2: Experiment and Theory, *Chemical Physics Letters*, Vol. 275, No. (5–6), pp. 457 - 462.

Nenes, A., Pandis, S. N. and Pilinis, C. (1999): Continued Development and Testing of a New Thermodynamic Aerosol Module for Urban and Regional Air Quality Models, *Atmospheric Environment*, Vol. 33, pp. 1553 - 1560.

Newman, L. (1981): Atmospheric Oxidation of Sulfur Dioxide: A Review as Viewed from Power Plant and Smelter Plume Studies, *Atmospheric Environment*, Vol. 15, No. 10 - 11, pp. 2231 - 2239.

Newman, L., Forrest, J. and Manowitz, B. (1975a): The Application of an Isotopic Ratio Technique to a Study of the Atmospheric Oxidation of Sulphur Dioxide in the Plume from an Oil-Fired Power Plant, *Atmospheric Environment*, Vol. 9, No. 10, pp. 959 - 968.

Newman, L., Forrest, J. and Manowitz, B. (1975b): The Application of an Isotopic Ratio Technique to A Study of the Atmospheric Oxidation of Sulphur Dioxide in the Plume from a Coal-Fired Power Plant, *Atmospheric Environment*, Vol. 9, No. 10, pp. 969 - 977.

Nguyen, B. C., Bonsang, B. and Gaudry, A. (1983): The Role of the Ocean in the Global Atmospheric Sulfur Cycle, *Journal of Geophysical Research*, Vol. 88, pp. 10903 - 10914.

Niki, H., Maker, P. D., Savage, C. M. and Breitenbach, L. P. (1983): An FTIR Study of the Mechanism for the Reaction HO + CH_3SCH_3, *International Journal of Chemical Kinetics*, Vol. 15, No. 7, pp. 647 - 654.

Norris, G., YoungPong, S. N., Koenig, J. Q., Larson, T. V., Sheppard, L. and Stout, J. W. (1999): An Association between Fine Particles and Asthma Emergency

Department Visits for Children in Seattle, *Environmental Health Perspectives*, Vol. 107, No. 6, pp. 489 - 493.

Nyden, M. R. and Petersson, G. A. (1981): Complete Basis Set Correlation Energies, I. The Asymptotic Convergence of Pair Natural Orbital Expansions, *Journal of Chemical Physics*, Vol. 75, pp. 1843 - 1862.

Ochterski, J. W., Petersson, G. A. and Montgomery Jr., J. A. (1996): Complete Basis Set Model Chemistry, V. Extensions to Six or More Heavy Atoms, *Journal of Chemical Physics*, Vol. 104, pp. 2598 - 2619.

Oke, T. R. (1987): Boundary Layer Climates, 2nd Edition, Methuen and Co. Inc, New York, 435p.

Omstedt, G. and Rodhe, H. (1978): Transformation and Removal Processes for Sulphur Compounds in the Atmosphere as Described by a One-Dimensional Time-Dependent Diffusion Model, *Atmospheric Environment*, Vol. 12, pp. 503 - 509.

Ott, W. R. (1995): Environmental Statistics and Data Analysis, 1st Edition, Lewis Pub. CRC Press Inc, Florida, 435p.

Paltridge, G. W. (1980): Cloud-radiation Feedback to Climate, *Quarterly Journal of the Royal Meteorological Society*, Vol. 106, No. 450, pp. 895 - 899.

Pandis, S. N., Harley, R. A., Cass, G. R. and Seinfeld, J. H. (1992): Secondary Organic Aerosol Formation and Transport, *Atmospheric Environment*, Vol. 26A, No. 13, pp. 2269 - 2282.

Panofsky, H. A. and Dutton, J. A. (1984): Atmospheric Turbulence: Models and Methods for Engineering Applications, John Wiley and Sons, New York, 417p.

Parthiban, S., Lee, T. J., Guha, S. and Francisco, J. S. (2003): Theoretical Study of Chlorine Nitrates: Implications for Stratospheric Chlorine Chemistry, *Journal of the American Chemical Society*, Vol. 125, pp. 10446 - 10458.

Pasquill, F. (1974): Atmospheric Diffusion, 2nd Edition, John Wiley and Sons, New York, 429p.

Patil, G. P. and Rao, C. R. (1993): Multivariate Environmental Statistics, Volume 12, North- Holland, Amsterdam.

Patil, G. P. and Rao, C. R. [Eds.] (1994): Handbook of Statistics, Volume 12, North-Holland, Amsterdam.

Perry, R. H. and Green, D. W. (1998): Perry's Chemical Engineer's Handbook, McGraw Hill Book Co. International Edition, 7th Edition, Singapore.

Perry, S. G. (1992): A Dispersion Model for Sources near Complex Topography. Part I: Technical Formulations, *Journal of Applied Meteorology*, Vol. 31, No. 7, pp. 633 – 645.

Petersson, G. A. and Al-Laham, M. A. (1991): A Complete Basis Set Model Chemistry, II. Open-Shell Systems and the Total Energies of the First-Row Atoms, *Journal of Chemical Physics*, Vol. 94, pp. 6081 - 6090.

Petersson, G. A., Tensfeldt, T. G. and Montgomery Jr., J. A. (1991): A Complete Basis Set Model Chemistry, III. The Complete Basis Set-Quadratic Configuration Interaction Family of Methods, *Journal of Chemical Physics*, Vol. 94, pp. 6091 - 6101.

Pienaar, J. J. and Helas, G. (1996): The Kinetics of Chemical Processes Affecting Acidity in the Atmosphere, *South African Journal of Science*, Vol. 92, pp. 128 - 132.

Piketh, S. J., Annegarn, H. J. and Tyson, P. D. (1999): Lower Tropospheric Aerosol Loadings over South Africa: The Relative Contribution of Aeolian Dust, Industrial Emissions and Biomass Burning, *Journal of Geophysical Research*, Vol. 104, No. D1, pp. 1597 - 1607.

Piketh, S. J. (2000): Transport of Aerosol and Trace Gases over Southern Africa, PhD Thesis, University of the Witwatersrand, Johannesburg, South Africa, 158p.

Pilinis, C. and Seinfeld, J. H. (1987): Continued Development of a General Equilibrium Model for Inorganic Multicomponent Atmospheric Aerosols, *Atmospheric Environment*, Vol. 21, No. 11, pp. 2453 - 2466.

Pilinis, C., Seinfeld, J. H. and Grosjean, D. (1989): Water Content of Atmospheric Aerosols, *Atmospheric Environment*, Vol. 23, pp. 1601 - 1606.

Platt, U. (1978): Dry Deposition of SO_2, *Atmospheric Environment*, Vol. 23, No. 1-3, pp. 363 - 367.

Podkrajsek, B., Bercic, G., Tursic, J. and Grgic, I. (2004): Aqueous Oxidation of Sulphur (IV) Catalyzed by Manganese (II): A Generalized Simple Kinetic Model, *Journal of Atmospheric Chemistry*, Vol. 47, pp. 287 - 303.

Pope, C. A., Burnett R. T., Thun, M. J., Calle, E. E., Krewski, D., Ito, K., Thurston, G. D. (2002): Lung Cancer, Cardiopulmonary Mortality, and Long-Term Exposure to Fine Particulate Air Pollution. *Journal of the American Medical Association*, Vol. 287, No. 9, pp. 1132 - 1141.

Prager, M. J., Stephens E. R. and Scott, W. E. (1960): Aerosol Formation from Gaseous Air Pollutants, *Industrial Engineering and Chemistry*, Vol. 52, pp. 521 - 524.

Prahm, L. P., Conradson, K. and Nielsen, L. B. (1980): Regional Source Quantification Model for Sulphur Oxides in Europe, *Atmospheric Environment*, Vol. 14, pp. 1027 - 1054.

Prather, M., Sausen, R., Grossman, A. S., Haywood, J. M., Rind, D., Subbaraya, Forster, P., Jain, A., Ponater, M., Schumann, U., Wang, W. -C., Wigley, T. M. L., and Wuebbles, D. J., (1999): Potential climate change from aviation. (1999) In: Penner, J., Lister, D., Griggs, D., Dokken, D. and McFarland, M. (Eds.), Aviation and the Global Atmosphere, IPCC [Intergovernmental Panel of Climate Change] (1999) Cambridge University Press, Cambridge, United Kingdom, pp. 185–215.

Pretorius, R. W., Auret, I., Held, G., Brassel, K. M., Dandord, I. R. and Waldie, D. D. (1986): The Climatology of the Boundary Layer in the Eastern Transvaal Highveld and Its Impact on Sulphur Dioxide Concentrations at Ground Level, *CSIR Report*, ATMOS/86/16, Pretoria, pp. 1 - 202.

Preston-Whyte, R. A. and Tyson, P. D. (1993): The Atmosphere and Weather of Southern Africa, Oxford University Press, Cape Town, 374p.

Priest, P., Navarre, J. L. and Ronneau, C. (1981): Elemental Background Concentration in the Atmosphere of an Industrialized Country**,** *Atmospheric Environment*, Vol. 15, No. 7, pp. 1325 - 1330.

Ragland, D. W. and Wilkening, D. E. (1982): Relationship between Mesoscale Acid Precipitation and Meteorological Factors, In: Acid Precipitation Effects on Ecological Systems, D'ltri, R. M. (Ed.), Ann Arbor Science, Ann Arbor, Michigan, pp. 123 - 141.

Rahn, K. A. and Lowenthal, D. H. (1984): Elemental Tracers of Distant Regional Pollution Aerosols, *Science*, Vol. 223, No. 4632, pp. 132 - 139.

Reiner, T. and Arnold, F. (1993): Laboratory Flow Reactor Measurements of the Reaction $SO_3 + H_2O + M \rightarrow H_2SO_4 + M$: Implications for Gaseous H_2SO_4 and Aerosol

Formation in the Plume of a Jet Aircraft, *Geophysical Research Letters*, Vol. 20, pp. 2659 - 2662.

Reiner, T. and Arnold, F. (1994): Laboratory Investigations of Gaseous Sulphuric Acid Formation via $SO_3 + H_2O + M \rightarrow H_2SO_4 + M$: Measurements of the Rate Constant and Product Identification, *Journal of Chemical Physics*, Vol. 101, pp. 7399 - 7407.

Robinson, E. and Robbins, R. C. (1970): Gaseous Sulfur Pollutants from Urban and Natural Sources, *Journal of Air Pollution Control Association*, Vol. 20, pp. 233 - 235.

Rodhe, H. (1970): On the Residence Time of Anthropogenic Sulphur in the Atmosphere, *Tellus*, Vol. 22, pp. 137 - 139.

Rodhe, H. (1978): Budgets and Turn-Over Times of Atmospheric Sulphur Compounds, *Atmospheric Environment*, Vol. 12, pp. 671 - 680.

Roedel, W. and Junkermann, W. (1978): High Volume Sampling of SO_2 for Isotopic Studies by Gas Absorption in Small Droplets, *Atmospheric Environment*, Vol. 12, No. 12, pp. 2399 - 2402.

Roessler, J. F., Stevenson, H. J. R. and Nader, J. S. (1965): Size Distribution of Sulphate Aerosols in the Ambient Air, *Journal of Air Pollution Control Association*, Vol. 15, pp. 576 - 579.

Ronneau, C. and Snappe-Jacob, N. (1978): Atmospheric Transport and Transformation Rate of Sulphur Dioxide, *Atmospheric Environment*, Vol. 12, No. 6 - 7, pp. 1517 – 1521.

Ross, K. (2003): Aerosol-Cloud Interactions over Southern Africa, PhD Thesis, University of the Witwatersrand, Johannesburg, South Africa, 184p.

RSA (2005): National Environment Management: Air Quality Act, No. 39 of 2004. *Republic of South Africa Government Gazette*, Vol. 476, No. 27318, 24 February 2004, Cape Town, .

Rupprecht and Patashnick (2001): Series 8400S Ambient Particulate Sulphate Monitor-Operations Manual, Revision A, R&P Part Number 42-007039, Rupprecht and Patashnick Co., Inc. Albany, New York, 340p.

Sampson, P. J. (1980): Trajectory Analysis of Summertime Sulfate Concentrations in the Northeastern United States, *Journal of Applied Meteorology*, Vol. 19, pp. 1382 - 1394.

Samson, P. J. and Ragland, K. W. (1977): Ozone and Visibility Reduction in the Midwest: Evidence for Large-Scale Transport, *Journal of Applied Meteorology*, Vol. 16, No. 10, pp. 1101 - 1106.

Santos, C. Y. M., Azevedo, D. A. and Aquino Neto, F. R. (2004): Atmospheric Distribution of Organic Compounds from Urban Areas Near a Coal-Fired Power Station, *Atmospheric Environment*, Vol. 38, pp. 1247 - 1257.

Sapse, A. M. and Jain, D. C. (1985): *Ab initio* studies of $F^-(H_2O)_n$ and $Cl^-(H_2O)_n$ clusters for n = 1, 2, *International Journal of Quantum Chemistry*, Vol. 27, No. 33, pp. 281 - 292.

Satterfield, C. N. (1991): Heterogeneous Catalysis in Industrial Practice, 2nd Edition, Prentice Hall Inc., New York, 554p.

Scheifinger, H. and Held, G. (1997): Aerosol Behaviour on the South African Highveld, *Atmospheric Environment*, Vol. 31, No. 21, pp. 3497 - 3509.

Schiesser, C. H. and Smart, B. A. (1995): An *Ab Initio* Study of Some Free-Radical Homolytic Substitution Reactions at Sulphur, Selenium and Tellurium, *Tetrahedron*, Vol. 51, No. 21, pp. 6051 - 6060.

Schreiner, P. R., Schleyer, P. v. R. and Hill, R. K. (1993): Reinvestigation of the S_N1 Reaction: The Ionization of Chlorosulfites, *Journal Organic Chemistry*, Vol. 58, pp. 2822 - 2829.

Scire, J. S., Robe, F. R., Fernau, M. E. and Yamartino, R. J. (2000a): A User's Guide for the CALMET Meteorological Model (Version 5), Earth Tech. Inc., U.S.A. http://www.src.com/verio/download/download.htm, 2005

Website accessed date: 20-04-2005.

Scire, J. S., Strimaitis, D. G. and Yamartino, R. J. (2000b): A User's Guide for the CALPUFF Dipsersion Model (Version 5), Earth Tech. Inc., U.S.A.

http://www.src.com/verio/download/download.htm, 2005.

Website accessed date: 20-04-2005

Scorgie, Y. (1999): Development of a Methodological Framework and Supporting Data Base for Air Pollution Impact Scoping in South Africa Industrial Planning, Dissertation, University of the Witwatersrand, Johannesburg, South Africa, 180p.

Scorgie, Y., Annegarn, H. and Randell, L. (2003): Final Report on the Air Quality Management Plan for the City of Johannesburg, No. MTX/03/JHB-01d, by Department of Development Planning, Transportation and Environment and the Department of Environmental Health, City of Johannesburg.

Scriven, R. A. and Fisher, B. E. A. (1975): The Long Range Transport of Airborne Material and Its Removal by Deposition and Washout-I. General Considerations, *Atmospheric Environment*, Vol. 9, No. 1, pp. 49 - 68.

Sehmel, G. A. (1980): Particle and Gas Dry Deposition: A Review, *Atmospheric Environment*, Vol. 14, pp. 983 - 1011.

Seigneur, C., Wu, X. A., Constantinou, E., Gillespie, P., Bergstom, R. E., Sykes, I., Venkatram, A. and Karamchandani, P. (1997): Formulation of a Second-Generation Reactive Plume and Visibility Model, *Journal of Air and Waste Management Association*, Vol. 47, pp. 176 - 184.

Seinfeld, J. H. (1986): Atmospheric Chemistry and Physics of Air Pollution, Wiley, New York, 738p.

Seinfeld, J. H. and Pandis, S. N. (1998): Atmospheric Chemistry and Physics: From Air Pollution to Climate Change, Wiley Interscience, New York, 1326p.

Sharpe, R. R., Schomberg, H. H., Harper, L. A., Endale, D. M., Jenkins, M. B. and Franzluebbers, A. J. (2004): Ammonia Volatilization from Surface-Applied Poultry Litter under Conservation Tillage Management Practices, *Journal of Environmental Quality*, Vol. 33, pp. 1183 - 1188.

Shaw, M. A. and Rood, M. J. (1990): Measurement of the Crystallization Humidities of Ambient Aerosol Particles, *Atmospheric Environment*, Vol. 21, pp. 1837 - 1841.

Shaw Jr., R. W. and Paur, R. J. (1983): Measurement of Sulfur in Gases and Particles during Sixteen Months in the Ohio River Valley, *Atmospheric Environment*, Vol. 17, No. 8, pp. 1431 - 1438.

Shaw Jr., R. W., Binkowski, F. S. and Courtney, W. J. (1982): Aerosols of High Chlorine Concentration Transported into Central and Eastern United States, *Nature*, Vol. 296, pp. 229 - 231.

Shir, C. C. and Shieh, L. J. (1978): Study of Parametric Effects on the SO_2 Concentration in St. Louis by a Numerical Simulation, *Atmospheric Environment*, Vol. 12, pp. 1087 - 1095.

Smith, F. B. and Jeffery, G. H. (1975): Airborne Transport of Sulphur Dioxide from the UK, *Atmospheric Environment*, Vol. 9, pp. 643 - 659.

Smith, J. M., Van Ness, H. C. and Abbott, M. M. (2004): Introduction to Chemical Engineering Thermodynamics, 7th Edition, McGraw Hill Co. Inc., New York, 848p.

Snyman, G. M., Held, G. and Brassel, K. M. (1990): Vertical Profiles of Particulates on the South Africa Highveld, *1st IUAPPA Regional Conference on Air Pollution Towards the 21st Century Implications*, *Challenges*, *Options and Solutions*, Vol. 1, No. 52, pp. 1 - 17.

Somerville, R. C. and Remer, L. A. (1984): Cloud Optical Thickness Feedbacks in the CO_2 Climate Problem, *Journal of Geophysical Research*, Vol. 89, No. D6, pp. 9668 - 9672.

Somnitz, H., Gleitsmann, G. and Zellner, R. (2003): Novel Rates of OH induced Sulphur Oxidation: Implications to the Plume Chemistry of Jet Aircraft, *AAC-Conference Proceedings*, *Friedrichshafen*, *Germany*, pp. 19 - 24.

Sorokin, A., Katragkon, E., Arnold, F., Busen, R. and Schumann, U. (2004): Gaseous SO_3 and H_2SO_4 in the Exhaust of an Aircraft Gas Turbine Engine: Measurements by CIMS and Implications for Fuel Sulfur Conversion to Sulfur (IV) and Conversion of SO_3 to H_2SO_4, *Atmospheric Environment*, Vol. 38, pp. 449 - 456.

Spengler, J. D., Brauer, M. and Koutrakis, P. (1990): Acid Air and Health, *Environmental Science and Technology*, Vol. 24, pp. 946 - 956.

Stern, A. C., Wohlers, H. C., Boubel, R. W. and Lowry, W. P. (1973): Fundamental of Air Pollution, Academic Press, New York.

Steven, R. K., Dzubay, T. G., Lewis, C. W. and Shaw Jr., R. W. (1984): Source Apportionment Methods Applied to the Determination of the Origin of Ambient Aerosols that Affect Visibility in Forested Areas, *Atmospheric Environment*, Vol. 18, No. 2, pp. 261 - 272.

Stockwell, W. R. (1986): A Homogeneous Gas Phase Mechanism for Use in a Regional Acid Deposition Model, *Atmospheric Environment*, Vol. 20, No. 8, pp. 1615 - 1632.

Stohl, A. (1998): Computation Accuracy and Applications of Trajectories – A Review and Bibliography, *Atmospheric Environment*, Vol. 32, pp 947 - 966.

Stolzenburg, M. R. and Hering, S. V. (2000): A New Method for the Automated Measurement of Atmospheric Fine Particle Nitrate, *Environmental Science and Technology*, Vol. 34, pp. 907 - 914.

Strimaitis, D. G., Yamartino, R. J., Insley, E. M. and Scire, J. S. (1995): A User's Guide for the Kinematic Simulation Particle (KSP) Model, Prepared for Institut fuer Meteorologie, Freie Universitaet Berlin, Germany, and Umwelbundesamt, Berlin, Germany, Document No. 1274-2, by Earth Tech Inc, Concord, MA.

Sze, N. D. and Ko, M. K. W. (1980): Photochemistry of COS, CS_2, CH_3SCH_3 and H_2S: Implications for the Atmospheric Sulfur Cycle, *Atmospheric Environment*, Vol. 14, pp. 1223 - 1239.

Szepesi, D. J. (1978): Transmission of Sulphur Dioxide on Local, Regional and Continental Scale, *Atmospheric Environment*, Vol. 12, pp. 529 - 535.

Tang, I. N. (1980): On the Equilibrium Partial Pressures of Nitric Acid and Ammonia in the Atmosphere, *Atmospheric Environment*, Vol. 14, pp. 819 - 828.

Tang, I. N. (1997): Thermodynamic and Optical Properties of Mixed-Salt Aerosols of Atmospheric Importance, *Journal of Geophysical Research*, Vol. 102, pp. 1883 - 1893.

Tang, I. N. and Munkelwitz, H. R. (1993): Composition and Temperature Dependence of the Deliquescence Properties of Hygroscopic Aerosols, *Atmospheric Environment*, Vol. 27A, pp. 467 - 473.

Tang, I. N. and Munkelwitz, H. R. (1994): Water Activities, Densities and Refractive Indices of Aqueous Sulfate and Nitrate Droplets of Atmospheric Importance, *Journal of Geophysical Research*, Vol. 99, pp. 18801 - 18808.

Tang, I. N., Wong, W. T. and Munkelwitz, H. R. (1981): The Relative Importance of Atmospheric Sulphates and Nitrates in Visibility Reduction, *Atmospheric Environment*, Vol. 15, No. 12, pp. 2463 - 2471.

Tanner, R., Marlow, W. H. and Newman, L. (1979): Chemical Composition Correlations of Size-fractionated Sulfate in New York City, *Environmental Science and Technology*, Vol. 13, pp. 75 - 78.

Terblanche, A. P. S., Danford, I. K. and Nel, C. M. E. (1993): Household Energy Use in South Africa, Air Pollution and Human Health, *Journal of Energy in South Africa*, pp. 54 - 57.

Thurston, G. D., Ito, K. and Lippman, M. (1993): The Role of Particulate Mass vs Acidity in the Sulphate-Respiratory Hospital Admissions Association, *Air and Waste Management Association*, 86th Annual Meeting and Exhibition, *93-MP-11.03*, Colorado, pp. 1 - 10.

Timko and Derrick (1989): Detection and Control of Spontaneous Heating in Coal Mine Pillars: A Case Study, US Bureau of Mines.

Toon, O. B., Hamill, P., Turco, R. P. and Pinto, J. (1986): Condensation of HNO_3 and HCl in the Winter Polar Stratosphere, *Geophysical Research Letter*, Vol. 13, pp. 1284 - 1287.

Tosen, G. R. and Jury, M. R. (1986): The Winter Nocturnal Wind Jet over the Eastern Transvaal Highveld, *South African Journal of Science*, Vol. 84, pp. 247 - 253.

Tsuang, B. -J. (2003): Quantification on the Source/Receptor Relationship of Primary Pollutants and Secondary Aerosols by a Gaussian Plume Trajectory Model: Part I – Theory, *Atmospheric Environment*, Vol. 37, pp. 3981 - 3991.

Tuncel, S. G., Olmez, I., Parrington, J. R., Gordon, G. E. and Stevens, R. K. (1985): Composition of Fine Particle Regional Sulphate Component in Shenandoah Valley, *Environmental Science and Technology*, Vol. 19, pp. 529 - 537.

Turner, D. B. (1974): Workbook of Atmospheric Dispersion Estimates, EPA Office of Air Program Publication AP-26, North Carolina, 56p.

Twomey, S. (1974): Pollution and the Planetary Albedo, *Atmospheric Environment*, Vol. 8, pp. 1251 - 1256.

Twomey, S. (1977): The Influence of Pollution on the Shortwave Albedo of Clouds, *Journal of Atmospheric Science*, Vol. 34, pp. 1149 - 1152.

Twomey, S. (1991): Aerosols, Clouds and Radiation, *Atmospheric Environment*, *Part A*, Vol. 25, pp. 2435 - 2442.

Tyson, P. D. and D'Abreton, P. C. (1995): Divergent and Non-divergent Water-Vapour Transport over Southern Africa during Wet and Dry Conditions, *Meteorology and Atmospheric Physics*, Vol. 55, pp. 47 - 59.

Tyson, P. D., Preston-Whyte, R. A. and Diab, R. D. (1976): Towards an Inversion Climatology of Southern Africa: Part 1, Surface Inversions, *South African Geographical Journal*, Vol. 58, pp. 151 - 163.

Tyson, P. D. and Preston-Whyte, R. A. (2000): The Weather and Climate of Southern Africa, 2nd Edition, Oxford University Press, Cape Town, 396p.

Van Ulden, A. P. and Holtslag, A. A. M. (1985): Estimation of Atmospheric Boundary Layer Parameters for Diffusion Applications, *Journal of Climate and Applied Meteorology*, Vol. 24, pp. 1196 - 1207.

Vasconcelos, L. A. P., Kahl, J. D. W., Liu, D., Macias, E. S. and White, W. H. (1996): Spatial Resolution of a Transport Inversion Technique, *Journal of Geophysical Research*, Vol. 101, pp. 19337 - 19342.

Venkatram, A. (1980a): Estimating the Monin-Obukhov Length in the Stable Boundary Layer for Dispersion Calculations, *Boundary Layer Meteorology*, Vol. 19, pp. 481 – 485.

Venkatram, A. (1980b): Dispersion from an Elevated Source in a Convective Boundary Layer, *Atmospheric Environment*, Vol. 14, pp. 1 - 10.

Viggiano, A. A., Perry, R. A., Albritton, D. L., Ferguson, E. E. and Fehsenfeld, F. C. (1980): The Role of H_2SO_4 Stratospheric Negative – Ion Chemistry, *Journal of Geophysical Research*, Vol. 85, No. C9, pp. 4551 - 4555.

Viggiano, A. A., Perry, R. A., Albritton, D. L., Ferguson, E. E. and Fehsenfeld, F. C. (1982): Stratospheric Negative – Ion Reaction Rates with H_2SO_4, *Journal of Geophysical Research*, Vol. 87, No. C9, pp. 7340 - 7342.

Villasenor, R., Claiborn, C., Lamb, B. and O'Neil, S. (2001): Mesoscale Modelling of Wintertime Particulate Matter Episodes in Eastern Washington, USA, *Atmospheric Environment*, Vol. 35, No. 36, pp. 6479 - 6491.

von Salzen, K. and Schlünzen, K. H. (1999): A Prognostic Physico-chemical Model of Secondary and Marine Inorganic Multicomponent Aerosols: I. Model Description, *Atmospheric Environment*, Vol. 33, pp. 567 - 576.

Waggoner, A. P., Vanderpol, A. H., Charlson, R. J., Larson, S., Granat, L. and Tragardh, C. (1976): Sulphate-Light Scattering as an Index of the Role of Sulphur in Tropospheric Optics, *Nature*, Vol. 261, pp. 120 - 122.

Walcek, C. J., Brost, R. A., Chang, J. S. and Wesley, M. L. (1986): SO_2, Sulphate and HNO_3 Deposition Velocities Computed using Regional Landuse and Meteorological Data, *Atmospheric Environment*, Vol. 20, No. 5, pp. 949 - 964.

Walker, J. T., Whitall, D. R., Robarge, W. and Paerl, H. W. (2004): Ambient Ammonia and Ammonium Aerosol across a Region of Variable Ammonia Emission Density, *Atmospheric Environment*, Vol. 38, No. 9, pp. 1235 - 1246.

Warneck, P. (1988): Chemistry of the Natural Atmosphere, Int. Geophysics Series, Vol. 41, Academic Press, New York, 757p.

Warneck, P. (1999): The Relative Importance of Various Pathways for the Oxidation of Sulphur Dioxide and Nitrogen Dioxide in Sunlit Continental Fair Weather Clouds, *Physical Chemistry Chemical Physics*, Vol. 1, pp. 5471 - 5483.

Watson, J. G., Chow, J. C., Lurmann, F. W. and Musarra, S. P. (1994): Ammonium Nitrate, Nitric Acid and Ammonium Equilibrium in Wintertime Phoenix, Arizona, *Journal of Air and Waste Management Association*, Vol. 44, pp. 405 - 412.

Wayne, T. D. [Ed.] (2000): Air Pollution Engineering Manual, 2nd Edition, Air and Waste Management Association, John Wiley and Sons, New York, 886p.

Webber, J. S., Dutkiewicz, V. A. and Husain, L. (1985): Identification of Submicrometer Coal Fly-Ash in a High-Sulfate Episode at Whiteface Mountain, New-York, *Atmospheric Environment*, Vol. 19, No. 2, pp. 285 - 292.

Weis, R. E., Waggonner, A. P., Charlson, R. J. and Ahlquist, N. C. (1977): Sulphate Aerosol: Its Geographical Extent in Midwestern and Southern United States, *Science*, Vol. 197, pp. 997 - 998.

Wesley, M. L. (1989): Parameterization of Surface Resistances to Gaseous Dry Deposition in Regional Scale Numerical Models, *Atmospheric Environment*, Vol. 23, pp. 1293 - 1304.

Wexler, A. S. and Seinfeld, J. H. (1990): The distribution of Ammonium Salts Among a Size And Composition Dispersed Aerosol, *Atmospheric Environment*, Vol. 24, pp. 1231 – 1246.

Whelpdale, D. M. (2002): An Overview of the Atmospheric Sulphur Cycle, Chapter 2. In: Scope 48 – Sulphur Cycling on the Continent,

http://www.icsu-scope.org/downloadpubs/scope48/chapter02.html,

Website accessed date: 10-11-2004.

Whitby, K. T. (1978): The Physical Characteristics of Sulfur Aerosols, *Atmospheric Environment*, Vol. 12, pp. 135 - 160.

White, W. H. and Roberts, P. T. (1977): On the Nature and Origins of Visibility-Reducing Aerosols in Los Angeles Air Basin, *Atmospheric Environment*, Vol. 11, pp. 803 - 812.

WHO (1979): Environmental Health Criteria 7: Photochemical Oxidants, World Health Organisation /U. N. Environmental Programme, Geneva.

WHO (1991): Indoor Air Pollution from Biomass Fuel, World Health Organisation Programme, *WHO/PEP/92.3A*, Geneva.

Wilson Jr., W. E. (1981): Sulphate Formation in Point Source Plumes: A Review of Recent Field Studies, *Atmospheric Environment*, Vol. 15, pp. 2573 - 2581.

Wolff, G. T., Lioy, P. J., Wight, G. D., Meyers, R. E. and Cederwall, R. T. (1977): An Investigation of Long-Range Transport of Ozone Across the Midwestern and Eastern United States, *Atmospheric Environment*, Vol. 12, pp. 135 - 160.

Wright, R. F. and Schindler, D. W. (1995): Interaction of Acid Rain and Global Changes: Effects on Terrestrial and Aquatic Ecosystems, *Water*, *Air and Soil Pollution*, Vol. 85, pp. 89 - 99.

www.angloamerican.co.uk, Website accessed date: 10-11-2004

www.eskom.co.za, Website accessed date: 10-11-2004

www.weathersa.co.za/RainfallMaps/RainMaps.jsp, Website accessed date: 12-11-2007

www.worldbank.org/html/fpd/em/power/standards/airqstd.stm,

Website accessed date: 12-11-2007

Wyngaard, J.C. (1988): Structure of the PBL, Lectures on Air-Pollution Modelling, Venkatram, A. and Wyngaard, J.C. (Eds.), *American Meteorological Society*, pp. 9 - 61.

Yang, K., Koo, I. S. and Lee, I. (1995): 1. Theoretical Studies on the Substitution Reactions of Sulfonyl Compounds. 2. Hydrolysis and Methanolysis of Methanesulfonyl Chloride, *Journal of Physical Chemistry*, Vol. 99, pp. 15035 - 15040.

Yamartino, R. J., Scire, J. S., Carmichael, G. R. and Chang, Y. S. (1992): The CALGRID Mesoscale Photochemical Grid Model - I. Model Formulation, *Atmospheric Environment*, Vol. 26A, pp. 1493 - 1512.

Yamartino, R. J., Strimaitis, D. and Graff, A. (1996): Evaluation of the Kinematic Simulation Particle Model using Tracer Experiments. In: Proceedings of the 4th Workshop on Harmonisation within Atmospheric Dispersion Modelling for Regular Purposes, Oostende, Belgium 1, pp. 59 - 66.

Yaws, C. L. (1999): Chemical Properties Handbook, McGraw Hill Co., New York, 779p.

Yin, F., Grosjean, D. and Seinfeld, J. H. (1986): Analysis of Atmospheric Photooxidation Mechanisms for Organo-Metallic Sulphur Compounds, *Journal of Geophysical Research*, Vol. 91, pp. 14417 - 14438.

Yu, F. and Turco, R. P. (1997): The Role of Ions in the Formation and Evolution of Particles in Aircraft Plumes, *Geophysical Research Letters*, Vol. 24, pp. 1927 - 1930.

Zhao, J. and Turco, R. P. (1995): Nucleation Simulation in the Wake of a Jet Aircraft in Stratospheric Flight, *Journal of Aerosol Science*, Vol. 26, pp. 779 - 795.

Zib, P. (1977): Urban Air Pollution Dispersion Models: A Critical Survey, Published by Department of Geography and Environmental Studies, University of the Witwatersrand, Johannesburg, South Africa, 44p.

Zilitinkevich, S. S. (1972): On the Determination of the Height of the Ekman Boundary Layer, *Boundary-Layer Meteorology*, Vol. 3, pp. 141 - 145.

Zunckel, M., Held, G., Preston-Whyte, R. A. and Joubert, A (1996): Low-level wind maxima and the transport of pyrogenic products over southern Africa, *Journal of Geophysical Research*, Vol. 101, No. D19, pp. 23,745 – 23,756.

Appendix A: Model Development and Calculations for Atmospheric SO_2 Oxidation during Diffusion

A-1: Rate Model Development for Atmospheric SO_2 Oxidation

To evaluate the disappearance of the reactant as a function of time, the solution of the rate change expressed in terms of a total differential equation is required. That is, the solution of equation (A-1) is essential.

Therefore, given the differential equation,

$$\frac{d[x(t)]}{dt} = -k[x(t)]^2 - k_d^{SO_2}[x(t)] \tag{A-1}$$

The most common technique suitable for evaluating equation (A-1) is the integrating factor (IF) method which, is used for solving first order ordinary differential equation. Rearranging equation (A-1) in the form of an integrating factor (IF) problem with variable right-hand side gives:

$$\frac{d[x(t)]}{dt} + k_d^{SO_2}[x(t)] = -k[x(t)]^2 \tag{A-2}$$

Simplifying equation (A-2) gives:

$$\frac{1}{[x(t)]^2}\frac{d[x(t)]}{dt} + \frac{k_d^{SO_2}}{[x(t)]} = -k \tag{A-3}$$

Let $v = x^{-1}$ (A-4)

and $dv = -x^{-2}dx$ (A-5)

or $-dv = \frac{dx}{x^2}$ (A-6)

Substituting equations (A-4) and (A-6) into equation (A-3) gives:

$$-\frac{dv}{dt} + k_d^{SO_2} v = -k \tag{A-7}$$

Rearranging equation (A-7) as the IF problem gives:

$$\frac{dv}{dt} - k_d^{SO_2} v = k \tag{A-8}$$

If $\ell^{\int(-k_d^{SO_2})dt} = \ell^{-k_d^{SO_2} t}$ =IF

Multipling equation (A-8) by the IF gives:

$$\ell^{-k_d^{SO_2} t} \frac{dv}{dt} - \ell^{-k_d^{SO_2} t} k_d^{SO_2} v = k\ell^{-k_d^{SO_2} t} \tag{A-9}$$

Integrating and simplifying equation (A-9)

$$v = \ell^{k_d^{SO_2} t}\left[\int k\ell^{-k_d^{SO_2} t} dt + C\right] = \ell^{k_d^{SO_2} t}\left[-\frac{k}{k_d^{SO_2}} \ell^{-k_d^{SO_2} t} + C\right] \tag{A-10}$$

$$\frac{1}{x} = v = -\frac{k}{k_d^{SO_2}} + C\ell^{k_d^{SO_2} t} \tag{A-11}$$

Taking boundary conditions on equation (A-11) with $x = x_0$ as $t = 0$ gives:

$$\frac{1}{x_0} = -\frac{k}{k_d^{SO_2}} + C$$

or

$$C = \frac{1}{x_0} + \frac{k}{k_d^{SO_2}} \tag{A-12}$$

Substituting equation (A-12) into equation (A-11) and simplifying after a sojourn time, τ, gives:

$$\frac{1}{x} = \left(\frac{1}{x_0} + \frac{k}{k_d^{SO_2}} \right) \ell^{k_d^{SO_2} \tau} - \frac{k}{k_d^{SO_2}} \tag{A-13}$$

The rate of formation of sulphate as a function of the disappearance of SO_2 by reaction and deposition is expressed as:

$$\frac{d[y(t)]}{dt} = -k_d^{SO_2}[x(t)] - k_d^{SO_4}\{[y(t)] - [x(t)]\} \tag{A-14}$$

Simplifying equation (A-14) gives:

$$\frac{dy}{dt} = -k_d^{SO_4} y + \{k_d^{SO_4} - k_d^{SO_2}\} x \tag{A-15}$$

Rearranging equation (A-15) gives:

$$\frac{1}{x}\frac{dy}{dt} + \frac{k_d^{SO_4}}{x} y = \{k_d^{SO_4} - k_d^{SO_2}\} \tag{A-16}$$

Substituting equation (A-13) into equation (A-16) gives:

$$\left[\left(\frac{1}{x_0} + \frac{k}{k_d^{SO_2}} \right) \ell^{k_d^{SO_2} t} - \frac{k}{k_d^{SO_2}} \right] \frac{dy}{dt} + \left[\left(\frac{1}{x_0} + \frac{k}{k_d^{SO_2}} \right) \ell^{k_d^{SO_2} t} - \frac{k}{k_d^{SO_2}} \right] k_d^{SO_4} y = \{k_d^{SO_4} - k_d^{SO_2}\} \tag{A-17}$$

Let $$m = \left(\frac{1}{x_0} + \frac{k}{k_d^{SO_2}} \right) \tag{A-18}$$

and $$n = \frac{k}{k_d^{SO_2}} \tag{A-19}$$

$$p = \{k_d^{SO_4} - k_d^{SO_2}\} \tag{A-20}$$

$$i = \frac{p}{m} = \left(\frac{k_d^{SO_4} - k_d^{SO_2}}{1/x_0 + k/k_d^{SO_2}} \right) \tag{A-21}$$

$$h = \frac{n}{m} = \left(\frac{k / k_d^{SO_2}}{1/x_0 + k / k_d^{SO_2}} \right) \tag{A-22}$$

Substituting equations (A-18) to (A-22) reduces equation (A-17) to:

$$\left[m\ell^{k_d^{SO_2} t} - n \right] \frac{dy}{dt} + \left[m\ell^{k_d^{SO_2} t} - n \right] k_d^{SO_4} y = p \tag{A-23}$$

Rearranging and simplifying equation (A-22) in the form of an IF expression gives:

$$\frac{dy}{dt} + k_d^{SO_4} y = \frac{p}{(m\ell^{k_d^{SO_2} t} - n)} = \frac{\frac{p}{m}}{(\ell^{k_d^{SO_2} t} - \frac{n}{m})} = \frac{i}{(\ell^{k_d^{SO_2} t} - h)} \tag{A-24}$$

Integrating equation (A-24) using an IF method gives:

$$y = \ell^{-k_d^{SO_4} t} \left[i \int \left(\frac{\ell^{k_d^{SO_4} t}}{\ell^{k_d^{SO_2} t} - h} \right) dt + C \right] \tag{A-25}$$

To integrate the right-hand side, the following evaluations are applied:

If $$I = \int \left(\frac{\ell^{k_d^{SO_4} t}}{\ell^{k_d^{SO_2} t} - h} \right) dt \tag{A-26}$$

let $$u = \ell^{k_d^{SO_2} t} - h \tag{A-27}$$

or $$\ell^{k_d^{SO_2} t} = u + h \tag{A-28}$$

and $$du = k_d^{SO_2} \ell^{k_d^{SO_2} t} dt \tag{A-29}$$

Rearranging and substituting equation (A-28) into equation (A-29) gives:

$$dt = \frac{du}{k_d^{SO_2} \ell^{k_d^{SO_2} t}} = \frac{du}{k_d^{SO_2} (u + h)} \tag{A-30}$$

and from mathematical manipulations,

$$\ell^{k_d^{SO_4} t} = \ell^{k_d^{SO_2} t\left(\frac{k_d^{SO_4}}{k_d^{SO_2}}\right)} = (u+h)^{\left(\frac{k_d^{SO_4}}{k_d^{SO_2}}\right)} \tag{A-31}$$

Substituting equations (A-27), (A-30) and (A-31) into equation (A-26) gives:

$$I = \frac{1}{k_d^{SO_2}} \int \frac{(u+h)^{\left(\frac{k_d^{SO_4}}{k_d^{SO_2}}\right)}}{u(u+h)} du = \frac{1}{k_d^{SO_2}} \int \frac{(u+h)^{\left(\frac{k_d^{SO_4}}{k_d^{SO_2}}-1\right)}}{u} du \tag{A-32}$$

To simplify equation (A-32), a binomial expansion on $(u+h)^{\left(\frac{k_d^{SO_4}}{k_d^{SO_2}}-1\right)}$ is useful. If $(u+h)^{\left(\frac{k_d^{SO_4}}{k_d^{SO_2}}-1\right)}$ consists of a variable *u*, and $\left(\frac{k_d^{SO_4}}{k_d^{SO_2}}-1\right)$ is assumed to be an integer, also if $f = \left(\frac{k_d^{SO_4}}{k_d^{SO_2}}-1\right)$, then

$$(u+h)^{\left(\frac{k_d^{SO_4}}{k_d^{SO_2}}-1\right)} = (u+h)^f \tag{A-33}$$

Rearranging equation (A-33) gives:

$$(u+h)^f = h^f \left(\frac{u}{h}+1\right)^f \tag{A-34}$$

$$h^f \left(\frac{u}{h}+1\right)^f \cong h^f \left[1 + \frac{f}{1!}\left(\frac{u}{h}\right) + \frac{f(f-1)}{2!}\left(\frac{u}{h}\right)^2 + \frac{f(f-1)(f-2)}{3!}\left(\frac{u}{h}\right)^3 + \frac{f(f-1)(f-2)(f-3)}{4!}\left(\frac{u}{h}\right)^4\right] \tag{A-35}$$

Substituting equation (A-35) into (A-32) and simplifying gives:

$$I = \frac{h^f}{k_d^{SO_2}} \int \left[\frac{1}{u} + \frac{f}{h} + \frac{f(f-1)u}{2h^2} + \frac{f(f-1)(f-2)u^2}{6h^3} + \frac{f(f-1)(f-2)(f-3)u^3}{24h^4}\right] du \tag{A-36}$$

Integrating equation (A-36) up to the fourth degree of the binomial expansion term gives:

$$I = \frac{h^f}{k_d^{SO_2}}\left[\ln u + \frac{fu}{h} + \frac{f(f-1)u^2}{4h^2} + \frac{f(f-1)(f-2)u^3}{18h^3} + \frac{f(f-1)(f-2)(f-3)u^4}{96h^4}\right] \tag{A-37}$$

Substituting equation (A-27) into (A-37) and replacing f gives:

$$I = \left(\frac{h^{\left(\frac{k_d^{SO_4}}{k_d^{SO_2}}-1\right)}}{k_d^{SO_2}}\right) I_A + I_B \tag{A-38}$$

where,

$$I_A = \left[\ln(\ell^{k_d^{SO_2}t} - h)\right] + \left[\left(\frac{k_d^{SO_4}}{k_d^{SO_2}}-1\right)\frac{(\ell^{k_d^{SO_2}t} - h)}{h}\right] + \left[\left(\frac{k_d^{SO_4}}{k_d^{SO_2}}-1\right)\left(\frac{k_d^{SO_4}}{k_d^{SO_2}}-2\right)\frac{(\ell^{k_d^{SO_2}t} - h)^2}{4h^2}\right]$$

and $I_B = \left[\left(\frac{k_d^{SO_4}}{k_d^{SO_2}}-1\right)\left(\frac{k_d^{SO_4}}{k_d^{SO_2}}-2\right)\left(\frac{k_d^{SO_4}}{k_d^{SO_2}}-3\right)\frac{(\ell^{k_d^{SO_2}t} - h)^3}{18h^3}\right] + \left[\left(\frac{k_d^{SO_4}}{k_d^{SO_2}}-1\right)\left(\frac{k_d^{SO_4}}{k_d^{SO_2}}-2\right)\left(\frac{k_d^{SO_4}}{k_d^{SO_2}}-3\right)\left(\frac{k_d^{SO_4}}{k_d^{SO_2}}-4\right)\frac{(\ell^{k_d^{SO_2}t} - h)^4}{96h^3}\right]$

Substituting equation (A-38) into equation (A-25) gives:

$$y \cong \ell^{-k_d^{SO_4}t}\left(j\xi + C\right) \tag{A-39}$$

where,

$$j = \frac{ih^{\left(\frac{k_d^{SO_4}}{k_d^{SO_2}}-1\right)}}{k_d^{SO_2}} \tag{A-40}$$

and

$$\xi = \ln(\ell^{k_d^{SO_2}t} - h) + \frac{a_1(\ell^{k_d^{SO_2}t} - h)}{h} + \frac{a_2(\ell^{k_d^{SO_2}t} - h)^2}{4h^2} + \frac{a_3(\ell^{k_d^{SO_2}t} - h)^3}{18h^3} + \frac{a_4(\ell^{k_d^{SO_2}t} - h)^4}{96h^3} \tag{A-41}$$

$$a_1 = \frac{k_d^{SO_4}}{k_d^{SO_2}} - 1 \tag{A-42}$$

$$a_2 = a_1\left(\frac{k_d^{SO_4}}{k_d^{SO_2}} - 2\right) \tag{A-43}$$

$$a_3 = a_2\left(\frac{k_d^{SO_4}}{k_d^{SO_2}} - 3\right) \tag{A-44}$$

and

$$a_4 = a_3\left(\frac{k_d^{SO_4}}{k_d^{SO_2}} - 4\right) \tag{A-45}$$

Taking boundary conditions for equation (A-39) with $y = x_0$ as $t = 0$ gives:

$$x_0 = j\Omega + C \tag{A-46}$$

where,

$$\Omega = \left[\ln(1-h) + \frac{a_1(1-h)}{h} + \frac{a_2(1-h)^2}{4h^2} + \frac{a_3(1-h)^3}{18h^3} + \frac{a_4(1-h)^4}{96h^4}\right] \tag{A-47}$$

Solving for C in equation (A-45) yields:

$$C = x_0 - j\Omega \tag{A-48}$$

Substituting equation (A-47) and (A-48) into (A-39) and simplifying gives:

$$y(t) \cong \ell^{-k_d^{SO_4}t}\left(x_0 + j(\xi - \Omega)\right) \tag{A-49}$$

Combining like terms in (A-41) and (A-47) and simplifying over a travelling time, τ, reduces equation (A-49) to:

$$[y(\tau)] \cong \ell^{-k_d^{SO_4}\tau}\left\{x_0 + j\left(\sum_{l=1}^{5}\nabla_l\right)\right\} \tag{A-50}$$

where

$$\nabla_1 = \ln(\ell^{k_d^{SO_2}\tau} - h) - \ln(1-h) = \ln\left\{\frac{\ell^{k_d^{SO_2}\tau} - h}{1-h}\right\} \tag{A-51}$$

$$\nabla_2 = \frac{a_1[(\ell^{k_d^{SO_2}\tau} - h) - (1-h)]}{h} = \frac{a_1(\ell^{k_d^{SO_2}\tau} - 1)}{h} \tag{A-52}$$

$$\nabla_3 = \frac{a_2[(\ell^{k_d^{SO_2}\tau} - h)^2 - (1-h)^2]}{4h^2} \tag{A-53}$$

$$\nabla_4 = \frac{a_3[(\ell^{k_d^{SO_2}\tau} - h)^3 - (1-h)^3]}{18h^3} \tag{A-54}$$

$$\nabla_5 = \frac{a_4[(\ell^{k_d^{SO_2}\tau} - h)^4 - (1-h)^4]}{96h^4} \tag{A-55}$$

If after travelling for a time, $t = \tau$, then the ratio of the mass concentration of sulphur dioxide to that of the total sulphur -sulphur dioxide and sulphate- expressed as a mass fractional rate $r(\tau)$ or $[x(\tau)]/[y(\tau)]$ for the disappearance of sulphur dioxide is expressed as:

$$\frac{1}{[r(\tau)]} = \frac{1}{[x(\tau)]}[y(\tau)] = \left\{\left(\frac{1}{x_0} + \frac{k}{k_d^{SO_2}}\right)\ell^{k_d^{SO_2}\tau} - \frac{k}{k_d^{SO_2}}\right\}\left\{x_0 + j\left(\sum_{l=1}^{5}\nabla_l\right)\ell^{-k_d^{SO_4}\tau}\right\} \tag{A-56}$$

$$\frac{1}{[r(\tau)]} = \sum_{p=1}^{6}\Delta_p \tag{A-57}$$

where,

$$\Delta_1 = \left(b_1 \exp[(k_d^{SO_2} - k_d^{SO_4})\tau]\right) - \left(b_0 \exp[(-k_d^{SO_4})\tau]\right) \tag{A-58}$$

$$\Delta_2 = \ln\left(h[\exp(k_d^{SO_2}\tau) - h]\right)\left\{\left(b_2 \exp[(k_d^{SO_2} - k_d^{SO_4})\tau]\right) - \left(b_3 \exp[(-k_d^{SO_4})\tau]\right)\right\} \tag{A-59}$$

$$\Delta_3 = \left[\frac{a_1}{h}\left([\exp(k_d^{SO_2}\tau) - h] + [1-h]\right)\right]\left\{\left(b_2 \exp[(k_d^{SO_2} - k_d^{SO_4})\tau]\right) - \left(b_3 \exp[(-k_d^{SO_2})\tau]\right)\right\} \tag{A-60}$$

$$\Delta_4 = \left[\frac{a_2}{4h^2}\left([\exp(k_d^{SO_2}\tau) - h]^2 + [1-h]^2\right)\right]\left\{\left(b_2 \exp[(k_d^{SO_2} - k_d^{SO_4})\tau]\right) - \left(b_3 \exp[(-k_d^{SO_2})\tau]\right)\right\} \quad \text{(A-61)}$$

$$\Delta_5 = \left[\frac{a_3}{18h^3}\left([\exp(k_d^{SO_2}\tau) - h]^3 + [1-h]^3\right)\right]\left\{\left(b_2 \exp[(k_d^{SO_2} - k_d^{SO_4})\tau]\right) - \left(b_3 \exp[(-k_d^{SO_4})\tau]\right)\right\} \quad \text{(A-62)}$$

$$\Delta_6 = \left[\frac{a_4}{96h^4}\left([\exp(k_d^{SO_2}\tau) - h]^4 + [1-h]^4\right)\right]\left\{\left(b_2 \exp[(k_d^{SO_2} - k_d^{SO_4})\tau]\right) - \left(b_3 \exp[(-k_d^{SO_4})\tau]\right)\right\} \quad \text{(A-63)}$$

and,

$$h = \left(\frac{kx_0}{k_d^{SO_2} + kx_0}\right) \quad \text{(A-64)}$$

$$1 - h = \left(\frac{k_d^{SO_2}}{k_d^{SO_2} + kx_0}\right) \quad \text{(A-65)}$$

$$b_0 = x_0 \frac{k}{k_d^{SO_2}} \quad \text{(A-66)}$$

$$b_1 = x_0 \frac{k}{k_d^{SO_2}} + 1 \quad \text{(A-67)}$$

$$b_2 = \frac{k_d^{SO_4} - k_d^{SO_2}}{k}\left(\frac{k_d^{SO_2} + kx_0}{k_d^{SO_2} x_0}\right)\left(\frac{kx_0}{k_d^{SO_2} + kx_0}\right)^{\frac{k_d^{SO_4}}{k_d^{SO_2}}} \quad \text{(A-68)}$$

$$b_3 = \frac{k_d^{SO_4} - k_d^{SO_2}}{k_d^{SO_2}}\left(\frac{kx_0}{k_d^{SO_2} + kx_0}\right)^{\frac{k_d^{SO_4}}{k_d^{SO_2}}} \quad \text{(A-69)}$$

Therefore, the reaction rate can be determined from equation (A-57) with known initial SO_2 concentration, x_0, dry deposition constants for SO_2, $k_d^{SO_2}$, and sulphate, $k_d^{SO_4}$, as well the mass fraction, $r(\tau)$ of SO_2 remaining after any particular sojourn time, (τ).

A-2: Temperature Dependency on Reaction Rates

To determine E_A, using the least squares method, equation (2.96a) may be likened to $y = a + bx$ when expressed as $\ln k = \ln k_\infty - \left(\frac{E_A}{R}\right)\frac{1}{T}$, Where $y = \ln k$, $a = \ln k_\infty$, $b = \left(-\frac{E_A}{R}\right)$ and $x = \frac{1}{T}$, then, applying the method of least squares, using the expressions given in equations (A-70) to (A-73) gives:

$$y = a + bx \tag{A-70}$$

$$an + b\sum x = \sum y \tag{A-71}$$

$$a\sum x + b\sum x^2 = \sum xy \tag{A-72}$$

$$a = \frac{\sum y \sum x^2 - \sum x \sum xy}{n\sum x^2 - (\sum x)^2} \tag{A-73) a}$$

$$b = \frac{n\sum xy - \sum x \sum y}{n\sum x^2 - (\sum x)^2} \tag{A-73) b}$$

Then with known R-value, E_A is determined from **b** in Table (A-1):

Table A-1: Calculated kinetics variables using the least squares method

	$x = \frac{1}{T}$ x 10^3	$y = \ln k$	$(x = \frac{1}{T})^2$ x 10^5	$(y = \ln k)$ $(x = \frac{1}{T})$ x 10^{-3}	**a**	**b**
	3.239	-11.9991	1.049	-38.86		
	3.343	-12.2101	1.118	-40.82		
	3.355	-12.6906	1.126	-42.58		
∑	9.937	-36.90	3.293	-0.1223	2.258092	-4394.871
	3.361	-12.3204	1.130	-41.41		
	3.412	-12.5859	1.164	-42.94		
	3.395	-12.5125	1.153	-42.48		
∑	10.169	-37.42	3.447	-0.1268	5.419812	-5278.872
	3.439	-12.7371	1.182	-43.80		
	3.464	-13.2445	1.200	-45.87		
	3.456	-12.4623	1.194	-43.07		
∑	10.358	-38.44	3.577	-0.1327	35.23031	-13914.81
	3.388	-12.4597	1.148	-42.21		

	3.351 3.334	-12.3026 -12.1707	1.123 1.112	-41.22 -40.58		
∑	10.073	-36.93	3.382	-0.124	5.170157	-5206.47

A-3: Model Development for Concentration Dispersion with Transformation

The assumptions considered during the model formulation were that the vertical concentration distribution is of the Gaussian pattern with the plume being made up of concentric elliptical rings (Freiberg, 1976). Within each ring, the concentration was assumed to be uniform (Briggs, 1969; Pasquil, 1974). In addition, the changes in concentration due to chemical reactions were assumed much smaller compared to those due to dispersion (Freidlander and Seinfeld, 1969). However, it is possible to obtain a rate of concentration due to chemical transformation of SO_2. When a chemical reaction takes place, the concentration at any given time, t, of the reacting species in the plume is expressed according to the Gaussian puff equation. The expression for a puff form of modelling smoke plume dispersion with reflection at the boundary layer and the Earth's surface is given as:

$$\bar{c}(t) = \frac{q(t)}{2\pi\sqrt{\bar{K}_{xx}\bar{K}_{yy}}} g \exp\left[-\frac{(x - x_0 - \bar{u}(t - t_0))^2}{4\bar{K}_{xx}} - \frac{(y - y_0)^2}{4\bar{K}_{yy}} \right] \qquad \text{(A-74)}$$

where

$$g = \sum_{n=1}^{\infty} \frac{(\lambda_n^2 + \beta^2)\cos[\lambda_n(H - z_0)]\cos[\lambda_n(H - z)]}{H(\lambda_n^2 + \beta^2) + \beta} \exp(-\lambda_n^2 \bar{K}_{zz}) \qquad \text{(A-74) a}$$

$$\lambda_n \tan \lambda_n H = \beta \qquad \text{(A-74) b}$$

$$\lambda_n = \frac{n\pi}{H} \qquad \text{(A-74) c}$$

$$K_{xx} = \frac{1}{2}\frac{d\sigma_x^2}{dt} \qquad \text{(A-74) d}$$

$$K_{yy} = \frac{1}{2}\frac{d\sigma_y^2}{dt} \qquad \text{(A-74) e}$$

$$K_{zz} = \frac{1}{2}\frac{d\sigma_z^2}{dt} \qquad \text{(A-74) f}$$

with the following boundary conditions that:

$$\bar{c} = 0 \qquad \text{as} \qquad \begin{matrix} x = \infty \\ y = \infty \end{matrix} \qquad \text{(A-75) a}$$

and

$$\frac{d\bar{c}}{dz} = 0 \qquad \text{as} \qquad z = H \qquad \text{(A-75) b}$$

also

$$\frac{d\bar{c}}{dz} = \frac{v_d}{K_{zz}} = \beta \qquad \text{as} \qquad z = 0 \qquad \text{(A-75) c}$$

At steady state (Seinfeld and Pandis, 1998):

$$\overline{K}_{xx} \cong \sigma_x^2 / 2 \qquad \text{(A-76) a}$$

$$\overline{K}_{yy} \cong \sigma_y^2 / 2 \qquad \text{(A-76) b}$$

$$\overline{K}_{zz} \cong \sigma_z^2 / 2 \qquad \text{(A-76) c}$$

Substituting equations (A-76a) to (A-76c) and (A-74c) into equations (A-74) and (A-74a) yields:

$$\bar{c}(t) = \frac{q(t)}{\pi\sigma_x\sigma_y} g \exp\left[-\frac{(x - x_0 - \bar{u}(t - t_0))^2}{2\sigma_x^2}\right] \exp\left[-\frac{(y - y_0)^2}{2\sigma_y^2}\right] \qquad \text{(A-77)}$$

$$g = \sum_{n=1}^{\infty} \frac{(\lambda_n^2 + \beta^2)}{H(\lambda_n^2 + \beta^2) + \beta} \exp - \left(\frac{\lambda_n^2 \sigma_z^2}{2} \right) \cos(n\pi - \lambda_n z_0) \cos(n\pi - \lambda_n z) \qquad \text{(A-77)a}$$

As described in Lusis and Phillips (1977), the emission strength, q, is related to the reaction rate, η, as:

$$\frac{1}{\bar{u}} \frac{dq(t)}{dt} = \int_0^H \int_{-\infty}^{\infty} \int_{-\infty}^{\infty} \eta_{SO_2}(\bar{c}, t) dx dy dz \qquad \text{(A-78)}$$

If the rate of SO_2 removal rate is expressed as:

For this Study: $$\eta_{SO_2} = \frac{d[SO_2]}{dt} = -k[SO_2]^2 - k_d^{SO_2}[SO_2] \qquad \text{(A-79)}$$

Carmichael and Peters (1984b): $$\eta_{SO_2} = \frac{d[SO_2]}{dt} = -2.22x10^{-4}[SO_2] \qquad \text{(A-80)}$$

Moller (1980): $$\eta_{SO_2} = -\frac{d[SO_2]}{dt} \geq 5.63x10^{-5}[SO_2] \qquad \text{(A-81)}$$

Combining equations (A-79), (A-77) into (A-78); (A-80), (A-77) into (A-78) as well as (A-81), (A-77) into (A-78) gives:

$$\frac{1}{\bar{u}} \frac{dq(t)}{dt} = -k \int_0^H \int_{-\infty}^{\infty} \int_{-\infty}^{\infty} \bar{c}^2 dx dy dz - k_d^{SO_2} \int_0^H \int_{-\infty}^{\infty} \int_{-\infty}^{\infty} \bar{c} dx dy dz \qquad \text{(A-82)}$$

$$\frac{1}{\bar{u}} \frac{dq(t)}{dt} \cong -3.69x10^{-6} \int_0^H \int_{-\infty}^{\infty} \int_{-\infty}^{\infty} \bar{c} dx dy dz \qquad \text{(A-83)}$$

$$\frac{1}{\bar{u}} \frac{dq(t)}{dt} \cong -5.64x10^{-5} \int_0^H \int_{-\infty}^{\infty} \int_{-\infty}^{\infty} \bar{c} dx dy dz \qquad \text{(A-84)}$$

Where $\bar{c}$ in equations (A-82) to (A-84) represents [SO_2] the equations (A-79) to (A-81). If from equation (A-77), $\left[\exp-\left(\frac{(x-x_0-\bar{u}(t-t_0))^2}{2\sigma_x^2}\right)\right]$ is simplified as $\left[\exp-\left(\frac{x^2}{2\sigma_x^2}\right)\right]$ and the crosswind -component $\left[\exp-\left(\frac{(y-y_0)^2}{2\sigma_y^2}\right)\right]$ is simplified as $\left[\exp-\left(\frac{y^2}{2\sigma_y^2}\right)\right]$, and if

$\int_{-\infty}^{\infty}\left[\ell^{-kx^2}\right]^2 dx = \int_{-\infty}^{\infty}\ell^{-kx^2}.\ell^{-kx^2}dx = \int_{-\infty}^{\infty}\ell^{-2kx^2}dx = \frac{\sqrt{\pi}}{2\sqrt{2k}}$, then the solution of the integration for the individual exponential terms of equation (A-77) are:

$$\int_{-\infty}^{\infty}\left[\exp-\left(\frac{x^2}{2\sigma_x^2}\right)\right]^2 dx = \int_{-\infty}^{\infty}\left[\exp-\left(\frac{x^2}{\sigma_x^2}\right)\right]dx = \frac{\sigma_x^2\sqrt{\pi}}{2} \quad \text{(A-i)}$$

$$\int_{-\infty}^{\infty}\left[\exp-\left(\frac{y^2}{2\sigma_y^2}\right)\right]^2 dy = \int_{-\infty}^{\infty}\left[\exp-\left(\frac{y^2}{\sigma_y^2}\right)\right]dy = \frac{\sigma_y^2\sqrt{\pi}}{2} \quad \text{(A-ii)}$$

$$\int_{-\infty}^{\infty}\left[\exp-\left(\frac{x^2}{2\sigma_x^2}\right)\right]dx = \frac{\sigma_x^2\sqrt{2\pi}}{2} \quad \text{(A-iii)}$$

$$\int_{-\infty}^{\infty}\left[\exp-\left(\frac{y^2}{2\sigma_y^2}\right)\right]dy = \frac{\sigma_y^2\sqrt{2\pi}}{2} \quad \text{(A-iv)}$$

Substituting the integrated exponential terms of $\bar{c}$ -equations (A-i) to (A-iv)- into equations (A-82) to (A-84) and integrating with respect to the x-, y-, z-coordinates over the distance travelled by the reacting fluid between the source and observation point yields the following expressions. From equation (A-82):

$$dq(t) = -k\bar{u}q(t)^2\int_{t_1}^{t_2}\left[\frac{1}{\sigma_x\sigma_y}\int_0^H g^2 dz\right]dt - k_d^{SO_2}\bar{u}q(t)\int_{t_1}^{t_2}\sum_{n=1}^{\infty}w_n\left[\exp-\left(\frac{\lambda_n^2\sigma_z^2}{2}\right)\right]dt \quad \text{(A-85)}$$

where,

$$w_n = \left(\frac{(\lambda_n^2 + \beta^2)}{H(\lambda_n^2 + \beta^2) + \beta} \right) \frac{\sin n\pi}{\lambda_n} \cos(n\pi - \lambda_n z_0) \qquad \text{(A-85) a}$$

and from equation (A-83):

$$dq(t) = -7.38x10^{-6}\, \bar{u} q(t) \int_{t_1}^{t_2} \sum_{n=1}^{\infty} w_n \left[\exp - \left(\frac{\lambda_n^2 \sigma_z^2}{2} \right) \right] dt \qquad \text{(A-86)}$$

and from equation (A-84):

$$dq(t) = -1.13x10^{-4}\, \bar{u} q(t) \int_{t_1}^{t_2} \sum_{n=1}^{\infty} w_n \left[\exp - \left(\frac{\lambda_n^2 \sigma_z^2}{2} \right) \right] dt \qquad \text{(A-87)}$$

From the boundary layer estimate, the ratio of the sampling highest to the Monin-Obukhov height is less than zero, that is, $z/L < 0$, and the deviations of wind velocities in the crosswind and vertical directions are given as:

$$\sigma_y(t) = \sigma_v f_{ly} t \qquad \text{(A-88) a}$$

$$\sigma_z(t) = \sigma_w f_{lz} t \qquad \text{(A-88) b}$$

where,

$$\sigma_v = 1.78u_*[1 + 0.059(-h_{us}/L)]^{1/3} \qquad \text{z/L < 0} \qquad \text{(A-88) c}$$

$$f_{ly} = \left[1 + \left(\frac{2.5u^* t}{z} \{1 + 0.0013(-z/L)\}^{1/3} \right)^{1/2} \right]^{-1} \qquad \text{z/L < 0} \qquad \text{(A-88) d}$$

and

$$\sigma_w = 2.891 w_* h_{us}^{-0.333} \qquad \text{(A-88) e}$$

where f is the Lagrangian time scale that specifies the characteristics of the atmospheric boundary layer. If *n=15* in equations (A-85) to (A-87), and for a symmetric puff with

$\sigma_x = \sigma_y$, substituting equations (A-88a) to (A-88e) into equation (A-85) and integrating gives:

$$\frac{dq(t)}{dt} = -k\frac{\bar{u}q(t)^2}{\sigma_v^2}\left[\frac{1}{f_{ly}^2 t^2}\int_0^H g^2 dz\right] - k_d^{SO_2}\bar{u}q(t)\sum_{n=1}^{15} w_n\left[\exp-\left(\frac{\lambda_n^2\sigma_w^2 f_{lz}^2 t^2}{2}\right)\right] \qquad \text{(A-89)}$$

or simplified as:

$$\frac{dq(t)}{dt} + k_d^{SO_2}\bar{u}q(t)\sum_{n=1}^{15} w_n\left[\exp-\left(\frac{\lambda_n^2\sigma_w^2 f_{lz}^2 t^2}{2}\right)\right] = -k\frac{\bar{u}q(t)^2}{\sigma_v^2}\left[\frac{1}{f_{ly}^2 t^2}\int_0^H g^2 dz\right] \qquad \text{(A-89) a}$$

If $$E = k_d^{SO_2}\bar{u}\sum_{n=1}^{15} w_n\left[\exp-\left(\frac{\lambda_n^2\sigma_w^2 f_{lz}^2 t^2}{2}\right)\right] \qquad \text{(A-89) b}$$

and $$F = -k\frac{\bar{u}}{\sigma_v^2}\left[\frac{1}{f_{ly}^2 t^2}\int_0^H g^2 dz\right] \qquad \text{(A-89) c}$$

then equation (A-89)a becomes:

$$-\frac{1}{q(t)^2}\frac{dq(t)}{dt} - \frac{E}{q(t)} = F \qquad \text{(A-89) d}$$

Also, if $v = \frac{1}{q}$ and $dv = -\frac{dq}{q^2}$, then equation (A-89d) is simplified to give a normal first order differential equation of the form:

$$\frac{dv}{dt} - Ev = F \qquad \text{(A-89) e}$$

Applying the integrating factor method gives:

$$v = \frac{1}{q} = \ell^{-\int E dt}\left[\left(\int F\ell^{\int E dt} dt\right) + C\right] \qquad \text{(A-89) f}$$

Solving equation (A-89e) gives the amount of transported air mass with dispersed concentrations.

$$\varepsilon_n = \frac{(\lambda_n^2 + \beta^2)}{H(\lambda_n^2 + \beta^2) + \beta} \exp - \left(\frac{\lambda_n^2 \sigma_z^2}{2} \right) \cos\left(n\pi - \lambda_n z_0 \right) \qquad \text{(A-89) g}$$

If equation (A-89f) is a constant relative to elevation, z, then the vertical term may be expressed as:

$$g = \sum \varepsilon_n \cos\left(n\pi - \lambda_n z \right) = \sum_{n=1}^{m} x_n \qquad \text{(A-89) h}$$

and if for very large values of *m*, the values of *g* are insignificant, then with *m = 15*;

$$\int_0^H g^2 dz = \int_0^H \left(\sum_{n=1}^{15} x_n \right)^2 dz = \int_0^H \left(x_1 + x_2 + x_3 + x_4 ..... + x_{15} \right)^2 dz \qquad \text{(A-90)}$$

Analogous to equation (A-90) is

$$(x + y + z + m)^2 \qquad \text{(A-91)}$$

Expanding the polynomial equation (A-91) gives:

$$(x^2 + y^2 + z^2 + m^2) + (2xy + 2xz + 2xm) + (2yz + 2ym) + 2zm \qquad \text{(A-91) b}$$

In a similar manner, expanding equation (A-90) gives:

$$\int_0^H \left(\sum_{n=1}^{15} x_n \right)^2 dz = \int_0^H \Phi_0 + \int_0^H \Phi_1 + \int_0^H \Phi_2 + \int_0^H \Phi_3 + ... + \int_0^H \Phi_{15} \qquad \text{(A-92)}$$

where

$$\int_0^H \Phi_0 = \int_0^H \left(x_1^2 + x_2^2 + x_3^2 + ... + x_{14}^2 + x_{15}^2 \right) dx \qquad \text{(A-93)}$$

If $x_n = \varepsilon_n \cos(n\pi - \lambda_n z)$, (A-93) a

and $x_n^2 = \varepsilon_n^2 \cos^2(n\pi - \lambda_n z)$ (A-93) b

then $\int_0^H x_n^2 dx = \frac{\varepsilon_n^2}{2} \int_0^H \cos^2(n\pi - \lambda_n z) dz$ (A-93) c

Simplifying equation (A-93c) gives:

$$\frac{\varepsilon_n^2}{2} \int_0^H \cos^2(n\pi - \lambda_n z) dz = \frac{\varepsilon_n^2}{2} \int_0^H [1 + \cos 2(n\pi - \lambda_n z)] dz \quad \text{(A-93) d}$$

Integrating the right hand side of equation (A-93c) yields:

$$\frac{\varepsilon_n^2}{2} \int_0^H [1 + \cos 2(n\pi - \lambda_n z)] dz = \frac{\varepsilon_n^2}{2} \left[z - \frac{\sin 2(n\pi - \lambda_n z)}{2\lambda_n} \right]_0^H \quad \text{(A-93) e}$$

Therefore

$$\int_0^H x_n^2 dx = \frac{\varepsilon_n^2}{2} \left(H + \frac{\sin(2n\pi)}{2\lambda_n} \right) \quad \text{(A-93) f}$$

The solution of equation (A-93f) was then substituted into (A-93) to give Φ_0. In a similar manner,

$$\int_0^H \Phi_1 = \int_0^H (2x_1x_2 + 2x_1x_3 + 2x_1x_4 + \ldots\ldots\ldots\ldots\ldots + 2x_1x_{14} + 2x_1x_{15}) dz \quad \text{(A-94)}$$

Applying equation (A-93a) gives:

$$\int_0^H 2x_m x_n = \int_0^H 2\varepsilon_m \varepsilon_n [\cos(m\pi - \lambda_m z) \cos(n\pi - \lambda_n z)] \quad \text{(A-94) a}$$

where n ≠ m

But $\cos A \cos B = \frac{1}{2}\cos(A + B) + \frac{1}{2}\cos(A - B)$ (A-94) b

Therefore applying (A-94b) to equation (A-94a) and simplifying gives:

$$\int_0^H 2x_m x_n = \int_0^H \varepsilon_m \varepsilon_n \left(\cos[(m+n)\pi - (\lambda_m + \lambda_n)z] + \cos[(m-n)\pi - (\lambda_m - \lambda_n)z]\right) \qquad \text{(A-94) c}$$

Integrating equation (A-94c) yields:

$$2x_m x_n = \varepsilon_m \varepsilon_n \left(\frac{\sin(m+n)\pi}{\lambda_m + \lambda_n} + \frac{\sin(m-n)\pi}{\lambda_m - \lambda_n}\right) \qquad \text{(A-94) d}$$

Evaluating equation (A-94a) for $m = 1, n = 2$ gives:

$$2x_1 x_2 = \varepsilon_1 \varepsilon_2 \left(\frac{\sin(3\pi)}{\lambda_1 + \lambda_2} + \frac{\sin(-\pi)}{\lambda_1 - \lambda_2}\right) \qquad \text{(A-94) e}$$

The solution of equation (A-94e) was then substituted into (A-94) to give Φ_1. In a similar fashion for,

$$\int_0^H \Phi_2 = \int_0^H \left(2x_2 x_3 + 2x_2 x_4 + \ldots\ldots\ldots\ldots\ldots + 2x_2 x_{15}\right) dz \qquad \text{(A-95) a}$$

$$2x_2 x_3 = \left[\varepsilon_2 \varepsilon_3 \left(\frac{\sin(5\pi)}{\lambda_2 + \lambda_3} + \frac{\sin(-\pi)}{\lambda_2 - \lambda_3}\right)\right] \qquad \text{(A-95) b}$$

$$2x_2 x_4 = \left[\varepsilon_2 \varepsilon_4 \left(\frac{\sin(6\pi)}{\lambda_2 + \lambda_4} + \frac{\sin(-2\pi)}{\lambda_2 - \lambda_4}\right)\right] \qquad \text{(A-95) c}$$

Likewise,

$$\int_0^H \Phi_3 = \int_0^H \left(2x_3 x_4 + 2x_3 x_5 + \ldots + 2x_3 x_{15}\right) dz \qquad \text{(A-96) a}$$

$$\int_0^H 2x_3 x_4 = \left[\varepsilon_3 \varepsilon_4 \left(\frac{\sin(7\pi)}{\lambda_3 + \lambda_4} + \frac{\sin(-\pi)}{\lambda_3 - \lambda_4}\right)\right] \qquad \text{(A-96) b}$$

Finally, the solution of equation (A-95c) and (A-96b) for variables beginning with x_2 and x_3 respectively, up to those with variables x_{15} was then substituted into (A-95) to give Φ_2, Φ_3 up to Φ_{15}. In a similar manner,

And $$\int_0^H 2x_m x_n dz = \varepsilon_m \varepsilon_n \left(\frac{\sin(m+n)\pi}{\lambda_m + \lambda_n} + \frac{\sin(m-n)\pi}{\lambda_m - \lambda_n} \right) \quad \text{where } m \neq n \qquad \text{(A-96) c}$$

Combining equations (A-92) to (A-96b) into equation (A-90) yields:

$$\int_0^H g^2 dz = \sum_{n=1}^{15} \frac{\varepsilon_n^2}{2} \left(\frac{\sin(2n\pi)}{2\lambda_n} + H \right) + \sum_{m=1}^{m=14} \sum_{n=m+1}^{n=15} \varepsilon_m \varepsilon_n \left(\frac{\sin(m+n)\pi}{\lambda_m + \lambda_n} + \frac{\sin(m-n)\pi}{\lambda_m - \lambda_n} \right) \qquad \text{(A-97)}$$

When equation (A-97) is substituted into equation (A-89c) and if the comprehensive for of equation (A-89c) obtained is introduced into equation (A-89f) and integrating with respect to t, gives the quantity of dispersed SO_2 after a particular travelling time given by equation (A-98). This is given as:

$$\left. \frac{1}{q(t)} \right|_{(Q_S/Q_S^0)_1}^{(Q_S/Q_S^0)_2} = e^{j(t)} . i(t) \qquad \text{(A-98)}$$

where,

$$i(t) = \left(\int_{t_1}^{t_2} e^{-j(t)} Q(t) dt \right)$$

$$Q(t) = \alpha \left[\sum_{n=1}^{15} V_n \exp\left(-\lambda_n^2 \sigma_z^2 \right) + \sum_{m=1}^{m=14} \sum_{n=m+1}^{n=15} U_{mn} \exp\left(-\frac{(\lambda_m^2 + \lambda_n^2)\sigma_z^2}{2} \right) \right]$$

or

$$Q(t) = \alpha \left[\sum_{n=1}^{15} V_n \exp\left(-\frac{\lambda_n^2 \sigma_w^2 t^2}{(1+0.9t^{0.5})^2} \right) + \sum_{m=1}^{m=14} \sum_{n=m+1}^{n=15} U_{mn} \exp\left(-\frac{(\lambda_m^2 + \lambda_n^2)\sigma_w^2 t^2}{2(1+0.9t^{0.5})^2} \right) \right] \qquad \text{(A-98)a}$$

$$V_n = \left[\frac{(\lambda_n^2+\beta^2)}{H(\lambda_n^2+\beta^2)+\beta}\cos\left(n\pi-\lambda_n z_0\right)\right]^2\left(\frac{\sin(2n\pi)}{4\lambda_n}+\frac{H}{2}\right) \quad \text{(A-98) b}$$

$$U_{mn} = \Gamma_{mn}\left(\frac{\sin(m+n)\pi}{\lambda_m+\lambda_n}+\frac{\sin(m-n)\pi}{\lambda_m-\lambda_n}\right) \quad \text{(A-98) c}$$

$$\Gamma_{mn} = \left[\frac{(\lambda_n^2+\beta^2)}{H(\lambda_n^2+\beta^2)+\beta}\cos\left(n\pi-\lambda_n z_0\right)\right]\left[\frac{(\lambda_m^2+\beta^2)}{H(\lambda_m^2+\beta^2)+\beta}\cos\left(m\pi-\lambda_m z_0\right)\right] \quad \text{(A-98) d}$$

$$j(t) = k_d^{SO_2}\delta(t) \quad \text{(A-98) e}$$

$$\delta(t) = \bar{u}\int_{t_1}^{t_2}\sum_{n=1}^{15} w_n\left[\exp-\left(\frac{\lambda_n^2\sigma_w^2 t^2}{2(1+0.9t^{0.5})^2}\right)\right]dt \quad \text{(A-98) f}$$

$$\alpha = -\frac{4.52x10^{-8}\bar{u}}{\sigma_v^2}\left(\frac{(T_i^{0.5}+t^{0.5})^2}{T_i t^2}\right) \quad \text{(A-98) g}$$

$$T_i = 50u_*\left(1+0.0013\left(-h_{us}/L\right)\right)^{-1/3} \quad \text{(A-98) h}$$

Equation (A-98) is the dispersed concentration distribution between the source and the monitoring station. It is based on the developed reaction and deposition rate constants of *model type-1* for the various seasons (Table 4-2b). The approximation to the exact solution of equation (A-98) was obtained using the Simpson's method of numerical approximations expressed below at a constant time interval of t = 1 hour.

The substitution of equations (A-88c) and (A-88d) into equation (A-86) yields:

$$\frac{dq(t)}{q(t)} = -7.38x10^{-6}\bar{u}\int_{t_1}^{t_2}\sum_{n=1}^{15} w_n\left[\exp-\left(\frac{\lambda_n^2\sigma_w^2 f_{lz}^2 t^2}{2}\right)\right]dt \quad \text{(A-99)}$$

Integrating equation (A-99) generates the results to of atmospheric dispersion of the SO_2 based on *model type-2A* expressed as:

$$q(t)\Big|_{(Q_S/Q_S^0)_1}^{(Q_S/Q_S^0)_2} = \ell^{-7.38x10^{-6}\delta(t)} \tag{A-100}$$

In similar manner, incorporating equations (A-88c) and (A-88d) into equation (A-87) gives:

$$\frac{dq(t)}{q(t)} = -1.13x10^{-4}\,\overline{u}\int_{t_1}^{t_2}\sum_{n=1}^{15} w_n\left[\exp-\left(\frac{\lambda_n^2\sigma_w^2 f_{lz}^2 t^2}{2}\right)\right]dt \tag{A-101}$$

Integrating equation (A-101) gives the results of the atmospheric dispersion of the SO_2 based on *model type-2B* expressed as:

$$q(t)\Big|_{(Q_S/Q_S^0)_1}^{(Q_S/Q_S^0)_2} = \ell^{-1.13x10^{-4}\delta(t)} \tag{A-102}$$

The solutions for equations (A-100) and (A-102) were obtained using the Simpson's approximation method similarly to the approach of equation (A-98). Similarly to equation (A-98), the developed equations (A-100) and (A-102) are the modelled amounts of SO_2 expected during advection between a source and the monitoring station with considerations on the boundary layer conditions.

The Simpson's method used for the determination of the change in source strength was evaluated as follows:

For a known downwind distance, the travel time given as:

$$t_q = \frac{s_q}{\overline{u}} \tag{A-103}$$

In Simpson's method, the integration of functions such as $j(t)$, $i(t)$ or $\delta(t)$ in equation (A-98), may be expressed with a general formula:

$$I = \int_{t_1}^{t_2} H(t) \cong \frac{\Delta t}{3}\left\{\left[\Psi(t_1)+\Psi(t_2)\right]+2\sum_{\substack{i=2\\ j=i+1}}^{\substack{i=q-2\\ j=q-1}}\left[2\Psi(t_i)+\Psi(t_j)\right]\right\} \tag{A-104}$$

Where $\Psi(t)$ represents any of the function expressions over a time interval given as:

$$\Delta t = \frac{t_{q+1} - t_q}{\kappa} \tag{A-105}$$

t_1 and t_2 are the start and finish times respectively and κ is an even number of divisions between the start and finish times, while q are equal distant locations generated from the κ-divisions.

Appendix B: Computational Methods for Evaluation of Thermochemical Properties

B-1: Model Input Requirements

Below is an example of the script file for the simulation of a typical input data for in Gaussian computational chemistry software (G03) for the theoretical computation of the electronic energies of molecule using the Gaussian-2 (G2) computational level. The Input data consists of the molecular geometry of the compound determined from the bond angles and bond lengths

♦	#T G2 Test				(Method to be Applied)
♦	HSO5*				(Molecule to be Evaluated)
♦	0	2			(Charge and Multiplicity)
♦	O 0	0.764587	1.098984	0.000000	(Structural Coordinate of the
♦	S 0	-0.111923	-0.419174	0.000000	Molecule Generated with
♦	O 0	-1.571000	0.387405	0.000015	GaussView package)
♦	O 0	2.037827	1.051620	-0.001129	
♦	O 0	0.051849	-1.057022	1.236359	
♦	O 0	0.051590	-1.057419	-1.236176	
♦	H 0	-2.364883	-0.128143	-0.000183	

The G2 computation is conducted as follows:

(a) Molecular Geometry Optimisation with Hartree-Fock (HF) method.

(b) Electronic Energy Calculation of optimised molecular structure with HF method.

(c) Optimisation and Calculation of Electronic Energy from step 2 with MP2 method.

(d) Optimisation and Calculation of Electronic Energy from step 2 with Quadratic Correlation Interaction Second Derivative (QCISD) method.

(e) Optimisation and Calculation of Electronic Energy from step 2 with MP4 method.

(f) Optimisation and Calculation of Electronic Energy from step 2 with MP2 method with full basis set.

B-2: Quick Tour of Gaussian Output

(1). Below is the copyright notice for Gaussian 03. Its appearance indicates that the program has begun.

Entering Link 1 = C:\G03W\l1.exe PID= 2536.

Copyright (c) 1988,1990,1992,1993,1995,1998,2003,2004, Gaussian, Inc.
All Rights Reserved.

This is the Gaussian(R) 03 program. It is based on the Gaussian(R) 98 system (copyright 1998, Gaussian, Inc.), Gaussian(R) 94 system (copyright 1995, Gaussian, Inc.), Gaussian 92(TM) system (copyright 1992, Gaussian, Inc.), Gaussian 90(TM) system (copyright 1990, Gaussian, Inc.), Gaussian 88(TM) system (copyright 1988, Gaussian, Inc.), Gaussian 86(TM) system (copyright 1986, Carnegie Mellon University), and the Gaussian 82(TM) system (copyright 1983, Carnegie Mellon University). Gaussian is a federally registered trademark of Gaussian, Inc.

This software contains proprietary and confidential information, including trade secrets, belonging to Gaussian, Inc.

This software is provided under written license and may be used, copied, transmitted, or stored only in accord with that written license.

---

(2). This section expressed below consists of the official citations, the version of Gaussian 03, the route section, title section and molecular specifications. It also show the standard orientation which is the coordinate system used internally by the program as it performs its calculation chosen to optimise performance.

Gaussian, Inc.
340 Quinnipiac St., Bldg. 40, Wallingford CT 06492

Warning -- This program may not be used in any manner that competes with the business of Gaussian, Inc. or will provide assistance to any competitor of Gaussian, Inc. The licensee of this program is prohibited from giving any competitor of Gaussian, Inc. access to this program. By using this program, the user acknowledges that Gaussian, Inc. is engaged in the business of creating and licensing software in the field of computational chemistry and represents and warrants to the licensee that it is not a competitor of Gaussian, Inc. and that it will not use this program in any manner prohibited above.

Cite this work as: Gaussian 03, Revision C.02,
M. J. Frisch, G. W. Trucks, H. B. Schlegel, G. E. Scuseria, M. A. Robb, J. R. Cheeseman, J. A. Montgomery, Jr., T. Vreven, K. N. Kudin, J. C. Burant, J. M. Millam, S. S. Iyengar, J. Tomasi, V. Barone, B. Mennucci, M. Cossi, G. Scalmani, N. Rega, G. A. Petersson, H. Nakatsuji, M. Hada, M. Ehara, K. Toyota, R. Fukuda, J. Hasegawa, M. Ishida, T. Nakajima, Y. Honda, O. Kitao, H. Nakai, M. Klene, X. Li, J. E. Knox, H. P. Hratchian, J. B. Cross, C. Adamo, J. Jaramillo, R. Gomperts, R. E. Stratmann, O. Yazyev, A. J. Austin, R. Cammi, C. Pomelli, J. W. Ochterski, P. Y. Ayala, K. Morokuma, G. A. Voth, P. Salvador, J. J. Dannenberg, V. G. Zakrzewski, S. Dapprich, A. D. Daniels, M. C. Strain, O. Farkas, D. K. Malick, A. D. Rabuck, K. Raghavachari, J. B. Foresman, J. V. Ortiz, Q. Cui, A. G. Baboul, S. Clifford, J. Cioslowski, B. B. Stefanov, G. Liu, A. Liashenko, P. Piskorz, I. Komaromi, R. L. Martin, D. J. Fox, T. Keith, M. A. Al-Laham, C. Y. Peng, A. Nanayakkara, M. Challacombe, P. M. W. Gill, B. Johnson, W. Chen, M. W. Wong, C. Gonzalez, and J. A. Pople, Gaussian, Inc., Wallingford CT, 2004.

****
Gaussian 03: IA32W-G03RevC.02 12-Jun-2004
27-May-2006
****

#T G2 Test

HOSO2OO

Symbolic Z-matrix:
Charge = 0 Multiplicity = 2

O	0	0.76459	1.09898	0.
S	0	-0.11192	-0.41917	0.
O	0	-1.571	0.38741	0.00002
O	0	2.03783	1.05162	-0.00113
O	0	0.05185	-1.05702	1.23636
O	0	0.05159	-1.05742	-1.23618
H	0	-2.36488	-0.12814	-0.00018

GradGradGradGradGradGradGradGradGradGradGradGradGradGradGradGradGradGrad
Initialisation pass.

! Initial Parameters !
! (Angstroms and Degrees) !

Name	**Definition**	**Value**	**Derivative Info.**
R1	R(1,2)	1.753	estimate D2E/DX2
R2	R(1,4)	1.2741	estimate D2E/DX2
R3	R(2,3)	1.6672	estimate D2E/DX2
R4	R(2,5)	1.4008	estimate D2E/DX2
R5	R(2,6)	1.4008	estimate D2E/DX2
R6	R(3,7)	0.9466	estimate D2E/DX2
A1	A(2,1,4)	117.8696	estimate D2E/DX2
A2	A(1,2,3)	91.0662	estimate D2E/DX2
A3	A(1,2,5)	109.6262	estimate D2E/DX2
A4	A(1,2,6)	109.6469	estimate D2E/DX2
A5	A(3,2,5)	108.8206	estimate D2E/DX2
A6	A(3,2,6)	108.8203	estimate D2E/DX2
A7	A(5,2,6)	123.9016	estimate D2E/DX2
A8	A(2,3,7)	118.0664	estimate D2E/DX2
D1	D(4,1,2,3)	-179.9431	estimate D2E/DX2
D2	D(4,1,2,5)	69.6185	estimate D2E/DX2
D3	D(4,1,2,6)	-69.5019	estimate D2E/DX2
D4	D(1,2,3,7)	179.9862	estimate D2E/DX2
D5	D(5,2,3,7)	-68.8362	estimate D2E/DX2
D6	D(6,2,3,7)	68.7865	estimate D2E/DX2

Number of steps in this run= 30 maximum allowed number of steps= 100.

GradGradGradGradGradGradGradGradGradGradGradGradGradGradGradGradGrad

Distance matrix (Angstroms):

		1	2	3	4	5
1	O	0.000000				
2	S	1.753018	0.000000			
3	O	2.441580	1.667176	0.000000		
4	O	1.274121	2.604738	3.669443	0.000000	
5	O	2.585525	1.400805	2.499711	3.149898	0.000000
6	O	2.585840	1.400794	2.499697	3.149369	2.472535
7	H	3.361461	2.271680	0.946594	4.558037	2.869224
		6	7			
6	O	0.000000				
7	H	2.868898	0.000000			

Framework group C1[X(HO5S)]
Deg. of freedom 15

Standard orientation:

Center Number	Atomic Number	Atomic Type	Coordinates (Angstroms) X	Y	Z
1	8	0	1.143278	0.678175	0.000134
2	16	0	-0.375542	-0.197187	0.000134
3	8	0	-1.234773	1.231518	0.000149
4	8	0	2.221742	-0.000277	-0.000995
5	8	0	-0.553114	-0.831332	1.236493
6	8	0	-0.553537	-0.831546	-1.236042
7	1	0	-2.180107	1.182695	-0.000049

Rotational constants (GHZ): 4.8046471 2.6285302 2.5310912
96 basis functions, 196 primitive gaussians, 96 cartesian basis functions
29 alpha electrons, 28 beta electrons
nuclear repulsion energy 353.4966523000 Hartrees.

(3). This section indicates the predicted **energy computed by our calculation**, the optimised molecular geometry, the estimated total atomic charge on each atom in the molecule and the dipole moment for this molecule in the standard as well as the optimised orientations. The end part shows the successful completion of the Gaussian Jobs with a quotation chosen at random as well as the CPU time and other resource usage information.

Rotational constants (GHZ): 4.9851124 2.9229502 2.8393866

96 basis functions, 196 primitive gaussians, 96 cartesian basis functions
29 alpha electrons, 28 beta electrons
nuclear repulsion energy 364.9797865163 Hartrees.
NAtoms= 7 NActive= 7 NUniq= 7 SFac= 1.00D+00 NAtFMM= 60 Big=F
Initial guess read from the read-write file:
Initial guess orbital symmetries:
Alpha Orbitals:
Occupied (A) (A) (A) (A) (A) (A) (A) (A) (A) (A) (A) (A)
(A) (A) (A) (A) (A) (A) (A) (A) (A) (A) (A) (A)
(A) (A) (A) (A) (A)
Virtual (A) (A) (A) (A) (A) (A) (A) (A) (A) (A) (A) (A)
……
(A) (A) (A) (A) (A) (A) (A)
Beta Orbitals:
Occupied (A) (A) (A) (A) (A) (A) (A) (A) (A) (A) (A) (A)
(A) (A) (A) (A) (A) (A) (A) (A) (A) (A) (A) (A)
(A) (A) (A) (A)
Virtual (A) (A) (A) (A) (A) (A) (A) (A) (A) (A) (A) (A)
……
(A) (A) (A) (A) (A) (A) (A) (A)
<S**2> of initial guess= 0.7590
SCF Done**: E(UHF) = -772.172370496** A.U. after 12 cycles
Convg = 0.2757D-08 -V/T = 2.0020
S**2 = 0.7590
Annihilation of the first spin contaminant:
S**2 before annihilation 0.7590, after 0.7501

GradGradGradGradGradGradGradGradGradGradGradGradGradGradGradGradGradGrad
Internal Forces: Max 0.000060350 RMS 0.000029470
Step number 7 out of a maximum of 30
All quantities printed in internal units (Hartrees-Bohrs-Radians)
Trust test= 9.87D-01 RLast= 1.71D-03 DXMaxT set to 4.24D-01
Eigenvalues 0.00595 0.01729 0.16153 0.16771 0.19925
Eigenvalues 0.20141 0.24735 0.27326 0.33302 0.36234
Eigenvalues 0.44865 0.52252 0.58365 1.18238 1.21743
Eigenvalues 1000.000001000.000001000.000001000.000001000.00000
Quartic linear search produced a step of -0.01224.
Iteration 1 RMS(Cart)= 0.00009702 RMS(Int)= 0.00000001
Iteration 2 RMS(Cart)= 0.00000001 RMS(Int)= 0.00000000

Variable	**Old X**	**-DE/DX (Linear)**	**Delta X (Quad)**	**Delta X (Total)**	**Delta X**	**New X**
R1	3.08325	0.00005	0.00001	0.00015	0.00015	3.08341
R2	2.49175	0.00004	-0.00001	0.00010	0.00009	2.49184
R3	2.95455	0.00004	0.00001	0.00007	0.00008	2.95463
R4	2.66237	-0.00006	0.00000	-0.00005	-0.00005	2.66231

R5	2.66237	-0.00006	0.00000	-0.00005	-0.00005	2.66232
R6	1.80653	0.00004	0.00000	0.00007	0.00007	1.80660
A1	1.91209	-0.00003	0.00001	-0.00014	-0.00013	1.91196
A2	1.59926	0.00000	0.00000	0.00003	0.00002	1.59928
A3	1.90700	0.00002	0.00000	0.00006	0.00006	1.90706
A4	1.90702	0.00002	0.00000	0.00006	0.00006	1.90708
A5	1.93380	0.00000	0.00000	-0.00002	-0.00001	1.93379
A6	1.93377	-0.00001	0.00000	-0.00002	-0.00002	1.93375
A7	2.11349	-0.00002	-0.00001	-0.00007	-0.00008	2.11341
A8	1.94113	-0.00001	0.00001	-0.00014	-0.00013	1.94099
D1	3.14145	0.00000	0.00000	-0.00001	-0.00001	3.14144
D2	1.17409	0.00000	0.00000	-0.00001	-0.00001	1.17408
D3	-1.17442	0.00000	0.00000	-0.00001	-0.00001	-1.17443
D4	3.14108	0.00000	0.00000	-0.00009	-0.00009	3.14099
D5	-1.19891	0.00002	0.00000	-0.00002	-0.00002	-1.19892
D6	1.19786	-0.00002	0.00000	-0.00016	-0.00016	1.19770

Item	Value	Threshold	Converged?
Maximum Force	0.000060	0.000450	YES
RMS Force	0.000029	0.000300	YES
Maximum Displacement	0.000219	0.001800	YES
RMS Displacement	0.000097	0.001200	YES

Optimisation completed.
-- Stationary point found.

Optimised Parameters
(Angstroms and Degrees)

Name	**Definition**	**Value**	**Derivative Info.**
R1	R(1,2)	1.6316	-DE/DX = 0.0001
R2	R(1,4)	1.3186	-DE/DX = 0.0
R3	R(2,3)	1.5635	-DE/DX = 0.0
R4	R(2,5)	1.4089	-DE/DX = -0.0001
R5	R(2,6)	1.4089	-DE/DX = -0.0001
R6	R(3,7)	0.956	-DE/DX = 0.0
A1	A(2,1,4)	109.5544	-DE/DX = 0.0
A2	A(1,2,3)	91.6307	-DE/DX = 0.0
A3	A(1,2,5)	109.2628	-DE/DX = 0.0
A4	A(1,2,6)	109.2639	-DE/DX = 0.0
A5	A(3,2,5)	110.7986	-DE/DX = 0.0
A6	A(3,2,6)	110.7966	-DE/DX = 0.0
A7	A(5,2,6)	121.0941	-DE/DX = 0.0
A8	A(2,3,7)	111.2183	-DE/DX = 0.0
D1	D(4,1,2,3)	179.9916	-DE/DX = 0.0
D2	D(4,1,2,5)	67.2706	-DE/DX = 0.0
D3	D(4,1,2,6)	-67.2894	-DE/DX = 0.0

```
! D4      D(1,2,3,7)      179.9706         -DE/DX =  0.0         !
! D5      D(5,2,3,7)      -68.6923         -DE/DX =  0.0         !
! D6      D(6,2,3,7)       68.6326         -DE/DX =  0.0         !
 ---------------------------------------------------------------------------
GradGradGradGradGradGradGradGradGradGradGradGradGradGradGradGradGrad
                     Distance matrix (angstroms):
                     1        2        3        4        5
    1  O    0.000000
    2  S    1.631586   0.000000
    3  O    2.291666   1.563481   0.000000
    4  O    1.318579   2.416788   3.514764   0.000000
    5  O    2.482670   1.408863   2.448198   2.911300   0.000000
    6  O    2.482689   1.408867   2.448172   2.911493   2.453566
    7  H    3.191631   2.107192   0.955976   4.345082   2.735439
                     6        7
    6  O    0.000000
    7  H    2.734991   0.000000
 Framework group  C1[X(HO5S)]
 Deg. of freedom    15
                    Standard orientation:
 ---------------------------------------------------------------------
 Center     Atomic     Atomic              Coordinates (Angstroms)
 Number     Number      Type              X           Y           Z
 ---------------------------------------------------------------------
    1          8           0       -0.998745    0.779098   -0.000002
    2         16           0        0.338400   -0.155844    0.000004
    3          8           0        1.270417    1.099471   -0.000308
    4          8           0       -2.072434    0.013695    0.000062
    5          8           0        0.424809   -0.843378   -1.226669
    6          8           0        0.425130   -0.842951    1.226897
    7          1           0        2.192184    0.846024    0.000089
 ---------------------------------------------------------------------
 Rotational constants (GHZ):      4.9851124      2.9229502      2.8393866
 ********************************************************************
          Population analysis using the SCF density.
 ********************************************************************
 Orbital symmetries:
 Alpha Orbitals:
       Occupied  (A)  (A)  (A)  (A)  (A)  (A)  (A)  (A)  (A)  (A)  (A)  (A)
                 (A)  (A)  (A)  (A)  (A)  (A)  (A)  (A)  (A)  (A)  (A)  (A)
                 (A)  (A)  (A)  (A)  (A)
       Virtual   (A)  (A)  (A)  (A)  (A)  (A)  (A)  (A)  (A)  (A)  (A)  (A)
                 ..........................................................
                 (A)  (A)  (A)  (A)  (A)  (A)  (A)
 Beta  Orbitals:
       Occupied  (A)  (A)  (A)  (A)  (A)  (A)  (A)  (A)  (A)  (A)  (A)  (A)
```

	(A)	(A)	(A)	(A)	(A)	(A)	(A)	(A)	(A)	(A)	(A)	(A)	
	(A)	(A)	(A)	(A)									
Virtual	(A)	(A)	(A)	(A)	(A)	(A)	(A)	(A)	(A)	(A)	(A)	(A)	
	…….												
	(A)	(A)	(A)	(A)	(A)	(A)	(A)	(A)					

The electronic state is 2-A.

Alpha occ. Eigenvalues: -92.30767 -20.75923 -20.74370 -20.68762 -20.61370

……

Alpha virt. Eigenvalues: 4.36091 4.42769

Beta occ. Eigenvalues: -92.30778 -20.73795 -20.71788 -20.68774 -20.61375

……

Beta virt. Eigenvalues: 4.25564 4.36486 4.42842

Condensed to atoms (all electrons):

Mulliken atomic charges:

		1
1	O	-0.342111
2	S	1.690990
3	O	-0.718568
4	O	0.017321
5	O	-0.582805
6	O	-0.582829
7	H	0.518003

Sum of Mulliken charges= 0.00000

Atomic charges with hydrogens summed into heavy atoms:

		1
1	O	-0.342111
2	S	1.690990
3	O	-0.200565
4	O	0.017321
5	O	-0.582805
6	O	-0.582829
7	H	0.000000

Sum of Mulliken charges= 0.00000

Atomic-Atomic Spin Densities.

		1	2	3	4	5	6
1	O	0.147132	-0.000791	0.000599	-0.092210	-0.000823	-0.000823
2	S	-0.000791	-0.004033	0.001255	-0.007876	0.000387	0.000386
3	O	0.000599	0.001255	-0.002885	0.000037	0.000000	0.000000
4	O	-0.092210	-0.007876	0.000037	1.058255	0.001056	0.001056
5	O	-0.000823	0.000387	0.000000	0.001056	-0.000835	-0.000111
6	O	-0.000823	0.000386	0.000000	0.001056	-0.000111	-0.000834
7	H	-0.000056	-0.000099	0.000015	-0.000001	0.000000	0.000000

		7
1	O	-0.000056

2	S	-0.000099
3	O	0.000015
4	O	-0.000001
5	O	0.000000
6	O	0.000000
7	H	-0.000805

Mulliken atomic spin densities:

		1
1	O	0.053029
2	S	-0.010771
3	O	-0.000977
4	O	0.960317
5	O	-0.000326
6	O	-0.000325
7	H	-0.000946

Sum of Mulliken spin densities= 1.00000
Electronic spatial extent (au): <R**2>= 501.6880
Charge= 0.0000 electrons
Dipole moment (field-independent basis, Debye):
X= 2.2017 Y= 1.5825 Z= 0.0003 Tot= 2.7114

Isotropic Fermi Contact Couplings

	Atom	a.u.	MegaHertz	Gauss	10(-4) cm-1
1	O(17)	0.05443	-32.99390	-11.77305	-11.00558
2	S(33)	-0.01782	-6.12065	-2.18400	-2.04163
3	O(17)	-0.00572	3.46649	1.23693	1.15630
4	O(17)	0.19289	-116.93121	-41.72396	-39.00405
5	O(17)	-0.00124	0.75137	0.26811	0.25063
6	O(17)	-0.00124	0.75097	0.26796	0.25050
7	H(1)	-0.00058	-2.59900	-0.92739	-0.86693

Center		---- Spin Dipole Couplings ---- 3XX-RR	3YY-RR	3ZZ-RR
1	Atom	-0.354416	-0.380956	0.735372
2	Atom	0.004571	-0.008709	0.004138
3	Atom	0.000491	-0.003155	0.002664
4	Atom	-1.849101	-1.822822	3.671923
5	Atom	-0.004202	0.007074	-0.002872
6	Atom	-0.004207	0.007079	-0.002872
7	Atom	0.003652	-0.001900	-0.001752

		XY	XZ	YZ
1	Atom	-0.118032	0.000045	0.000044
2	Atom	0.021929	-0.000001	-0.000001
3	Atom	-0.000467	0.000006	0.000003

```
   4   Atom       0.024939     0.000159     0.000256
   5   Atom       0.000535    -0.003210     0.002959
   6   Atom       0.000534     0.003210    -0.002962
   7   Atom       0.001100     0.000000     0.000000
-------------------------------------------------------
-------------------------------------------------------------------------------
          Anisotropic Spin Dipole Couplings in Principal Axis System
-------------------------------------------------------------------------------
     Atom           a.u.   MegaHertz   Gauss  10(-4) cm-1       Axes

         Baa    -0.4865    35.200    12.560    11.741  0.6664  0.7456 -0.0001
   1 O(17)  Bbb    -0.2489    18.011     6.427     6.008  0.7456 -0.6664  0.0000
         Bcc     0.7354   -53.211   -18.987   -17.749  0.0000  0.0000  1.0000
……
         Baa    -0.0021    -1.126    -0.402    -0.375 -0.1875  0.9823 -0.0010
   7 H(1)   Bbb    -0.0018    -0.935    -0.334    -0.312 -0.0001  0.0010  1.0000
         Bcc     0.0039     2.061     0.735     0.687  0.9823  0.1875  0.0000
 -------------------------------------------------------------------------------
Test job not archived.
1|1|UNPC-UNK|FOpt|UHF|6-31G(d)|H1O5S1(2)|PCUSER|27-May-2006|0||#T G2 T
EST||HOSO2OO||0,2|O,0.5679550477,1.1322158338,-0.0003124698|S,-0.23882
51102,-0.2859446238,0.000080024|O,-1.619239652,0.4481733496,0.00027275
49|O,1.8661775321,0.9014162169,-0.0003804611|O,-0.0218782771,-0.943759
319,1.2269087561|O,-0.0224697942,-0.9441326513,-1.2266572406|H,-2.3431
5709,-0.1761934587,0.0000689007||Version=IA32W-G03RevC.02|State=2-A|HF
=-772.1723705|S2=0.759025|S2-1=0.|S2A=0.750061|RMSD=2.757e-009|RMSF=3.
702e-005|Dipole=-1.0495502,0.1908095,-0.0001273|PG=C01 [X(H1O5S1)]||@

HE WHO LOVES TO READ, AND KNOWS HOW TO REFLECT,
HAS LAID BY A PERPETUAL FEAST FOR HIS OLD AGE.
-- UNCLE ESEK, "SCRIBNER'S MONTHLY", SEPT. 1880
Job cpu time:  0 days  0 hours  5 minutes 31.0 seconds.
File lengths (MBytes):  RWF=     20 Int=      0 D2E=      0 Chk=      5 Scr=      1
Normal termination of Gaussian 03 at Sat May 27 14:19:41 2006.
```

(4). This section shows the result pattern for the compounded methods such as the G2 described in this part of the appendix. It provides the operating temperature and pressure, the zero potential energy, its thermal energy, the G1, G2 and G2 (with MP2 added) total energies, enthalpies and Gibbs free energies at 0 and 298 Kelvin respectively.

Temperature=	298.150000	Pressure=	1.000000
E(ZPE)=	0.028832	E(Thermal)=	0.034449
E(QCISD(T))=	-773.448241	E(Empiric)=	-0.110710
DE(Plus)=	-0.024310	DE(2DF)=	-0.312497
G1(0 K)=	-773.866926	G1 Energy=	-773.861309

G1 Enthalpy=	-773.860364	G1 Free Energy=	-773.897449
E(Delta-G2)=	-0.026785	E(G2-Empiric)=	0.020520
G2(0 K)=	-773.873191	G2 Energy=	-773.867573
G2 Enthalpy=	-773.866629	G2 Free Energy=	-773.903714
DE(MP2)=	-0.346854		
G2MP2(0 K)=	-773.856452	G2MP2 Energy=	-773.850835
G2MP2 Enthalpy=	-773.849891	G2MP2 Free Energy=	-773.886976

Test job not archived.
1|1|UNPC-UNK|Mixed|G2|G2|H1O5S1(2)|PCUSER|28-May-2006|0||#T G2 TEST||H
OSO2OO||0,2|O,0,0.4953428504,1.2347465571,-0.051160824|S,0,-0.21739575
8,-0.3469634557,0.0602438787|O,0,-1.7015022981,0.2245468047,0.26122498
71|O,0,1.7883395178,1.0882368041,-0.3172781766|O,0,0.1980295066,-0.937
9227912,1.3030577575|O,0,-0.0833142481,-0.9655284814,-1.2388047178|H,0
,-2.0968305021,0.3987841441,-0.6202142687||Version=IA32W-G03RevC.02|St
ate=2-A|MP2/6-311G(d,p)=-773.3938017|QCISD(T)/6-311G(d,p)=-773.4482406
|MP4/6-311G(d,p)=-773.4545576|MP2/6-311+G(d,p)=-773.4154838|MP4/6-311+
G(d,p)=-773.4788677|MP2/6-311G(2df,p)=-773.6921883|MP4/6-311G(2df,p)=-
773.7670545|MP2/6-311+G(3df,2p)=-773.7406554|G1=-773.8669256|G2MP2=-77
……
70,0.00000267|||@
Job cpu time: 0 days 0 hours 52 minutes 55.0 seconds.
File lengths (MBytes): RWF= 4963 Int= 0 D2E= 0 Chk= 11 Scr= 1
Normal termination of Gaussian 03 at Sun May 28 15:25:03 2006.

B-3: Enthalpies and Gibbs Free Energy Computed Using G03 Model Package

Table B-3a: Computed enthalpies of the individual chemical species in Hartrees at 298K

Methods / Species	B3LYP/ 6-311+G(2df,p)	G1	G2	G2MP2	G3	CBS-4	CBS-Q
S^*	-398.130895	-397.652564	-397.65258	-397.644634	-397.958749	-397.649546	-397.654527
H^*	-0.499795	-0.497639	-0.497639	-0.497639	-0.498642	-0.500991	-0.497457
HS^*	-398.765191	-398.282177	-398.283669	-398.276156	-398.592012	-398.285416	-398.286504
HSO^*	-474.002898	-473.416264	-473.419768	-473.41183	-473.777686	-473.420467	-473.431973
O^*	-75.087699	-74.979688	-74.979669	-74.976317	-75.02863	-74.991202	-74.984699
SO^*	-473.411301	-472.825232	-472.826155	-472.815982	-473.184673	-472.840923	-472.838573
OH^*	-75.751415	-75.638837	-75.640603	-75.637619	-75.691601	-75.655185	-75.645593
HO_2^*	-150.944854	-150.722042	-150.724116	-150.718973	-150.8231	-150.738822	-150.734376
$HOSO_2^*$ / HSO_3^*	-624.469192	-623.686972	-623.694125	-623.682487	-624.070633	-623.741859	-623.722747
$HO_2SO_2^*$	-699.58403	-698.719	-698.725	-698.711	-699.230253	-698.783926	-698.765259
$HOSO_2O^*$	-699.630875	-698.726496	-698.729064	-698.714738	-699.233905	-698.757454	-698.764972
$HOSO_2OO^*$ / HSO_5^*	-774.837324	-773.860364	-773.866629	-773.849891	-774.423127	-773.906901	-773.905176

Methods / Species	B3LYP/ 6-311+G(2df,p)	G1	G2	G2MP2	G3	CBS-4	CBS-Q
$HOSO_2OH$	-700.338694	-699.470124	-699.479785	-699.46584	-699.987638	-699.531493	-699.512391
$HOSO_2O_2H$	-775.482818	-774.508231	-774.517271	-774.501183	-775.073204	-774.576485	-774.555132
$HOSO_2ONO^*$	-829.651264	-828.598545	-828.605697	-828.588224	-829.205554	-828.667149	-828.645292
$HOSO_2ONO_2^*$	-904.792909	-903.635695	-903.641761	-903.622122	-904.289843	-903.709151	-903.686794
CH_3O^*	-115.054619	-114.860436	-114.863575	-114.859534	-114.958746	-114.88607	-114.868273
$CH_3O_2^*$	-190.236782	-189.938986	-189.942085	-189.936106	-190.085252	-189.963672	-190.020314
$CH_3OSO_2^*$	-663.926923	-662.842406	-662.849111	-662.829078	-663.39110	-662.961137	-662.934542
$CH_3CO_2^*$	-228.439433	-228.06628	-228.068587	-228.061694	-228.255072	-228.107132	-228.078202
$CH_3COO_2^*$	-303.603179	-303.13525	-303.136561	-303.127374	-303.371528	-303.177623	-303.150345
$CH_3COO_2SO_2^*$	-852.278445	-851.111352	-851.115032	-851.089238	-851.774745	-851.230322	-851.191092
$(CH_3)_3CO^*$	-232.954498	-232.545855	-232.5522	-232.545837	-232.784404	-232.615818	-232.558794
$(CH_3)_3CO_2^*$	-308.140365	-307.6294	-307.635496	-307.627076	-307.915545	-307.696379	-307.647727
CH_3CHO^*	-153.825738	-153.56918	-153.571946	-153.568072	-153.709898	-153.606824	-153.575968
CH_3CHOO^*	-229.103079	-228.744919	-228.748271	-228.742051	-228.934396	-228.79269	-228.757745
H_2S	-399.4065	-398.924012	-398.926906	-398.920274	-399.234573	-398.932908	-398.929686
SO_2	-548.682607	-548.007907	-548.011733	-548.003069	-548.417722	-548.034327	-548.032082

Methods / Species	B3LYP/ 6-311+G(2df,p)	G1	G2	G2MP2	G3	CBS-4	CBS-Q
SO_3	-623.883984	-623.113762	-623.120863	-623.110157	-623.576597	-623.155424	-623.147367
O_2	-150.367638	-150.144583	-150.144905	-150.138759	-150.244899	-150.170421	-150.159327
O_3	-225.478966	-225.17126	-225.170606	-225.163183	-225.314369	-225.184562	-225.184673
H_2O	-76.434455	-76.324561	-76.328274	-76.326231	-76.378264	-76.346171	-76.332724
NO	-129.926508	-129.73583	-129.736663	-129.732916	-129.830603	-129.745884	-129.743765
NO_2	-205.133399	-204.831769	-204.83298	-204.826643	-204.975723	-204.863135	-204.84782
NO_3	-280.302903	-279.885457	-279.886734	-279.877393	-280.07722	-279.927687	-279.910028
N_2O_4	-410.242	-409.680906	-409.680514	-409.668124	-409.96171	-409.728917	-409.704294
N_2O_5	-485.462141	-484.768276	-484.767352	-484.752112	-485.097753	-484.828436	-484.796785
CO	-113.343672	-113.173919	-113.174192	-113.172104	-113.264063	-113.186812	-113.178226
CO_2	-188.635425	-188.357508	-188.357752	-188.353048	-188.496729	-188.379391	-188.367756
OCS	-511.592635	-510.945346	-510.944176	-510.935721	-511.342819	-510.955711	-510.953932
HNO_2	-205.752637	-205.455569	-205.457646	-205.451798	-205.598914	-205.485164	-205.469135
HNO_3	-280.956617	-280.55174	-280.554354	-280.545695	-280.744209	-280.59383	-280.571578
H_2SO_3	-625.107478	-624.327305	-624.332812	-624.321535	-624.789257	-624.370595	-624.356852
H_2SO_4	-700.338689	-699.470122	-699.479783	-699.465837	-699.987635	-699.531476	-699.512388

Methods / Species	B3LYP/ 6-311+G(2df,p)	G1	G2	G2MP2	G3	CBS-4	CBS-Q
NH_3	-56.54581	-56.450961	-56.454838	-56.453372	-56.503215	-56.47102	-56.455314
H_2O_2	-151.61305	-151.358736	-151.361599	-151.357144	-151.459967	-151.386648	-151.371963
HOONO	-280.972798	-280.501499	-280.50275	-280.494657	-280.691848	-280.53709	-280.519753
$HOONO_2$	-356.107233	-355.598437	-355.600023	-355.589764	-355.839747	-355.643557	-355.580079
HCHO	-114.513977	-114.333462	-114.335098	-114.332257	-114.427241	-114.356264	-114.338949
HCOOH	-189.794124	-189.509768	-189.512342	-189.50712	-189.652572	-189.542922	-189.521466
CH_3OH	-115.71223	-115.526307	-115.530605	-115.527525	-115.624923	-115.558975	-115.534036
CH_3OOH	-190.865249	-190.574179	-190.578024	-190.572711	-190.720502	-190.612263	-190.587153
$CH_2(OH)_2$	-190.960963	-190.669747	-190.675205	-190.669968	-190.817361	-190.710906	-190.683694
Cl	-460.164695	-459.67433	-459.674267	-459.664356	-459.988598	-459.674576	-459.6805
Cl_2	-920.413869	-919.442349	-919.438707	-919.422227	-920.067768	-919.44035	-919.456192
H^+	-0.499795	-0.497639	-0.497639	-0.497639	-0.498642	-0.500991	-0.497457
O2-	-150.222598	-150.16194	-150.162047	-150.154214	-150.259627	-150.079968	-150.176497
H_3O^+	-76.693382	-76.584808	-76.588086	-76.586049	-76.638609	-76.604392	-76.591738
OH^-	-75.815936	-75.706701	-75.709473	-75.70667	-75.75694	-75.726583	-75.710964
SO_3^-	-623.975821	-623.195131	-623.201983	-623.188954	-623.659972	-623.250044	-623.232187

Methods / Species	B3LYP/ 6-311+G(2df,p)	G1	G2	G2MP2	G3	CBS-4	CBS-Q
SO_3^{2-}	-623.850814	-623.073863	-623.079987	-623.064691	-623.53523	-623.119706	-623.102867
SO_4^{-}	-699.196508	-698.315256	-698.32212	-698.304977	-698.83234	-698.366635	-698.354261
SO_4^{2-}	-699.134604	-698.263498	-698.27587	-698.259388	-698.78288	-698.331639	-698.309539
SO_5^{-}	-774.376538	-773.392143	-773.399061	-773.380993	-773.955565	-773.445003	-773.439693
HSO_3^{-}	-624.593611	-623.813276	-623.819017	-623.806419	-624.275532	-623.857849	-623.843988
HSO_3^{2-}	-624.400073	-623.585957	-623.598477	-623.585114	-624.05922	-623.653698	-623.6321
HSO_4^{-}	-699.84795	-698.977184	-698.987752	-698.972826	-699.495744	-699.041459	-699.022216
HSO_5^{-}	-774.940866	-773.961026	-773.96914	-773.952105	-774.524844	-774.023641	-774.013583
NO_3^{-}	-280.446353	-280.039688	-280.04077	-280.030567	-280.229962	-280.080464	-280.059147
Cl^{-}	-460.301367	-459.805569	-459.806635	-459.797359	-460.121239	-459.809901	-459.809901
$HOCHSO_3^{-}$	-738.468642	-737.518397	-737.529901	-737.5141	-738.019343	-737.592357	-737.583235
$HOCH_2SO_3^{-}$	-738.970049	-738.187073	-738.198755	-738.183391	-738.483429	-738.056175	-738.056175
COO^{-}	-188.623935	-188.336564	-188.334588	-188.327976	-188.474348	-188.365305	-188.346688
$HCOO^{-}$	-189.252142	-188.968329	-188.967454	-188.961482	-189.10644	-188.998663	-188.976357

Table B-3b: Computed Gibbs free energies of the individual chemical species in Hartrees at 298K

Methods / Species	B3LYP/ 6-311 +G(2df,p)	G1	G2	G2MP2	G3	CBS-4	CBS-Q
S^*	-398.149189	-397.670858	-397.670874	-397.662928	-397.977043	-397.667839	-397.672821
H^*	-0.51281	-0.510654	-0.510654	-0.510654	-0.511657	-0.514005	-0.510472
HS^*	-398.787001	-398.303961	-398.305454	-398.297941	-398.613797	-398.307201	-398.308289
HSO^*	-474.030336	-473.443783	-473.447288	-473.439349	-473.805206	-473.44805	-473.45948
O^*	-75.105012	-74.997001	-74.996982	-74.99363	-75.045943	-75.008515	-75.002011
SO^*	-473.436507	-472.850392	-472.851315	-472.841143	-473.209833	-472.866111	-472.863728
OH^*	-75.771649	-75.659037	-75.660802	-75.657818	-75.7118	-75.675437	-75.665781
HO_2^*	-150.970837	-150.747975	-150.750049	-150.744906	-150.849033	-150.765033	-150.760278
$HOSO_2^*$ / HSO_3^*	-624.502061	-623.719718	-623.726871	-623.715233	-624.105018	-623.774841	-623.755394
$HO_2SO_2^*$	-699.632462	-698.756	-698.761	-698.747	-699.266517	-698.820233	-698.800931
$HOSO_2O^*$	-699.667175	-698.762643	-698.765211	-698.750885	-699.270052	-698.793582	-698.800782
$HOSO_2OO^*$ / HSO_5^*	-774.875294	-773.897449	-773.903714	-773.886976	-774.460212	-773.944132	-773.942072
$HOSO_2OH$	-700.374515	-699.503765	-699.513426	-699.499481	-700.021279	-699.565159	-699.545884
$HOSO_2O_2H$	-775.520399	-774.545523	-774.554563	-774.538475	-775.110496	-774.614228	-774.592193
$HOSO_2ONO^*$	-829.693181	-828.638607	-828.645758	-828.628286	-829.245616	-828.708492	-828.6855

Methods / Species	B3LYP/ 6-311 +G(2df,p)	G1	G2	G2MP2	G3	CBS-4	CBS-Q
$HOSO_2ONO_2^*$	-904.837459	-903.679644	-903.685709	-903.66607	-904.333791	-903.753653	-903.731909
CH_3O^*	-115.081544	-114.88733	-114.890469	-114.886428	-114.98564	-114.913057	-114.895147
$CH_3O_2^*$	-190.267318	-189.969309	-189.972407	-189.966429	-190.115574	-189.99428	-190.050122
$CH_3OSO_2^*$	-663.951507	-662.911583	-662.922394	-662.901533	-663.421985	-662.998721	-662.969639
$CH_3CO_2^*$	-228.470597	-228.099888	-228.102195	-228.095302	-228.28868	-228.140054	-228.111704
$CH_3COO_2^*$	-303.639427	-303.171085	-303.172396	-303.163209	-303.407363	-303.213544	-303.185981
$CH_3COO_2SO_2^*$	-852.322322	-851.156378	-851.160059	-851.134266	-851.819731	-851.275582	-851.236095
$(CH_3)_3CO^*$	-232.991623	-232.583118	-232.589464	-232.5831	-232.821668	-232.652342	-232.595863
$(CH_3)_3CO_2^*$	-308.180312	-307.669216	-307.675313	-307.666892	-307.955362	-307.736147	-307.687296
CH_3CHO^*	-153.855493	-153.599092	-153.601857	-153.597984	-153.73981	-153.636664	-153.605799
CH_3CHOO^*	-229.135954	-228.777478	-228.780829	-228.77461	-228.966954	-228.825075	-228.790178
H_2S	-399.429848	-398.947322	-398.950215	-398.943583	-399.257882	-398.956215	-398.952993
SO_2	-548.710821	-548.036025	-548.039852	-548.031187	-548.445841	-548.062432	-548.032082
SO_3	-623.914899	-623.144555	-623.151656	-623.14095	-623.60739	-623.186194	-623.178087
O_2	-150.390914	-150.167794	-150.168116	-150.16197	-150.268109	-150.193749	-150.182519
O_3	-225.505981	-225.198132	-225.197478	-225.190055	-225.34124	-225.211948	-225.211499

Methods / Species	B3LYP/ 6-311 +G(2df,p)	G1	G2	G2MP2	G3	CBS-4	CBS-Q
H_2O	-76.455879	-76.345938	-76.349651	-76.347607	-76.39964	-76.367595	-76.354078
NO	-129.9498	-129.759089	-129.759922	-129.756174	-129.853861	-129.769413	-129.76701
NO_2	-205.161287	-204.859567	-204.860778	-204.854442	-205.003522	-204.891093	-204.875577
NO_3	-280.33444	-279.915545	-279.916822	-279.907481	-280.107308	-279.958167	-279.939101
N_2O_4	-410.279	-409.717722	-409.71733	-409.704939	-409.998525	-409.765826	-409.740761
N_2O_5	-485.501225	-484.803956	-484.803032	-484.787792	-485.133432	-484.86793	-484.836521
CO	-113.366094	-113.196321	-113.196595	-113.194507	-113.286466	-113.20924	-113.200622
CO_2	-188.659674	-188.381742	-188.381986	-188.377282	-188.520963	-188.403736	-188.391954
OCS	-511.618919	-510.971683	-510.970512	-510.962058	-511.369155	-510.981977	-510.980206
HNO_2	-205.780827	-205.483588	-205.485665	-205.479817	-205.626933	-205.513493	-205.497095
HNO_3	-280.98685	-280.581768	-280.584381	-280.575722	-280.774236	-280.624288	-280.60151
H_2SO_3	-625.141307	-624.360479	-624.365987	-624.354709	-624.822431	-624.403514	-624.389928
H_2SO_4	-700.374512	-699.503766	-699.513427	-699.499481	-700.021279	-699.565144	-699.545881
NH_3	-56.568694	-56.473803	-56.477681	-56.476214	-56.526057	-56.493932	-56.478148
H_2O_2	-151.639507	-151.38514	-151.388003	-151.383548	-151.486371	-151.414479	-151.398377
HOONO	-281.004354	-280.532984	-280.534234	-280.526142	-280.723332	-280.569318	-280.551097

Methods / Species	B3LYP/ 6-311 +G(2df,p)	G1	G2	G2MP2	G3	CBS-4	CBS-Q
$HOONO_2$	-356.14096	-355.631945	-355.63353	-355.623272	-355.87325	-355.678006	-355.614289
HCHO	-114.539445	-114.358892	-114.360528	-114.357687	-114.452671	-114.381706	-114.364373
HCOOH	-189.822319	-189.537954	-189.540529	-189.535306	-189.680758	-189.571171	-189.5496
CH_3OH	-115.739312	-115.553322	-115.55762	-115.55454	-115.651937	-115.585995	-115.560998
CH_3OOH	-190.894887	-190.603768	-190.607614	-190.6023	-190.750091	-190.643699	-190.61667
$CH_2(OH)_2$	-191.020281	-190.699855	-190.705313	-190.700077	-190.84747	-190.741453	-190.713591
Cl	-460.182732	-459.692368	-459.692305	-459.682394	-460.006636	-459.692614	-459.698538
Cl_2	-920.439208	-919.467647	-919.464005	-919.447525	-920.093066	-919.465674	-919.481475
H^+	-0.51281	-0.510654	-0.510654	-0.510654	-0.511657	-0.514005	-0.510472
O2-	-150.246155	-150.184976	-150.185083	-150.17725	-150.282663	-150.104135	-150.19952
H_3O^+	-76.715335	-76.606731	-76.610009	-76.607972	-76.660531	-76.626532	-76.613732
OH^-	-75.835497	-75.726253	-75.729025	-75.726222	-75.776493	-75.745318	-75.730515
SO_3^-	-624.007593	-623.226751	-623.233603	-623.220574	-623.691592	-623.281605	-623.263739
SO_3^{2-}	-623.882171	-623.104986	-623.11111	-623.095814	-623.566353	-623.150717	-623.133917
SO_4^-	-699.230247	-698.332302	-698.344674	-698.328191	-698.851711	-698.400215	-698.387916
SO_4^{2-}	-699.167243	-698.295918	-698.30829	-698.291808	-698.8153	-698.363828	-698.34184

Methods / Species	B3LYP/ 6-311 +G(2df,p)	G1	G2	G2MP2	G3	CBS-4	CBS-Q
SO_5^-	-774.414449	-773.42873	-773.435648	-773.41758	-773.992152	-773.481559	-773.476097
HSO_3^-	-624.625501	-623.844672	-623.850412	-623.837815	-624.306927	-623.889102	-623.875298
HSO_3^{2-}	-624.431838	-623.61977	-623.63229	-623.618927	-624.093033	-623.68735	-623.66573
HSO_4^-	-699.880952	-699.009947	-699.020514	-699.005588	-699.528507	-699.075367	-699.054845
HSO_5^-	-774.978408	-773.998839	-774.006953	-773.989918	-774.562657	-774.061711	-774.051287
NO_3^-	-280.475964	-280.069188	-280.070271	-280.060067	-280.259462	-280.110372	-280.088588
Cl^-	-460.31875	-459.822953	-459.824019	-459.814742	-460.138623	-459.827285	-459.827285
$HOCHSO_3^-$	-738.507562	-737.55725	-737.568754	-737.552953	-738.051841	-737.631372	-737.620444
$HOCH_2SO_3^-$	-739.008364	-738.223568	-738.23525	-738.219886	-738.515792	-738.095058	-738.095058
COO^-	-188.651794	-188.36442	-188.362444	-188.355832	-188.502204	-188.393206	-188.374526
$HCOO^-$	-189.279869	-188.995999	-188.995124	-188.989152	-189.13411	-189.02636	-189.004006

Table B-3c: Calculated and experimental enthalpies of the gas-phase reactions (kJ mol^{-1}) at 298K

S/N	Gas-phase Reactions	B3LYP	G1	G2	G2MP2	G3	CBS-4	CBS-Q	Experiment
1	$H_2S + OH^* \rightarrow H_2O + SH^*$	-109.6	-115.2	-116.7	-116.8	-115.8	-114.2	-115.4	-117.6[†]
2	$HS^* + O_2 \rightarrow SO^* + OH^*$	-78.5	-98.0	-100.3	-101.6	-103.4	-105.7	-100.7	-98.7[†]
3	$HS^* + O_2 \rightarrow SO_2 + H^*$	-130.2	-206.9	-212.1	-225.3	-208.6	-208.7	-219.8	-212.8[†]
4	$HS^* + O_3 \rightarrow HSO + O_2$	- 331.8	-282.0	-289.9	-292.1	-305.1	-317.5	-315.4	-289.7[†]
5	$HS^* + O_3 \rightarrow OH^* + SO^* + O^*$	-16.4	25.4	20.6	24.7	3.9	-45.5	6.1	7.8[†]
6	$HSO^* + O_2 \rightarrow HO_2^* + SO^*$	37.8	35.6	37.8	41.1	38.9	29.3	48.2	23.6[†]
7	$HSO^* + O_3 \rightarrow OH^* + SO^* + O_2$	-127.3	-55.5	-55.9	-45.6	-76.5	-161.5	-70.5	-94.4[†]
8	$SO_2 + O^* \rightarrow SO_3$	-298.5	-331.3	-339.9	-343.3	-342.0	-341.0	-342.9	-348.1[†];-348.5[‡]
9	$SO_2 + OH^* \rightarrow HOSO_2^*$	-92.3	-105.6	-109.7	-109.7	101.6	-137.4	-118.3	-127.5[†];-154.8[‡]
10	$HOSO_2^* + O_2 \rightarrow HO_2^* + SO_3$	21.0	-11.2	-15.6	-20.7	-221.0	47.4	0.9	3.9[†]
11	$SO_2 + HO_2^* \rightarrow OH^* + SO_3$	-20.8	-59.5	-67.3	-67.5	-71.9	-98.4	-69.6	-74.1[†];-80.8[‡]
12	$SO_2 + HO_2^* \rightarrow HO_2SO_2^*$	114.0	28.8	28.5	29.0	27.8	-28.3	3.2	-29.3[‡]
13	$HO_2SO_2^* \rightarrow HO^* + SO_3$	-134.9	-88.2	-95.7	-96.6	-99.6	-70.1	-72.7	-50.2[‡]
14	$SO_2 + CH_3O^* \rightarrow CH_3OSO_2^*$	-498.1	68.1	68.8	88.0	38.4	-107.0	-89.8	-100.4[‡]
15	$SO_2 + CH_3O_2^* \rightarrow CH_3O^* + SO_3$	-50.4	-71.7	-80.4	-80.1	-85.0	-114.2	96.5	-90.7[†];-113.0[‡]
16	$SO_2 + CH_3CHOO^* \rightarrow CH_3CHO^* + SO_3$	199.4	183.5	176.4	175.6	172.3	170.1	174.6	NA

S/N	Gas-phase Reactions	B3LYP	G1	G2	G2MP2	G3	CBS-4	CBS-Q	Experiment
17	$SO_2 + (CH_3)_3CO_2^* \rightarrow (CH_3)_3CO^* + SO_3$	-40.7	-58.6	-67.8	-67.9	-72.8	-106.4	-69.2	-108.8[‡]
18	$SO_2 + CH_3COO_2^* \rightarrow CH_3CO_2^* + SO_3$	-98.8	-96.8	-108.1	-108.7	-111.4	-132.9	-113.3	-134.4[†];-138.1[‡]
19	$SO_2 + CH_3COO_2^* \rightarrow CH_3COO_2SO_2^*$	19.3	83.5	87.3	108.2	38.1	-48.24	-22.8	-154.8[‡]
20	$SO_2 + O_3 \rightarrow O_2 + SO_3$	-236.4	-207.9	-0.1	-217.0	-234.7	-280.8	-236.1	-241.6[†];-241.9[‡]
21	$SO_2 + NO_2 \rightarrow NO + SO_3$	14.5	-26.0	-33.6	-35.1	-36.1	-10.1	-29.5	-41.7[†];-41.8[‡]
22	$SO_2 + NO_3 \rightarrow NO_2 + SO_3$	-83.7	-137.0	-145.4	-147.9	-150.6	-148.5	-139.4	-138.4[†];-137.2[‡]
23	$SO_2 + N_2O_5 \rightarrow N_2O_4 + SO_3$	49.3	-48.5	-58.5	-60.7	-59.9	-56.65	-59.9	-101.0[†];-102.9[‡]
24	$OCS + O^* \rightarrow CO + SO$	-196.0	-194.6	-200.9	-199.7	-202.9	-212.2	-205.2	-185.5[†]
25	$OCS + OH^* \rightarrow CO_2 + HS$	-148.5	-145.7	-147.7	-146.7	-142.6	-141.5	-143.7	-120.7[†]
26	$SO^* + O^* \rightarrow SO_2$	-482.1	-532.9	-540.61	-553.4	-536.7	-530.9	-548.2	-551.0[†]
27	$SO^* + SO^* \rightarrow S + SO_2$	23.9	-26.3	-31.51	-41.3	-18.7	-5.3	-24.9	-29.6[†]
28	$SO^* + OH^* \rightarrow H + SO_2$	-51.7	-108.9	-111.9	-123.7	-105.3	-103.0	-119.1	-123.2[†]
29	$SO^* + SO_3 \rightarrow SO_2 + SO_2$	-183.6	-201.7	-200.7	-210.0	-194.7	-189.8	-205.3	-202.9[†]
30	$SO^* + NO_2 \rightarrow NO + SO_2$	-169.1	-227.7	-234.4	-245.1	-230.9	-199.9	-234.9	-244.7[†]
31	$SO^* + O_2 \rightarrow O^* + SO_2$	22.7	-46.7	-53.4	-64.7	-44.1	-37.2	-49.6	-52.6[†]
32	$SO^* + O_2 \rightarrow SO_3$	-275.8	-377.9	-393.3	-408.1	-386.0	-378.3	-392.4	-400.7[†]
33	$SO^* + O_3 \rightarrow O^* + SO_3$	-213.8	-254.6	-272.5	-281.7	-278.8	-318.1	-285.7	-294.2[†]

S/N	Gas-phase Reactions	B3LYP	G1	G2	G2MP2	G3	CBS-4	CBS-Q	Experiment
34	$SO^* + O_3 \rightarrow SO_2 + O_2$	-420.0	-409.6	-419.8	-427.1	-429.5	-470.7	-441.5	-444.5[†]
35	$HOSO_2^* + O_2 \rightarrow HOSO_2OO^*$	-1.3	-75.6	-72.5	-75.2	-282.5	14.1	-60.7	-66.9[‡]
36	$HOSO_2OO^* + NO \rightarrow HOSO_2O^* + NO_2$	-1.2	99.6	108.3	108.8	115.8	84.5	94.9	-104.6[‡]
37	$HOSO_2OO^* + NO_2 \rightarrow HOSO_2O^* + NO_3$	97.0	210.5	220.1	221.6	230.3	222.9	204.8	-8.4[‡]
38	$HOSO_2OO^* + HO_2 \rightarrow HOSO_2O_2H + O_2$	-179.3	-184.9	-187.5	-186.6	-188.7	-265.7	-196.7	-179.9[‡]
39	$2HOSO_2OO^* \rightarrow 2HOSO_2O^* + O_2$	118.8	323.3	341.9	345.4	350.6	337.3	317.9	-92.0[‡]
40	$HOSO_2O^* + NO \rightarrow HOSO_2ONO^*$	-246.5	-357.6	-367.5	-369.1	-370.3	-430.1	-358.5	-108.8[‡]
41	$HOSO_2O^* + NO_2 \rightarrow HOSO_2ONO_2^*$	-75.2	-203.3	-209.3	-212.0	-210.6	-232.5	-194.3	-92.0[‡]
42	$HOSO_2O^* + HO_2 \rightarrow HOSO_2OH + O_2$	-342.9	-436.3	-450.3	-448.7	-460.9	-539.9	-452.6	-238.5[‡]
43	$HOSO_2ONO^* + H_2O \rightarrow H_2SO_4 + HNO_2$	-14.7	-6.8	-9.1	-8.4	-7.2	-8.7	-9.2	NA
44	$HOSO_2ONO_2^* + H_2O \rightarrow H_2SO_4 + HNO_3$	-178.4	-161.8	-168.3	-165.9	-167.3	-183.7	-169.2	NA
45	$SO_3 + O^* \rightarrow SO_2 + O_2$	-206.3	-155.0	-147.3	-145.3	-150.7	-152.6	-155.8	-150.3[†];-150.2[‡]
46	$SO_3 + H_2O \rightarrow H_2SO_4$	-53.2	-83.5	-80.5	-77.3	-86.1	-78.4	-84.8	-92.6[†];-102.9[‡]

In all the reactions involving O_2 in air, the O_2 is the dominant reactant. [†]Enthalpies for gas-phase reactions were determined from individual enthalpies of formation obtained from Yaws (1999) and Lide (2002). All reactions were obtained courtesy of [‡]Calvert *et al*, 1978; Eggleton and Cox (1978); Hegg and Hobbs (1980); Britton and Clarke (1980); Moller (1980); Warneck (1988); Eisele and Tanner (1991); Pienaar and Helas (1996); Seinfeld and Pandis (1998); Warneck (1999).

Table B-3d: Calculated and experimental enthalpies of the aqueous-phase reactions (kJ mol^{-1}) at 298K

S/N	Aqueous-phase Reactions	B3LYP	G1	G2	G2MP2	G3	CBS-4	CBS-Q	Experiment
1	$SO_2 + H_2O \rightarrow H_2SO_3$	25.1	13.6	18.9	20.4	17.667	26.0	20.9	NA
2	$SO_3^{2-} + O_3 \rightarrow O_2 + SO_4^{2-}$	-452.8	-427.9	-446.8	-447.1	-467.812	-519.3	-476.1	-416.5[†]
3	$SO_3^{2-} + O_2 \rightarrow O^* + SO_4^{2-}$	-10.1	-65.0	-80.5	-84.7	-82.391	-85.9	-84.1	-24.6[†]
4	$HSO_3^- + OH^* \rightarrow OH^- + HSO_3^*$	157.3	153.4	-147.1	144.1	366.415	117.1	146.7	-28.2[†]
5	$HSO_3^* + O_2 \rightarrow HSO_5^*$	-1.3	-75.6	-72.5	-75.2	-282.5	14.1	-60.7	NA
6	$HSO_3^- + HSO_5^* \rightarrow HSO_3^* + HSO_5^-$	54.8	67.3	58.8	57.0	270.9	-2.0	33.7	NA
7	$HSO_3^- + HSO_5^- + H^+ \rightarrow 2SO_4^{2-} + 3H^+$	697.5	661.7	633.1	641.9	623.115	567.7	639.6	NA
8	$HSO_3^- + H_2O \rightarrow SO_3^{2-} + H_3O^+$	1270.4	1258.1	1258.2	1265.3	1260.127	1260.0	1265.8	NA
9	$HCHO + HSO_3^- \rightarrow HOCH_2SO_3^-$	361.1	-105.9	-117.2	-117.4	575.9	414.7	332.8	NA
10	$HCHO + SO_3^{2-} + H^+ \rightarrow HOCH_2SO_3^-$	-276.9	-740.7	-751.0	-758.3	-58.6	-208.0	-306.9	NA
11	$HOCH_2SO_3^- + OH^- \rightarrow CH_2(OH)_2 + SO_3^{2-}$	-67.7	394.3	401.8	408.0	-294.6	-125.6	-51.0	NA
12	$OH^* + HOCH_2SO_3^- \rightarrow HOCHSO_3^- + H_2O$	-476.9	-44.8	-49.4	-50.7	-584.4	-596.4	-562.4	NA
13	$HOCHSO_3^- + O_2 + H_2O \rightarrow HCOOH + HSO_3^- + HO_2^*$	1154.1	1604.5	1618.5	1617.0	933.1	1137.3	1177.3	NA
14	$O_3 + HSO_3^- \rightarrow HSO_4^- + O_2$	-375.5	-360.3	-375.5	-372.8	-395.8	-444.9	-401.4	-403.8[†]
15	$O_3 + SO_2 + H_2O \rightarrow HSO_4^- + O_2 + H^+$	-313.4	-303.7	-314.2	-306.5	-338.5	-388.1	-340.1	NA
16	$HSO_3^- + H_2O_2 \rightarrow HSO_4^- + H_2O$	-198.9	-340.6	-355.5	-355.7	-363.7	-375.8	-364.9	-366.6[†]

S/N	Aqueous-phase Reactions	B3LYP	G1	G2	G2MP2	G3	CBS-4	CBS-Q	Experiment
17	$HSO_3^- + CH_3OOH \rightarrow HSO_4^- + CH_3OH$	-266.0	-304.7	-318.5	-318.3	-327.2	-342.2	-328.5	NA
18	$HSO_3^- + HOONO_2 \rightarrow HSO_4^- + NO_3^- + H^+$	-244.8	-269.9	-281.3	-275.3	-286.4	-319.0	-406.3	NA
19	$HSO_3^- + HOONO \rightarrow HSO_4^- + HNO_2$	-89.7	-309.8	-324.6	-324.4	-334.2	-345.7	-335.0	NA
20	$HSO_3^- + HSO_5^- \rightarrow 2HSO_4^-$	-423.8	-472.8	-491.9	-491.3	-501.8	-528.9	-490.6	NA
21	$HSO_3^{2-} + Cl_2 \rightarrow SO_3^- + 2Cl^- + H^+$	-694.2	-723.6	-723.9	-719.3	-719.7	-726.7	-685.7	NA
22	$OH^* + HSO_3^- \rightarrow SO_3^- + H_2O$	-171.3	-177.4	-185.5	-186.8	-186.7	-218.4	-197.8	NA
23	$OH^* + SO_3^{2-} \rightarrow SO_3^- + OH^-$	-497.6	-496.6	-501.1	-507.6	-499.1	-529.7	-511.2	NA
24	$OH^* + HSO_5^- \rightarrow SO_5^- + H_2O$	-311.7	-306.8	-308.7	-308.5	-308.2	-295.0	-297.3	NA
25	$OH^* + HSO_4^- \rightarrow SO_4^- + H_2O$	-83.0	-64.5	-57.9	-54.5	-61.1	-42.4	-50.4	NA
26	$SO_3^- + O_2 \rightarrow SO_5^-$	-86.9	-137.7	-137.0	-139.9	-133.1	-64.4	-126.5	NA
27	$SO_5^- + HSO_3^- \rightarrow HSO_5^- + SO_3^-$	140.4	129.3	123.3	-121.7	121.5	76.6	99.5	NA
28	$SO_5^- + HSO_3^- \rightarrow SO_4^{2-} + SO_4^- + H^+$	0.1	0.1	0.1	0.1	0.1	0.1	0.1	NA
29	$SO_5^- + SO_3^{2-} + H^+ \rightarrow HSO_5^- + SO_3^-$	-497.6	-505.4	-504.8	-519.2	-513.0	-546.1	-540.2	NA
30	$SO_5^- + SO_3^{2-} \rightarrow SO_4^{2-} + SO_4^-$	-272.4	-296.0	-312.3	-311.6	-326.7	-350.7	-318.3	NA
31	$SO_5^- + SO_5^- \rightarrow 2SO_4^- + O_2$	-19.9	24.1	23.6	34.9	4.1	-35.9	30.3	NA
32	$SO_5^- + HO_2^* \rightarrow HSO_5^- + O_2$	33.8	22.5	23.0	23.9	23.4	-26.9	3.0	NA
33	$SO_5^- + O_2^- + H^+ \rightarrow HSO_5^- + O_2$	-550.2	-141.5	-139.5	-152.3	-146.8	-441.4	-155.6	NA
34	$SO_4^- + HSO_3^- \rightarrow HSO_4^- + SO_3^-$	-88.4	-115.0	-127.6	-132.3	-125.6	-176.0	-147.4	NA

S/N	Aqueous-phase Reactions	B3LYP	G1	G2	G2MP2	G3	CBS-4	CBS-Q	Experiment
35	$SO_4^- + O_2^- \rightarrow SO_4^{2-} + O_2$	-218.3	340.7	325.4	160.3	168.5	-145.6	162.5	NA
36	$SO_4^- + SO_3^{2-} \rightarrow SO_4^{2-} + SO_3^-$	-165.7	-182.5	-198.9	-206.6	-197.7	-250.3	-222.1	NA
37	$SO_4^- + NO_3^- \rightarrow SO_4^{2-} + NO_3$	539.2	540.8	525.9	521.9	530.9	493.0	508.9	NA
38	$SO_4^- + OH^- \rightarrow SO_4^{2-} + OH^*$	331.9	314.1	302.3	301.0	301.4	279.3	289.1	NA
39	$SO_4^- + H_2O \rightarrow SO_4^{2-} + H^+ + OH^*$	0.3	0.2	0.2	0.2	0.2	0.2	0.2	NA
40	$SO_4^- + H_2O_2 \rightarrow HSO_4^- + HO_2^*$	44.0	-66.3	-73.9	-77.9	-69.7	-70.9	-79.7	NA
41	$SO_4^- + HCOOH \rightarrow HSO_4^- + H^+ + COO^-$	49.8	35.8	32.4	35.9	42.5	4.7	24.6	NA
42	$SO_4^- + HCOO^- \rightarrow HSO_4^- + COO^-$	-61.0	-79.2	-86.0	-90.2	-82.2	-108.9	-100.5	NA
43	$SO_4^- + CH_2(OH)_2 + O_2 \rightarrow HSO_4^- + HO_2^* + HCOOH$	-162.3	-208.5	-215.2	-223.7	-201.7	-197.6	-212.1	NA
44	$SO_4^- + CH_2(OH)_2 + O_2 \rightarrow HSO_4^- + HO_2^* + HCHO + O^*$	343.0	307.7	303.5	297.6	314.8	315.6	307.3	NA
45	$SO_4^- + Cl^- \rightarrow SO_4^{2-} + Cl$	521.4	480.5	468.9	468.8	-478.1	447.2	457.2	NA
46	$H_2SO_4 + NO_3^- \rightarrow HSO_4^- + HNO_3$	-51.3	-50.2	-56.6	-58.1	-53.7	-61.3	-58.4	-152.2[†]

[†]Enthalpies for aqueous-phase reactions were determined from individual enthalpies of formation obtained from Yaws (1999) and Lide (2002). All reactions were obtained courtesy of Beilke and Gravenhorst (1978); Moller (1980); Britton and Clarke (1980); Viggiano *et al* (1982); Breytenbach *et al* (1984); Eisele and Tanner (1991); Herrmann *et al* (2000); Warneck (1999); Grgic and Bercic (2001).

Table B-3e: Calculated and experimental Gibbs free energies of the gas-phase reactions (kJ mol^{-1}) at 298K

S/N	Gas-phase Reactions	B3LYP	G1	G2	G2MP2	G3	CBS-4	CBS-Q	Experiment
1	$H_2S + OH^* \rightarrow H_2O + SH^*$	-108.7	-114.3	-115.8	-115.9	-114.9	-113.3	-114.5	NA
2	$HS^* + O_2 \rightarrow SO^* + OH^*$	-79.4	-98.9	-101.2	-102.5	-104.3	-106.6	-101.6	NA
3	$HS^* + O_2 \rightarrow SO_2 + H^*$	-120.0	-196.7	-202.0	-215.1	-198.5	-198.2	-135.9	NA
4	$HS^* + O_3 \rightarrow HSO + O_2$	-336.8	-287.5	-295.3	-297.5	-310.5	-322.0	-320.9	NA
5	$HS^* + O_3 \rightarrow OH^* + SO^* + O^*$	-53.0	-11.4	-16.2	-12.1	-32.9	-81.2	-30.8	NA
6	$HSO^* + O_2 \rightarrow HO_2^* + SO^*$	36.5	34.7	36.9	40.1	37.9	28.0	47.2	NA
7	$HSO^* + O_3 \rightarrow OH^* + SO^* + O_2$	-164.8	-92.7	-93.1	-82.8	-113.7	-197.7	-107.8	NA
8	$SO_2 + O^* \rightarrow SO_3$	-260.1	-292.8	-301.5	-304.9	-303.5	-302.6	-378.1	$-302.8^{\dagger}$
9	$SO_2 + OH^* \rightarrow HOSO_2^*$	-51.4	-64.7	-68.8	-68.9	138.1	-97.1	-151.1	NA
10	$HOSO_2^* + O_2 \rightarrow HO_2^* + SO_3$	19.0	-13.2	-17.6	-22.7	-218.7	45.6	-1.2	NA
11	$SO_2 + HO_2^* \rightarrow OH^* + SO_3$	-12.8	-51.4	-59.2	-59.5	-63.8	-89.7	-135.2	NA
12	$SO_2 + HO_2^* \rightarrow HO_2SO_2^*$	129.2	73.5	75.9	76.4	74.5	19.0	-22.5	NA
13	$HO_2SO_2^* \rightarrow HO^* + SO_3$	-142.0	-125.0	-135.1	-135.9	-138.3	-108.7	-112.7	NA
14	$SO_2 + CH_3O^* \rightarrow CH_3OSO_2^*$	-417.8	30.9	20.8	42.2	24.9	-61.0	-111.4	NA
15	$SO_2 + CH_3O_2^* \rightarrow CH_3O^* + SO_3$	-48.1	-69.7	-78.4	-78.1	-83.0	-111.7	23.6	NA
16	$SO_2 + CH_3CHOO^* \rightarrow CH_3CHO^* + SO_3$	200.5	183.4	176.4	175.6	172.2	169.7	100.8	NA

S/N	Gas-phase Reactions	B3LYP	G1	G2	G2MP2	G3	CBS-4	CBS-Q	Experiment
17	$SO_2 + (CH_3)_3CO_2^* \rightarrow (CH_3)_3CO^* + SO_3$	-40.4	-58.9	-68.2	-68.2	-73.1	-104.9	-143.3	NA
18	$SO_2 + CH_3COO_2^* \rightarrow CH_3CO_2^* + SO_3$	-92.5	-98.0	-109.2	-109.9	-112.6	-132.0	-188.3	NA
19	$SO_2 + CH_3COO_2^* \rightarrow CH_3COO_2SO_2^*$	73.3	133.2	137.0	157.9	87.9	1.0	-47.3	NA
20	$SO_2 + O_3 \rightarrow O_2 + SO_3$	-233.7	-205.3	-0.1	-214.5	-232.1	-277.2	-307.3	-234.2[†]
21	$SO_2 + NO_2 \rightarrow NO + SO_3$	19.5	-21.1	-28.7	-30.2	-31.2	-5.5	-98.3	-39.5[†]
22	$SO_2 + NO_3 \rightarrow NO_2 + SO_3$	-81.2	-138.0	-146.4	-148.9	-151.7	-148.8	-216.6	NA
23	$SO_2 + N_2O_5 \rightarrow N_2O_4 + SO_3$	47.7	-58.5	-68.5	-70.6	-70.0	-56.9	-131.9	-88.2[†]
24	$OCS + O^* \rightarrow CO + SO$	-206.6	-204.9	-211.1	-209.9	-213.2	-222.8	-215.6	NA
25	$OCS + OH^* \rightarrow CO_2 + HS$	-147.3	-144.4	-147.4	-145.3	-141.3	-140.5	-142.5	NA
26	$SO^* + O^* \rightarrow SO_2$	-444.5	-495.3	-502.9	-515.7	-499.0	-493.1	-436.7	NA
27	$SO^* + SO^* \rightarrow S + SO_2$	34.1	-16.0	-21.3	-31.1	-8.5	5.1	59.2	NA
28	$SO^* + OH^* \rightarrow H + SO_2$	-40.6	-97.8	-100.8	-112.6	-94.2	-91.6	-34.3	NA
29	$SO^* + SO_3 \rightarrow SO_2 + SO_2$	-184.4	-202.4	-201.5	-210.8	-195.5	-190.5	-58.7	NA
30	$SO^* + NO_2 \rightarrow NO + SO_2$	-165.0	-223.6	-230.2	-241.0	-226.7	-196.0	-157.0	NA
31	$SO^* + O_2 \rightarrow O^* + SO_2$	30.4	-39.0	-45.7	-57.0	-36.3	-29.1	31.9	NA
32	$SO^* + O_2 \rightarrow SO_3$	-229.7	-331.8	-347.2	-361.9	-339.9	-331.7	-346.2	NA
33	$SO^* + O_3 \rightarrow O^* + SO_3$	-203.3	-244.3	-262.1	-271.4	-268.5	-306.3	-275.3	NA
34	$SO^* + O_3 \rightarrow SO_2 + O_2$	-418.1	-407.7	-417.9	-425.2	-427.6	-467.7	-365.9	NA

S/N	Gas-phase Reactions	B3LYP	G1	G2	G2MP2	G3	CBS-4	CBS-Q	Experiment
35	$HOSO_2^* + O_2 \rightarrow HOSO_2OO^*$	46.4	-26.1	-22.9	-25.7	-228.6	64.2	-10.9	NA
36	$HOSO_2OO^* + NO \rightarrow HOSO_2O^* + NO_2$	-8.8	90.1	98.8	99.3	106.3	75.8	85.9	NA
37	$HOSO_2OO^* + NO_2 \rightarrow HOSO_2O^* + NO_3$	91.8	207.0	216.5	218.1	226.8	219.2	204.2	NA
38	$HOSO_2OO^* + HO_2 \rightarrow HOSO_2O_2H + O_2$	-171.1	-178.3	-180.9	-180.0	-182.1	-259.4	-190.0	NA
39	$2HOSO_2OO^* \rightarrow 2HOSO_2O^* + O_2$	66.5	267.3	285.9	289.4	294.6	281.9	262.7	NA
40	$HOSO_2O^* + NO \rightarrow HOSO_2ONO^*$	-200.1	-306.9	-316.7	-318.3	-319.5	-382.0	-309.0	NA
41	$HOSO_2O^* + NO_2 \rightarrow HOSO_2ONO_2^*$	-23.6	-150.8	-156.8	-159.5	-158.1	-181.1	-145.9	NA
42	$HOSO_2O^* + HO_2 \rightarrow HOSO_2OH + O_2$	-334.5	-422.6	-436.6	-434.9	-447.1	-525.9	-439.4	NA
43	$HOSO_2ONO^* + H_2O \rightarrow H_2SO_4 + HNO_2$	-16.5	-7.4	-9.7	-8.9	-7.8	-6.7	-8.9	NA
44	$HOSO_2ONO_2^* + H_2O \rightarrow H_2SO_4 + HNO_3$	-178.6	-157.4	-164.0	-161.5	-163.0	-179.0	-161.2	NA
45	$SO_3 + O^* \rightarrow SO_2 + O_2$	-214.9	-163.5	-155.8	-153.8	-159.2	-161.4	-90.6	-160.7[†]
46	$SO_3 + H_2O \rightarrow H_2SO_4$	-9.8	-34.9	-31.8	-28.7	-37.4	-29.8	-36.0	-53.8[†]

[†]Free energies gas-phase reactions were determined from individual free energies of formation obtained from Yaws (1999) and Lide (2002).

Table B-3f: Calculated and experimental Gibb's free energies of the aqueous-phase reactions (kJ mol^{-1}) at 298K

S/N	Aqueous-phase Reactions	B3LYP	G1	G2	G2MP2	G3	CBS-4	CBS-Q	Experiment
1	$SO_2 + H_2O \rightarrow H_2SO_3$	66.7	56.4	61.7	63.2	60.5	69.6	-9.9	NA
2	$SO_3^{2-} + O_3 \rightarrow O_2 + SO_4^{2-}$	-446.4	-421.6	-440.6	-440.9	-461.6	-511.7	-469.8	-421.2[†]
3	$SO_3^{2-} + O_2 \rightarrow O^* + SO_4^{2-}$	2.2	-52.9	-68.4	-72.6	-70.3	-73.2	-72.0	-26.3[†]
4	$HSO_3^- + OH^* \rightarrow OH^- + HSO_3^*$	156.5	151.6	-145.2	142.2	360.3	116.5	144.9	NA
5	$HSO_3^* + O_2 \rightarrow HSO_5^*$	46.4	-26.1	-22.9	-25.7	-228.6	64.2	-10.9	NA
6	$HSO_3^- + HSO_5^* \rightarrow HSO_3^* + HSO_5^-$	53.4	61.9	53.3	51.6	261.2	-8.7	28.1	NA
7	$HSO_3^- + HSO_5^- + H^+ \rightarrow 2SO_4^{2-} + 3H^+$	640.1	604.9	576.2	585.0	566.2	512.4	582.8	NA
8	$HSO_3^- + H_2O \rightarrow SO_3^{2-} + H_3O^+$	1270.4	1257.3	1257.5	1264.5	1259.4	1258.8	1264.8	NA
9	$HCHO + HSO_3^- \rightarrow HOCH_2SO_3^-$	411.1	-52.5	-63.8	-64.0	-640.1	461.4	379.7	NA
10	$HCHO + SO_3^{2-} + H^+ \rightarrow HOCH_2SO_3^-$	-194.1	-653.8	-664.1	-671.4	39.1	-127.7	-226.6	NA
11	$HOCH_2SO_3^- + OH^- \rightarrow CH_2(OH)_2 + SO_3^{2-}$	-153.8	380.7	388.2	394.4	-319.1	-136.0	-57.6	NA
12	$OH^* + HOCH_2SO_3^- \rightarrow HOCHSO_3^- + H_2O$	-481.6	-54.0	-58.7	-60.0	-587.8	-599.9	-561.0	NA
13	$HOCHSO_3^- + O_2 + H_2O \rightarrow HCOOH + HSO_3^- + HO_2^*$	1146.0	1592.9	1606.9	1605.3	910.6	1131.8	1172.2	NA
14	$O_3 + HSO_3^- \rightarrow HSO_4^- + O_2$	-368.6	-354.3	-369.5	-366.8	-389.8	-441.3	-395.3	-391.4[†]
15	$O_3 + SO_2 + H_2O \rightarrow HSO_4^- + O_2 + H^+$	-294.0	-284.3	-294.9	-287.1	-319.1	-370.6	-394.3	NA
16	$HSO_3^- + H_2O_2 \rightarrow HSO_4^- + H_2O$	-188.6	-331.0	-345.9	-346.1	-354.1	-366.0	-355.1	-351.2[†]

S/N	Aqueous-phase Reactions	B3LYP	G1	G2	G2MP2	G3	CBS-4	CBS-Q	Experiment
17	$HSO_3^- + CH_3OOH \rightarrow HSO_4^- + CH_3OH$	-262.2	-301.5	-315.3	-315.1	-324.1	-337.5	-325.2	NA
18	$HSO_3^- + HOONO_2 \rightarrow HSO_4^- + NO_3^- + H^+$	-271.1	-297.1	-308.5	-302.5	-313.6	-348.2	-431.4	NA
19	$HSO_3^- + HOONO \rightarrow HSO_4^- + HNO_2$	-83.8	304.2	-319.1	-318.9	-328.7	-342.5	-329.6	NA
20	$HSO_3^- + HSO_5^- \rightarrow 2HSO_4^-$	-414.8	-463.0	-482.2	-481.6	-492.1	-524.9	-480.7	NA
21	$HSO_3^{2-} + Cl_2 \rightarrow SO_3^- + 2Cl^- + H^+$	-753.1	-776.9	-777.2	-772.6	-772.9	-780.2	-739.3	NA
22	$OH^* + HSO_3^- \rightarrow SO_3^- + H_2O$	-174.1	-181.1	-189.1	-190.5	-190.4	-222.3	-201.5	NA
23	$OH^* + SO_3^{2-} \rightarrow SO_3^- + OH^-$	-496.9	-496.2	-500.7	-507.2	-498.7	-527.1	-510.8	NA
24	$OH^* + HSO_5^- \rightarrow SO_5^- + H_2O$	-315.8	-306.6	-308.6	-308.4	-308.1	-294.1	-297.0	NA
25	$OH^* + HSO_4^- \rightarrow SO_4^- + H_2O$	-88.0	-24.3	-34.2	-32.5	-29.0	-44.7	-56.1	NA
26	$SO_3^- + O_2 \rightarrow SO_5^-$	-41.9	-89.8	-89.1	-92.0	-85.2	-16.3	-78.3	NA
27	$SO_5^- + HSO_3^- \rightarrow HSO_5^- + SO_3^-$	141.6	125.5	119.5	117.9	117.7	71.8	95.5	NA
28	$SO_5^- + HSO_3^- \rightarrow SO_4^{2-} + SO_4^- + H^+$	0.1	0.1	0.1	0.1	0.1	0.1	0.1	NA
29	$SO_5^- + SO_3^{2-} + H^+ \rightarrow HSO_5^- + SO_3^-$	-463.6	-475.8	-475.2	-489.5	-483.3	-517.3	-510.8	NA
30	$SO_5^- + SO_3^{2-} \rightarrow SO_4^{2-} + SO_4^-$	-264.8	-248.1	-278.8	-279.9	-284.9	-346.0	-314.3	NA
31	$SO_5^- + SO_5^- \rightarrow 2SO_4^- + O_2$	-59.1	65.8	-36.3	44.1	33.5	-81.6	-16.2	NA
32	$SO_5^- + HO_2^* \rightarrow HSO_5^- + O_2$	41.9	26.4	27.9	27.8	27.4	-23.3	6.8	NA
33	$SO_5^- + O_2^- + H^+ \rightarrow HSO_5^- + O_2$	514.9	-111.0	-109.0	-121.8	-116.3	-409.0	-125.3	NA
34	$SO_4^- + HSO_3^- \rightarrow HSO_4^- + SO_3^-$	-86.1	-156.8	-155.0	-157.9	-161.4	-177.6	-145.4	NA

S/N	Aqueous-phase Reactions	B3LYP	G1	G2	G2MP2	G3	CBS-4	CBS-Q	Experiment
35	$SO_4^- + O_2^- \rightarrow SO_4^{2-} + O_2$	-214.7	301.3	300.4	135.6	-133.8	-139.8	165.6	NA
36	$SO_4^- + SO_3^{2-} \rightarrow SO_4^{2-} + SO_3^-$	-163.9	-224.2	-226.1	-232.0	-233.2	-248.1	-219.9	NA
37	$SO_4^- + NO_3^- \rightarrow SO_4^{2-} + NO_3$	537.0	498.9	498.4	496.1	495.1	495.2	513.5	NA
38	$SO_4^- + OH^- \rightarrow SO_4^{2-} + OH^*$	333.1	272.0	274.7	275.1	265.5	279.0	290.9	NA
39	$SO_4^- + H_2O \rightarrow SO_4^{2-} + H^+ + OH^*$	0.2	0.2	0.2	0.2	0.2	0.2	0.2	NA
40	$SO_4^- + H_2O_2 \rightarrow HSO_4^- + HO_2^*$	47.2	-106.3	-99.5	-101.8	-103.6	-67.5	-75.7	NA
41	$SO_4^- + HCOOH \rightarrow HSO_4^- + H^+ + COO^-$	18.4	-38.3	-27.7	-22.5	-26.0	-29.4	-6.1	NA
42	$SO_4^- + HCOO^- \rightarrow HSO_4^- + COO^-$	-59.4	-120.9	-113.3	-115.7	-117.9	-110.3	-98.3	NA
43	$SO_4^- + CH_2(OH)_2 + O_2 \rightarrow HSO_4^- + HO_2^* + HCOOH$	-85.8	-251.9	-244.1	-250.9	-238.9	-199.9	-211.9	NA
44	$SO_4^- + CH_2(OH)_2 + O_2 \rightarrow HSO_4^- + HO_2^* + HCHO + O^*$	381.2	226.2	236.4	232.2	239.3	275.1	269.2	NA
45	$SO_4^- + Cl^- \rightarrow SO_4^{2-} + Cl$	522.5	438.4	441.3	443.0	-442.1	449.1	459.0	NA
46	$H_2SO_4 + NO_3^- \rightarrow HSO_4^- + HNO_3$	-45.5	-49.3	-55.7	-57.1	-57.8	-63.4	-57.5	-102.4[†]

[†] Free energies for the aqueous-phase reactions were determined from individual free energies of formation obtained from Yaws (1999) and Lide (2002).